Cloning of the vanilloid-like receptor VR-L and investigation of its interaction with members of the Transient Receptor Potential family of receptors

by

Anastasia Liapi

Submitted to the University of London for the degree of doctor of philosophy

Biology Department,

University College London

2001

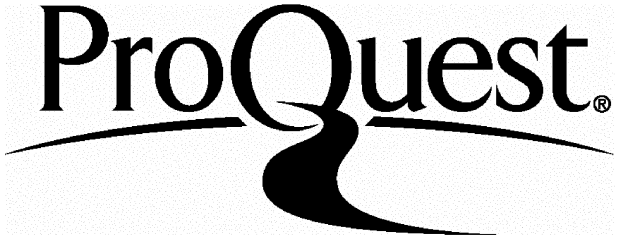

To my parents,
my first teachers

An Eskimo father fishes with his son by a stream that crosses an ice field. They just got a glimpse of a fish that is swimming close to them.

Eskimo Son *(with excitement)*: What a wonderful fish! What a wonderful fish!
Eskimo Father *(pleasantly surprised he slowly moves his fishing rod towards it)*: Oh yes, wonderful.
E.S.: We have to catch it today! We will catch it today!
E.F. *(with reassuring voice)*: Today.
E.S. (*startled, he points out*): Do the eyes start on the other side of the head?
E.F. *(straightens his back, attaching importance to his narration)*: Yes, it is a very strange fish. When it is time to become an adult, one eye moves across and joins the other.
E.S.: Why do they do that?
E.F. *(keeps talking while following the fish with his eyes)*: Maybe it is like a... a badge of maturity. It shows they passed through the nightmare.
E.S.: What nightmare?
E.F.: The nightmare that separates children from adults. *(suddenly interrupted, bends over)* Come quickly! Quickly! *(the son helps stabilise the vibrating fishing rod)* We've got it! Slowly.. slowly.. *(the fish is dragged out of the water).* Don't move!
(The father gives the fish to the son to hold it, while the father beats it to death)
E.F.: Look. Its colour changes to match the ocean floor.
E.S.: Camouflage!
E.F.: If one Arrow-tooth halibut sinks on top of the head of another, the bottom one does not create a disturbance, but waits until the other fish moves on.
E.S.: I wouldn't like anyone to sit on my head!
E.F. *(laughing)*: My boy, you are still young.. One eye just begins to move to the other side..
E.S.: Then it is better to have both eyes on the same side!
E.F.: Not better, different.
E.S.: What do you lose?
EF: Your other side. You lose something, but you also gain something..

From the film "Arizona Dream" (1992)
Directed by Emir Kusturica
Written by David Atkins

CONTENTS

Acknowledgements

There are a number of people I would like to thank from the bottom of my heart for having contributed one way or another to me presenting this thesis today. I would like to thank my supervisor Prof. John Wood and the Wellcome Trust for giving me the opportunity to study for a Ph.D. degree. I am mostly grateful to my supervisor for his guidance throughout the doctorate training and his support especially in the last few months.

I would also like to thank Dr. Garcia for teaching me bioinformatics and for his major contribution to the cloning of the VR-L receptor, Dr. Cesare and Dr. Wafford's group at Merck for their electrophysiology recordings and Dr. Sihra for devoting the time to teach me fluorometry. I am indebted to Dr. Sukumaran for always been available to discuss experiments with me and for his support and understanding at difficult times. I am also grateful to my second supervisor Prof. Richardson for his advice and support and to Dr. Akopian and Dr. Souslova for the scientific inspiration. My thanks to Prof. Stephenson, Dr. Perkinton and Dr. Brandon for discussing the immunoprecipitation method with me. Moreover I am grateful to Dr. Perkinton and Melissa Barber for making me realise how much I enjoy teaching. My gratitude to Prof. Parnavelas for the inspiring scientific discussions, his friendship and help. I am indebted to my friends Litsa, Fleur and Anjan for the much-needed coffee breaks and for dragging me out of the lab at times of despair! My friends Ali, Maria, Marianthi, Eunice and Thomas outside the lab helped to keep things in perspective. Katerina, Paolo and Dexter managed to electronically transmit loads of warmth and encouragement from abroad and an amazing cheeky humour, that proved indispensable on long, tiring days. I am also indebted to colleagues all around the world, that I'll never be able to thank personally, who took the time to answer my questions in the (life saving) biology forum at www.nwfsc.noaa.gov/protocols/methods/methods.html.

I should also thank the people who inspired me to do science and made it possible for me to study for this degree. Prof. Lichtenstein is my prototype of an educator, as he taught me the fundamentals of how to think, do and present science. Moreover, his friendship, support and advice at the most difficult times of this Ph.D. proved an invaluable safety net. If there is anybody to blame for the existence of this thesis today is him and his contagious enthusiasm! But the real culprits are my biggest fans, my family! I would like to thank my brother, who in an incredible act of serendipity made my studies in UK possible and for proving to me that a Ph.D. is not out of reach. My father for teaching me first the ropes in scientific methodology and for reminding me that stubbornness is an advantageous quality to a scientist (unless natural selection eliminates you first for it). My mother for teaching me the importance of meticulous analysis and for indicating the viewpoint's relativity to happiness (otherwise "stop whining, it could always be worse"). Finally, I would like to thank Navin for helping me see the big picture and for fuelling my efforts in research with his addictive rum-chocolate truffles! The fact that he never complained about being dragged to the university the most ridiculous hours deserves him sainthood. Most importantly, I am grateful to him for carrying out extensive behavioural experiments, trying to identify the comedy programme capable of treating my Ph.D. blues. With a sample number n= 10 episode series, he concluded that Ali G induced a consistent response (95% confidence in the extreme conditions of a Ph.D. student's t-test) by providing the absolute freedom of mind for 4min 36 seconds average, exactly the time it takes for me to recover after falling off the couch laughing with tears..

Publications that resulted from this work

- A. Liapi, R.Garcia, P. Cesare, T. Bonnert, K. Wafford, S. Clark, J. Young, P. Whiting, P. McNaughton and J.N. Wood (2001). The capsaicin receptor VR1 interacts with the Vanilloid Receptor-like protein VR-L (in preparation).

- Ian F.James , Rey Garcia, Anastasia Liapi and John N.Wood (2000). Capsaicin and vanilloid receptors. Molecular Basis of Pain Induction, Wiley-Liss, USA, pp: 175-192

- John N. Wood, Armen N. Akopian, Paolo Cesare, Yanning Ding, Rey Garcia, Mark Heath, Anastasia Liapi, Misbah Malik-Hall, Mohammed Nassar, Kenji Okuse, Samantha Ravenall, Oro Rufian, Veronika Souslova and Madhu Sukumaran (1999). The primary nociceptor: Special functions, special receptors. Proceedings of the 9th world congress on pain. Progress in pain research and management, IASP Press, Seattle, vol. 16, pp: 47-62

- R. Garcia, A. Liapi, P. Cesare, T. Bonnert, K. Wafford, S. Clark, J. Young, P. Delmas, P. Whiting, P. McNaughton and J.N. Wood, (1999). VR-L, a vanilloid receptor-like orphan receptor, is expressed in T-cells and sensory neurons. Meeting of the Physiology Society, vol. 518P, Ion channels 126P

List of tables and figures

Prologue

CHAPTER 1

Introduction

Experimental results

Discussion

CHAPTER 2

Introduction

Experimental Results

tissue distribution of the VR-L gene. **Figure 2.3A:** Tissue distribution of VR-L (cont). **Figure 2.3B:** Genomic DNA contamination control in the same RNA samples as the ones used in figure 2.3A. **Figure 2.4:** Sensitivity of RT-PCR in identifying differences in concentrations. **Figure 2.5:** Determining the exponential amplification of the genes studied. **Figure 2.6:** Determining the exponential amplification of the genes studied (cont.). **Figure 2.7:** Normalisation of the cDNA amounts of the differently treated samples. **Figure 2.8:** Upregulation of VR1 by NGF in cultured DRG. **Figure 2.9:** Upregulation of VR1 and VR-L by NGF in cultured DRG. **Figure 2.10:** Upregulation of VR-L by NGF *in vivo*. **Figure 2.11:** Upregulation of VR-L by NGF in cultured DRG. **Figure 2.12:** Upregulation of VR-L by NGF *in vivo*. **Figure 2.13:** Expression of VR-L in DRG neurons that do not respond to capsaicin. **Figure 2.14:** Examples of responses of VR1, VR-L and untransfected COS7 cells to 1μM capsaicin and pH change from 7.4 to 6. **Figure 2.15:** Statistical analyses of VR1, VR-L transfected and naïve cells' responses. **Figure 2.16:** VR1 responses to 1μM capsaicin (A) and pH reduction from 7.4 to 6 (B). **Figure 2.17:** Co-application (A) or sequential application of 1μM capsaicin and pH reduction from 7.4 to 6 (B and C) in VR1 transfected COS7 cells. **Figure 2.18:** Membrane inward currents measured at -60 mV evoked by fast application of high temperature 52^{0}C (T), pH 5.4 (pH) and 500 nM capsaicin (caps) in HEK293 cells transfected with either GFP, GFP/VR-L or GFP/VR1. **Figure 2.19:** Statistical analysis of high temperature 55^{0}C, pH 6.0 and 1μM capsaicin responses in HEK293 cells transfected with either GFP, GFP/VR-L or GFP/VR1. **Figure 2.20:** Epitope tagging PCR strategy. **Figure 2.21:** Subcloning the tagged gene sequence. **Figure 2.22:** PCR amplification of AB and CD regions of rat VR-L. **Figure 2.23:** Amplification of the AD region of rat VR-L, incorporating the *c-myc* epitope. **Figure 2.24:** Digestion of rat VR-L in pcDNAI with NarI and Eco47III. **Figure 2.25:** Digestion of PCR product AD with NarI and Eco47III. **Figure 2.26:** *In vitro* transcription and translation of the original rat VR-L and of the rat VR-L with the *c-myc* epitope on the extracellular loop. **Figure 2.27:** Detection of rat VR-L mycX with fluorescent immunocytochemistry on non-permeabilised HEK293 cells.

CHAPTER 3

Introduction, **Table 1:** Summary of the TRP channel characteristics.

Experimental results

Figure 3.1: Expression of TRP channels in rat tissues. **Figure 3.2:** Expression of TRP channels in normalised capsaicin treated and control rat DRG cultures. **Figure 3.3 :** PCR strategy for addition of epitope tags. **Figure 3.4:** Addition of the c-myc epitope on VR1 with PCR. **Figure 3.5:** Insertion of FLAG epitope with PCR in human VR-L. **Figure 3.6:** Insertion of the c-myc epitope into the rat VR-L gene. **Figure 3.7:** Insertion of c-myc epitope in human TRP1. **Figure 3.8:** Insertion of FLAG epitope in human TRP3. **Figure 3.9:** Insertion of the c-myc epitope into mouse TRP6. **Figure 3.10:** Diagnostic restriction enzyme digestions of the VR and TRP constructs. **Figure 3.11:** *In vitro* transcription and translation of VR and TRP constructs. **Figure 3.12:** Immunocytochemistry of VR and TRP constructs in HEK293 cells. **Figure 3.13:** Patch-clamp recordings from HEK293 cells transfected with VR1 constructs in the presence of 3μM capsaicin for 6 sec. **Figure 3.14 (A):** Autoradiography of Western blot of rat VR-L/FLAG protein probed with anti-FLAG antibody. **Figure 3.14 (B):** Autoradiography of the same Western blot of rat VR-L/FLAG protein as picture A, probed with anti-VR-L antibody. **Figure 3.15:** log of protein mass versus the log of distance covered by each of the protein markers. **Figure 3.16.** Picture A: expression of rat VR-L/FLAG in HEK293 and COS cells. Picture B: expression of rat VR-L/FLAG in HEK293 and COS

cells in the presence and absence of protease inhibitors. Picture C: immunoprecipitation with non-immune IgG and without antibody in rat VR-L/FLAG transfected cells. **Figure 3.17:** Anti-FLAG western blot of VR-L/FLAG protein immunoprecipitations from membrane and cytoplasmic preparations of transfected HEK293 and COS cells. **Figure 3.18:** PNGaseF treatment of crude lysates and immunoprecipitates from rat VR-L/FLAG transfected HEK293 cells. **Figure 3.19:** Co-immunoprecipitation of rat VR-L/FLAG and VR-L/MYC proteins. **Figure 3.20:** Immunoprecipitations of VR and TRP constructs. **Figure 3.21:** Co-immunoprecipitations of VR and TRP proteins. **Figure 3.22:** Negative control for protein interactions. **Figure 3.23:** Insertion of a SacII site into pcDNA3. **Figure 3.24:** Diagnostic digestion of the rat VR-L/FLAG construct in pcDNA3. **Figure 3.25:** *In vitro* transcription and translation of the rat VR-L/FLAG construct in pcDNA3. **Figure 3.26:** Plot of percentage of CHO cell survival versus increasing concentrations of geneticin after the period of 2 weeks. **Figure 3.27:** Western blot analysis of the rat VR-L/FLAG CHO cell line.

Abbreviations list

5HT: 5-hydroxytryptamine (serotonin)
a.a.: amino acid
ATP: adenosine triphosphate
BDNF: brain-derived neurotrophic factor
BK: bradykinin receptor
BLAST: basic local algnment search tool
BLOSUM: blocks substitution matrix
cAMP: adenosine 3,5,-cyclic monophosphate
CB1: cannabinoid receptor subtype 1
CCE: capacitative calcium entry
cDNA: coding DNA
CGRP: calcitonin gene-related peptide
CHO: chinese hamster ovary
CNS: Central Nervous System
CRAC: calcium release-activated channel
DAG: diacylglycerol
dbEST: database expressed sequence tag
DEPC: diethylene pyrocarbonate.
DMEM: Dilbecco's modified eagle medium
DMSO: dimethyl sulfoxide
DRG: dorsal root ganglia
DTT: dithiothreitol
EBI: European bioinformatics institute
EDTA: ethylenediaminetetraacetate
EGF: epidermal growth factor
GABA: γ-aminobutyric acid
GDNF: glial-derived neurotrophic factor
GenBank: Genome Bank
GFP: green fluorescent protein
HEK: human embryo kidney
HEPES: N-2-Hydroxyehtylpiperazine-N'-2-ethanesulfonic acid
HGI: human gene index
IB_4: Griffonia simplicifolia lectin B4

IGF-I: insulin-like growth factor I
IP3: inositol triphosphate
IPTG: isopropylthiogalactoside
MES: 2-(N-morpholino)ethanesulphonic acid
MOPS: 3-(N-morpholino)propanesulfonic acid
NGF: nerve growth factor
NIH: national institute of health
NMDA: N-methyl-D-aspartate
PBS: phosphate buffer solution
PCR: polymerase chain reaction
PDGF: platelet-derived growth factor
Pfam: protein families database
PI-3: phosphatidylinositol-3 kinase
PIP_2 : phosphatidylinositol 4,5- biphosphate
PIP3: phosphatidylinositol 3,4,5-triphosphate
PKC: protein kinase C
PLC: phospholipase C
PMSF: phenylmethanesulfonyl fluoride
PNGase F: peptide-N-glycosidase F
RACE: rapid amplification of cDNA ends
RTX: resiniferatoxin
SDS: sodium dodecyl sulphate
SDS-PAGE: SDS-polyacrylamide gel electrophoresis
SMART: simple modular architecture research tool
SOC: store-operated channel
TAE: tris-acetate EDTA buffer
TE: tris-EDTA
TEMED: N,N,N',N'-Tetramethyl-1,2-diaminomethane
THC: tentative human consensus sequenc
TIGR: institute for genome research
trkA/B: tyrosine kinase receptor A/B
TRP: transient receptor potential
UTR: untranslated region
UV: ultra-violet
VR1: vanilloid receptor subtype 1
VR-L: vanilloid receptor-like

Abstract

Early pharmacological studies (Szolcsanyi and Jancso-Gabor, 1975, Wood, 1988) showed that capsaicin, the pungent ingredient of chilli peppers and other vanilloids, can specifically stimulate the C unmyelinated fibres which transmit nociceptive information i.e. information about noxious thermal, chemical and mechanical stimuli. The specific action of capsaicin on this subset of sensory neurons led researchers to postulate the existence of a capsaicin receptor.

Caterina *et al.* (1997) cloned Vanilloid Receptor 1 (VR1) from dorsal root ganglia, where the somata of C fibres reside. VR1 responds to capsaicin, heat, protons and to the cannabinoid ligand, anandamide (Zygmunt *et al.*, 1999). Discrepancies between the pharmacological profile of VR1 and native vanilloid responses fuelled research for the identification of other vanilloid receptors. In this thesis, the cloning of a new member of the vanilloid receptor family is described using bioinformatics tools. The novel receptor was named Vanilloid Receptor-like (VR-L) and was found to share 49% identity with VR1 and 20% with members of the Transient Receptor Potential (TRP) family. VR-L transcripts were identified in a wide range of tissues including the capsaicin insensitive dorsal root ganglia neurons. The expression of the channel in these neurons can be upregulated by Nerve Growth Factor, as it was established with semi-quantitative RT-PCR. Co-immunoprecipitation studies were carried out to investigate the possibility that VR-L interacts with VR1 and other members of the TRP family to regulate indirectly vanilloid and other responses. VR1 and VR-L were found to form homomultimers and also to interact with each other and with members of the TRP family. A VR-L stable cell line was generated to study the functional significance of the interactions identified.

PROLOGUE

Pain and nociceptors

Pain can be broadly defined as an unpleasant experience associated with actual or potential tissue damage and serves to warn and protect from injury. Although it comprises a sensory modality, it also has emotional qualities that make pain a subjective experience difficult to describe. Pain is overall an emotional state, of which intensity and severity depends on the nature of the stimulus but also on subjective experiences and factors such as gender and cultural background. The need to treat clinically the causes of pain led to attempts to classify states of pain on the basis of pathophysiological processes (reviewed by Chapman and Stillman, 1996). Although the following definitions do not always reflect an organic contribution, they have proved useful in the evaluation and treatment of pain: Allodynia describes the sensation of pain from a stimulus that is not normally painful. The term analgesia represents the absence of pain following exposure to painful stimuli. Central pain infers pain induced by a lesion in the central nervous system. Deafferentation pain is associated with the loss of input from afferent nerves e.g. as it happens in amputation. Hyperalgesia describes augmented responses to noxious stimuli i.e. hypersensitivity. The term neuralgia describes pain of the nerves. Neuropathic pain refers to pain that results from the disturbed function of nerves in the peripheral or central nervous system. Inflammatory pain is initiated by inflammation that follows tissue damage. Idiopathic pain has no detectable pathological origin and is attributed to psychiatric disorder. Pain is also described as acute, when it can be readily associated with a cause and its duration does not exceed the healing period, while chronic pain is prolonged and is associated with signs of psychological distress. Although pain perception has evolved to alert to damaging stimuli, cases like chronic pain and phantom limb pain, associated with amputated limbs, serve no adaptive role indicating that pain perception is not an infallible sensory system.

Physiological pain is initiated at the periphery with the activation of specialised receptors by noxious stimuli. In the 1890's Max von Frey in a series of histological observations identified the existence of tactile, warm, cold and pain spots on the skin. In 1906 Sherrington, supporting von Frey's observations, reported that noxious stimuli are conducted along unmyelinated or thin axons. Later in 1967 Burgess and Perl proposed the existence of receptors after they had identified fibers that responded with different conductances to different stimuli (reviewed by Perl and Kruger, 1996). Today, we know

that all somatosensory information is conveyed by dorsal root ganglia neurons that innervate the periphery. Dorsal root ganglia (DRG) are located at the dorsal entry of the spinal cord on the level of each vertebra and contain the somata of the neurons (figure 1). The axon of a DRG neuron, otherwise called primary afferent fiber, has two branches, one projecting to the central nervous system (in the dorsal horn of the spinal cord) and the other to the periphery. The terminals of the afferent fiber contain receptors that respond to noxious stimuli. For this reason, these neurons are called nociceptors (Latin *nocere*, to injure). Provided that the stimulation of the nociceptors is sufficient, action potentials are generated that travel along the afferent and transmit pain-related information to the central nervous system. There are three major classes of nociceptors: the rapid thermal and mechanical nociceptors with small diameter, thinly myelinated Aδ fibers conducting at 5-30m/sec and the slow polymodal nociceptors with small diameter, unmyelinated C fibers responding to mechanical, chemical and thermal stimuli at 1m/sec conductance.

Figure 1: The location of dorsal root ganglia
(from http://www.owecc.net/breynolds/ap1ppt/cusisld043.htm)

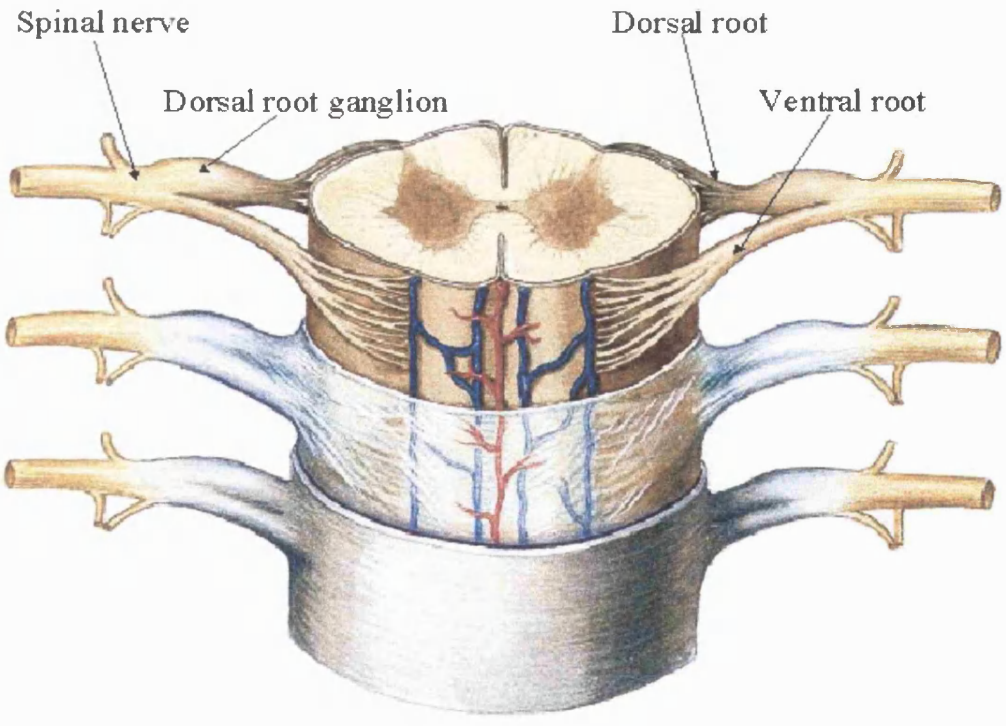

Apart from their function and velocity with which they convey signals, the different classes of nociceptors are also delineated according to markers and proteins they

express e.g. substance P, CGRP, their neurotrophic factor requirement e.g. NGF, GDNF and their connectivity to neurons of the dorsal horn in the spinal cord (reviewed by Basbaum and Woolf). The dorsal horn can be subdivided in six laminae with distinct types of neurons inhabiting them. Aδ and C fibers predominantly project to laminae I, II and V (figure 2). The nociceptive input is relayed from the spinal cord to the thalamus and the cerebral cortex via five ascending pathways. These pathways do not only involve sensory regions of the thalamus and the cortex but also the limbic system, in particular the amygdala that are thought to contribute to the emotional aspect of pain. Study of injuries in the thalamus and the cerebral cortex have established the importance of neurons in these areas in perceiving and processing nociceptive information. The central nervous system does not only process pain-related information but also controls pain, as it was established by the production of analgesia following electric stimulation of a variety of brain structures, most importantly the periaqueductal gray (reviewed by Basbaum and Jessell). This structure was also found to participate in opiate-induced analgesia. Descending pathways starting from the periaqueductal gray can inhibit the nociceptor afferent fibers in the spinal cord and thus regulate the transduction of pain-related information.

Figure 2: Summary of the pain pathway. Signals from nociceptors are propagated along the afferents to the somata of the dorsal root ganglia and then projected to the dorsal horn. The connectivity of two classes of C polymodal nociceptors is shown. From there the signals are transduced to the brain. (source: http://www.nature.com/nrn/journal/v2/n2/slideshow.nrn0201_083a_F1.html)

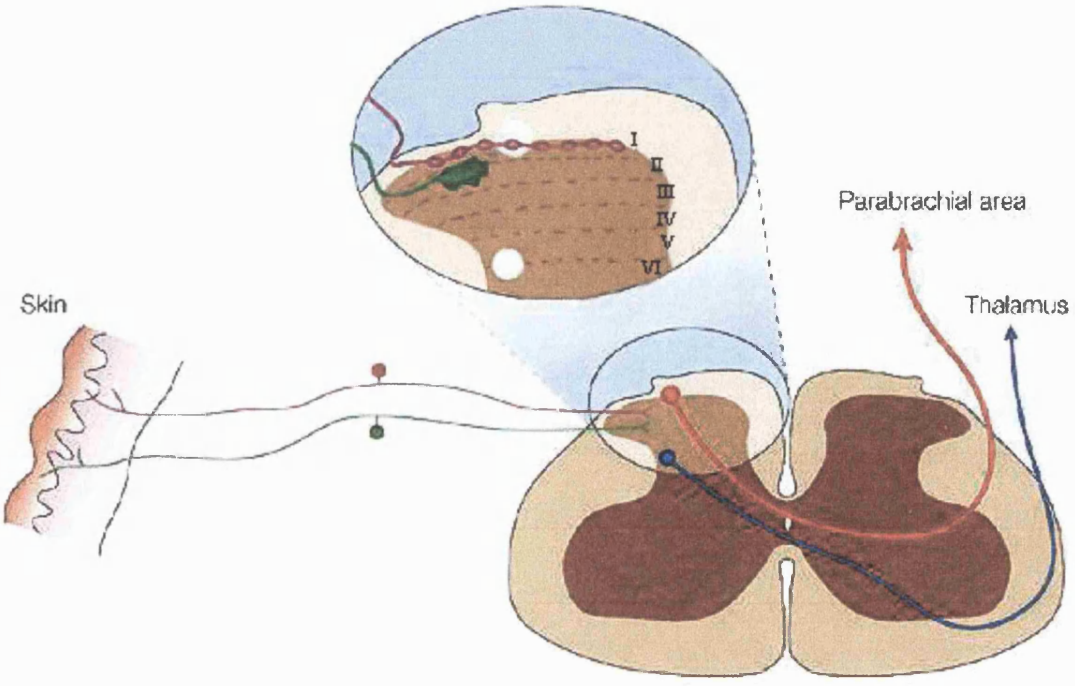

Capsaicin as a pharmacological tool in the study of nociceptors

1) ***What is capsaicin and where the site of its action is ?***

Capsaicin (8-methyl N-vanillyl-6-noneamide) is the pungent, algogenic ingredient of red hot peppers of the *Capsicum* family. It has been found to activate selectively a subset of mammalian peripheral sensory neurons: the small diameter primary afferent neurons, which transmit nociceptive information to the CNS about noxious thermal, mechanical and chemical stimuli. These neurons also have efferent functions, since they release neurotransmitters from their central and peripheral terminals after the application of capsaicin, such as the calcitonin gene-related peptide (CGRP), tachykinins, substance P, neurokinin A, eledoisin like peptide, somatostatin etc.(reviewed by Lawson, 1996). These neuropeptides are responsible for symptoms of inflammation e.g. vasodilation, plasma exudation, mucus secretion in a variety of tissues and organs such as the gastrointestinal, the genitourinary system, airway smooth muscles, heart etc.

2) ***Electrophysiological and pharmacological characterisation of the vanilloid action.***

Voltage-clamp experiments on nodose ganglia and DRG neurons revealed that capsaicin elicits an inward depolarising current in most of the neurons in negative potentials (Vlachova and Vyklicky, 1993, Oh *et al.*, 1996). The increase in conductance shows that an ion channel is opened by capsaicin, which was found to permit the entry of monovalent and divalent cations in the following permeability sequence: Ca^{2+}>Mg^{2+} >K^+ >Na^+. Even large organic ions such as choline and arginine are allowed to pass through the capsaicin-activated channel. The permeability to Ca^{2+}, Na^+ and big molecules such as guanidine in response to capsaicin was also shown in pharmacological studies of cultured DRG neurons (Wood *et al.*, 1988). The large capsaicin-induced Ca^{2+} uptake was not inhibited with voltage-sensitive calcium channel antagonists, suggesting that the capsaicin response cannot be attributed to such channels. Current-voltage relationships for the capsaicin-evoked current are linear and reverse close to 0mV. Single channel conductance was measured to be 20-40pS at membrane potentials between –80mV and -50mV and 80-100pS at +60mV, which suggest outward rectification. The open channel probability (P_O) is voltage-dependent (-60mV to +60mV). Efflux experiments with radioactive anions showed that capsaicin acts with an EC_{50} of 100-300nM. Electrophysiological experiments showed similar results (an EC_{50} of 1.1μM in membrane patches and an EC_{50} of 200-400nM in voltage-clamped cells).

The Hill coefficient was calculated to be 1.8, which shows that more than one vanilloid molecule needs to bind to the receptor to activate it (reviewed by James *et al.*, 1993).

High concentrations of capsaicin (20-300μM) can inhibit voltage-gated Na^+ and K^+ channels in a variety of tissues. Specifically in DRG, capsaicin has a long lasting inhibitory effect on voltage-gated Ca^{2+} channels, which is dependent on the Ca^{2+} influx induced by capsaicin (Docherty *et al.*, 1991). This phenomenon might underlie the functional desensitisation exhibited by capsaicin, where high concentrations of the drug can inhibit responses to other noxious stimuli. Capsaicin also induces pharmacological desensitisation, where repeated capsaicin exposure reduces subsequent responses to the drug itself. Docherty *et al.* (1996) reported the pharmacological desensitisation to be mostly calcium-dependent and to be regulated by calcineurin, as it was demonstrated by the use of specific inhibitors of the enzyme.

3)*Neurotoxicity and desensitisation: therapeutic applications*

Capsaicin concentrations at the 10-500nM range initially excite the C fiber and some A δ fiber neurons in culture, causing depolarisation. The current elicited is non-specific and can be studied by $^{45}Ca^{2+}$ influx, or efflux of [^{14}C]guanidinium, $^{86}Rb^+$ or $^{22}Na^+$ (Wood *et al.*, 1988). At higher concentrations (1-5 μM range) capsaicin can desensitise neuronal responses to other noxious stimuli e.g. it can inhibit neurogenic inflammation (Jancso *et al.*, 1967), increase thermal nociceptive thresholds and impair responses to mechanical pressure and chemical irritants like formalin (Nagy and van der Kooy, 1983). Moreover, application of capsaicin in large concentrations (>5μM) especially in neonatal animals has neurotoxic effects that can lead to a great loss of neural cells and neuropeptide depletion (Nagy *et al.*, 1980, Jancso and Kiraly, 1981, Jancso *et al.*, 1985). The neurotoxicity is believed to be due to an increase in intracellular Ca^{2+} that follows capsaicin application. The Ca^{2+} is probably taken up by mitochondria, since inhibitors of mitochondrial respiration can block the Ca^{2+} accumulation (Bevan and Szolcsanyi, 1990). Application of capsaicin also allows the influx of Na^+, which, when combined with the passive influx of Cl^- to give NaCl, causes the osmotic uptake of water and lysis of the cell.

The characteristic desensitisation caused by capsaicin can be used therapeutically. Systemic application of capsaicin activates afferent nerve terminals in the spinal cord, followed by inactivation of voltage-gated Ca^{2+} channels and thus blockade of

neurotransmitter release, which results in antinociception and anti-inflammation. Local application of capsaicin inactivates the C fibres and as a result, inhibits neurotransmitter release from peripheral nerve endings (Dray *et al.*, 1990a). Local administration of capsaicin has been used to alleviate painful conditions such as cluster headache, post herpetic neuralgesia, rheumatoid arthritis etc.(Watson *et al.*,1988). The analgesic effect of capsaicin follows an initial undesirable burning sensation. For that reason, attempts have been made to develop drugs like olvanil (Brand *et al.*, 1987) with the antinociceptive effect of capsaicin without the initial irritation.

4) *Evidence for the existence of a vanilloid receptor.*

Avian sensory neurons in culture do not respond to capsaicin, reinforcing the finding that capsaicin acts specifically on mammals (Wood *et al.*, 1988). Capsaicin excites nociceptive neurons and particularly the RT97 negative populations (Winter *et al.*, 1987). Capsaicin can elicit its effects on membrane patches of DRG, suggesting that it interacts with a membrane protein and that no second messenger systems are involved (Bevan and Forbes, 1988). Nevertheless, the capsaicin-induced rise in intracellular Ca^{2+} can increase the levels of intracellular mediators such as cGMP, resulting from activation of the arachidonic acid metabolism (Wood *et al*, 1989). Therefore, there is specificity of action, which probably accounts for the existence of a capsaicin receptor. This specificity was first proposed by Szolcsanyi and Jancso-Gabor (1975), who reported that capsaicin and its analogues exhibit a chemical structure-activity relationship that is reflected in their pungency. Moreover, capsaicin sensitivity of adult DRG neurons in culture was found to be NGF-dependent (Winter *et al.*, 1988) and therefore like other receptors is under cellular control. Szallasi and Blumberg (1991) found that the size of vanilloid receptors in pig DRG is approximately 300kDa by using inactivation of agonist binding by radiation, which suggests the vanilloid receptor to consist of subunits.

Capsaicin analogues have been used, like the naturally occurring piperine from black peppers and resiniferatoxin (RTX) from the cactus *Euphorbia resinifera* or the synthetic compounds olvanil and nuvanil. Szallasi and Blumberg (1990) identified $[^3H]$RTX binding sites on sensory neurons but not on capsaicin-insensitive neurons, reinforcing the postulation for the existence of a vanilloid receptor. Winter *et al.* (1990) reported that RTX-elicited $^{45}Ca^{2+}$ uptake by cobalt-sensitive, RT97-negative DRG neurons in culture and neurotoxic effects evoked by prolonged exposure to RTX. The common moiety

among all these compounds is the vanilloid moiety, hence the name of the receptor (Fig 3). Ruthenium red antagonises capsaicin non-competitively (Dray *et al.*, 1990b), while capsazepine, a synthetic compound, acts specifically as a competitive capsaicin antagonist, as established in radioactive ion flux experiments (Bevan *et al.*, 1992). Bevan and Yeats (1991) identified a proton-gated current specifically conducted by capsaicin sensitive neurons and regulated by NGF. The proton and the capsaicin responses have a similar time course and similar amplitudes. Petersen *et al.* (1993) reported that low pH can potentiate capsaicin responses in DRG and trigeminal neurons. Szallasi *et al.* (1995a) reported that acidification inhibited [^{3}H]RTX binding in the spinal cord. These results suggested protons to be candidates for the endogenous ligand of the vanilloid receptor.

5) *Subtypes of vanilloid receptors*

Resiniferatoxin (RTX), an extract from plants of the genus *Euphorbia* is a capsaicin agonist. It causes similar behavioural effects as capsaicin e.g. hypothermia and it exhibits cross-desensitisation with capsaicin. The major difference to capsaicin is that RTX is active at 100-10000 times lower concentrations compared to capsaicin and it has higher affinity for the receptor (Bevan and Szolcsanyi, 1990). RTX opens the vanilloid receptor more slowly but it keeps it open for longer (Winter *et al.*, 1990). Capsaicin is not appropriate for binding assays since it is very lipophilic and exhibits low potency for the receptor. [^{3}H]RTX was used instead for binding assays on membranes of DRG ganglia, in the hope of revealing the vanilloid receptor. By using [^{3}H]RTX on intact DRG neurons in culture or suspension, Acs *et al.* (1996) showed that RTX exhibits 10-fold higher potency for receptor binding than $^{45}Ca^{2+}$ uptake, while capsaicin and capsazepine show 10-fold higher potency for calcium uptake than receptor binding. These findings argue for the existence of two classes of vanilloid receptors, R and C respectively. Studies using capsazepine and ruthenium red and comparing the potency of blocking desensitisation and $^{45}Ca^{2+}$ uptake gave extra support to the argument (Acs *et al.*, 1997). Affinity for RTX differs among species (rat tissues show higher RTX affinity than guinea pig tissues) and also among tissues of the same animal (nervous tissue shows higher affinity for RTX than airways and urinary bladder), which probably indicates the existence of multiple receptors (reviewed by Szallasi, 1994).

Capsaicin was found to evoke oxygen consumption by the perfused hindlimb, followed by depression of that phenomenon due to vasoconstriction. Colquhoun *et al.* (1995) proposed the existence of two capsaicin receptors in the rat hindlimb: a high affinity

capsaicin receptor, which stimulates oxygen consumption and vasoconstriction depending on the presence of external Ca^{2+} and oxygen and a low affinity capsaicin receptor that evokes decreased oxygen consumption and vasoconstriction, independently of Ca^{2+} and oxygen. Another piece of evidence that supports the existence of vanilloid receptor subtypes, came from Liu and Simon (1996) who recorded two capsaicin specific inward currents in trigeminal ganglia with different kinetics: one rapid (1.7sec time to peak), RTX-insensitive current and one slower (24.5 sec time to peak), RTX-sensitive current.

The accumulating evidence for the existence of a capsaicin receptor fuelled attempts to isolate it. Wood *et al.* (1990) used a photoaffinity probe with capsaicin-like activity to label neurons and other tissues. These tissues were subsequently analysed with an anti-capsaicin antibody that specifically recognised capsaicin-binding proteins in DRG neurons with a major band at about 58kDa.Ninkina *et al.* (1994) isolated RTX binding proteins by screening an expressed rat DRG library with an RTX photoaffinity probe. One of the clones identified encoded a 235 amino acid protein that lacked channel-like characteristics. Its expression was identified in dorsal root ganglia and also in capsaicin-insensitive tissues. This protein was found able to displace capsaicin and RTX in binding studies but functional experiments failed to elucidate its role. The ultimate evidence for the existence of a capsaicin receptor was provided by Caterina *et al.* (1997), who cloned the Vanilloid Receptor subtype 1 (VR1) from a rat DRG library using calcium imaging expression studies. The cloned receptor exhibited the pharmacological and electrophysiological characteristics associated with capsaicin application, as it is described in detail in the following section.

Figure 3 : Structure comparison of capsaicin and RTX. The common vanilloid moiety is indicated.

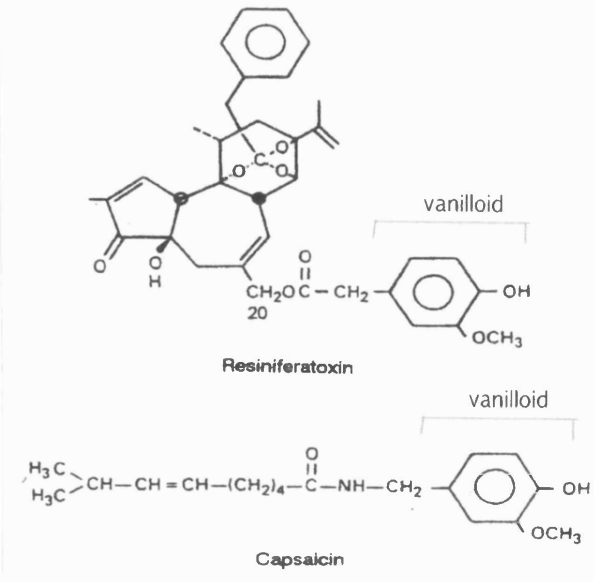

CHAPTER 1

In silico cloning of VR-L, a new member of the vanilloid receptor family

INTRODUCTION

CLONING OF VANILLOID RECEPTOR SUBTYPE 1: THE CAPSAICIN RECEPTOR

Early studies carried out by Jancso *et al.* (1967) on inhibiting neurogenic inflammation by using large capsaicin concentrations indicated that capsaicin acts specifically on nociceptors. Later, Szolcsanyi and Jancso-Gabor (1975) conducted behavioural experiments on rats to identify relations between the pungency of capsaicin-like drugs and their chemical structure. The finding that there are structural requirements for activity of capsaicin and its analogues led the researchers to propose the existence of a capsaicin receptor in nociceptors. Wood *et al.* (1988) reported that capsaicin-induced cobalt and $^{45}Ca^{2+}$ uptake by a specific population of DRG neurons, showing that capsaicin affects a particular subtype of nociceptors. Since these cells were negative for neurofilament immunoreactivity, it was concluded that they were small diameter DRG neurons. These studies spurred attempts to isolate and characterise the capsaicin receptor.

Electrophysiological and pharmacological studies in the past had shown that the activation of the capsaicin receptor resulted in Ca^{2+} influx in DRG neurons (Wood *et al.*, 1988, Oh *et al.*, 1996). Caterina *et al.* (1997), taking advantage of the channel's permeability to Ca^{2+}, used the calcium imaging technique to clone the capsaicin receptor, where fluorescent indicator dyes exhibit different excitation wavelength when they bind Ca^{2+}, compared to their free state. A rat DRG cDNA library was divided into pools, which were transfected in human embryonic kidney-derived HEK293 cells, loaded with the calcium-sensitive fluorescent dye, Fura-2. Calcium imaging analysis identified cells that responded to capsaicin with a Ca^{2+} influx. A positive pool was identified which was subdivided and subjected to calcium imaging repeatedly until a single clone was isolated. The insert identified was named Vanilloid Receptor 1 (VR1), from the chemical moiety present in capsaicin.

The cDNA clone contains 2,514 nucleotides that encode for a protein of 838 amino acids. The receptor consists of three ankyrin repeats followed by six transmembrane domains with a hydrophobic linker between domains five and six. Structural and amino acid sequence similarity was found between the VR1 and TRP channels. The TRP (transient receptor potential) channels are probably the best known CRAC (Ca^{2+} release activated Ca^{2+}) channels or SOC channels (store operated Ca^{2+} channel) first found in Drosophila. These channels, expressed on the plasma membrane, allow an inward

calcium current into the cell, when Ca^{2+} is depleted from intracellular storing organelles (Funayama *et al.*, 1996). It is not known what signal informs the cell about Ca^{2+} depletion and what initiates the Ca^{2+} influx. Not only do both TRP and VR1 have similar structure containing six transmembrane domains, but they also share great sequence homology between domains five and six. Studies using thapsigargin to deplete intracellular Ca^{2+} stores or SKF96365 to inhibit depletion-induced Ca^{2+} entry showed that VR1 is not a store operated Ca^{2+} channel (Caterina *et al.*, 1997).

Electrophysiological studies on *Xenopus* oocytes injected with the VR1 cDNA, showed that the cloned receptor responded to capsaicin and RTX. Similar to the desensitisation observed in native vanilloid receptors (Blumberg *et al.*, 1993), washing out of the RTX failed to recover the current. The Hill coefficient of 1.95 for capsaicin on VR1 showed that more than one molecule of agonist is required to activate the receptor, as known for native vanilloid receptors from previous studies (reviewed by Wood and Docherty, 1997). The competitive antagonist, capsazepine, and the non-competitive antagonist, ruthenium red, blocked the activation of VR1.

Subjecting VR1 expressing cells to different ionic solutions showed that the receptor is selective for divalent cations in the following order of decreasing permeability: $Ca^{2+} > Mg^{2+} > Na^+$, $\sim K^+$, $\sim Cs^+$, as observed in the case of native vanilloid receptors. Desensitisation of VR1 seemed to depend on the presence of Ca^{2+} in the bathing solution. Capsaicin currents were produced on either side of VR1 expressing membrane patches, which proves that either there are binding sites of the receptor on both sides of the membrane or that lipophilic capsaicin can cross the lipid bilayer and reach its binding site. The EC_{50} was estimated to be 39.1nM, the reversal potential was found close to 0 mV and the unitary conductance 76.7pS at positive potentials and 35.4pS at negative potentials. Large concentrations of capsaicin caused nuclear fragmentation in VR1 expressing non-neuronal cells, proving that the capsaicin cytotoxicity caused by large concentrations of the drug is specific to the receptor.

Northern blot analysis revealed that VR1 is expressed in trigeminal and dorsal root ganglia and maybe in the kidney. No expression was found in the brain and the spinal cord, although capsaicin sensitivity of brain regions had been reported in the past (Jancso and Wollemann, 1977, Szallasi *et al.*, 1995b). Also, *in situ* hybridisation

histochemistry in sensory ganglia showed that VR1 is expressed in the neurons with small diameter, which is in agreement with previous studies (Winter, 1987).

VR1 RESPONDS TO HEAT

Calcium imaging and patch clamp studies of HEK293 cells expressing VR1 showed the receptor to respond to heat above a temperature threshold of 42^0 C with currents similar to those produced by capsaicin treatment. The current not only exhibited similar kinetics but also similar cation permeability. Ruthenium red and capsazepine inhibited the response, while their washout led to the current recovery, which shows VR1 to be directly involved in sensing thermal changes. Unlike desensitisation by capsaicin, desensitisation of VR1 by repeated heat application was found to be independent of Ca^{2+} in the bathing solution. Heat and capsaicin exhibited cross-desensitisation both in presence and absence of Ca^{2+} (Tominaga *et al.*, 1998), implying an overlap in the mechanism by which these stimuli activate the receptor. Interestingly, co-application of the two stimuli was found to overcome the desensitisation. Heat currents were also observed in patches of VR1 transfected HEK293 cells, which could be reversibly inhibited by capsazepine. They exhibited an outwardly rectifying current-voltage relationship and single channel conductance similar to capsaicin currents (reversal potential close to 0 mV, single channel conductance for Na^+ between 0 and +66mV was 83.4 +/- 2.9 pS). Very similar pharmacology and kinetics were observed for the human vanilloid receptor subtype 1 (Smart *et al.*, 2001).

Nagy and Rang (1999) performed electrophysiological studies in cultured rat DRG neurons and detected many differences between capsaicin and heat responses in small diameter neurons e.g. the current amplitudes were different and the permeability of Ca^{2+} versus Na^+ was found to be greater for capsaicin responses than heat responses. Interestingly, capsazepine failed to block heat responses. Overall, they observed that only 4% of the studied neurons exhibited both heat and capsaicin sensitivity, arguing against the possibility of VR1 integrating both responses (Caterina *et al.*, 1997, Tominaga *et al.*, 1998). Similarly, Liu and Simon (2000) identified heat currents in trigeminal ganglia that could be partially inhibited or unaffected by capsazepine. One can infer the existence of more heat detecting channels or the possibility of VR1 accounting for both responses in DRG neurons depending on its phosphorylation or glycosylation state or on interactions with other proteins. Nagy and Rang later (2000) proposed that the comparison of rat VR1 and chick VR1 would reveal

interesting information regarding the channel's gating by capsaicin and heat, since chicken neurons exhibited the same heat responses as rat neurons but were insensitive to capsaicin.

VR1 RESPONDS TO ACIDIC STIMULI

Bevan and Yeats (1991) identified a proton-activated sustained current in capsaicin-sensitive DRG neurons. Tominaga *et al.* (1998) reported that protons potentiate the capsaicin and heat responses of VR1 at pH 6.4. Additionally, reduction in pH was found to potentiate heat responses of VR1 to such an extent that a pH drop from neutral 7.4 to 6.4 could open the channel at the physiological temperature of 37^0C. This phenomenon bears tremendous significance as acidification (pH<6) occurs in pathological conditions such as tissue injury, inflammation, ischemia and can evoke pain and lead to hyperalgesia. Lowering the pH further to 5.4 caused the VR1 receptor to open at room temperature. The current observed was an inward predominantly Ca^{2+} current, exhibiting outward rectification (EC_{50} at 5.5). This phenomenon was also observed in membrane patches and particularly when the protons were applied to outside-out patches, which implies that they recognise a site on an extracellular portion of the receptor.

In 1998, Vyvlicky *et al.* made the interesting observation that capsaicin-sensitive DRG neurons also responded to a cocktail of inflammatory mediators (5HT, bradykinin and prostaglandin E_2) at pH 6.1. Furthermore, the combination of these mediators caused the release of CGRP from cultured DRGs. The DRG response to the inflammatory mediators could be blocked by capsazepine, but was not affected by acidification (Averbeck *et al.*, 2000). These experiments suggest the involvement of VR1. The mechanism behind this phenomenon remains elusive, as application of inflammatory mediators in an acidic environment in rat skin-saphenous nerve preparation, resulted in an enhanced response to protons that could not be blocked by capsazepine (Habelt *et al.*, 2000). Experiments on VR1 expressed in a heterologous system could answer whether protons sensitise the receptor to inflammatory mediators.

VR1 EXPRESSION IN DORSAL ROOT GANGLIA

The nociceptors are delineated in two major classes according to protein markers they express and their neurotrophic factor requirements, suggesting specificity of function. During development, 70-80% of the DRG neurons express trkA, the receptor for Nerve

Growth Factor. In adulthood, the trkA expression is downregulated, at which point 40-45% of the neurons express trkA. These neurons also express

CGRP and substance P and they project into lamina I and outer lamina II of the dorsal horn. The neurons that have lost the trkA phenotype express the receptor RET for GDNF and bind the lectin IB4. These neurons project to the inner lamina II. The functional importance of this differentiation has been supported by identifying genes that follow this specified pattern of expression and confer distinct phenotypes (reviewed by Snider and McMahon, 1998) e.g. the ATP gated P_2X_3 receptor is mainly expressed in the IB_4 positive population of neurons. The division of nociceptors in two major classes according to markers they express is routinely used as a blueprint on which to base the characterisation of new genes expressed in these neurons. The VR1 gene was not an exception.

The Julius group developed a polyclonal antibody against the carboxyl end of VR1 (Tominaga *et al.*, 1998), which they used to characterise the receptor expression. They reported that in DRG, ~85% of substance P positive cells (NGF-sensitive cells) also stained for VR1, while ~60-80% of IB4 (CGRP-sensitive) cells co-stained for VR1. The VR1 immunoreactivity was restricted to small to medium size DRG neurons. Michael and Priestley (1999) examined the distribution of the VR1 protein in more detail. They showed that VR1 does not colocalise with N52 positive cells, the large diameter neurons in DRG. About 65% of trkA cells also stained for VR1 and in agreement with Tominaga, about 75% of IB4 positive cells exhibited VR1 staining. They observed trkA and IB4 positive cells that did not stain for VR1, as well as VR1 positive cells that were negative for the two markers but positive for RET and thus GDNF-sensitive, indicating a considerable diversity in DRG neurons. VR1 was also found to colocalise with CGRP in the trkA population and somatostatin in the IB4 population.

VR1 EXPRESSION IN THE SPINAL CORD

Tominaga *et al.* (1998) reported VR1 immunoreactivity mainly in unmyelinated axons in lamina I and II of the dorsal horn with a few axons travelling along the medial edge staining in the neck of the dorsal horn and around the central canal (also observed by Guo *et al.*, 1999). In the sacral part of the spinal cord, staining was found throughout the dorsal horn and in vagal afferents. This group identified VR1 immunoreactivity in the vagus, the sciatic nerve and at nerve terminals but not in the central nervous system. In the superficial dorsal horn cells, staining for both substance P and VR1 were found in

lamina I and outer lamina II (as expected since peptidergic neurons project in these areas), while VR1 and IB4 positive cells were found in the medial part of lamina II. This observation together with the finding that there is heavy IB4 staining in the inner lamina II, revealed heterogeneity in the IB4 positive cell population. Guo *et al.* (1999) on the other hand reported VR1 expression predominantly in the inner lamina II in rats, colocalising with P_2X_3, the ATP-sensitive channel. In DRG 75% of P_2X_3 neurons also expressed VR1. Unilateral dorsal rhizotomies performed by this group resulted in abolishing the VR1 signal in the superficial dorsal horn, demonstrating the primary afferent origin of VR1 in that area. Nakatsuka and Gu (2000) demonstrated, with functional studies using capsaicin and ATP analogues, that P_2X and vanilloid receptor terminals synapsed differentially to lamina V and II respectively in the dorsal horn.

The contradictions between the three groups can be explained by different antibody specificities especially if they happen to recognise different vanilloid receptors and not just VR1. Additionally, Guo *et al.* (2000) advised caution in interpreting immunostaining results, as studies in mice show a different distribution pattern of VR1 from rats, with VR1 and neuropeptides coexpressing in the dorsal horn.

VR1 EXPRESSION IN THE PERIPHERY

Michael and Priestley (1999) observed that sciatic lesion caused a massive reduction in VR1 expression (from 46% in the injured side to 2.3% in the contralateral uninjured side), while axotomy resulted in almost complete loss. This observation in conjunction with the report (Winter *et al.*,1988, 1993) that capsaicin sensitivity in DRG culture is lost with NGF withdrawal, indicate the possibility that the axotomy-related VR1 loss might be due to target-derived neurotrophic factor deprivation. Sciatic nerve ligation resulted in the VR1 signal concentrating prior to the ligation site, intimating the VR1 transport to the periphery. As was mentioned in the previous section, Guo *et al.* (1999) made the interesting observation that VR1 does not colocalise with CGRP and substance P in central projections (lamina I). Similarly, in the peripheral terminals VR1 did not colocalise with substance P or CGRP. Studies investigating the neuropeptides transport after sciatic nerve ligation showed VR1 not to be associated with the same fibres as CGRP and substance P, although these neuropeptides are co-expressed to a large extent with VR1 in the DRG somata.

VR1 EXPRESSION IN TISSUES OTHER THAN DRG

Michael and Priestley reported that 80% of the nodose ganglia neurons express VR1 but with variable intensity. Large N52 cells were also found to express VR1. In contrast to DRG neurons, the majority of trkB staining population of nodose cells co-expressed VR1.Guo *et al.* (1999) reported the expression of VR1 in small and medium sizes neurons of the trigeminal ganglia.

Although Caterina *et al.* (1997) and Tominaga *et al.* (1998) failed to identify VR1 in the central nervous system using Northern blot analysis, Mezey *et al.* (2000) reported the expression of VR1 in the rat and human brain using immunocytochemistry and *in situ* hybridisation. VR1 positive areas include the inferior olive, substantia nigra, cortex, septum, hippocampus and dentate gyrus. Other structures like the central amygdala, hypothalamic nuclei, the nucleus of the spinal trigeminal tract, solitary tract nucleus showed a weaker signal. These results supported previous findings capsaicin sensitivity in the central nervous system (Sasamura *et al.*, 1998).

Birder *et al.* (2000) reported VR1 immunostaining in denervated bladder epithelial cells. They also reported the absence of capsaicin related cytotoxicity in these cells. Capsaicin and protons elicited nitric oxide release that could be blocked by capsazepine.

Biro *et al.* (1998a) examined the activation of mast cell lines with vanilloids exhibiting pharmacological characteristics similar to those observed in DRG. These responses were demonstrated using $^{45}Ca^{2+}$ uptake and they were blocked with ruthenium red and capsazepine. The vanilloid receptors in these cells seemed to be of the C type (associated with Ca^{2+} uptake more than RTX binding) and their activation was not dependent on mast cell degranulation, associated with the release of proinflammatory mediators. Capsaicin did not evoke any toxic effects but induced the production of IL-4, a cytokine that acts on B cells to stimulate antibody secretion and the expression of cell surface molecules involved in antigen recognition in immune responses. Biro *et al.* (1998b) also observed vanilloid responses in C6 rat glioma cells. Similarly to the vanilloid receptors in mast cells, the C6 glioma cells exhibited the C-type vanilloid receptors. Although these papers did not investigate the expression of VR1 in mast

cells, they offer challenging clues towards the possible varied roles of vanilloid receptors.

STRUCTURAL STUDIES ON VR1

Jung *et al.* (1999) investigated the topology of the capsaicin binding site in DRG neurons using the water soluble capsaicin analogue, AD (AD-5018.HCl), which is charged at physiological pH and thus cannot cross the plasma membrane. Electrophysiological studies in DRG patches in inside-out and cell-attached configurations showed vanilloid receptor activation with AD only when it was applied intracellularly, implying an intracellular binding site. Capsaicin and RTX on the other hand activated the receptor even when they were applied extracellularly, although the activation was less rapid compared to intracellular application. Capsaicin has lipophilic nature and thus it can diffuse across the membrane and reach an intracellular binding site. The inhibition of the capsaicin response by capsazepine was faster when it was applied intracellularly. The same results were obtained in studies of VR1 expressing *Xenopus* oocytes challenged with AD, supporting the finding that the capsaicin binding site is intracellular.

Jordt *et al.* (2000) studied VR1 mutants in an attempt to identify functionally significant amino acids in the receptor. Replacement of a glutamic acid residue with glutamine (E600Q) or a positively charged amino acid created a mutant conferring deleterious effect to the host cells, probably due to making the channel constitutively open. When this amino acid was replaced with a negatively charged one e.g. aspartic acid, the deleterious effect was abolished, proving that an increase in positive charge on this amino acid position promotes channel activity. The E600Q mutation also increased the sensitivity of the receptor both to heat and capsaicin, a phenomenon similar to sensitisation by protons (Tominaga *et al.*, 1998). Interestingly, the proton evoked responses in E600Q were similar to wild-type. Therefore, the charge on amino acid 600 only sets the proton mediated potentiation of the receptor and not the proton responses *per se*. An E648A mutant showed reduced responses to protons, while exhibiting wild type capsaicin and heat responses, indicating that proton potentiation and proton activation of the receptor are two distinct mechanisms. Both amino acid positions (600 and 648) are found extracellularly, which is in accordance with the observation made by Tominaga *et al.* (1998) that the VR1 receptor is activated by protons only extracellularly.

Kwak *et al.* (2000) observed that the vanilloid receptors activation in sensory neurons in cell-attached configuration was consistently higher than in inside-out patches. They hypothesised the existence of a cytosolic substance that regulates channel activity, which is lost in the inside-out patch formation. Since ATP controls activity via phosphorylation in many channels, they tested ATP application in inside–out patches of DRG, concomitantly with capsaicin stimulation. ATP was found to increase channel activity to the levels observed in cell-attached configuration. It should be noted that ATP alone did not elicit any current on these patches. The ATP heightened capsaicin response was found not to depend on Mg^{2+} and ATP hydrolysis, implying that ATP is not regulating the capsaicin channel via phosphorylation. In agreement to this observation, the application of protein kinase inhibitors did not alter the ATP-induced elevation of the capsaicin response. Mutating the Walker A-type and B-type motifs in VR1, proved that the ATP effect in augmenting the capsaicin response is due to its direct binding on these nucleotide binding domains.

Garcia-Martinez and colleagues (2000) identified aspartic acid at position 646 as the amino acid that regulates the pore properties of VR1. Neutralisation of this amino acid reduced sensitivity to ruthenium red and the channel permeability to Mg^{2+}. On the contrary, neutralisation of E636 increased blockade by ruthenium red. VR1 resembles *Shaker*-type K^{+} channels with a pore loop between transmembrane domains 5 and 6 consisting of acidic residues in certain sequence motifs. According to the *Shaker* type channel model, the pore loop should comprise a selectivity filter and a pore helix. Residues 625-640 presumably form that helix with residue 636 interacting with residue 639 creating an intrahelical salt bridge. The neutralisation of 636 probably disrupts that interaction, making the channel non-functional. The functional significance of these acidic amino acids is manifested by the fact that positively charged synthetic and natural arginine-rich peptides block VR1 and display analgesic properties (Planells-Cases *et al,* 2000). Additionally, a methionine residue in position 644 was mutated to tyrosine, creating a channel exhibiting capsaicin currents with very slow kinetics, demonstrating the importance of this amino acid in channel gating.

Mutant studies carried out by Welch and colleagues (2000) offered additional information on some of the interesting amino acids mentioned above (picture 1.1). Neutralisation of E648, E636 and E646 increased sensitivity to capsaicin three fold,

while decreased sensitivity to protons. E648Q and E636Q exhibited increased Ca^{2+}/K^{+} permeability ratios, indicating the importance of these residues in the channel's selectivity filter. These experiments further support the notion that separable pathways involving different VR1 residues modulate the channel activation.

Picture 1.1: Location of important residues (E636, E648 and D646 highlighted in bold) on VR1 (from Welch *et al.*, 2000)

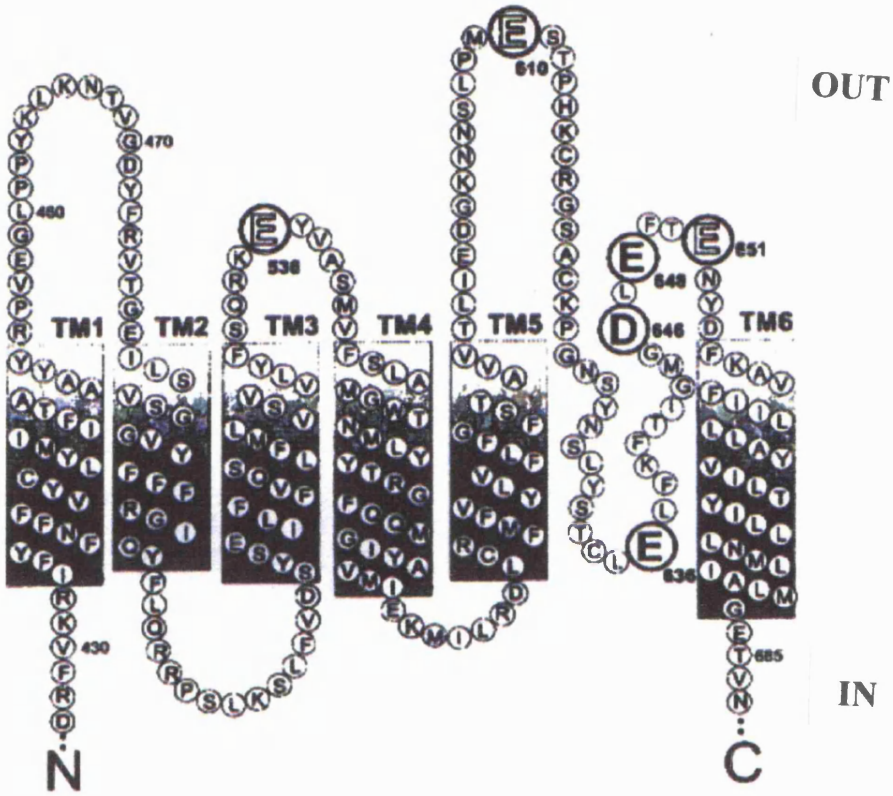

THE VR1 KNOCKOUT

Both the D.Julius and the J.Davis group developed VR1 knockout mice (Caterina *et al.*, 2000, Davis *et al.*, 2000) . The knockout mice seemed physiologically normal and their nociceptors were found to have developed properly. Cultured DRG neurons from $VR1^{-/-}$ animals responded as wild-type neurons to mechanical stimuli and to neurotransmitters like ATP and GABA, but failed to respond to capsaicin and RTX. Knockout mice did not respond to intraplantar capsaicin injection and they drank normally from capsaicin-contaminated water, exhibiting the significance of VR1 in trigeminal and DRG mediated nociception. Nevertheless, injection of formalin to the hind paw evoked wild type pain related behaviour, indicating that VR1 is not involved in chemically-induced pain perception. Subcutaneous capsaicin injection failed to induce hypothermia in the

knockout mice, expanding the VR1 related thermal deficit in the autonomous nervous system. $VR1^{-/-}$ neurons and unmyelinated fibers in skin-nerve preparations did not respond to protons with sustained currents but exhibited only transient currents, in contrast to wild type. As it has been proposed elsewhere (Liu and Simon, 2000), the transient proton evoked currents are due to members of the proton gated ASIC channel family and thus do not involve VR1 activation. Cultured neurons and unmyelinated fibres from the knockout animals exhibited small or no responses to heat stimuli. These results were replicated in lamina V neurons in the dorsal horn that receive nociceptive signals from the periphery, implicating VR1 in the CNS processing of nociceptive information.

The Julius group reported that $VR1^{-/-}$ mice displayed longer withdrawal latency in the tail immersion test at temperatures $<48^0$C, but exhibited significantly longer latencies only at temperatures higher than 50 ^{0}C in the hotplate test. On the contrary, no wild-type and knockout mice differences were observed by the Davis group in the hotplate test. This phenomenon could be due to differences in the construction of the knockout cassette, as the Julius group knocked out part of the 5^{th} and the whole 6^{th} transmembrane domain of mouse VR1, while the Davis group VR1 knock-out mouse lacked the region encompassing domains 2^{nd}- 4^{th}. VR1 was not found to contribute to neuropathic pain, as partial sciatic nerve ligation did not change the heat responses in $VR1^{-/-}$ or $VR1^{+/+}$ mice. The most important observation reported by both groups is that in the mustard oil and the carrageenan test (for tissue injury and inflammation) the treated $VR1^{-/-}$ mice did not show any change in hotplate latency compared to untreated animals, indicating that they did not develop thermal hyperalgesia.

These results demonstrate that VR1 is not solely responsible for detecting thermal and acidic noxious stimuli, since these responses were not completely abolished in the knockout animals. However, the VR1 contribution in the development of thermal hyperalgesia was proven to be imperative, rendering this molecule salient in the therapy of related medical conditions.

VR1 AND CELL SIGNALLING

Regulation by neurotrophins

The majority of the nociceptors that are sensitive to capsaicin also express the neuropeptides CGRP and substance P, as well as

trkA, the high affinity receptor for NGF (Tominaga *et al.*, 1998, Michael and Priestley, 1999). Capsaicin treatment causes the release of neuropeptides such as CGRP and substance P from the central and peripheral terminals of nociceptors. Under inflammatory conditions, the concentration of NGF peripherally increases and causes the degranulation of mast cells, which release more NGF, histamine and serotonin and subsequently sensitise the nociceptors (Shu and Mendell, 1999). The NGF after binding trkA on nerve terminals is internalised and retrogradely transported to the cell bodies in DRG, where it can increase gene expression levels e.g. BDNF (Michael *et al.*, 1997). Capsaicin sensitivity of adult rat DRG neurons in culture is NGF-dependent (Winter *et al.*, 1988). In agreement to this, NGF deprivation due to axotomy reduces capsaicin sensitivity as well as neuropeptide levels (McMahon *et al.*, 1995). After sciatic nerve axotomy, Michael and Priestley (1999) observed VR1 mRNA reduction as well as downregulation of CGRP, trkA expression and IB4 binding, that might be due to target derived neurotrophic factor deprivation.

Recently Winston and colleagues (2001) examined the regulation of VR1 expression by NGF in DRG cultures. NGF treatment resulted in the increase of VR1 mRNA levels. The presence of NGF was necessary in causing CGRP release from cultured DRGs after capsaicin stimulation. Other neurotrophins seem to affect VR1 expression as well. Ogun-Muyiwa *et al.* (1999) reported that

GDNF , whose receptor is expressed in the IB4 DRG population, upregulates VR1 in a similar way to NGF. In addition to the changes in the VR1 protein levels elicited by neurotrophic factors, Shu and Mendell (1999) observed that NGF also has a direct effect on the vanilloid receptor. Administration of NGF intermediately to capsaicin applications in DRG neurons prevented tachyphylaxis (smaller currents observed in further receptor stimulation compared to initial response). This phenomenon does not involve gene regulation as it took place in a short time scale. These studies together with the finding that NGF increases capsaicin responses in DRG neurons innervating inflamed tissue (Nicholas *et al.*, 1999), suggest a possible role of VR1 in inflammation.

Dissecting the cell signalling pathway

One of the most common mechanisms in regulating receptor function is via phosphorylation. NGF can indirectly trigger phosphorylation of receptors, via binding onto its receptor trkA, which causes receptor dimerisation and subsequent activation of its tyrosine kinase activity. The tyrosine kinase activity of the two receptor subunits not

only leads to each other's phosphorylation (autophosphorylation of trkA) but also to the phosphorylation and thus activation of other proteins that recognise and bind onto the phosphorylated domains of trkA. Phosphotases like calcineurin, which is activated by calcium, can reverse the phosphorylation and alter the receptor activity. The fast tachyphylaxis prevention effect of NGF on DRG vanilloid receptors described by Shu and Mendell (1999) suggests the involvement of the phosphorylation/dephosphorylation mechanism. The receptor trkA is associated with phospholipase C, among other proteins, which catalyses the hydrolysis of the membrane phospholipid phosphatidylinositol 4,5-biphosphate (PIP_2) into diacylglycerol (DAG) and inositol triphosphate (IP_3), which are second messengers. The enzyme phosphatidylinositol-3 kinase (PI-3) binds onto the phosphorylated domains of trkA as well as other growth receptors. The phosphorylation activity of this kinase leads to the production of phosphatidylinositol 3,4,5- triphosphate (PIP_3) from phosphoinositides like PIP_2, which are membrane phospholipids. PIP_3 can activate members of the protein kinase C family (PKCs), which in their turn can phosphorylate other proteins. PKC can also be activated by DAG, which is a product of PLC activity as it was stated above (figure 1.2).

PKCs have been involved in nociceptors' sensitisation to heat (Cesare *et al.*,1999a) and in thermal and acid-induced hyperalgesia (Khasar *et al.*, 1999). Additionally, the neuropeptide bradykinin has been shown to elicit its algesic effect on nociceptors through PKC activation. Considering that PKC participates in signalling of noxious stimuli that have also been shown to be mediated via VR1 i.e. heat and proton responses, Premkumar and Ahern (2000) hypothesised the functional interaction of the two molecules. They discovered that PKC activation in DRG neurons and *Xenopus* oocytes injected with VR1 produced currents very similar to capsaicin induced responses. They also showed that bradykinin can activate vanilloid receptors in DRG via PKC. In support of the VR1 activation by PKC, Smart *et al.* (2001) reported that PKC inhibition prevented the capsaicin activation of the human VR1 homologue.

Lopshire *et al.* (1998) reported that prostaglandin E_2 sensitises the capsaicin response in DRG via protein kinase A (PKA) phosphorylation. To examine whether this phenomenon is mediated by direct VR1 phosphorylation by PKA De Petrocelis *et al.* (2001) used 8-Br-cAMP, a cAMP analogue and forskolin, an adenylyl cyclase activator to trigger the PKA pathway in HEK cells expressing VR1. The drug application enhanced capsaicin responses and responses to anandamide, another VR1 agonist (see

next section). The latter responses were also potentiated with phorbol esters that activate PKC. Application of anandamide on DRG causes release of neurotransmitters like substance P. Forskolin increased the release of substance P three-fold in DRG, proving that activation of PKA enhances the vanilloid receptor action in a native environment as well.

Lee *et al.* (2000) reported that application of the same drugs (forskolin and 8-Br-cAMP) on VR1 expressed in *Xenopus* oocytes and *Aplysia* neurons failed to sensitise the receptor to capsaicin. It is possible that these heterologous systems cannot replicate the PKA pathway existing in DRG and HEK cells. Another study showing discrepancies between *Xenopus* oocytes and HEK cells as heterologous systems for the study of VR1 regulation is the study conducted by Tominaga *et al.* (2001), who reported the potentiation of the capsaicin response by ATP similarly to Kwak *et al.* (see section "Structural Studies on VR1" above). The latter group contacted their studies in *Xenopus* oocytes and failed to identify the participation of PKC in this phenomenon. On the contrary, Tominaga *et al.* (2001) found that the VR1 capsaicin, heat and proton response potentiation by ATP in HEK cells is regulated by PKC activation. By using specific PKC inhibitors and activators they managed to eliminate or trigger the potentiation respectively. They reasoned that PKC could be triggered by DAG, which is generated by phospholipase C stimulation following G protein coupled receptors activation (see figure 1.2 below). Metabotropic receptors that could be activated by ATP in these neurons are the P2Y receptors. By using specific agonists against P2Y subtypes in VR1 expressing HEK cells and in DRG neurons, they identified $P2Y_1$ as the receptor involved in the VR1 potentiation. This finding could explain the nociceptor sensitisation by ATP release during tissue injury or inflammation.

In the light of the studies reporting VR1 regulation by inflammatory mediators via second messenger systems, Chuang *et al.* (2001) inquired into the tachyphylaxis prevention of VR1 responses by NGF, first described by Shu and Mendell (see "regulation by neurotrophins" in this section). Chuang and colleagues reported that injection of bradykinin or NGF in VR1 null mice did not evoke hyperalgesia as observed in wild type mice. They found that bradykinin enhanced capsaicin and proton responses in HEK cells transfected with VR1 and BK_2, the bradykinin receptor. Similarly, they observed that NGF potentiated proton and heat responses in oocytes co-expressing VR1 and trkA. Since BK_2 and trkA activation involves PLC stimulation, the

researchers set out to investigate the role of PLC in the potentiation of VR1 currents. When they co-expressed VR1 and a mutant trkA that abolishes the interaction with PLC-γ, they failed to record NGF induced potentiation. On the contrary, application of recombinant PLC on excised patches of VR1 expressing HEK cells enhanced capsaicin currents. Application of an antibody that sequesters PIP_2 and thus mimics its hydrolysis by PLC, resulted in enhancing capsaicin elicited currents both in a heterologous system and in DRG neurons. These results suggest that PIP_2 represses VR1 activity. As a result, the PIP_2 hydrolysis by PLC alleviates the receptor inhibition, which manifests itself as potentiation of the receptor's responses. Therefore, the tachyphylaxis prevention of capsaicin currents observed by Shu and Mendell (1999) is due to NGF stimulating PLC, which hydrolyses PIP_2 and relieves VR1 suppression. Interestingly, PLC-γ ,trkA and VR1 were found to co-immunoprecipitate. Although the researchers did not examine direct stimulation of the receptor by PKC, which can result by PLC activation, they observed that PKC inhibitors did not alter NGF induced potentiation of VR1. Further careful dissection of the cell signalling system is necessary to establish whether the VR1 activation and potentiation are regulated through different mechanisms. Picture 1.2 below sums up all the pathways found to regulate VR1 function.

Figure 1.2: Schematic diagram integrating VR1 modulating pathways. PI3 kinase: phosphatidylinositol-3 kinase, PLC: phospholipase C, PKC: protein kinase C, PKA: protein kinase A, DAG: diacylglycerol, IP3: inositol triphosphate, PIP3: phosphatidylinositol 3,4,5- triphosphate, PIP2: phosphatidylinositol 4,5-biphosphate, AC: adenylate cyclase, cAMP: adenosine 3',5'-cyclic monophosphate.

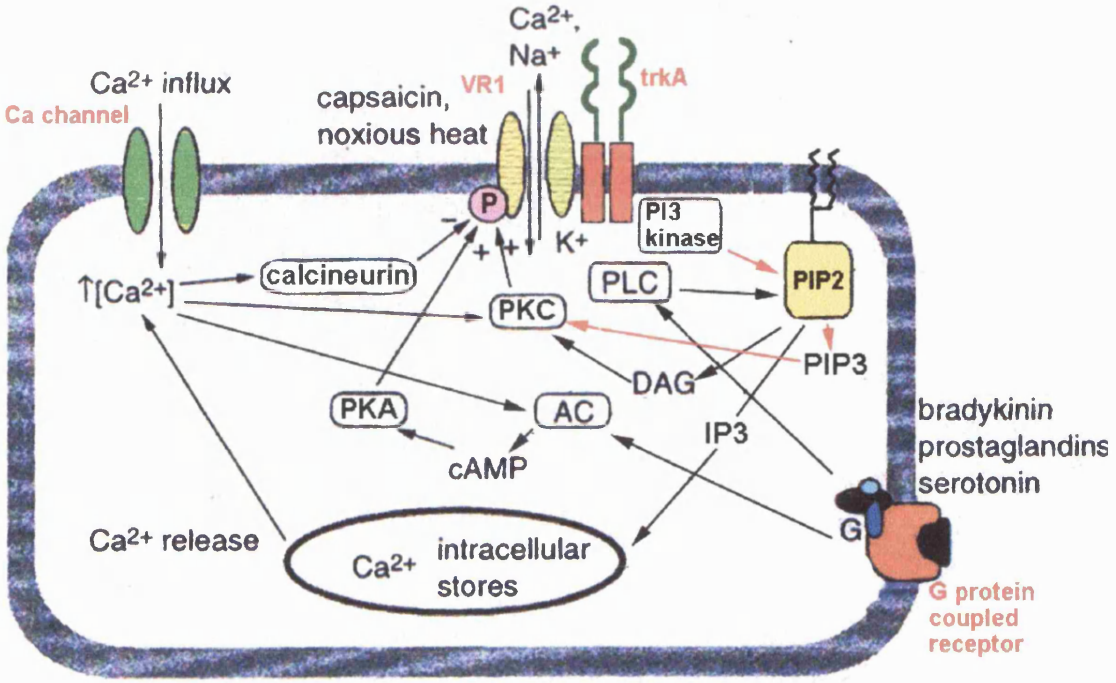

THE ENDOGENOUS AGONIST

The endogenous cannabinoid ligand, anandamide, is a lipid, structurally similar to capsaicin. Moreover, anandamide has been shown to act on capsaicin sensitive neurons innervating mesenteric arteries and mediate vasodilation by causing the release of CGRP, indicating that the anandamide and capsaicin pathways might be interrelated (Zygmunt *et al.*, 1999). The researchers observed that CGRP antagonist and capsaicin treatment of perivascular sensory nerves abolished the anandamide vasodilation effect. Cannabinoid receptor 1 (CB1) and calcium channel antagonists failed to block the anandamide action, showing that these channels do not mediate the anandamide effect. Capsazepine succeeded in inhibiting the anandamide vasodilation effect, implicating the capsaicin receptor in this phenomenon. In order to investigate whether anandamide acts directly on vanilloid receptors, the cloned receptor VR1 was expressed in HEK cells and *Xenopus* oocytes and challenged with anandamide. 10μM of anandamide caused a response similar to 100nM capsaicin, while control untransfected cells failed to respond. Smart *et al.* (2000) identified anandamide as an agonist for the human VR1 homologue using a Ca^{2+} based assay. The anandamide responses were inhibited by capsazepine and exhibited cross-desensitisation with capsaicin.

The cannabinoid agonist is less potent on VR1 compared to capsaicin, but it elicits the same type of outwardly rectifying currents, blocked by capsazepine. Premkumar and Ahern *et al.* (2000) reported that anandamide enhances its own activity by triggering PKC, which leads to VR1 phosphorylation and the latter to increased agonist potency. Other lipids like diacylglycerol and arachidonic acid did not elicit any responses from VR1. Interestingly, Ahluwalia *et al.* (2000) observed colocalisation of VR1 and CB1 in DRG neurons to a great extent (98% of VR1 neurons showed CB1 immunostaining). Considering that both VR1, a prominent receptor in the transmission of nociceptive information, and CB1, a receptor that mediates inhibition of pain responses, are activated by anandamide and expressed in the same type of DRG neurons, an interesting mechanism of regulating pain signalling emerges. Millns *et al.* (2001) showed that the CB1 receptors in DRG have an antinociceptive role by using the synthetic cannabinoid agonist, HU210, to inhibit capsaicin responses. HU210 alone did not evoke any vanilloid-like responses and its effect on capsaicin elicited currents was reversed by a CB1 antagonist. These preliminary data offer only a glimpse in the functional interaction between CB1 and capsaicin receptors that constitutes a challenging

mechanism for relaying nociceptive information. Identification of other regulating components will help dissect this mechanism further.

The presence of anandamide extracellularly is transient as it is transferred into the cell via a protein transporter, where it is hydrolysed and inactivated. AM404 is a synthetic substance that was designed to inhibit the anandamide transporter and thus extend anandamide's activity by preventing its re-uptake by the cell. Zygmunt *et al.* (2000) found that AM404 activates vanilloid receptors in neurons innervating rat hepatic arteries and causes vasodilation like anandamide. This effect was blocked by capsazepine and a CGRP antagonist, while a CB1 antagonist had no effect. AM404 activated VR1 expressed in heterologous systems, which showed that the anandamide transporter inhibitor acts directly on the vanilloid receptor. These experiments triggered further research into related lipids and the effect of changing their structure in VR1 activation. The lipid methanandamide was also found to evoke responses in perivascular neurons that were inhibited by capsazepine and a CGRP receptor antagonist (Ralevic *et al.*, 2000). Melck *et al.* (1999) found that by changing the length and degree of unsaturation of the fatty acid chain in olvanil, a capsaicin receptor agonist, they created substances that could inhibit the anandamide transport and could bind onto CB1 in addition to activating VR1. On the other hand, Petrocellis *et al.* (2000) identified anandamide derivatives that inhibit anandamide re-uptake but are not VR1 or cannabinoid receptor ligands.

Despite the wealth of information related to VR1 activating lipids, the mechanism of anandamide action remained elusive. Petrocellis and colleagues (2001) used novel anandamide transporter inhibitors that do not bind directly onto VR1, unlike AM404, to illustrate that it is necessary for anandamide to cross the plasma membrane and enter the cell in order to activate VR1. This is consistent with the finding that the capsaicin binding site is intracellular (see the section "structural studies on VR1" above). Once inside the cell, hydrolysis of anandamide was found to reduce VR1 activation. Olah *et al.* (2001a) demonstrated that vanilloids competed with radioactive anandamide for binding onto VR1, providing further evidence for anandamide being a VR1 agonist. Furthermore, they showed that protons potentiated the anandamide response both in VR1 transfected cells and in DRG, suggesting that tissue acidification during inflammation can sensitise vanilloid receptors to anandamide. Hwang *et al.* (2000) examined whether other eicosanoids, byproducts of the arachidonic acid metabolism

involved in inflammatory reactions, can activate vanilloid receptors. Arachidonic acid is converted to prostaglandins via the activity of the enzyme cyclo-oxygenase and to leukotrienes via catalysis by the enzyme lipoxygenase. Only byproducts of the latter pathway were found to activate VR1. This finding accentuates the role of the capsaicin receptor in inflammatory hyperalgesia, as lipoxygenase products are produced during tissue injury and inflammation and cause hyperalgesia when injected intradermally (Levine *et al.*, 1986).

VANILLOID RECEPTOR HETEROGENEITY

The comparison of VR1 currents in heterologous systems to vanilloid responses *in vivo* provided evidence towards the existence of more vanilloid receptor subtypes. Nagy and Rang (1999) noticed small DRG neurons that responded to heat but were capsaicin insensitive. Similarly trigeminal ganglion cells were found that responded to heat and capsaicin but not protons, while other neurons were heat responsive only (Liu and Simon, 2000). Additionally, Nagy and Rang (1999) reported that the heat and capsaicin current amplitudes in DRG neurons exhibited poor correlation, while the capsaicin evoked Ca^{2+} uptake was greater compared to the one induced by heat. Although capsazepine is an effective capsaicin antagonist, it did not inhibit heat responses as potently.

Taking into consideration that VR1 integrates both heat and capsaicin responses, the discrepancies observed *in vivo* could be explained by either the interaction of VR1 with proteins that would modulate its function or by the existence of other vanilloid receptors. Additional data on discrepancies between VR1 and native vanilloid receptors followed. The characterisation of rat VR1 (Caterina *et al.*, 1997) and the human VR1 by Smart *et al.* (2001) revealed that RTX was only 20 fold more potent than capsaicin on the cloned receptor, in contrast to the reported thousand fold higher affinity for binding on native vanilloid receptors in tissues. Shin *et al.* (2001) reported differences in activation of vanilloid receptors in cultured DRG neurons and VR1 expressed in a heterologous system. In particular, DA-5018.HCl, a synthetic capsaicin analogue was more potent on the cloned receptor, while resiniferatoxin activated native vanilloid receptors more efficiently. Welch *et al.* (2000) reported that the vanilloid receptor conductance in DRG neurons was much smaller than the recorded VR1 conductance. Szallasi *et al.* (1999) found that the cloned VR1 receptor exhibits both affinity for RTX (R-type) and $^{45}Ca^{2+}$ uptake efficacy when challenged with capsaicin (C-type), while studies in DRG neurons demonstrated distinct C and R type native

vanilloid receptors. The variation in R and C-type responses observed in DRG has attributed to speculating the existence of vanilloid receptor subtypes. Finally, Ringkamp *et al.* (2001) reported the existence of heat-sensitive, mechanically insensitive A-fibers that respond to capsaicin, as well as A-fibers that were sensititive to capsaicin only innervating monkey hairy skin. Considering that A-fiber nociceptors do not express VR1, the capsaicin sensitivity can be ascribed to other vanilloid receptors.

AIM OF PROJECT

The discrepancies between the pharmacological profile of VR1 and the native vanilloid responses suggest the existence of a family of vanilloid receptors. The possibility remains that these variations can be ascribed to regulation of VR1 by modulatory proteins in different tissues or could be due to differences between native and heterologous expression systems. However, taking also into consideration past studies preceding the VR1 cloning that proposed the existence of a vanilloid receptor family (see section 5 of prologue "subtypes of vanilloid receptors"), it was inevitable that a pursuit for more vanilloid receptors was sparked off. The aim of this project was to isolate and characterise novel vanilloid receptors.

CHAPTER 1

***In silico* cloning of VR-L, a new member of the vanilloid receptor family**

MATERIALS & METHODS

1.1 Bioinformatics tools

The tBLASTn search was performed at http://www.ncbi.nlm.nih.gov/blast/blast.cgi, using BLOSUM62 and filtering low complexity regions.

To blast two sequences against each other the programme http://www.ncbi.nlm.nih.gov/blast/bl2seq/bl2.html was used, with the default settings: reward for match=1, penalty for mismatch -2, gap opening 5, gap extension 2, checking both strands.

Multiple alignments were carried out at http://www.expasy.org/tools/dna.html

The settings used were gap opening penalty 10, gap extension 5.

The human index was searched at http://www.tigr.org/tdb/hgi/searching/reports.html

Sequences were translated using the translation tool in the Expasy server: http://www.expasy.org/tools/dna.html

Phylogenetic tree prediction was carried out at the address: http://www.genebee.msu.su/services/phtree_reduced.html. The matrices used by this programme are the Dayhoff, BLOSUM62 and the Johnson matrix.

A protein family search for identifying patterns of interest was done at: http://www.sanger.ac.uk/Software/Pfam/search.shtml. In this programme models from the SMART and TIGR databases were searched as well. A pattern search, including abundant motifs, was also at performed at http://www2.ebi.ac.uk/ppsearch/

For transmembrane regions detection the following programmes were deployed: http://www.ch.embnet.org/software/TMPRED_form.html. This programme compares the protein of interest with a database of known transmembrane proteins. http://www.sbc.su.se/~erikw/toppred2/. This is a similar programme that allows the user to specify the search for eukaryotic proteins.

1.2 Culturing Jurkat cells

1) A vial of frozen Jurkat cells, kept at -70^0 C, was defrosted quickly and was resuspended in 10ml of medium containing Dulbecco's modified eagle medium (DMEM), 10% (v/v) foetal bovine serum, 1% (v/v) of 5units/ml penicillin, 5mg/ml streptomycin and 100X L-glutamine (GibcoBRL).
2) The tube was centrifuged at 1000g for 5min and the supernatant was discarded. The pellet was resuspended in 10ml of fresh medium and the cells were plated in a 10ml culture flask. The cells are cultured in suspension in a humidified incubator in the presence of 5% CO_2 at 37^0C.

3) When the culture was confluent, the cells were centrifuged at 1000g for 5min and resuspending the pellet in 10ml of medium. The cells were then plated in a 1:5 ratio. On average the culture was split twice a week.

N.B. To create a frozen stock of Jurkat cells, a 10ml flask of culture was spun down at 1000g for 5min. The pellet was resuspended in medium containing 10%(v/v) DMSO and was quickly dispensed in 1ml aliquots in vials. The cells were kept at -20^0 C for 1 hour and then transferred at -70^0 C. All the materials used were from GibcoBRL. For companies information please see appendix 3.4

1.3 RNA extraction from Jurkat cells

The protocol used is a variation of the method developed by Chomczynski and Sacchi (Current Protocols in Molecular Biology 4.2.5). It is based on the observation that RNA is denser than DNA and protein. It can separate from the latter two in an acidic environment (pH 4), in the presence of guanidinium thiocyanate and an organic phase. All the materials used were from Sigma and were prepared as following:

Denaturing solution: 250g of guanidinium thiocyanate were dissolved in a solution of 293ml distilled water, 17.7ml of 0.75M sodium citrate pH7 and 26.4ml of 10% (w/v) Sarkosyl at 60-65^0 C with stirring. The stock solution can be stored for up to 3 months. The working solution was prepared by adding 0.35ml of 2-mercaptoethanol in 50ml of stock solution. It can be stored up to a month at room temperature.

2M sodium acetate pH4: 16.42g of sodium acetate were dissolved in 40ml of distilled water and 35ml of glacial acetic acid. The pH was adjusted to pH 4 with glacial acetic acid. The final volume was made up to 100ml with distilled water and the solution was autoclaved.

Water saturated phenol: 100g of phenol crystals were dissolved in distilled water at 60-65^0 C with stirring. The upper water phase was aspirated the solution was kept up to a month at 4^0 C.

1) 10ml of Jurkat cells culture was centrifuged at 1000g for 5min. The pellet was resuspended in 1ml of denaturing solution and the solution transferred in a glass homogeniser. The Jurkat cell solution was homogenised with 10-20 strokes.
2) The cell homogenate was transferred in a 10ml falcon tube. 0.1ml of 2M sodium acetate pH4 was added and the solution was mixed by inversion. 1ml of water-saturated phenol was dispensed followed by thorough mixing. Then 0.2ml of 49:1

chloroform/isoamyl alcohol was added and the solution was mixed well and was left at 4^0 C to incubate for 15min.

3) The solution was centrifuged for 20min at 10,000g at 4^0 C. The upper aqueous phase containing the RNA was transferred into a fresh tube.
4) The RNA was precipitated with 1ml of 100% isopropanol at -20^0 C for 30min. The sample was centrifuged at 10,000g for 10min at 4^0 C and the supernatant was discarded.
5) The RNA pellet was resuspended in 0.3ml denaturing solution and transferred into a 1.5ml eppendorf tube.
6) 0.3ml 100% isopropanol was added into the sample. The RNA was left to precipitate at -20^0 C for 30min. The solution was centrifuged at 10,000g, 4^0 C for 10min.
7) The supernatant was discarded and the RNA pellet was washed with 75% ethanol. The sample was vortexed and was left to incubate for 15min at room temperature for any residual guanidinium to be dissolved.
8) The solution was centrifuged for 5min at 10,000g and the supernatant was discarded. The RNA pellet was left to dry in a vacuum for 5min. Attention was paid not to overdry the pellet, as that would make the RNA difficult to dissolve.
9) The RNA pellet was resuspended in 100µl of DEPC-treated water and the concentration was measured with a spectrophotometer. The RNA sample was stored at -20^0 C.

1.4 cDNA synthesis

The first strand cDNA synthesis was accomplished by using the Superscript™ RNase H⁻ reverse transcriptase (GibcoBRL). This transcriptase is produced from a cloned M-MLV RT gene with the RNase H sequence deleted.

DNaseI treatment

This treatment is necessary to destroy genomic DNA that might have contaminated the RNA preparation. A 10µl reaction was prepared by adding the following materials from Promega: 6.2µl sterile distilled water, 1µl of 10X Taq DNA polymerase buffer (500mM KCL, 100mM Tris-HCl pH9, 0.1% Triton X-100), 0.6µl of 25mM well resuspended $MgCl_2$, 2µg RNA, 0.1µl DNaseI RNase free, 0.1µl RNasin Ribonuclease inhibitor. The solution was well mixed and placed at 37^0C for 15min. To stop the reaction the tube was placed at 99^0C for 10min. Subsequently, it was left to cool on ice for 2min.

Reverse transcription

The materials used in this reaction were from GibcoBRL. The following were added in the DNaseI treated RNA solution: 4.4µl 5X First Strand buffer (250mM Tris-HCl pH8.3, 375mM KCl 15mM $MgCl_2$), 2µl DTT, 4µl of 5mM dNTP, 0.1µl RNasin Ribonuclease inhibitor, 1µl Superscript, 0.2µl of 500µg/ml random primers and 0.3µl sterile distilled water. The reaction mixture was vortexed and incubated at 37^0 C for 1 hour. To stop the reaction the tube was placed at 99^0C for 10min and then on ice to cool down before proceeding with PCR.

1.5 Polymerase Chain reaction using Pfu DNA polymerase

The DNA polymerase Pfu is isolated from *Pyrococcus furiosus,* has proof-reading activity and exhibits the smallest error in copying DNA from all the known DNA polymerases. For that reason it is used in cloning techniques that require PCR amplification.

The conditions for optimum enzyme activity are: Mg^{2+}>1.5mM, dNTP<1mM, pH of Tris-based buffers>8. Because the polymerase has 3'-5' exonuclease activity, it can degrade the primers in absence of dNTPs. To avoid this possibility the dNTP concentration is maintained at 100-200 µM each and the primers at 0.1-0.5 µM. Pfu polymerase lacks terminal deoxynucleotidyltransferase activity, i.e. does not add non-specific nucleotides at the 3' ends of the PCR products. As a result the PCR products are blunt ended. In order to clone Pfu amplified PCR products, 1 unit of Taq polymerase was used at 72^0C for 10min at the end of the PCR cycles to add adenines at the 3' end of the product. This would subsequently allow cloning into a T-vector.

The PCR reaction was set up in a room different from the one used for DNA cloning. This was necessary to avoid DNA contamination of the PCR samples. For the same reason gloves were worn and extreme care was taken not to contaminate any of the PCR reagents or the pipettes. Aerosol resistant tips were utilised to avoid the transfer of any DNA from the pipettes to the samples. DNA can adhere onto surfaces and in order to ensure that the PCR template concentration would not vary, sterile eppendorfs with thin walls were used.

The PCR mixture contained the following: 5 µl of 10X buffer (200mM Tris-HCl pH8.8, 20mM $MgSO_4$, 100mM KCl, 100mM $(NH_4)_2SO_4$, 1% (v/v) Triton X-100, 1mg/ml

nuclease free BSA), 1 µl of 10mM dNTPs (0.2mM final), 1 µl of each of the 20µM primers (0.4µM final), 100ng of DNA template, 5 units of Pfu polymerase and sterile distilled water to make up the reaction volume to 50 µl. The mixture was vortexed for a few seconds and centrifuged shortly to ensure the solution remained at the bottom of the tube. One drop of sterile mineral oil was used to layer the sample in order to prevent its evaporation during the PCR.

The following PCR programme was used:
94^0C for 3 min to denature the DNA completely
For 35 cycles:
Denaturation step: 94^0C for 30sec
Primer annealing step: 55^0C for 40sec
Primer extension step: 68^0C for 40sec

At the end of the cycles, there was a further step of 5min at 68^0C to ensure completion of extension. The reagents were purchased from Stratagene.

Primer design: the primers used were designed following a set of principles: 1) the GC content was kept at about 60%. 2) the primer length was 20-30bp 3) regions of repeats were avoided 4) primers with no hairpin structures were selected to ensure their successful annealing onto the template 5) in order to avoid primer dimer formation, primers with no regions of complementarity to each other were selected. The primers were ordered from Sigma Genosys.

1.6 Agarose gel electrophoresis

The materials used were from Sigma.

1) The appropriate amount of agarose was weigh ed and diluted in 1X TAE buffer (50X TAE buffer contains 121g of Tris base, 28.55ml of glacial acetic acid, 50ml of 0.5M EDTA pH8 in total volume 500ml) to achieve the desirable concentration.

   N.B. The gels used for visualisation of DNA bands above 1kb were of 0.8% (w/v) agarose concentration. To view smaller bands, 1.5% (w/v) gels were prepared.

2) The agarose solution was heated in the microwave for 5-7 min, shaking occasionally and then left to cool down to about 50^0C.
3) Ethidium bromide was added, to achieve a concentration of 0.7 µg/ml in the final solution.

4) About 100 ml of the mixture was poured in the gel electrophoresis tray, containing a comb with the appropriate number and size of teeth to create wells with about 50 μl capacity. The gel was left to set for about 20 min.
5) The comb was removed and the tray with the gel was placed in the electrophoresis apparatus and covered with 1X TAE buffer. Ethidium bromide was added in the running buffer to a final concentration of 0.7 μg/ml, to achieve good visualisation of the bands.
6) The DNA samples were loaded together with a DNA ladder. Between 600ng-1000ng of 1kb ladder or 100bp ladder were used for the experiments.
7) The electrophoresis conditions were set in the apparatus (voltage of ~100V for a 0.8% (w/v) gel or 80V for a 1.5% (w/v) gel). Electrophoresis was carried out for the appropriate length of time, depending on the size of the DNA bands expected.
8) Subsequently the gel was viewed under UV light emitted by a high-power ultra violet transilluminator (short wavelength) and a photograph was taken by using the special apparatus provided.

1.7 Glassmilk DNA extraction (GENECLEAN® kit)

In order to purify DNA from a gel for cloning purposes, the Geneclean kit was used (Bio 101 Inc.). It is based on a silica matrix (Glassmilk) that can bind to DNA, removing it from impurities. The manufacturer's protocol was followed, which is described here briefly:

1) The part of the gel containing the DNA of interest was cut with a scalpel blade and kept aside, after visualising it under UV for as short time as possible (because UV can create nicks in DNA).
2) 2.5- 3ml of 6M NaI was added per gram of gel slice. The tube was placed in a waterbath of 50^0C for the agarose to be dissolved.
3) 5μl of well-suspended Glassmilk were added to extract 5μg or less of DNA. The mixture was vortexed and placed on ice for 5 min to allow binding of the DNA. The solution was mixed every minute.
4) The solution was centrifuged for 5 sec. Then the pellet was washed three times with 10-50 volumes of NEW (a washing solution containing NaCl, ethanol, Tris and EDTA) to remove any agarose residues.
5) The pellet was resuspended in 10μl of distilled water and was placed in the 50^0C waterbath for 2-3 min to allow elution of the DNA from the matrix.

6) The tube was centrifuged for 2-3 min and the supernatant containing the eluted DNA was removed carefully and placed in another tube.

1.8 Vector dephosphorylation and ligation to inserts

Shrimp alkaline phosphotase (Roche) was used to dephosphorylate 5' phosphates from DNA blunt or "sticky" ends. This enzyme can be inactivated at 65^0C. The manufacturer's protocol was followed with a few modifications:

1) The digested vector was always purified from the gel using glassmilk. 50ng of vector were mixed with 1μl of 10X dephosphorylation buffer (0.5M Tris-HCl, 50mM $MgCl_2$, pH8.5) and 1 μl (1 unit) of shrimp alkaline phosphotase.
2) The reaction was left to incubate at 37^0 C for 30min. In the case of blunt ended vector, the reaction was incubated for 60min.
3) The enzyme was inactivated with incubation at 65^0 C for 15min.

To ligate a DNA fragment into a vector, a molar ratio of 3:1 of insert:vector is traditionally used. The superfluous number of insert molecules to vector increases the chance of a ligation to take place.

$$\frac{\text{Z moles of insert ends to ligate}}{\text{Y moles of vector ends to ligate}} = \frac{3}{1} \quad (1) \Leftrightarrow$$

because 1mole of every substance contains 6.023×10^{23} molecules (Avogadro's number) then:

$$\frac{\text{Z x } 6.023\text{x}10^{23} \text{ insert molecules}}{\text{Y x } 6.023\text{x}10^{23} \text{ vector molecules}} = \frac{\text{Z insert molecules}}{\text{Y vector molecules}} = \frac{3}{1} \quad (2)$$

since 10^9 base pairs of DNA weigh 1pg, it is possible to convert the DNA weight measured spectrophotometrically into the total number of base pairs that weigh that amount. So, if a solution of "Y" vector molecules of size "vector kb" base pairs each, weighs "vector pg" picograms, then the whole solution consists of 10^9 x vector pg base pairs. If the size "kb" of each fragment is known, the number "Y" of molecules in the solution that give a total of 10^9 x vector pg base pairs can be calculated:

$$\text{Y vector molecules} = \frac{10^9 \text{ x vector pg}}{\text{vector kb}} \quad (3)$$

By substituting the equation (3) into (2), the following equation is derived:

$$\frac{\frac{10^9 \times \text{insert pg}}{\text{insert kb}}}{\frac{10^9 \times \text{vector pg}}{\text{vector kb}}} = \frac{\text{insert pg} \times \text{vector kb}}{\text{vector pg} \times \text{insert kb}} = \frac{3}{1} \quad (4) \quad \Leftrightarrow$$

therefore to calculate the amount of insert one needs to ligate into a known amount of vector of known size:

$$\text{insert pg} = \frac{\text{vector pg} \times \text{insert kb}}{\text{vector kb}} \times 3 \qquad (5)$$

Formula (5) was applied in ligations using T4 DNA ligase from *Escherichia coli.* This enzyme creates a phosphodiester bond between 5'-P and 3'-OH in cohesive or blunt ends of double stranded DNA. It can also repair DNA nicks. The reaction was carried out by mixing the following: 2 µl of 10X ligation buffer (660 mM Tris-HCl, 50 mM $MgCl_2$, 10mM dithioerythritol, 10mM ATP, pH 7.5), 1 µl of T4 ligase, the appropriate amount of insert and vector to give a molar ratio of 3:1 and sterile distilled water to make up the volume to 20 µl. The reaction was left at 14^0C overnight to incubate.

In the case of T-easy vector (Promega), the ligase and ligation buffer that come with the kit were used as follows: 1 µl of 10X ligation buffer (300mM Tris-HCl pH 7.8, 100mM $MgCl_2$, 100mM DTT, 10mM ATP), 50ng of T-easy vector, the appropriate amount of PCR product, 1 µl of T4 ligase and sterile distilled water to make up the volume to 10 µl. The reaction was mixed and left to incubate overnight at 4^0 C.

Cloning of an insert into the T-easy vector disrupts the coding sequence of the β-galactosidase gene. As a result, successful recombinants should result in white colonies when transformed into *Escherichia coli* cells, while empty vectors should give blue colonies. Background blue colonies can result from vectors that had not been digested or T-tailed, but also from inserts that had been cloned in frame with the β-galactosidase gene. To examine these possibilities, a control ligation was included where no insert was added in the ligation reaction. If the experimental ligation would yield more blue colonies than the control ligation, then real recombinants were present in some of these blue colonies.

1.9 Preparation and testing of competent cells for heat shock transformation

1) 4-5 colonies of the DH5-α strain of *Escherichia coli* cells (ampicillin-sensitive, tetracycline-resistant) were inoculated into 1ml of Luria Broth (containing bactopeptone, NaCl, yeast extract, agar, NaOH and sterile distilled water) with 20mM $MgSO_4$ and left to grow overnight at 37^0 C shaking (250-300cycles/min).
2) The following day the culture was inoculated with 200ml of Luria Broth in a flask of 2l capacity at 37^0 C shaking for 3 hours.
3) The culture was collected into four 50ml falcon tubes and left on ice for 10min. It was then centrifuged in a fixed angle rotor at 1000g for 10min.
4) The supernatant was decanted and the pellets were resuspended gently into two tubes with 30ml of solution RF1 pH 5.8 each (100mM RbCl, 50mM $MnCl_2 \cdot 4H_2O$, 30mM KOAc pH7.5, 10mM $CaCl_2 \cdot 2H_2O$, 15% v/v glycerol). They were left on ice for 15min to incubate.
5) The tubes were centrifuged at 1000g for 10min. The supernatant was discarded.
6) All the pellets were collected into one tube with 16ml of solution RF2 pH 6.8 (10mM MOPS, 10mM $RbCl_2$, 75mM $CaCl_2 \cdot 2H_2O$, 15% v/v glycerol) and left on ice for 15min.
7) 300 µl of the cell suspension was dispensed into ice cold screw cap tubes and flash frozen in liquid nitrogen. The tubes were stored at -80^0 C.

To test the transformation efficiency of the cells, they were transformed with 1µg of DNA (as seen in section 1.8) and plated in 1:10 and 1:100 dilutions. After overnight incubation at 37^0 C, the colonies in the 1:10 plate should overgrow. The colonies in the 1:100 were counted and the transformation efficiency (number of colonies resulting from transformation with 1µg of DNA) was calculated with the formula:

$$\frac{\text{No of colonies x dilution factor}}{\text{No of µg of DNA}} = \text{colonies/ µg of DNA}$$

The transformation efficiency should be about 10^8 colonies/µg. The materials used were from Sigma.

1.10 Transformation using heat shock

1) Competent cells were thawed slowly on ice. 50µl of cells were used per transformation and dispensed in an eppendorf tube kept on ice.

2) 100ng of DNA were added in each tube and mixed by pipetting slowly. The mixture was left on ice for 15min.
3) The tube was transferred in a 42^0 C waterbath for 50sec. Immediately afterwards, it was kept on ice for 2 min.
4) 1ml of Luria Broth was added in the eppendorf tube and was left in a 37^0 C shaking incubator for 1 hour for the cells to recover.
5) 100-200µl of the cell suspension was plated onto Luria Broth plates (autoclaved 1l of LB with 15g agar, that had been poured in 25ml aliquots onto sterile petri dishes) containing 100µg/ml ampicillin, as all the constructs used in this project should render the *E.coli* cells ampicillin resistant. In the case of T-easy vector, the plates also contained 80µg/ml X-gal, the substrate for β-galactosidase to allow for blue-white colony selection and 0.5mM IPTG to induce the *LacZ* promoter.

1.11 Qiagen kit mini DNA preparation

In order to prepare DNA of good quality for sequencing and transfections, the spin miniprep kit from Qiagen was used. The manufacturer's protocol was followed:

1) A single bacterial colony containing the plasmid of interest was selected and inoculated overnight at 37^0C with shaking in Luria Broth containing 50µg/ml ampicillin.
2) The culture was centrifuged at 4800 rpm for 10min at 4^0C. The supernatant was discarded and the tube was inverted to dry off the excess medium.
3) The bacterial pellet was resuspended in 250µl of buffer P1 containing RNase A to destroy the cellular RNA.
4) The cells were lysed with 250 µl of buffer P2, which contains NaOH and SDS. The tube was inverted a few times gently to ensure lysis of the bacteria without shearing the genomic DNA. The SDS solubilises the cell membrane, while the alkaline conditions denature the plasmid and genomic DNA. The reaction was left for no longer than 5min to prevent the plasmid DNA from becoming irreversibly denatured.
5) 350 µl of buffer P3 were added to neutralise the solution and the tube was inverted 5-6 times gently to mix the content. The high salt concentration of this buffer ensures the precipitation of SDS, proteins, genomic DNA and cellular debris, while the plasmid DNA remains in solution.
6) The solution was centrifuged for 10min at 13,000 rpm at room temperature.

7) The supernatant was loaded in the column provided containing a special matrix for binding the DNA and was spun down at 13,000 rpm for 30sec. The flow-through was discarded.
8) The bound DNA was washed with 0.75ml buffer PB that removes excess salt. The tube was spun down at 13,000 rpm for 30 sec.
9) The flow-through was discarded and the tube was centrifuged for 1min to ensure the complete removal of wash buffer.
10) The column was transferred in a fresh 1.5ml eppendorf tube and 50 μl of sterile water were placed on the top of the matrix. The tube was left to stand for 1min and it was subsequently centrifuged for 2min at 13,000 rpm to elute the DNA.
11) The concentration of the DNA was measured with a spectrophotometer. 2μl of the DNA was mixed in 498μl of distilled water and was dispensed in a quartz cuvette. The cuvette was placed in the spectrophotometer that had been set to zero previously with only water in the cuvette. The absorbance reading ($\lambda = 260nm$) was taken and it was multiplied with the dilution factor (x250) and the number 0.05 to convert the reading into a concentration value (μg/μl).

1.12 Restriction enzyme digestion

1) For single enzyme restriction digestion or double digestion with enzymes that require the same buffer the DNA was mixed with sterile distilled water and the appropriate volume of 10X buffer. The mixture was vortexed for 2 sec.
2) The required units of enzyme(s) were added very quickly and the mixture was vortexed again.

   N.B. 1 unit of enzyme digests 1μg of DNA in 1 hour.
3) The mixture was centrifuged for a few seconds and then it was kept in the optimum temperature for two hours.

   N.B. After digestion is complete, the DNA can be stored in the fridge. The volume of the enzyme should not exceed the 10% of the total reaction volume, because the enzymes are supplied in 50% (v/v) glycerol, which in big amounts can inhibit the reaction. Some enzymes require the addition of bovine serum albumin to be stabilised.

For digestion with enzymes that require different buffer, the digestion with the low salt concentration buffer was carried out first. For the second digestion, the volume was doubled

by adding water, the new buffer and enzyme and the digestion was left to complete for two more hours. The enzymes and buffers were purchased from Roche.

1.13 DNA sequencing

DNA sequencing was carried out in an ABI PRISM 377 DNA sequencer. The sequencing reaction was carried out according to manufacturer's protocol (Perkin-Elmer), which is summarised here:

1) 4 µl of terminator ready reaction mix was mixed with 0.4 µg of DNA template, 3.2pmol of the appropriate primer and enough sterile distilled water to make up the volume to 10µl. The mixture was vortexed and layered with one drop of mineral oil.

   N.B. Apart from the AmpliTaq DNA polymerase the premix contains A-dye terminator, G-dye terminator, C-dye terminator, T-dye terminator, Tris-HCl pH9, $MgCl_2$, thermal stable pyrophosphotase, dATP, dTTP, dCTP and dITP (instead of dGTP to avoid band compression).
2) the mixture was subjected in the following PCR programme of 25 cycles: 96^0C for 30sec, 50^0C for 20sec and 60^0C for 4 min.
3) 50µl of chloroform were added to separate the PCR sample from the oil. The PCR reaction was removed and transferred to another eppendorf tube.
4) 1 µl of 3M NaAc pH 5.2 was added and the solution was mixed by pippeting. 25 µl of 100% ethanol was added, the solution was vortexed and left on ice for 10min.
5) The tube was centrifuged for 30min at 20^0C at 14,000rpm. The ethanol solution was carefully removed and the pellet was washed with 250µl of 70% ethanol. The solution was centrifuged for 5min at 20^0C at 14,000rpm.
6) The ethanol supernatant was carefully removed and the pellet was dried in a vacuum for 5-10min. The pellet was resuspended in 4 µl of loading buffer. This buffer contained a ratio of 1 dye: 5 formamide. The dye constitution is 25mM EDTA pH8 with 50mg/ml blue dextran. The sample was stored at -20^0C until ready to load in a sequencing gel.
7) The sequencing gel consisted of 18g urea, 5.7 ml 40% (w/v) acrylamide stock, 25ml autoclaved millipure water and 0.5g mixed bed resin. After sterilising it through a 0.22µm filter and degassing for 5min in a vacuum, 50ml of TBE buffer were added.
8) When the gel tray was set up, 10% (w/v) of ammonium persulphate and 35 µl of TEMED were added. The appropriate software for the sequencer was used to run the gel and visualise the sequences.

CHAPTER 1

In silico cloning of VR-L, a new member of the vanilloid receptor family

EXPERIMENTAL RESULTS

1.a Cloning using bioinformatics tools: the methodology

Comparison of the VR1 pharmacological profile with the native vanilloid responses suggested the existence of multiple vanilloid receptors. In collaboration with Dr. Garcia (UCL) we deployed an *in silico* cloning approach i.e. a computational method, to attempt to clone another member of the vanilloid receptor family, which has the advantage of being more rapid than traditional cloning methods.

We used information deposited in GenBank, which is part of the International Nucleotide Sequence Database Collaboration. GenBank is a collection of annotated genetic information that is publicly available and is maintained by NIH. Specifically, the dbEST division of GenBank was used; a repository of expressed sequence tags (ESTs), which are partial, single pass cDNA sequences derived from randomly selected library clones. These ESTs come from different libraries, generated from different tissues. Many ESTs can represent the same gene in a library; hence the frequency of such ESTs gives a rough indication of the gene's expression levels in the tissue used to generate the library. Additionally, the existence of ESTs representing the same gene in different libraries from different tissues can reveal the tissue distribution of that gene. ESTs with a degree of homology to a known gene have been traditionally used as probes to screen a library and identify a novel gene of the same family. More recently, ESTs, assembled into consensus sequences, were used to create a virtual transcript of a gene that could be subsequently cloned with library screening (Wei *et al.*,1998). We used a similar method to cluster ESTs together that share a degree of homology to VR1. Specifically, we performed a tBLASTn (Basic Local Alignment Search Tool) search of the dbEST database using the VR1 amino acid sequence as query.

The blast algorithm tries to identify local regions of alignment between sequences. Scores are assigned according to the extension of alignment and high-scoring segment pairs (HSPs), i.e. alignments that cannot be optimised any further, are identified. Specifically, the score of an alignment is calculated as a sum of substitution and gap scores. Gap scores are empirically set penalties for the creation of gaps in aligning sequences and the extension of these gaps. Score for substitution (change to a different amino acid due to mutation during evolution) for each pair in an alignment is calculated according to a scoring system or matrix. In our search we used the **Blo**cks **Su**bstitution **M**atrix (BLOSUM), where the frequency of substitution for each amino acid is

estimated from the substitution frequencies occurring in an alignment of a known family of related proteins. In our search we used BLOSUM62, where the related sequences used have maximum 62% identity (default setting). We used the tBLASTn algorithm, which compares the amino acid sequence of the query (VR1), against the dbEST database translated in all possible reading frames. The search (appendix 1.1) identified overlapping, partially homologous entries, which can be assembled into a virtual transcript. The ESTs selected for the contig assembly were the ones with $P<10^{-5}$ (the entries with $P>10^{-5}$ are omitted in appendix 1.1), where P is the probability of the alignment occurring in the database with the calculated score S or score better than S. The probability value is estimated in relation to similar or better scores of alignments, that can occur by chance in the database. The most significant P values are the ones close to 0, i.e. sequences in almost perfect alignment. Therefore, to avoid selecting ESTs that were actually representing VR1, we selected ESTs with $P<10^{-5}$, hoping to identify new members of the VR family. The human entries were selected to generate the virtual transcript (table 1.1), albeit interrupted by gaps, which represented sequences analogous to the amino acid positions 86 to 763 of rat VR1 (figures 1.1 and 1.10). Since the ESTs were obtained from different cDNA libraries and hence tissues, a RT-PCR approach was used to fill in the gaps and to prove that the virtual transcript is not a computation artefact.

In order to assemble overlapping ESTs into contigs, the longest EST reading frames aligning to the VR1 amino acid sequence were considered correct and taken into account (e.g. contig 1, figure 1.1. In addition, refer to appendix 1.1). There were also cases where alignments from different reading frames of the same EST were considered (e.g. contig 2, figure 1.1, entries N23395, frame +1A and N23395, frame +3A), unless they were refuting each other (e.g.N21167, frame -1 and N21167, frame –2, appendix 1.1). The disruption of the alignment and its continuation in a different frame can be explained as the result of sequencing mistakes, which are very common in the single pass, low quality sequences of ESTs. Only the human entries (26 ESTs) were selected for the construction of contigs (table 1.1), apart from the case of contig 5, where also a mouse entry, with extended homology to the corresponding human EST, was used.

Table 1.1. EST clones showing homology to the rat vanilloid receptor subtype 1 (VR1).

GenBank Accession Number	Library/Tissue Source	Region of Homology to VR1 (amino acid numbers)
W44731	parathyroid tumour (human)	281-401
AA476107	mammary gland (mouse)	541-689
W38665	parathyroid tumour (human)	319-456
AA139413	kidney (mouse)	305-441
AA304033	aorta endothelial cells, TNF alpha-treated (human)	649-755
W82502	total foetus (mouse)	127-264
N23395	foreskin melanocytes (human)	248-401
AA281349	tonsillar cells enriched for germinal center B cells (human)	248-344
AA236416	Pooled melanocyte, foetal heart and pregnant uterus (human)	95-231
W92895	foetal liver and spleen (subtracted) (human)	537-658
AA741232	tonsillar cells enriched for germinal center B cells (human)	86-209
H20025	adult brain (human)	86-209
AA461295	total foetus (human)	86-209
AA357145	Jurkat T-cells (human)	364-456
AA321554	lymphoid tissue / CCRF-CEM cells, cyclohexamide treated (human)	774-838
H51393	adult brain (human)	87-209
AA768829	tonsillar cells enriched for germinal center B cells (human)	86-203
AA236417	Pooled melanocyte, foetal heart and pregnant uterus (human)	86-203
T12251	heart (human)	624-692
N26729	foreskin melanocytes (human)	119-209
H50364	adult brain (human)	127-209
W53556	embryos (mouse)	110-273
H21490	adult brain (human)	138-209
H49060	adult brain (human)	135-209
N21167	foreskin melanocytes (human)	127-209
N35179	foreskin melanocytes (human)	687-763
AA015295	placenta (mouse)	709-763
H27879	adult brain (human)	127-203
AA281348	tonsillar cells enriched for germinal center B cells (human)	717-763
AA274980	total foetus (mouse)	722-763
AA078617	placenta (human)	325-389
N24224	foreskin melanocytes (human)	385-487
AA144832	testis (mouse)	200-354

Figure 1.1: Alignment of overlapping ESTs and deduction of contigs (in blue letters). Discrepancies in the alignment are shown in red color. Different reading frames are represented by numbered (+) or (-), followed by capital letters e.g. A, B, that represent the first, second etc. aligned segment reported in the tBLASTn search result (where applicable). Each contig is aligned against the rat VR1 amino acid sequence.

CONTIG 1

```
>AA768829(-3)                ASQPDPNRFDRDRLFNAVSRGVPEDLAGLPEYLSKTSKYLTDSEYTEGSTGKTCLMKAVLN
>AA741232(-2)                ASQPDPNRFDRDRLFNAVSRGVPEDLAGLPEYLSKTSKYLTDSEYTEGSTGKTCLMKAVLN
>H20025(-1)                  ASQPDPNRFDRDRLFNAVSRGVPEDLAGLPEYLSKTSKYLTDSEYTEGSTGKTCLMKAVLN
>AA461295(-3)                ASQPDPNRFDRDRLFNAVSRGVPEDLAGLPEYLSKTSKYLTDSEYTEGSTGKTCLMKAVLN
>AA236417(-3)                ASQPDPNRFDRDRLFNAVSRGVPEDLAGLPEYLSKTSKYLTDSEYTEGSTGKTCLMKAVLN
>N26729(-3)                                  NAVSRGVPEDLAGLPEYLSKTSKYLTDSEYTEGSTGKTCLMKAVLN
>H51393 (-3)                                 EDLAGLPEYLSKTSKYLTDSEYTEGSTGKTCLMKAVLN
>H50364(-3)                                  EDLAGLPEYLSKTSKYLTDSEYTEGSTGKTCLMKAVLN
>H27879(-2)                                                          TGKTCLMKAVLN
>AA236416(+1)                                EDLAGLPEYLSKTSKYLTDSEYTEGSTGKTCLMKAVLN
>AA236416(+2)        QPQLPKGTGASQDPDNRFDRDRLFNAVSR
>H21490(-2)                                                    RPSKYLTDSEYTEGSTGKTCLMKAVLN
>H49060(-1)                                                          TGKTCLMKAVLN
>N21167(-1)                                  EDLAGLPEYLSKTSKYLTDSEYTEGSTGKTCLMKAVLN

>AA768829(-3)        LKDGVNACILPLLQIDRDSGNPQPLVNAQCTDDYYRGHS
>AA741232(-2)        LKDGVNACILPLLQIDRDSGNPQPLVNAQCTDDYYRGHSALHIAI
>H20025(-1)          LKDGVNACILPLLQIDRDSGNPQPLVNAQCTDDYYRGHSALHIAI
>AA461295(-3)        LKDGVNACILPLLQIDRDSGNPQPLVNAQCTDDYYRGHSALHIAI
>AA236417(-3)        LKDGVNACILPLLQIDRDSGNPQPLVNAQCTDDYYRGHS
>N26729(-3)          LKDGVNAXILPLLQIDRDSGNPQPLVNAQCTDDYYRGHSALHIAI
>H51393(-3)          LKDGVNACILPLLQIDRDSGNPQPLVNAQCTDDYYRGHSALHIAI
>H50364(-3)          LKDGVNACILPLLQIDRDSGNPQPLVNAQCTDDYYRGHSALHIAI
>H27879(-2)          LKDGVNACILPLLQIDRDSGNPQPLVNAQCTDDYYRGHS
>AA236416(+1)        LKDGVNACILPLLQIDRDSGNPQPLVNAQCTDDYYRGHSALHIAIEKRSLQCVKLLVENGANVHARA
>H21490(-2)          LKDGVNACILPLLQIDRDSGNPQPLVNAQCTDDYYRGHSALHIAI
>H49060(-1)          LKDGVNACILPLLQIDRDSGNPQPLVNAQCTDDYYRGHSALHIAI
>N21167(-1)          LKDG
```

```
Score =  118 bits (296), Expect = 3e-25
Identities = 61/137 (44%), Positives = 88/137 (63%)

rat VR1:  95  RPSSQDSVSAGEKPPRLYDRRSIFDAVAQSNCQELESLLPFLQRSKKRLTDSEFKDPETG 154
              +P       A + P   +DR  +F+AV++   ++L  L  +L ++ K LTDSE+ +  TG
Contig 1: 1   QPQLPKGTGASQDPDNRFDRDRLFNAVSRGVPEDLAGLPEYLSKTSKYLTDSEYTEGSTG 60

Rat VR1:   155 KTCLLKAMLNLHNGQNDTIALLLDVARKTDSLKQFVNASYTDSYYKGQTALHIAIERRNM 214
               KTCL+KA+LNL +G N  I  LL + R + + +  VNA  TD YY+G +ALHIAIE+R++
Contig 1:  61  KTCLMKAVLNLKDGVNACILPLLQIDRDSGNPQPLVNAQCTDDYYRGHSALHIAIEKRSL 120

Rat VR1:  215 TLVTLLVENGADVQAAA 231
               V LLVENGA+V A A
Contig 1: 121 QCVKLLVENGANVHARA 137
```

CONTIG 2

```
>AA281349(+3)            GELPLSLAACTKQWDVVSYLLENPHQPASLQATDSQGNTVLHALVMISDNSAENIAL
>N23395(+1A)             GELPLSLAACTKQWDVVSYLLENPHQPASLQA
>N23395(+3A)                                                DSQGNTVLHALVMISDNSAENIAL
>W44731(+2A)                                                DSQGNTVLHALVMISDNSAENIAL
>W44731(+3A)             GELPLSLAACTKQWDVVSYLLENPHQPASL

>AA281349(+3)             VTSMYDGLLQAGARLCPTVQLEDIRNLQDLTPLKLAAKEG
>N23395(+3A)              VTSMYDGLLQAGARLCPTVQ
>W44731(+2A)              VTSMYDGLLQAGARLCPTVQLEDIRNLQDLTPLKLAAKEGKIEIFRHILQRE
>W38665(-3)                                LCPTVQLEDIRNLQDLTPLKXAAKEGKIEIFRHILQRGVXRTE
```

```
Score =  129 bits (323), Expect = 2e-28
Identities = 65/114 (57%), Positives = 83/114 (72%)

Rat VR1:  248 GELPLSLAACTNQLAIVKFLLQNSWQPADISARDSVGNTVLHALVEVADNTVDNTKFVTS 307
              GELPLSLAACT Q  +V +LL+N  QPA + A DS GNTVLHALV ++DN+ +N   VTS
Contig 2: 1   GELPLSLAACTKQWDVVSYLLENPHQPASLQATDSQGNTVLHALVMISDNSAENIALVTS 60

Rat VR1:  308 MYNEILILGAKLHPTLKLEEITNRKGLTPLALAASSGKIGVLAYILQREIHEPE 361
              MY+ +L  GA+L PT++LE+I N + LTPL LAA  GKI +  +ILQRE+   E
Contig 2: 61  MYDGLLQAGARLCPTVQLEDIRNLQDLTPLKLAAKEGKIEIFRHILQREVXRTE 114
```

CONTIG 3

```
>W44731(+2B)          HLSRKFTEWCYGPVRVSLYDLASVDSCEENSVLEIIAF
>AA357145(+2A)        HLSRKFTEWCYGPVRVSLYDLASXDSCXENSVLEIIAF
>N23395(+3B)                                  VDSCEENSVLGIIAF
>W38665(-1A)          HLSRKFTEWCYGPVRVSLYDLASVDSCEENSVLEIIAF

Score = 67.0 bits (162), Expect = 1e-09
Identities = 28/38 (73%), Positives = 34/38 (88%)

Rat VR1:  364 HLSRKFTEWAYGPVHSSLYDLSCIDTCEKNSVLEVIAY 401
              HLSRKFTEW YGPV  SLYDL+ +D+CE+NSVLE+IA+
Contig 3: 1   HLSRKFTEWCYGPVRVSLYDLASVDSCEENSVLEIIAF 38
```

CONTIG 4

```
>N24224(+1)           KSPXRHRMVVLEPLNKLLQAKWDLLIPKFFLNFLCNLXYMFIFTAVAYHQPT
>AA357145(+2B)        KSPHRHRMVVLEPLNKLLQ
>W38665(-1B)          KSPHRHRMVVLEPLNKLLQAKWDLLIPKFF

>N24224(+1)           LKKQAAPHLKAEVGNSMLLTGHILILLGGIY

Score = 72.8 bits (177), Expect = 2e-11
Identities = 38/85 (44%), Positives = 56/85 (65%), Gaps = 4/85 (4%)

Rat VR1:  405 ETPNRHDMLLVEPLNRLLQDKWDRFVKRIFYFNFFVYCLYMIIFTAAAYYRPV--EGLPP 462
              ++P+RH M+++EPLN+LLQ KWD  + + F+ NF     YM IFTA AY++P   +   P
Contig 4: 1   KSPHRHRMVVLEPLNKLLQAKWDLLIPK-FFLNFLCNLXYMFIFTAVAYHQPTLKKQAAP 59

Rat VR1:  463 YKLKNTVGDYFRVTGEILSVSGGVY 487
              + LK  VG+   +TG IL + GG+Y
Contig 4: 60  H-LKAEVGNSMLLTGHILILLGGIY 83
```

CONTIG 5

```
>W92895(+1)                YLPLLVSALVLGWLNLLYYTRGFQHTGIYSVMIQK
>AA476107(MOUSE)+1             LVSSLVLGWLNLLYYTRGFQHTGIYSVMIQKVILRDLLRFLLVYLVF

>AA476107(MOUSE)+1         LFGFAVALVSLSRDGRSPKAPEDS

Score = 97.4 bits (241), Expect = 7e-19
Identities = 44/75 (58%), Positives = 59/75 (78%)

Rat VR1:  537 YVASMVFSLAMGWTNMLYYTRGFQQMGIYAVMIEKMILRDLCRFMFVYLVFLFGFSTAVV 596
              Y+  +V +L +GW N+LYYTRGFQ  GIY+VMI+K+ILRDL RF+ VYLVFLFGF+ A+V
Contig 5: 1   YLPLLVSALVLGWLNLLYYTRGFQHTGIYSVMIQKVILRDLLRFLLVYLVFLFGFAVALV 60

Rat VR1:  597 TLIEDGKNNSLPMES 611
              +L  DG++   P +S
Contig 5: 61  SLSRDGRSPKAPEDS 75
```

CONTIG 6

```
>T12251(+3)           GAQYRGILVASLELFKFTIGMGELAFQEQLHFRGMVLLLLL
>AA304033(+1)                                   FQXQLHFRGMVLLLLL

>T12251(+3)       AYVLLTYILLLNMLIALMSETVNSVATD
>AA304033(+1)     AYVLLTYILLLNMLIALMSETVNSVATDSWSIWKLQKAIXVLEMENGYWWCRKK
>N35179(-1)                                                        KK
>AA281348(-2)                                                      RKK

>N35179(-1)               QRAGVMLXVGTKPDGSPDERWCFRVEEVNWASWEQTLPTLCEDP
>AA281348(-2)             QRAGVMLTVGTKPDGSPDERWCFRVEEVNWASWEQTLPTLCEDP

Score =  160 bits (404), Expect = 9e-38
Identities = 78/140 (55%), Positives = 98/140 (69%), Gaps = 1/140 (0%)

Rat VR1:  624 GNSYNSLYSTCLELFKFTIGMGDLEFTENYDFKAVFIILLLAYVILTYILLLNMLIALMG 683
              G  Y  +    LELFKFTIGMG+L F E   F+ + ++LLLAYV+LTYILLLNMLIALM
Contig 6: 1   GAQYRGILVASLELFKFTIGMGELAFQEQLHFRGMVLLLLLAYVLLTYILLLNMLIALMS 60

Rat VR1:  684 ETVNKIAQESKNIWKLQRAITILDTEKSFLKCMRKAFRSGKLLQVGFTPDGKDDYRWCFR 743
              ETVN +A +S +IWKLQ+AI +L+ E  +  C RK  R+G +L VG  PDG  D RWCFR
Contig 6: 61  ETVNSVATDSWSIWKLQKAIXVLEMENGYWWC-RKKQRAGVMLTVGTKPDGSPDERWCFR 119

Rat VR1:  744 VDEVNWTTWNTNVGIINEDP 763
              V+EVNW +W   +  + EDP
Contig 6: 120 VEEVNWASWEQTLPTLCEDP 139
```

CONTIG 7

>AA321554(+2) SFSLRSSRVSGRHWKNFALVPLLREASXRXRQSAQPEEVYLRQFSGSLKPEDAEVFKSPAASGEK

```
Score = 94.4 bits (233), Expect = 6e-18
Identities = 46/65 (70%), Positives = 52/65 (79%)

Rat VR1:  774 SFSLRSGRVSGRNWKNFALVPLLRDASTRDRHATQQEEVQLKHYTGSLKPEDAEVFKDSM 833
              SFSLRS RVSGR+WKNFALVPLLR+AS R R + Q EEV L+ ++GSLKPEDAEVFK
Contig 7: 1   SFSLRSSRVSGRHWKNFALVPLLREASXRXRQSAQPEEVYLRQFSGSLKPEDAEVFKSPA 60

Rat VR1:  834 VPGEK 838
                GEK
Contig 7: 61  ASGEK 65
```

As it is evident from the contig-VR1 alignments, there is no contig representing the N-terminus of the VR1 sequence. In order to identify ESTs closer to the 5' end, information deposited in the Institute for Genome Research (TIGR) was used. One of the databases maintained in this institute is the Human Gene Index (HGI), which stores information from human genome projects worldwide. One subdivision is the database of tentative human consensus sequences (THCs), a regularly updated collection of human EST clusters. The ESTs used are non-redundant cDNA and coding genomic DNA entries in GenBank, that were assembled under strict criteria (minimum of 40 bases overlap, 95% sequence identity) to create transcripts with consensus sequence and to avoid the generation of chimeric contigs. One of the most 5' EST identified by the tBLASTn search was used (H20025) to search the THC reports. This resulted in retrieving a THC report (figure 1.2) that extended the consensus sequence to the N terminus of the virtual transcript.

Figure 1.2: The THC report using the EST with gb#H20025 as query

HGI THC Report: THC176254

```
GCTAGCCTGTCCTGACAGGGgAGAGTTAAGCTCCCGtTCTCCACCGTGCCGGCTGgCAGGTGGGCTGAGGGTGACCGAGA
GACCAGAACCTGCTTGCTGGAGCTTAGTGCTCAGAGCTGGGGAGGGAGGTTCCGCCGCTCCTCTGCTGTCAGCGCCGGCA
GCCCCTCCCGGCTTCACTTCCTCCCGCAGCCCCTGCTACTGAGAAGCTCCGGGATCCCAGCAGCCGCCACGCCCTGGCCT
CAGCCTGCGGGGCTCCAGTCAGGCCAACACCGACGCGCAnTGGnGAGGAAGACAGGACCCTTGACATCTCCATCTGCACA
GAGGTCCTGGCTGGACgAGCAGCCTCCTCCTCCTAGGATGACCTCACCCTCCAGCTCTCCAGTTTTCAGGTTGGAGACAT
TAGATGGAGGCCAAGAAGATGGCTCTGAGGCGGACAGAGGAAAGCTGGATTTTGGGAGCGGGCTGCCTCCCATGGAGTCA
CAGTTCCAGGGCGAGGACCGGAAATTCGCCCCTCAGATAAGAGTCAACCTCAACTACCGAAAGGGAACAGGTGCCaGTCA
GCCGGATCCAAACCGATTTGACCgAGATCGGCTcTTCAATGCGGTCTCCCgGGGTGTCCCCGAGGATCTGGCTGGACTTC
CAGAGTACCTGAGCAAGACCAGCAAGTACCTCACCGACTCGGAATACACAGAGGGCTcCACAGGTAAGACGTGCCTGATG
AAGGCTGTGCTGAACCTTAAGGACGGGGTCAATGCCTGCATTCTGCCACTGCTGCAGATCGACCGGGACTCTGGCAATCC
TCAGCCCCTGGTAAATGCCCAGTGCACAGATGACTATTACCGAGGCCACAGCGCTCTGCACATCGCCATT
```

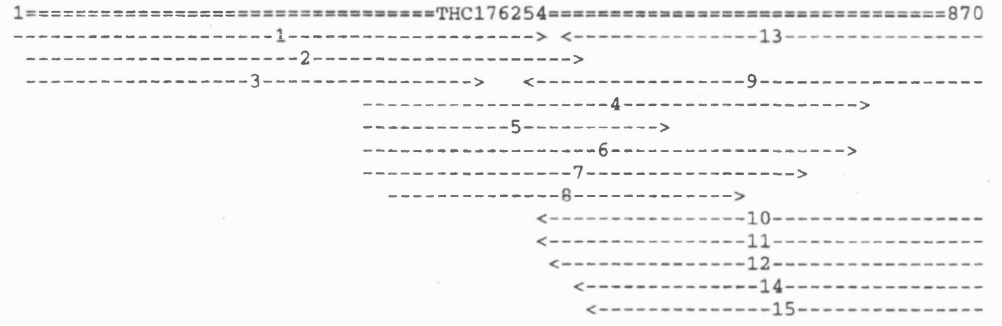

#		EST Id	GB#	ATCC#	left	right	library
1	F	yx50h11.r1	N28029	522334	1	476	melanocyte 2NbHM, Soares
2	F	yx47e06.r1	N29128	522011	14	506	melanocyte 2NbHM, Soares
3	F	yx62c11.r1	N34617	523437	15	424	melanocyte 2NbHM, Soares
4	F	yn55e02.r1	H20101	419091	320	771	adult brain N2b5HB55Y, Soares
5	F	yn79h03.r1	H40615	421422	320	591	adult brain N2b5HB55Y, Soares
6	F	yo21f05.r1	H49128	425338	320	757	adult brain N2b5HB55Y, Soares
7	F	yo29h05.r1	H50404	426130	320	713	adult brain N2b5HB55Y, Soares
8	F	yo30f10.r1	H51392	426212	340	654	adult brain N2b5HB55Y, Soares
9	F	yn55e02.s1	H20025	419091	464	870	adult brain N2b5HB55Y, Soares
10	F	yx47e06.s1	N21167	522011	475	870	melanocyte 2NbHM, Soares
11	F	yo30f10.s1	H51393	426212	478	870	adult brain N2b5HB55Y, Soares
12	F	yo29h05.s1	H50364	426130	493	870	adult brain N2b5HB55Y, Soares
13	F	yx62c11.s1	N26729	523437	501	870	melanocyte 2NbHM, Soares
14	F	yn76c11.s1	H21490	421101	506	870	adult brain N2b5HB55Y, Soares
15	F	yo21f05.s1	H49060	425338	525	870	adult brain N2b5HB55Y, Soares

Sequence source codes:
F = WashU/Merck

The report contains the consensus sequence derived from collating the overlapping ESTs together. The horizontal parallel lines represent the alignment of each EST on the consensus sequence, followed by the list of ESTs used to generate the report. In order to establish whether or not the THC report contains the initiation methionine, the consensus sequence was translated in all reading frames. The translation revealed the first forward reading frame as the correct frame containing the start codon and lacking proceeding stop codons (figure 1.3).

Figure 1.3: Translation of THC176254 in all possible frames. The initiation methionine is highlighted.

5'3' Frame 1
A S L S **Stop** Q G R V K L P F S T V P A G R W A E G D R E T R T C L L E L S A Q S W G G R F R R S S A V S A G S P S R
L H F L P Q P L L L R S S G I P A A A T P W P Q P A G L Q S G Q H R R A X X R K T G P L T S P S A Q R S W L D E Q P P
P P R **Met** T S P S S S P V F R L E T L D G G Q E D G S E A D R G K L D F G S G L P P **Met** E S Q F Q G E D R K F A P Q I
R V N L N Y R K G T G A S Q P D P N R F D R D R L F N A V S R G V P E D L A G L P E Y L S K T S K Y L T D S E Y T E
G S T G K T C L **Met** K A V L N L K D G V N A C I L P L L Q I D R D S G N P Q P L V N A Q C T D D Y Y R G H S A L H I
A N

5'3' Frame 2
L A C P D R G E L S S R S P P C R L A G G L R V T E R P E P A C W S L V L R A G E G G S A A P L L S A P A A P P G F T
S S R S P C Y **Stop** E A P G S Q Q P P R P G L S L R G S S Q A N T D A X W X G R Q D P **Stop** H L H L H R G P G W T S S
L L L L G **Stop** P H P P A L Q F S G W R H **Stop** **Met** E A K K **Met** A L R R T E E S W I L G A G C L P W S H S S R A R T G
N S P L R **Stop** E S T S T T E R E Q V P V S R I Q T D L T E I G S S **Met** R S P G V S P R I W L D F Q S T **Stop** A R P A S T S
P T R N T Q R A P Q V R R A **Stop** **Stop** R L C **Stop** T L R T G S **Met** P A F C H C C R S T G T L A I L S P W **Stop** **Met** P S A
Q **Met** T I T E A T A L C T S P I

5'3' Frame 3
Stop P V L T G E S **Stop** A P V L H R A G W Q V G **Stop** G **Stop** P R D Q N L L A G A **Stop** C S E L G R E V P P L L C C Q R
R Q P L P A S L P P A A P A T E K L R D P S S R H A L A S A C G A P V R P T P T R X X E E D R T L D I S I C T E V L A G
R A A S S S **Stop** D D L T L Q L S S F Q V G D I R W R P R R W L **Stop** G G Q R K A G F W E R A A S H G V T V P G R G P
E I R P S D K S Q P Q L P K G N R C Q S A G S K P I **Stop** P R S A L Q C G L P G C P R G S G W T S R V P E Q D Q Q V P H
R L G I H R G L H R **Stop** D V P D E G C A E P **Stop** G R G Q C L H S A T A A D R P G L W Q S S A P G K C P V H R **Stop** L
L P R P Q R S A H R Q

3'5' Frame 1
N W R C A E R C G L G N S H L C T G H L P G A E D C Q S P G R S A A V A E C R H **Stop** P R P **Stop** G S A Q P S S G T S
Y L W S P L C I P S R **Stop** G T C W S C S G T L E V Q P D P R G H P G R P H **Stop** R A D L G Q I G L D P A D W H L F P F
G S **Stop** G **Stop** L L S E G R I S G P R P G T V T P W E A A R S Q N P A F L C P P Q S H L L G L H L **Met** S P T **Stop** K L E
S W R V R S S **Stop** E E E A A R P A R T S V Q **Met** E **Met** S R V L S S X P X R V G V G L T G A P Q A E A R A W R L L G
S R S F S V A G A A G G S E A G R G C R R **Stop** Q Q R S G G T S L P S S E H **Stop** A P A S R F W S L G H P Q P T C Q P A
R W R T G A **Stop** L S P V R T G **Stop**

3'5' Frame 2
I G D V Q S A V A S V I V I C A L G I Y Q G L R I A R V P V D L Q Q W Q N A G I D P V L K V Q H S L H Q A R L T C G A
L C V F R V G E V L A G L A Q V L W K S S Q I L G D T P G D R I E E P I S V K S V W I R L T G T C S L S V V E V D S Y
L R G E F P V L A L E L **Stop** L H G R Q P A P K I Q L S S V R L R A I F L A S I **Stop** C L Q P E N W R A G G **Stop** G H P R
R R R L L V Q P G P L C R W R C Q G S C L P X X C A S V L A **Stop** L E P R R L R P G R G G C W D P G A S Q **Stop** Q G L
R E E V K P G G A A G A D S R G A A E P P S P A L S T K L Q Q A G S G L S V T L S P P A S R H G G E R E L N S P L S G
Q A S

3'5' Frame 3
L A **Met** C R A L W P R **Stop Stop** S S V H W A F T R G **Stop** G L P E S R S I C S S G R **Met** Q A L T P S L R F S T A F I R H
V L P V E P S V Y S E S V R Y L L V L L R Y S G S P A R S S G T P R E T A L K S R S R S N R F G S G **Stop** L A P V P F R
Stop L R L T L I **Stop** G A N F R S S P W N C D S **Met** G G S P L P K S S F P L S A S E P S S W P P S N V S N L K T G E L E
G E V I L G G G G C S S S Q D L C A D G D V K G P V F L X X A R R C W P D W S P A G **Stop** G Q G V A A A G I P E L L
S S R G C G R K **Stop** S R E G L P A L T A E E R R N L P P Q L **Stop** A L S S S K Q V L V S R S P S A H L P A G T V E N G
S L T L P C Q D R L

The highlighted initiation methionine is preceded by a stop codon as expected. Unlike the other frames, the first forward frame is not interrupted by further stop codons.

The THC report (figure 1.2) contains many of the ESTs covered by contig 1(figure 1.1); therefore contig 1 can be represented by the combination of the THC report with the tBLASTn search result for this region (figure 1.4).

Figure 1.4: Contig 1 with 5'UTR

ASLS**Stop**QGRVKLPFSTVPAGRWAEGDRETRTCLLELSAQSWGGRFRRSSAVSAGSPSRLHFLPQPLLLRSSGIPAAATPWP
QPAGLQSGQHRRAXXRKTGPLTSPSAQRSWLDEQPPPPR**M**TSPSSSPVFRLETLDGGQEDGSEADRGKLDFGSGLPP**M**ESQ
FQGEDRKFAPQIRVNLNYRKGTGASQPDPNRFDRDRLFNAVSRGVPEDLAGLPEYLSKTSKYLTDSEYTEGSTGKTCL**M**K
AVLNLKDGVNACILPLLQIIDRDSGNPQPLVNAQCTDDYYRGHSALHIAI

```
Identities = 46/105 (43%), Positives = 68/105 (63%)

Rat VR1:        104 AGEKPPRLYDRRSIFDAVAQSNCQELESLLPFLQRSKKRLTDSEFKDPETGKTCLLKAML 163
                    A + P   +DR  +F+AV++   ++L  L  +L ++ K LTDSE+ +  TGKTCL+KA+L
Contig 1/5UTR: 184 ASQPDPNRFDRDRLFNAVSRGVPEDLAGLPEYLSKTSKYLTDSEYTEGSTGKTCLMKAVL 243

Rat VR1:        164 NLHNGQNDTIALLLDVARKTDSLKQFVNASYTDSYYKGQTALHIAI 209
                    NL +G N  I  LL + R + + +  VNA  TD YY+G +ALHIAI
Contig 1/5UTR: 244 NLKDGVNACILPLLQIDRDSGNPQPLVNAQCTDDYYRGHSALHIAI 289
```

The EST AA236416 (see contig 1, figure 1.1) has not been included, since it did not meet the strict criteria applied for the construction of the THC report. In summary, by combining EST and THC database mining with VR1 as a "probe", a virtual transcript of a gene related to the capsaicin receptor was generated. Notwithstanding this accomplishment, computational cloning methods are prone to errors due to redundancy and low sequencing quality of the EST database. It was therefore necessary to obtain experimental verification for the existence of the virtual transcript.

1.b Cloning of the full length gene using classic PCR and ligations

In order to prove that VR-L is not a computational artefact but it represents an expressed gene, primers were designed based on the contig sequence that would allow the gene amplification with RT-PCR. The alignment of the contigs against the VR1

protein reveals parts of the latter that are not covered by ESTs. The RT-PCR approach would result in filling in these gaps and also offer the experimental validation for the existence of this gene. If the virtual transcript was real, further analysis would be required to examine that it represents a novel member of the vanilloid receptor family.

RNA from Jurkat cells was used, a leukemic T cell line, the tissue source of one cDNA library that gave the positive EST hit AA357145. Primers covering the whole length of the virtual transcript were used (see table 1.2 and appendix 1.6 for their sequence and figure 1.10 for their relative position on the transcript). The Pfu polymerase with proof-reading activity was used, in order to avoid introducing mistakes in the sequence. An initial RT-PCR was performed attempting to ligate contigs 2-4, 3-4, 4-5 and 6-7 (consult figure 1.10 for the primer location and table 1.2 for the expected size of the products. For size of ladders used see appendix 1.7).

Figure 1.5: RT- PCR using Jurkat cells RNA and primers designed from the virtual VR transcript
Lane 1: 100bp ladder
Lane 2: J1-J5 primers product (~740 bp expected)
Lane3: J2-J3 primers product (~270 bp expected)
Lane 4: J1-J3 primers product (~620bp expected)
Lane 5: J2-J5 primers product (~360 bp expected)
Lane 6: J4-J6 primers product (~420 bp expected)
Lane 7: J7-J9 primers product (~260 bp expected)
Lane 8: J7-J10 primers product (~230bp expected)

The size prediction was derived from the relative position of these primers on the contigs and the corresponding position on VR1. With the exception of the last two RT-PCR reactions (lanes 7 and 8), products of the expected size were acquired proving that the virtual transcript represents a real gene. The primers used in the last two reactions were designed from the last two contigs, reflecting the putative 3' end of the gene. Subsequent efforts to repeat the RT-PCR for this region of the gene failed. This failure combined with the fact that the last contig comprises only one EST hit and thus is not very reliable, led to the conclusion that maybe this contig forms part of a different vanilloid receptor gene. Consequently, whereas the rest of the primer pairs successfully traverse along gaps and bridge gene regions covered by different contigs, primers J7, J9, J10 fail to connect contigs 6 and 7, since they probably recognise different genes. As it was proven later with the cloning of human VR1 (Hayes *et al.*, 2000), contig 7 sequence actually represents the C terminus of human VR1 (figure 1.6).

Figure 1.6: Alignment of contig 7 with human VR1

Identities = 63/65 (96%), Positives = 63/65 (96%)

```
Human VR1: 775 SFSLRSSRVSGRHWKNFALVPLLREASARDRQSAQPEEVYLRQFSGSLKPEDAEVFKSPA 834
               SFSLRSSRVSGRHWKNFALVPLLREAS R RQSAQPEEVYLRQFSGSLKPEDAEVFKSPA
Contig 7:  1   SFSLRSSRVSGRHWKNFALVPLLREASXRXRQSAQPEEVYLRQFSGSLKPEDAEVFKSPA 60


Human VR1: 835 ASGEK 839
               ASGEK
Contig 7:  61  ASGEK 65
```

In order to identify the 3' end of the transcript represented by contigs 1-6, the THC reports were once more examined, using AA281348, the most 3' EST from contig 6, as a query. This search resulted in retrieving a promising THC that might contain the C terminus of the virtual transcript (figure 1.7).

Figure 1.7: The THC report using the EST with gb#AA281348 as query. The stop codon is highlighted

HGI THC REPORT: THC 161190

```
TTAGTTAGTGAAAATATATATTTGCCACCAGAATTCACTGGGACCCCAGAGCCAGCAGATGTGGTTGGAAAGATCCTCTGCTCTGTCC
TCTGGCCTCCTGCTGCATCTGGGCCATCAGTTGGACTGGAGGAGCTGGACGGGCACATAGTTTTCCTCAGAGGCACCATCCTCATCCT
CCTTGGGAGGGGAAGCCAGGACAGGGTTCTCGAGAGTTCGAGGGACACCTGCCCCTGACGGGTCCTCACACAGCGTAGGCAGCGTCTG
CTCCCATGAAGCCCAGTTCACCTCCTCCACCCTGAAGCACCAGCGCTCATCGGGGCTGCCATCTGGCTTAGTGCCAACGGTCAGCATC
ACACCTGCCCGCTGCTTCTTCCTGCACCACCAATAGCCATTCTCCATCTCCAGGACAGAGATGGCTTTCTGCAGCTTCCAGATGCTCC
AGCTGTCAGTGGCGACACTGTTGACGGTCTCGCTCATGAGGGCGATGAGCATGTTGAGCAGCAGGATGTAGGTGAGCAGCACGTAGGC
CAGCAGCAGCAGCAGCACCATGCCGCGGAAGTGCAGCTGCTCCTGGAAGGCCAGCTCGCCCATGCCGATGGTGAATTTGAAGAGCTCC
AAGGAGGCTTCCAGGATACCCCTGTACTGGGCCCCGTTGCCCTCGTCCTCCTGTCG
```

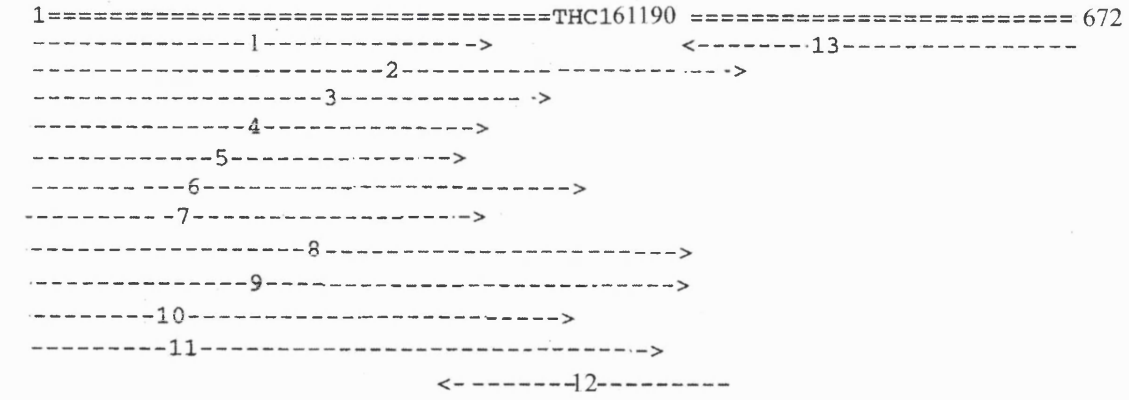

#	Src	EST Id	GB#	Clone	left	right	Library
1	GB	wd88b03.x1	AI912253	IMAGE:2338637	1	364	
2	GB	tx28h02.x1	AI801897	IMAGE:2270931	3	628	NCI_CGAP_Lu24
3	GB	qb96b07.x1	AI126953	IMAGE:1707925	3	370	fetal heart NbHH19W, Soares
4	F	yx53c07.s1	N21284	IMAGE:265452	3	335	melanocyte 2NbHM, Soares
5	F	vx21a11.s1	H99578	IMAGE:262436	3	310	melanocyte 2NbHM, Soares
6	F	zs94g12.r1	AA281348	IMAGE:705190	4	428	Germinal B-cell, Soares NbHTGBC
7	GB	ti37g04.x1	AI433222	IMAGE:2132694	5	337	lymphoma, follicular mixed small and large c
8	GB	ou38h02.s1	AA994465	IMAGE:1628595	7	486	fetal lung, testis, B-cell (Soares NFL T GBC
9	GB	g190c09.x1	AI305201	IMAGE:1879600	7	476	pooled human melanocyte, fetal heart, and p1
10	F	zh80h02.s1	W92818	IMAGE:418419	7	410	fetal liver and spleen 1NFLS S1 subtracted,
11	F	yx83e12.r1	N35179	IMAGE:268366	33	474	melanocyte 2NbHM, Soares
12	T	EST16729	AA304033	HAFAU18	270	529	Aorta endothelial + TNF alpha
13	G	A468F	T12251	A468	453	672	heart

The THC report for this region contains ESTs that comprise contig 6. Therefore contig 6 and THC 161190 can be abridged to one contig. The amino acid sequence of this new contig was derived from the translation of THC 161190 (figure 1.8). By translating the consensus sequence in all frames, the stop codon was identified. As expected, the correct reading frame corresponds to the reading frame of the EST used to search the THC database. New primers were designed from the new contig 6 to amplify the 3'end of the virtual transcript.

Figure 1.8: Translation of contig 6 containing the 3'UTR. The stop codon is highlighted.

5'3' Frame 1
L V S E N I Y L P P E F T G T P E P A D V V G K I L C S V L W P P A A S G P S V G L E E L D G H I V F L R G T I L I L L G
R G S Q D R V L E S S R D T C P **Stop** R V L T Q R R Q R L L P **Stop** S P V H L L H P E A P A L I G A A I W L S A N G Q H
H T C P L L L P A P P I A I L H L Q D R D G F L Q L P D A P A V S G D T V D G L A H E G D E H V E Q Q D V G E Q H V
G Q Q Q Q Q H H A A E V Q L L L E G Q L A H A D G E F E E L Q G G F Q D T P V L G P V A L V L L S

5'3' Frame 2
Stop L V K I Y I C H Q N S L G P Q S Q Q **Met** W L E R S S A L S S G L L L H L G H Q L D W R S W T G T **Stop** F S S E A P
S S S S L G G E A R T G F S R V R G T P A P D G S S H S V G S V C S H E A Q F T S S T L K H Q R S S G L P S G L V P T V
S I T P A R C F F L H H Q **Stop** P F S I S R T E **Met** A F C S F Q **Met** L Q L S V A T L L T V S L **Met** R A **Met** S **Met** L S S R
Met **Stop** V S S T **Stop** A S S S S S T **Met** P R K C S C S W K A S S P **Met** P **Met** V N L K S S K E A S R I P L Y W A P L P S
S S C

5'3' Frame 3
S **Stop** **Stop** K Y I F A T R I H W D P R A S R C G W K D P L L C P L A S C C I W A I S W T G G A G R A H S F P Q R H H P
H P P W E G K P G Q G S R E F E G H L P L T G P H T A **Stop** A A S A P **Met** K P S S P P P P **Stop** S T S A H R G C H L A
Stop C Q R S A S H L P A A S S C T T N S H S P S P G Q R W L S A A S R C S S C Q W R H C **Stop** R S R S **Stop** G R **Stop** A
C **Stop** A A G C R **Stop** A A R R P A A A A A P C R G S A A A P G R P A R P C R W **Stop** I **Stop** R A P R R L P G Y P C T G
P R C P R P P V

3'5' Frame 1
R Q E D E G N G A Q Y R G I L E A S L E L F K F T I G **Met** G E L A F Q E Q L H F R G **Met** V L L L L L A Y V L L T Y I L
L L N **Met** L I A L **Met** S E T V N S V A T D S W S I W K L Q K A I S V L E **Met** E N G Y W W C R K K Q R A G V **Met** L T
V G T K P D G S P D E R W C F R V E E V N W A S W E Q T L P T L C E D P S G A G V P R T L E N P V L A S P P K E D E
D G A S E E N Y V P V Q L L Q S N **Stop** W P R C S R R P E D R A E D L S N H I C W L W G P S E F W W Q I Y I F T N
Stop

3'5' Frame 2
D R R T R A T G P S T G V S W K P P W S S S N S P S A W A S W P S R S S C T S A A W C C C C C W P T C C S P T S C C
S T C S S P S **Stop** A R P S T V S P L T A G A S G S C R K P S L S W R W R **Met** A I G G A G R S S G Q V **Stop** C **Stop** P L A
L S Q **Met** A A P **Met** S A G A S G W R R **Stop** T G L H G S R R C L R C V R T R Q G Q V S L E L S R T L S W L P L P R R
Met R **Met** V P L R K T **Met** C P S S S S S P T D G P D A A G G Q R T E Q R I F P T T S A G S G V P V N S G G K Y I F S L
T

3'5' Frame 3
T G G R G Q R G P V Q G Y P G S L L G A L Q I H H R H G R A G L P G A A A L P R H G A A A A A G L R A A H L H P A
A Q H A H R P H E R D R Q Q C R H **Stop** Q L E H L E A A E S H L C P G D G E W L L V V Q E E A A G R C D A D R W H
Stop A R W Q P R **Stop** A L V L Q G G G G E L G F **Met** G A D A A Y A V **Stop** G P V R G R C P S N S R E P C P G F P S Q
G G **Stop** G W C L **Stop** G K L C A R P A P P V Q L **Met** A Q **Met** Q Q E A R G Q S R G S F Q P H L L A L G S Q **Stop** I L V
A N I Y F H **Stop** L

The right frame is 3'5' frame 1, since it agrees with the translation of the pre-existing contig 6. This is the only frame where the stop codon is not followed by methionines, indicating that it is indeed the stop signal for the gene transcription. The alignment of the THC report with the rat VR1 protein sequence revealed that the former shares 55% a.a. identity with the capsaicin receptor (figure 1.9). This percentage is more promising for

representing a new family member compared to the 70% identity to VR1 exhibited by contig 7.

Figure 1.9: New contig 6 with 3' UTR

RQEDEGNGAQYRGILEASLELFKFTIGMGELAFQEQLHFRGMVLLLLLAYVLLTYILLLNMLIALMSETVNSVATDSWSIW
KLQKAISVLEMENGYWWCRKKQRAGVMLTVGTKPDGSPDERWCFRVEEVNWASWEQTLPTLCEDPSGAGVPRTLENPV
LASPPKEDEDGASEENYVPVQLLQSN**Stop**WPRCSRRPEDRAEDLSNHICWLWGPSEFWWQIYIFTN**Stop**

Identities = 83/150 (55%), Positives = 104/150 (69%), Gaps = 2/150 (1%)

```
Rat VR1:        624 GNSYNSLYSTCLELFKFTIGMGDLEFTENYDFKAVFIILLLAYVILTYILLLNMLIALMG 683
                    G  Y  +    LELFKFTIGMG+L F E   F+ + ++LLLAYV+LTYILLLNMLIALM
Contig 6/3UTR: 8    GAQYRGILEASLELFKFTIGMGELAFQEQLHFRGMVLLLLLAYVLLTYILLLNMLIALMS 67

Rat VR1:        684 ETVNKIAQESKNIWKLQRAITILDTEKSFLKCMRKAFRSGKLLQVGFTPDGKDDYRWCFR 743
                    ETVN +A +S +IWKLQ+AI++L+ E  +  C RK  R+G +L VG  PDG  D RWCFR
Contig 6/3UTR: 68   ETVNSVATDSWSIWKLQKAISVLEMENGYWWC-RKKQRAGVMLTVGTKPDGSPDERWCFR 126

Rat VR1:        744 VDEVNWTTWNTNVGIINEDPGNCEGVKRTL 773
                    V+EVNW +W   +  + EDP    GV RTL
Contig 6/3UTR: 127  VEEVNWASWEQTLPTLCEDPSGA-GVPRTL 155
```

Once putative 5' and 3' ends of the virtual gene have been identified, more primers were designed to carry out the RT-PCR (table 1.2). The primer sequence and their position on the contigs can be seen below in figure 1.10 (for the exact primer location on EST sequences, refer to appendix 1.6).

Table 1.2: Primers used for cloning human VR-L fragments (for the exact position of these primers on the EST sequences, please refer to appendix 1.6)

Primer name	Direction on VR1	EST or THC corresponding to primer	Relation to the rat VR1 sequence (a.a. No.)	Primer Sequence (5' to 3')
J1	forward	W44731	248	GGT GAG CTA CCC CTC TCT TTG
J2	forward	AA357145	364	CAC CTT TCC CGA AAG TTC ACC
J3	reverse	N24224	455	AGG CTG ATG GTA GGC AAC AGC
J4	forward	N24224	477	CCA CAT CCT TAT CCT GCT AG
J5	reverse	N24224	484	CTA GCA GGA TAA GGA TGT GG
J6	reverse	W92895	618	CAA GGA GGC TTC CAG GAT ACC
J7	forward	AA281348	746	GAG GTG AAC TGG GCT TCA TGG
J8	reverse	AA281348	752	CCA TGA AGC CCA GTT CAC CTC
J9	reverse	AA321554	839	TCA CTT CTC CCC GGA AGC GGC AG
J10	reverse	AA321554	829	GAA GAC CTC AGC GTC CTC TGG
J11	reverse	W44731	263	CAC ATC CCA CTG CTT GGT GCA
J12	reverse	H21490	149	TGT GTA TTC CGA GTC GGT GAG
J13	forward	H20025	113	ACC GAG ATC GGC TCT TCA ATG
J14	reverse	(THC161190)	3' UTR (47 bp from stop)	GAA AGA TCC TCT GCT CTG TCC
J15	reverse	(THC161190)	3' UTR (30 bp from stop)	GTC CTC TGG CCT CCT GCT GCA
J16	reverse	(THC161190)	Stop codon	TCA GTT GGA CTG GAG GAG CTG
J17	forward	W92895	583	GAA GCT CCT ACA GGC CCC AAT G
UTR	forward	(THC176254)	5' UTR (165 bp 5' of Met)	TGC TAC TGA GAA GCT CCG GGA TCC
Met	forward	H49128	(deduced by walking through THC)	ATG ACC TCA CCC TCC AGC TCT CCA

Figure 1.10: Representation of the VR1 sequence covered by the contigs and the relative position of the primers designed for RT-PCR. The red numbers represent the contigs. The blue lines indicate the relative position of enzymes used in the cloning of the full length gene (cDNA).

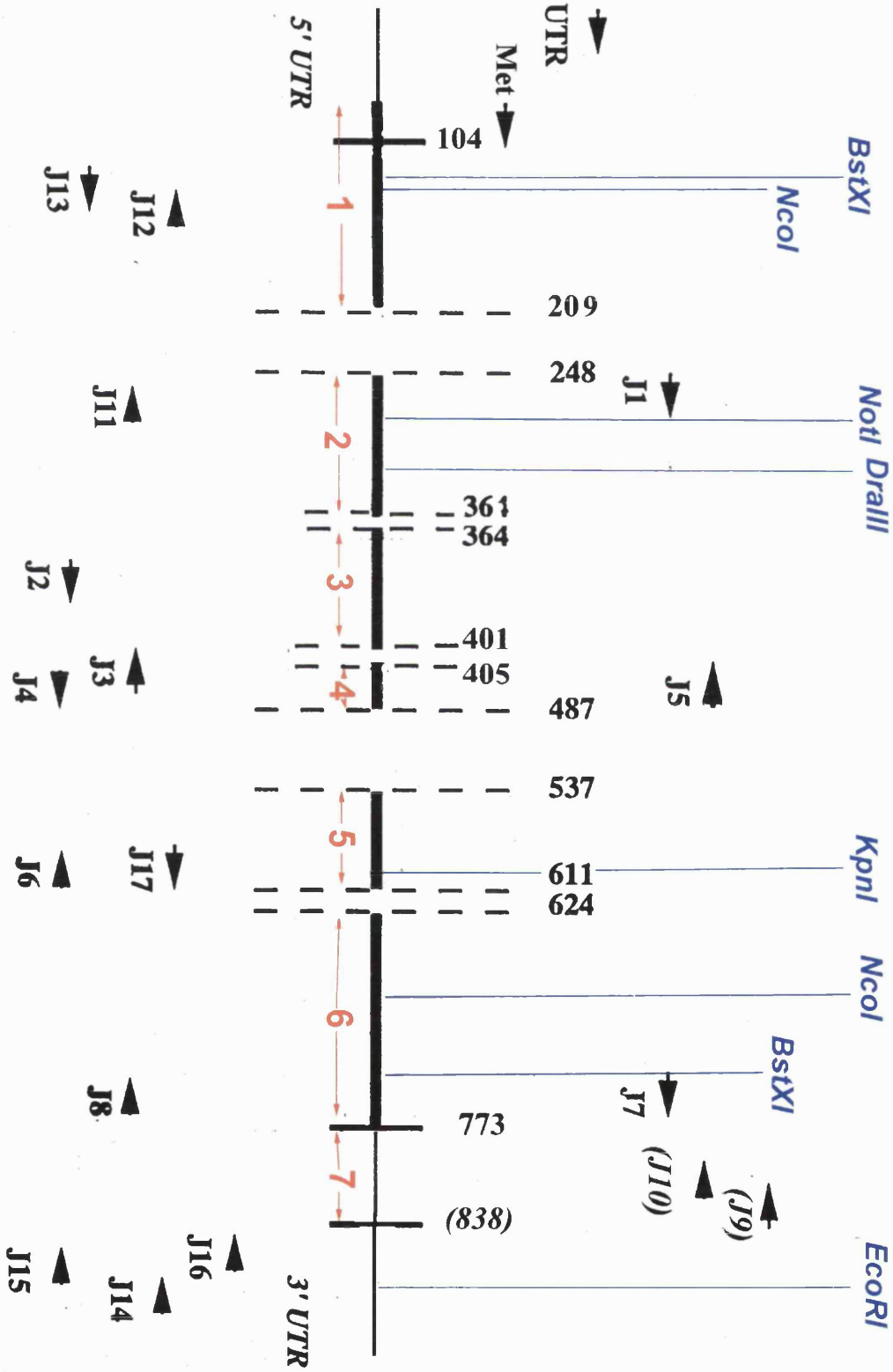

To prove that the primers recognise the same gene and to obtain larger gene fragments, the following PCR was carried out, using Jurkat cells cDNA as the template.

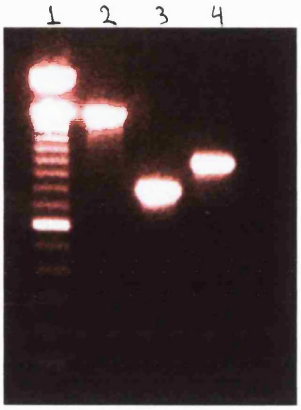

Figure 1.11: PCR reactions interconnecting the 5'end of the virtual transcript with contig 4, contig 4 with contig 5, contig 4 with the 3'end of the transcript.

Lane 1: 100bp ladder
Lane 2: UTR-J5 primers product (expected size ~1494bp)
Lane 3: J2-J6 primers product (expected size ~762bp)
Lane 4: J4-J14 primers product (expected size ~ 1044bp)

To exclude the likelihood that the above PCR bands represent different members of a possible VR family in Jurkat cells, the products UTR-J5, J2-J6 and J4-J14 were purified from the gel and used as templates for splicing by overlap PCR (figure 1.12). In this method templates with an overlapping region are used, aiming at the primers to extend over that region and amplify products that constitute of the "ligated" templates.

Figure 1.12: The principle of splicing by overlap extension

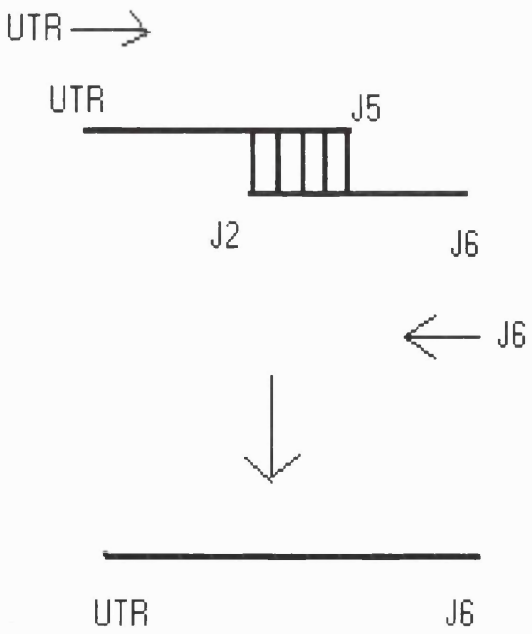

Figure 1.13 shows the PCR products that resulted from attempting to connect the 5'UTR region with contig 5 and contig 3 with the 3'UTR

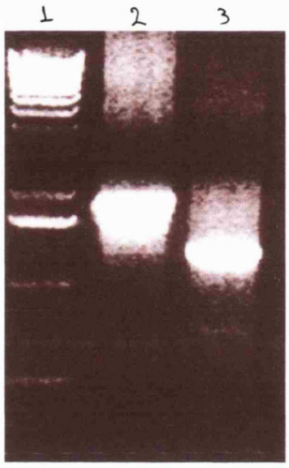

Figure 1.13: PCR reaction amplifying the region between 5' UTR and contig 5 (lane 2) and between contig 3 and the 3' UTR (lane 3).

Lane 1: 1kb ladder
Lane 2: UTR-J6 product (templates UTR-J5, J2-J6, expected size ~2100bp)
Lane 3: J2-J14 product (templates J2-J6, J4-J14 expected size ~1000bp)

Products of approximately the expected sizes were amplified (consult figure 1.10 and table 1.2). The PCR was carried out using Pfu polymerase that has proof-reading activity and thus high copying fidelity, but results in blunt ended products. Half a unit of Taq polymerase was used in the last extension step to add adenine overhangs on the 3' end of the PCR products and make subcloning into T-vector possible (vector with T overhangs on either side of the multiple cloning site). The PCR products were glass milk purified from the gel and ligated to T vector to facilitate detailed sequencing of the gene (for sequencing reports and restriction maps refer to appendix 1.3 and appendix 1.4 respectively). The ligations were transformed into bacteria and colonies were picked to perform DNA mini preparations. Examples of such DNA digestions are shown below (for size prediction please refer to figure 1.10 and appendix 1.4).

Figure 1.14: Digestion of UTR-J6 in T vector with EcoRI
Lane 1: 1kb ladder
Lane 2: digestion with EcoRI (expected band sizes ~3kb vector, 1.9kb insert)

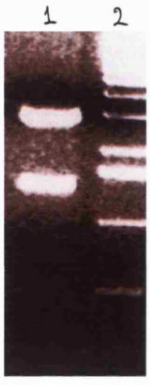

Figure 1.15: Digestion of J2-J14 in T vector with EcoRI
Lane 1: digested with EcoRI (expected band sizes ~3kb vector, 1.3kb insert)
Lane 2: 1kb ladder

The T vector is 3kb long; it can be cut with DraIII at position 2.6kb and it contains NcoI and BstXI in the multiple cloning site (appendix 1.2). According to the restriction enzyme maps (table 1.2, figure 1.10, appendix 1.4), the enzyme NcoI can digest the insert J2-J14 in two products of size 760bp and 610bp, whereas digestion with enzyme BstXI should yield products of about 850bp and 520bp size. A double digestion of the UTR-J6 PCR product with NcoI and DraIII should result in 4 bands of size 280bp, 880bp, 740bp and 60bp approximately. Taking this information into account and the fact that the PCR products can be inserted into the T vector in either orientation, mini DNA preparations of ligated PCR products in T vector were subjected to diagnostic digestions (figure 1.16).

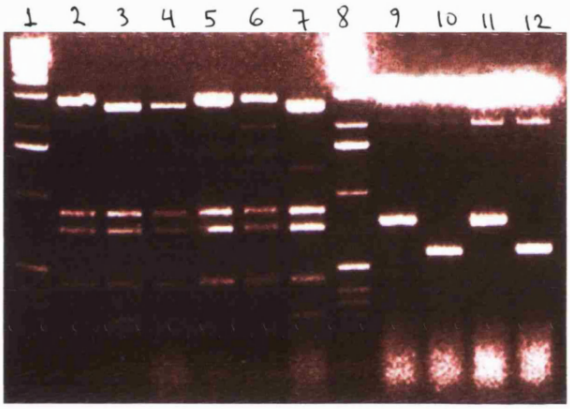

Figure 1.16: Digestion of clones containing T vector cloned PCR fragments.
Lanes 1and 8: 1kb ladder
Lanes 2-7: T vector with UTR-J6 fragment clones digested with NcoI and DraIII (predicted sizes depending on orientation ~2.8kb, 0.8kb, 07kb, 0.3kb or 2.6kb, 0,8kb, 0.7kb, 0.5kb)
Lanes 9 and 11: T vector with J2-J14 fragment clones digested with NcoI (sizes expected ~ 3.6kb and 0.7kb or 3.7kb and 0.6kb)
Lanes 10 and 12: T vector with J2-J14 fragment clones digested with BstXI (sizes expected 3.8kb and 0.5kb or 3.5kb or 0.8kb)

Note: additional bands close to the linearised vector are uncut plasmid.

The fragments UTR-J6 and J2-J14 cover the virtual transcript from the 5'UTR to the 3'UTR. Since they contain an overlapping region, they could be ligated together in a common restriction enzyme site, resulting in the full gene sequence (figure 1.17).

Figure 1.17: Subcloning strategy to obtain the full length transcript

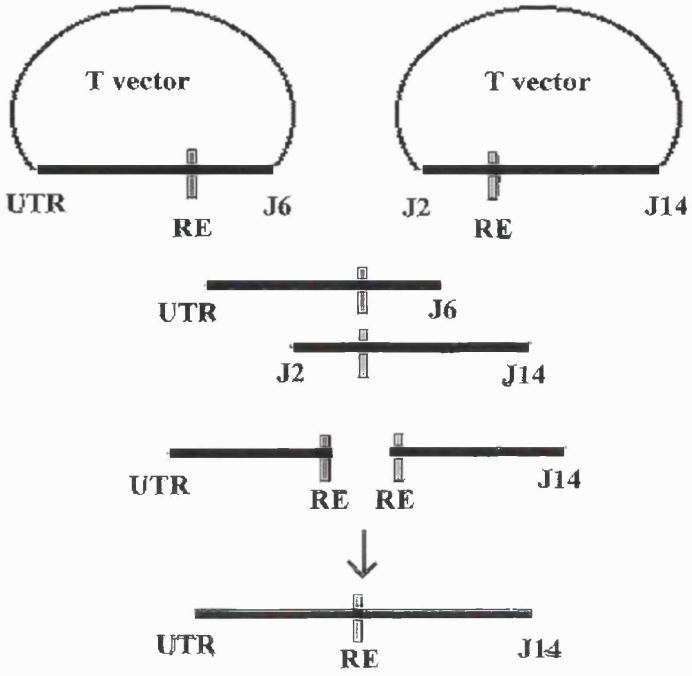

According to the sequencing information (appendix 1.4 and figure 1.10), NotI may cut the UTR-J6 sequence about 750bp after the beginning of the UTR primer, whereas EcoRI should not cut the fragment. KpnI should cut UTR-J6 at 1.6kb and J2-J14 at 0.5kb after the beginning of the sequence. KpnI does not cut the T vector. The enzymes NotI and EcoRI, by being on each side of the multiple cloning site, should splice the insert out of the vector. The enzymes EcoRI and KpnI as rare 6bp cutters, Not I a 8bp cutter and DraIII a 9bp cutter would be ideal enzymes to use for ligating UTR-J6 and J2-J14 together. To test that they cut as predicted, the following digestions were carried out (figure 1.18).

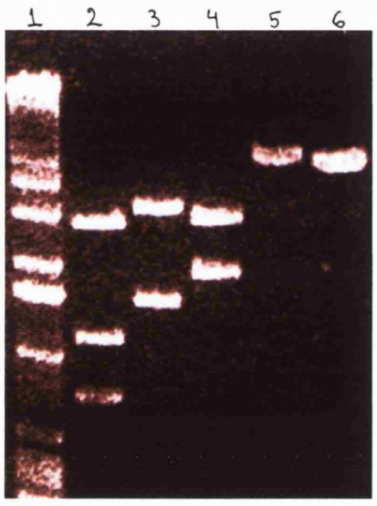

Figure 1.18: Diagnostic digestions for identification of enzymes to be used for subcloning
Lane 1: 1kb ladder
Lane 2: UTR-J6 in T vector cut with NotI (expected bands ~ 3kb, 1.2kb, 0.7kb)
Lane 3: UTR-J6 in T vector cut with DraIII (expected bands ~ 3.4kn and 1.4kb or 3.7kb and 1.1kb)
Lane 4: UTR-J6 in T vector cut with EcoRI (expected bands ~ 3kb and 1.9kb)
Lane 5: UTR-J6 in T vector cut with KpnI (expected band ~ 4.9kb)
Lane 6: J2-J14 in T vector cut with KpnI (expected band ~ 4.3kb)

Unfortunately, as it was predicted NotI could not be used to extract the two inserts out of the T vector (as it cut the PCR product internally too) and ligate them together in the common DraIII or KpnI site. On the other hand, the EcoRI enzyme was suitable, since it does not digest within the inserts. Since DraIII also cuts within the vector, the common KpnI site can be used to ligate the two inserts together, as seen in figure 1.19.

Figure 1.19: Subcloning strategy using the enzymes KpnI and EcoRI

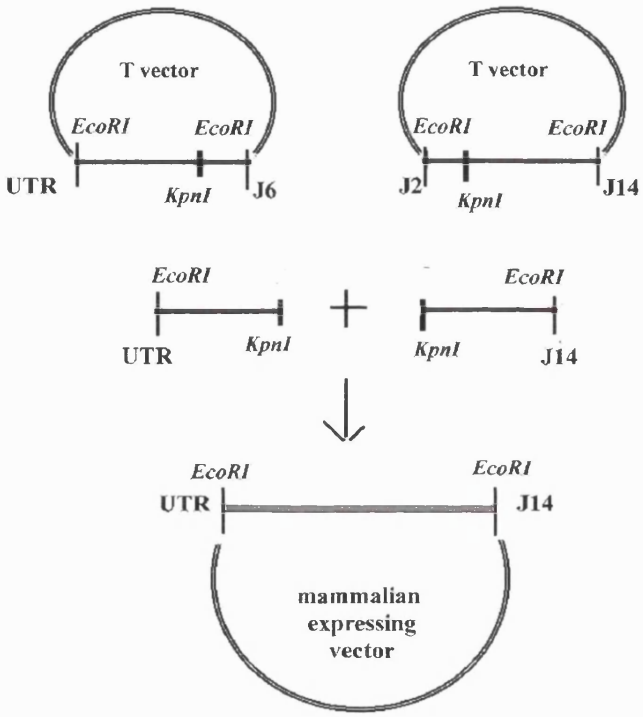

The T vector cloned PCR fragments UTR-J6 and J2-J14 were double digested with KpnI and EcoRI (figure 1.20). For product size prediction consult figure 1.10 and appendix 1.4

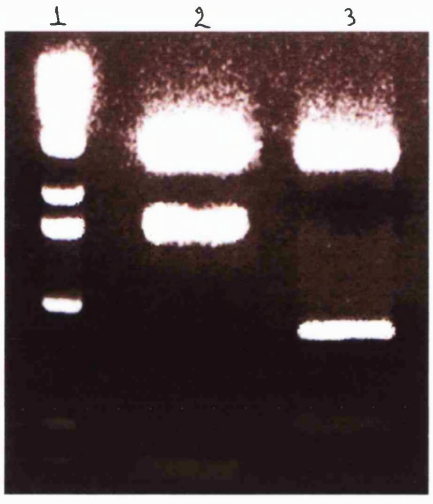

Figure 1.20: Double digestions of UTR-J6 and J2-J14

Lane 1: 1 kb ladder
Lane 2: UTR-J6 cut with KpnI and EcoRI (expected bands ~ 3kb, 1.6kb and 0.3kb)
Lane 3: J2-J14 cut with KpnI and EcoRI (expected bands ~ 3kb, 0.8kb and 0.5kb)

The 1.6kb and 0.8kb bands were purified from the gel to be ligated into the EcoRI digested mammalian expression vector pcDNA3 (figure 1.21. For a map of pcDNA3 refer to appendix 1.8).

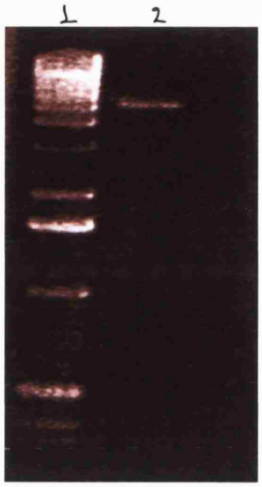

Figure 1.21: Digestion of the pcDNA3 vector.
Lane 1: 1kb ladder
Ladder 2: EcoRI linearised pcDNA3 (expected size: 5.4kb)

The linearised vector was excised from the gel and glass milk purified. Subsequently it was dephosphorylated to avoid recircularisation of the plasmid during ligation. A three way ligation was attempted, where one segment, consisting of the two PCR fragments ligated in the common KpnI site, would then be ligated into the pcDNA3 vector via its EcoRI overhangs. The ligation was transformed in bacterial cells and colonies were picked to perform mini DNA preparations.

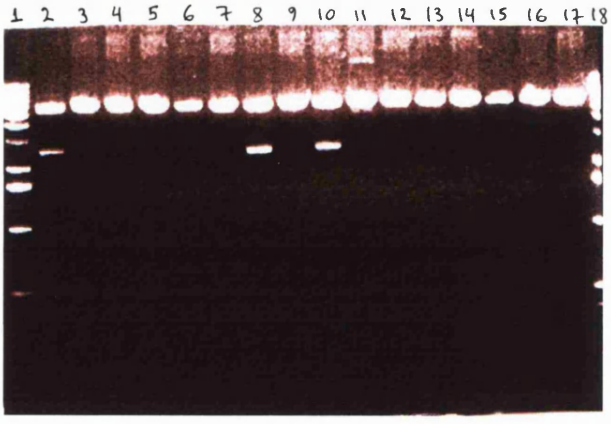

Figure 1.22: EcoRI digested DNA mini preparations of colonies containing the putative UTR-J14 fragment cloned into pcDNA3.
Lanes 1 and 18: 1kb ladder
Lanes 2-17: mini-preps of putative UTR-J14 in pcDNA3 digested with EcoRI. (bands expected: ~5.4kb and 2.4kb)

Only the DNA mini preparations in lanes 2, 8 and 10 contain the full length gene that is possibly a new member of the vanilloid receptor family. The rest of the DNA digestions seem to be of vectors that had circularised without taking an insert in, possibly due to insufficient dephosphorylation. The insert containing EcoRI overhangs on both ends

could have been ligated into the vector in two orientations. In order to ascertain the clone(s) with the correct orientation of insert, a digestion with KpnI was carried out (figure 1.23), since both the insert and the vector can be cut with this enzyme. If the insert is in the correct orientation, the products of the digestion should be two bands of 6.2kb and 1.6kb. Digestion of an insert in the opposite orientation would result in two bands of 7kb and 0.8kb.

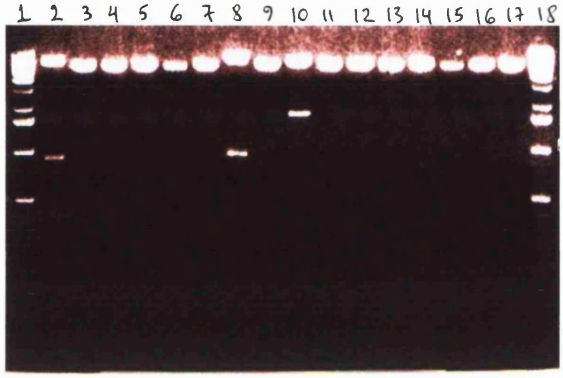

Figure 1.23: KpnI digested DNA mini preparations of colonies containing the putative UTR-J14 fragment cloned into pcDNA3.
Lanes 1 and 18: 1kb ladder
Lanes 2-17: mini-preps of putative UTR-J14 in pcDNA3 digested with KpnI.

Only the clone in lane 10 gave the right digestion products, indicating that it contains the insert in a 5'-3' orientation. Therefore, by using the information derived from the EST assembly a possible vanilloid related gene was amplified using a classic RT-PCR approach.

1.c Cloning of the full length gene using splicing by overlap

In parallel to the classic RT-PCR approach coupled to ligations, an alternative method was also used to obtain a full length clone in order to confirm the results. The method of splicing by overlap (figure 1.12) was deployed, where the PCR fragments UTR-J6 and J2-J14 (figure 1.13) were used as templates and the primers UTR and J14 to perform a PCR. It was hoped that the primers would keep extending over the region of overlap, amplifying the whole gene. Figure 1.24 shows the PCR results.

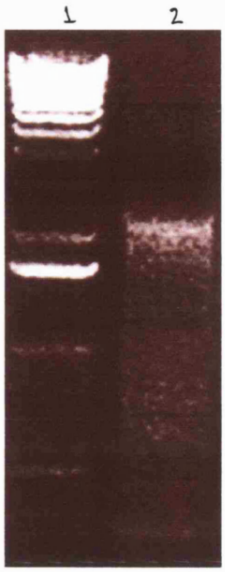

Figure 1.24: Cloning the full length gene with splicing by overlap
Lane 1: 1kb ladder
Lane 2: the PCR product using UTR-J6, J2-J14 as templates and UTR. J14 as primers.

In order to establish that the UTR-J14 PCR product is indeed the full length gene, a diagnostic double digestion was done using the enzymes NcoI and DraIII. DraIII should cut at 1.1kb after the beginning of the sequence, whereas NcoI should cut at 0.3kb and 1.9kb (refer to figure 1.10 and appendix 1.4). Therefore, digestion of the correct PCR product should result in 4 bands of sizes 0.9kb, 0.75kb, 0.6kb and 0.2kb approximately (figure 1.25).

Figure 1.25: Diagnostic digestion of the UTR-J14 PCR product
Line 1: 1kb ladder
Lane 2: UTR-J14 PCR product digested with NcoI and DraIII

The correct bands appeared on the gel, except for the 0.2kb band, which was probably too weak to be visualised. The full length gene was named Vanilloid Receptor-like Protein (VR-L), as it was found to share 49% a.a. identity with the rat VR1 (see figure 1.26 for alignment with VR1), indicating that this gene is a new member of the vanilloid receptor family and not a human homologue of VR1.

Figure 1.26: Alignment of rat VR1 with human VR-L. Identities are highlighted in red colour. Conservative substitutions are indicated with blue colour. The dashes represent gaps introduced to maximise the alignment and not gaps that exist in the sequences.

```
humanVRL    1 ----------------------MTSPSSSP------------VFRLETLDGGQEDGSEADR
ratVR1      1 MEQRASLDSEESESPPQENSCLDPPDRDPNCKPPPVKPHIFTTRSRTRLFGKGDSEEASP

humanVRL   28 GKLDFGSG-----LPPMESQFQGEDRKFASQIRVNLNYRKGTGASQPDPNRFDRDRLFNA
ratVR1     61 LDCPYEEGGLASCPIITVSSVLTIQRPGDGPASVRPSSQDSVSAGEKPPRLYDRRSIFDA

humanVRL   83 VSRGVPEDLAGLPEYLSKTSKYLTDSEYTEGSTGKTCLMKAVLNLKDGVNACILPLLQID
ratVR1    121 VAQSNCQELESLLPFLQRSKKRLTDSEFKDPETGKTCLLKAMLNLHNGQNDTIALLLDVA

humanVRL  143 RDSGNPQPLVNAQCTDDYYRGHSALHIAIEKRSLQCVKLLVENGANVHARACGRFFQKGQ
ratVR1    181 RKTDSLKQFVNASYTDSYYKGQTALHIAIERRNMTLVTLLVENGADVQAAANGDFFKKTK

humanVRL  203 G-TCFYFGELPLSLAACTKQWDVVSYLLENPHQPASLQATDSQGNTVLHALVMISDNSAE
ratVR1    241 GRPGFYFGELPLSLAACTNQLAIVKFLLQNSWQPADISARDSVGNTVLHALVEVADNTVD

humanVRL  262 NIALVTSMYDGLLQAGARLCPTVQLEDIRNLQDLTPLKLAAKEGKIEIFRHILQREFSG-
ratVR1    301 NTKFVTSMYNEILILGAKLHPTLKLEEITNRKGLTPLALAASSGKIGVLAYILQREIHEP

humanVRL  321 -LSHLSRKFTEWCYGPVRVSLYDLASVDSCEENSVLEIIAFH-CKSPHRHRMVVLEPLNK
ratVR1    361 ECRHLSRKFTEWAYGPVHSSLYDLSCIDTCEKNSVLEVIAYSSSETPNRHDMLLVEPLNR

humanVRL  379 LLQAKWDLLIP-KFFLNFLCNLIYMFIFTAVAYHQPTLKKQAAPHLKAEVGNSMLLTGHI
ratVR1    421 LLQDKWDRFVKRIFYFNFFVYCLYMIIFTAAAYYRP-VEGLPPYKLKNTVGDYFRVTGEI

humanVRL  438 LILLGGIYLLVGQLWYFWRRHVFIWISFIDSYFEILFLFQALLTVVSQVLCFLAIEWYLP
ratVR1    480 LSVSGGVYFFFRGIQYFLQRRPSLKSLFVDSYSEILFFVQSLFMLVSVVLYFSQRKEYVA

humanVRL  498 LLVSALVLGWLNLLYYTRGFQHTGIYSVMIQKVILRDLVRFLVIYLVFLFGFAVALVSLS
ratVR1    540 SMVFSLAMGWTNMLYYTRGFQQMGIYAVMIEKMILRDLCRFMFVYLVFLFGFSTAVVTLI

humanVRL  558 QEAWRPEAPTGPNATESVQPMEGQEDEGNGAQYRGILEASLELFKFTIGMGELAFQEQLH
ratVR1    600 EDGKNNSLP-----MESTPHKCRGSACKPGNSYNSLYSTCLELFKFTIGMGDLEFTENYD

humanVRL  618 FRGMVLLLLLAYVLLTYILLLNMLIALMSETVNSVATDSWSIWKLQKAIXVLEMENGYWW
ratVR1    655 FKAVFIILLLAYVILTYILLLNMLIALMGETVNKIAQESKNIWKLQRAITILDTEKSFLK

humanVRL  678 CR-KKQRAGVMLTVGTKPDGSPDERWCFRVEEVNWASWEQTLPTLCEDP-----------
ratVR1    715 CMRKAFRSGKLLQVGFTPDGKDDYRWCFRVDEVNWTTWNTNVGIINEDPGNCEGVKRTLS

humanVRL  726 --------SGAGVPRTLENPVLASPPKEDEDGASEENYVPVQLLQSN-------------
ratVR1    775 FSLRSGRVSGRNWKNFALVPLLRDASTRDRHATQQEEVQLKHYTGSLKPEDAEVFKDSMV

humanVRL      ----
ratVR1    835 PGEK
```

In summary, a new member of the vanilloid receptor family was cloned by applying computational nucleotide database mining and by acquiring experimental confirmation for the existence of the transcript via RT-PCR. In order to assert the protein identity it was necessary to obtain some preliminary information on the protein structure. This data would substantiate that VR-L is a member of the vanilloid protein family.

1.d Secondary structure and protein pattern predictions

Further computational analysis followed in order to investigate whether VR-L shares any common characteristics with VR1 on the level of protein secondary structure. The secondary structure of the protein was predicted computationally using the programme TopPred2 with the default parameters, run by the Institut Pasteur (http://bioweb.pasteur.fr/seqanal/interfaces/toppred.html).

Figure 1.27: Representation of the TopPred2 results

Helix	Begin (amino acid number on VR-L)	End (amino acid number on VR-L)	Score	Certainty
1	201	221	0.751	Putative
2	391	411	1.719	Certain
3	429	449	1.781	Certain
4	472	492	1.640	Certain
5	495	515	1.401	Certain
6	538	558	2.331	Certain
7	620	640	2.117	Certain

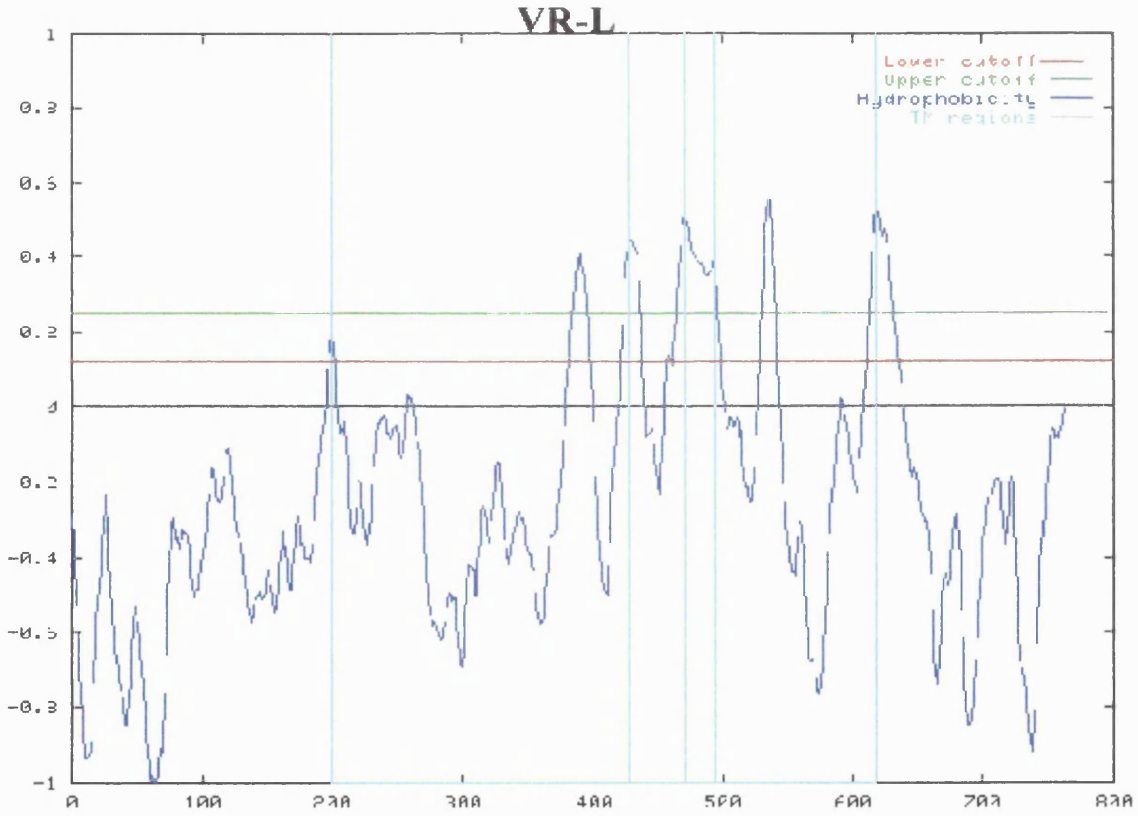

Comparison of this data with the predicted structure of transient receptor potential channels (Chapter3) and results run by the programme TMPred

(http://www.ch.embnet.org/ software/TMPRED_form.html) curated by the European Molecular Biology Network, suggests the existence of 6 transmembrane domains, with the N and C termini being intracellular. A pattern search at EBI (http://www2.ebi.ac.uk/ ppsearch/) revealed a possible Asn glycosylation site at amino acid position 570 and many myristoylation sites important for membrane attachment (positions 18, 63, 130, 201, 272, 592, 685, 729). Other features of interest include cAMP and cGMP dependent protein kinase phosphorylation sites (positions 61 and 326), PKC phosphorylation sites (positions 101, 115, 325, 414), tyrosine kinase phosphorylation sites (positions 106, 223 and 329) and a leucine zipper pattern (positions 532-553), important for protein dimerisation and DNA binding. The existence of the phosphorylation sites implies possible changes in the ion channel properties (e.g. by PKC) with functional implications and the transmission of cell signals through the receptor (e.g. via tyrosine kinase phosphorylation).

The Pfam programme (Protein families database of alignments and Hidden Markov Models) at the Sanger centre (http://www.sanger.ac.uk/Software/ Pfam/) was deployed to identify patterns of interest. The programme compares the query sequence with models derived from aligned protein families that might represent conserved domains of functional significance. Ankyrin-like repeats were identified at positions 162-194, 208-243 and 293-326. Ankyrin repeats are sequences of about 33 amino acids that appear successively in at least four copies. They have a helix-loop-helix structure, important in mediating protein-protein interactions e.g. with the cytoskeleton or the cell membrane. Finally the region 441-645 amino acids was identified as ion transporter protein signature. Members of this family of proteins have 6 transmembrane helices, as already predicted by the hydrophilicity plot for VR-L. The last two helices form a loop, which is important for the ion selectivity. This information is summarised in figure 1.28.

Figure 1.28: The VR-L protein sequence. The transmembrane domains are shown as bold, red, underlined letters. The ankyrin-like repeats are highlighted in yellow. The PKC phosphorylation sites are indicated in light blue, the cAMP-cGMP phosphorylation sites in green and the tyrosine kinase phosphorylation sites in pink. The putative pore loop is shown in bold Italics.

MTSPSSSPVFRLETLDGGQEDGSEADRGKLDFGSGLPPMESQFQGEDRKFASQIRVNLNYRKGT
GASQPDPNRFDRDRLFNAVSRGVPEDLAGLPEYLSKTSKYLTDSEYTEGSTGKTCLMKAVLNLK
DGVNACILPLLQIDRDSGNPQPLVNAQCTDDYYRGHSALHIAIEKRSLQCVKLLVENGANVHAR
ACGRFFQKGQGTCFYFGELPLSLAACTKQWDVVSYLLENPHQPASLQATDSQGNTVLHALVMI
SDNSAENIALVTSMYDGLLQAGARLCPTVQLEDIRNLQDLTPLKLAAKEGKIEIFRHILQREFSGL
SHLSRKFTEWCYGPVRVSLYDLASVDSCEENSVLEIIAFHCKSPHRHRMVVLEPLNKLLQAKWD
LLIPKFFLNFLCNLIYMFIFTAVAYHQPTLKKQAAPHLKAEVGNSMLLTGHILI
LLGGIYLLVGQLWYFWRRHVFIWISFIDSYFEILFLFQALLTVVSQVLCFLAIEWYLPLLVSA
LVLGWLNLLYYTRGFQHTGIYSVMIQKVILRDLVRFLVIYLVFLFGFAVALVSLSQEAWRP
EAPTGPNATESVQPMEGQEDEGN*GAQYRGILEASLELFKFTIGMG*ELAFQEQLHFRGMVLLL
LLAYVLLTYILLLNMLIALMSETVNSVATDSWSIWKLQKAISVLEMENGYWWCRKKQRAG
VMLTVGTKPDGSPDERWCFRVEEVNWASWEQTLPTLCEDPSGAGVPRTLENPVLASPPKEDED
GASEENYVPVQLLQSN

1.e VR-L is a member of the Transient Receptor Potential family

A tBLASTn search of the GenBank database reveals that VR-L, like VR1, is very similar to the transient receptor potential channels. On average it shares 20% identity with this family (for an alignment with TRP channels, refer to appendix 1.5). These calcium channels were first discovered as mutants of the phototransduction system in *Drosophila.* Most of them are activated by depletion of intracellular Ca^{2+} stores (for more information on TRP channels, refer to Chapter 3).

The phylogenetic tree prediction programme at http://www.genebee.msu.su constructed a phylogenetic tree by aligning the VRs protein sequences against known TRP protein sequences. The programme runs two algorithms; one topological that focuses on the way the tree nodes connect with each other and a cluster algorithm, where the order of the node connections and the branch lengths reveal the distance among the compared proteins (figure 1.29). Both algorithms revealed the same relationship between VR-L and the rest members of the vanilloid receptor family. The phylogenetic trees show the association of VR-L with TRP channels and particularly a close link with VR-1 and OSM-9. The latter is a *Caenorhabditis elegans* channel involved in olfaction and mechanosensation.

Figure 1.29: Phylogenetic trees of the Transient Receptor Potential superfamily of ion channels

CLUSTER ALGORITHM

TOPOLOGICAL ALGORITHM

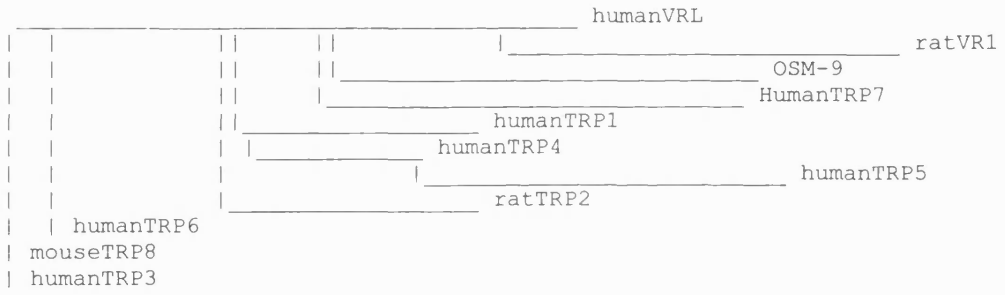

Figure 1.30: Predicted secondary structure of the VR-L protein

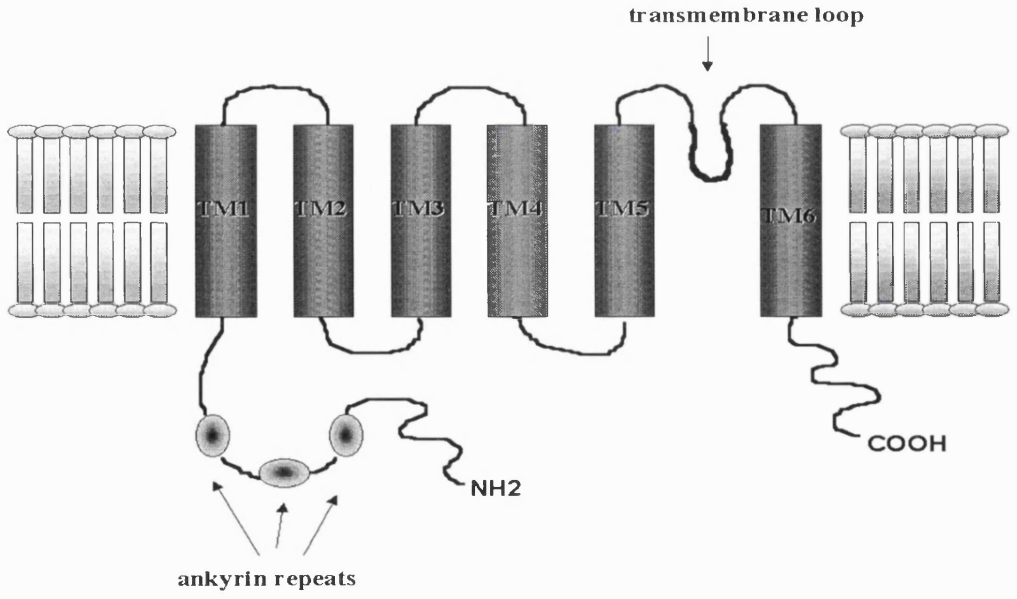

The computational analysis of the secondary structure of VR-L revealed a clear correlation with the TRP family of receptors. VR-L exhibits the same structure (figure 1.30) of 6 transmembrane domains with a putative pore loop between domains 5 and 6. The predicted structure and the protein patterns found in VR-L indicate that the *in silico* cloning method was successful in identifying a new member of the vanilloid family of proteins (Garcia *et al.*, 1999). Although the computation analysis offers a few hints on the function of this receptor, it was necessary to establish experimentally the role of this protein and its possible participation in the pain perception processes.

CHAPTER 1

In silico cloning of VR-L, a new member of the vanilloid receptor family

DISCUSSION

The *in silico* cloning strategy: its merits and its problems

The cloning of the capsaicin receptor opened new possibilities in the field of pain perception and alleviation. Undoubtedly, it also offered an invaluable tool in the pursuit for new members of the vanilloid receptor family. In this chapter the cloning of a new vanilloid-like receptor is described by utilising the VR1 protein sequence and a computational cloning approach. The dbEST division in GenBank was used containing Expressed Sequence Tags (ESTs), which are 5' and 3' sequences of cDNAs and thus they represent expressed genes. The EST sequencing data constituted the source from which the new vanilloid receptor sequence was retrieved by applying a computational screening method called tBLASTn. This is an algorithm that compares the query protein sequence (VR1 in this case) with the conceptual translation of the annotated genome database GenBank and attempts to identify regions of alignment. By analogy to performing a hybridisation screen of a cDNA library, where one sets the stringency parameters, the stringency of the tBLASTn search can be adjusted. The algorithm assigns scores to the comparisons performed according to how good the alignment is. Misalignments and substitution penalties are scored. The substitution penalties are allocated according to a score system (matrix) that has been calculated by comparing members of a known family of proteins. Choosing the degree of identity among the protein family members that give rise to the scoring system is one of the tBLASTn parameters. Choosing a low degree of identity will set up a low stringency search that might reveal distantly related proteins but also allows room for false positives by allowing mismatches due to sequencing errors. In the VR1 search the default setting of 62% a.a. identity was selected, which is neither too lax nor too limiting. Another parameter is the probability by which the calculated score of a comparison can occur in the database. The probability 0 represents perfectly aligned sequences. In order to avoid "background noise" by picking VR1 in the database, only the entries with probability $P<10^{-5}$ were selected. Values such as this have been found optimal through test BLAST searches (Huminiecki and Bicknell, 2000).

The aim of the tBLASTn search was to identify ESTs that when assembled together would unveil a new member of the vanilloid receptor family. In order to avoid the formation of chimeras, ESTs from the same species were selected. 26 human entries were retrieved, most of which were overlapping and as a result they formed a virtual transcript aligning to the VR1 amino acid positions 95 to 838. The novel transcript was named VR-L for Vanilloid Receptor-like Protein. Since ESTs are only partial

sequences, it was inevitable that gaps appeared in the transcript. The overlapping ESTs were grouped into contigs and primers were designed from their sequence in order to bridge the gaps using PCR.

The last contig (number 7) consisted of only one entry representing the 3' end of the virtual transcript. PCRs attempting to connect the last two contigs (6 and 7) failed, indicating the possibility the two contigs did not form part of the same transcript. An alternative method was deployed using the tentative human consensus sequences database (THCs) of the Institute of Genome Research (TIGR). These sequences comprise aligned ESTs clustered together under strict criteria to avoid the formation of chimeras and as a result each THC report probably represents a unique gene. The requirement of 40 bases minimum overlap for two ESTs to be linked results in forming clusters in a manner similar to the gene walking method. The THC database was screened using the most 3' EST, hoping that it would be part of a cluster containing the stop codon of the virtual transcript. The cluster identified diverted from the one suggested by contig 7.

As it was revealed later with the cloning of VR1 homologues, contig 7 represented the human homologue of VR1 (cloned by Hayes *et al.,* 2000). This is one of the most common caveats occurring in *in silico* cloning that results from the compromise one has to make when setting the search stringency. Relatively low stringency results in picking gene homologues, but setting the stringency higher might result in missing an overall closely related gene as VR-L is to VR1. Despite the wealth of information contained in the nucleotide sequence databases the analytical tools are in need of further sophistication in order to avoid computation artefacts. During electronic analysis one should exercise caution in interpreting the EST data. In the case of VR-L, the absence of other ESTs overlapping with EST AA321554 in contig 7 was a good indication for this EST's invalidity. The 3' end of VR-L diverged so extensively from VR1 that the tBLASTn search missed the relative EST entries. On the contrary the THC reports following an assimilated gene walking method had assembled a cluster representing VR-L's C terminus containing the right ESTs. An algorithm often used to identify distant protein relatives is the **P**osition-**S**pecific **I**terative BLAST (PSI-BLAST). Results of the initial BLAST search are used to build a profile, which is applied in subsequent BLAST searches. As a result the profile is refined in each cycle, identifying small regions of similarity that are probably conserved domains. In the case of VR-L, the PSI-

BLAST would not be the appropriate algorithm to use because VR-L is overall close to VR1 with the exemption of the C terminus.

In the absence of ESTs covering the N terminus, the THC strategy was deployed one more time to identify a relative cluster. Following the completion of this search, the contigs identified covered the residues 104-773 of the VR1 amino acid sequence. Linking the contigs with PCR using cDNA from a human T cell line proved that the virtual transcript represents a real gene. The PCR products were collated with conventional ligations and by using the PCR method of "splicing by overlap", where overlapping templates are interconnected by primer extension over the common region. This offered further proof that the PCR products constitute part of the same gene. The resulting product named Vanilloid Receptor-like Protein (VR-L) was found to share 49% identity with the rat VR1 and about 20% identity with the TRP family of receptors. Like the rest members of this superfamily, VR-L has the same topological structure of 6 transmembrane domains with a loop region between the last two domains and the N and C termini located intracellularly. A computational search for protein patterns revealed that VR-L like VR1 contains phosphorylation sites. The PKC and tyrosine kinase phosphorylation sites are of particular interest because they present the possibility of VR-L being regulated by neurotrophic factors and activated by PKC phosphorylation like VR1. An immunohistochemical analysis of VR-L's location in DRG could provide further clues to which neurotrophins might regulate its function as well as to what its function might be.

In summary, despite the risks *in silico* cloning presents, a new member of the vanilloid receptor family was successfully cloned by using this method. Because the poor EST sequence quality and annotation can lead to computational artefacts, the data generated by *in silico* cloning methods require critical interpretation to ensure they are biologically meaningful. Nevertheless, the virtual cloning methods are more rapid and provide a useful alternative to the traditional cloning approaches, especially when the source of RNA is hard to obtain e.g. human DRG. This advantage and the increasing wealth of electronically deposited genomic information will undoubtedly lead to the development of sophisticated software that will shorten the gene discovery procedure even further and will allow scientists to concentrate on the functional analysis of the genome.

Alternative computational cloning strategies

The expansion of nucleotide sequence databases due to genome projects around the world and the development of new biologically orientated software led to the increasing appearance of *in silico* gene cloning reports presenting ingenuous strategies for database mining. Prigent *et al.* (1999) described the cloning of Aik2, a protein kinase related to Drosophila Aurora using the ESTBlast tool. In this method the query sequence is blasted against the EST dataset. One can specify the tissue source of the ESTs to be searched, offering an advantage in tissue specific gene searches. The high scoring ESTs are selected that are subsequently aligned to be assembled in contigs. The resulting consensus sequence is then re-blasted against the database. This reciprocal process continues until the consensus sequence has been extended as far as possible, hoping to reveal the full length gene (figure 1).

Figure 1: The principle of the ESTBlast tool. The query sequence (1) is used to retrieve partially homologous ESTs (2 & 3) that are assembled into contigs (4). The consensus sequence (5) created is used to retrieve further ESTs that will extend the virtual transcript (6). (From www.hgmp.mrc.ac.uk/ESTblast/Tutorial/externalTUT.html)

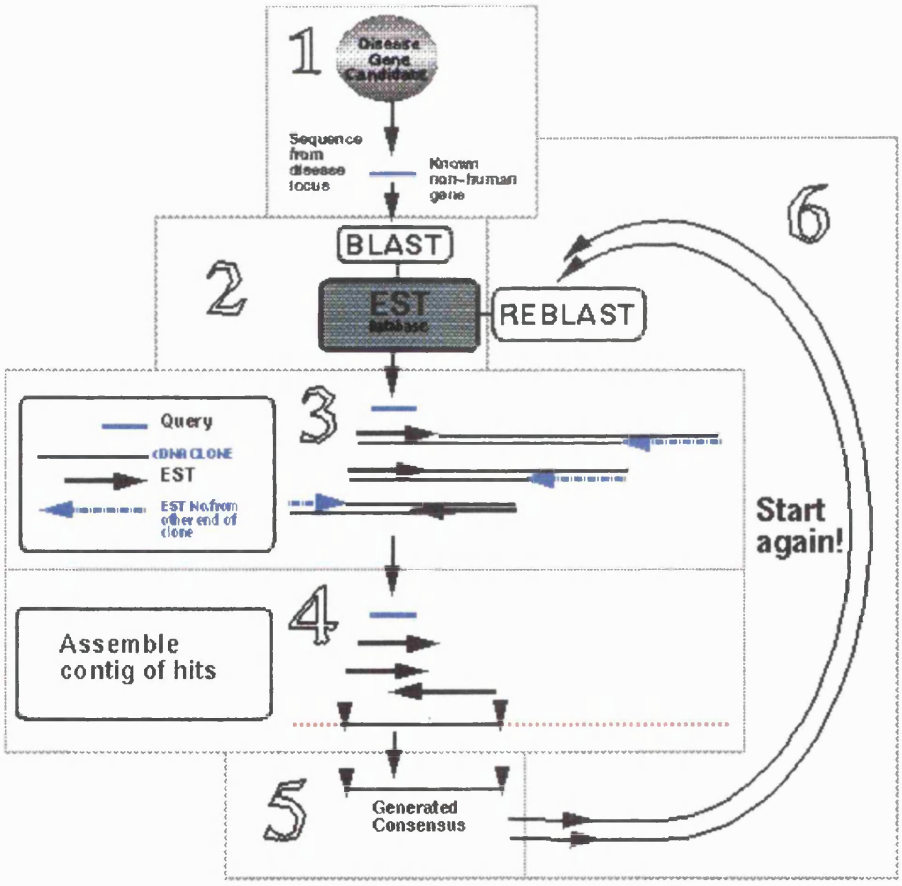

This process is similar to the database curating method followed by the Institute of Genome Research that generates the Tentative Human Consensus (THC) reports. The

advantage of following this procedure is that one does not have to rely on the completion of the human gene reports created by TIGR, as it can be applied to any nucleotide database, setting parameters specific to the experimental purposes.

Vasmatzis *et al.* (1998) simulated subtractive cDNA library construction in order to clone prostate specific genes. A dbEST search specifying the organism and tissue source was conducted to identify human ESTs that contained the acronym "prost". The generated file was blasted against all human ESTs in GenBank in high stringency. This search resulted in retrieving ESTs with high identity to the query sequences. These entries corresponding to each query EST were segregated in two groups: hits in prostate ESTs and hits in non-prostate ESTs. The latter list was used to attach a specificity index to each query EST. If an EST was represented by many hits in the non-prostate group it was attached a low specificity index, indicating that it represents a gene that is not specifically expressed in the prostate. The prostate ESTs were clustered into contigs and their specificity index was considered. Only the highly specific clusters were selected. RNA hybridisation with probes designed from the prostate EST clusters confirmed the expression of seven novel transcripts in this tissue. Huminiecki and Bicknell (2000) took advantage of a library subtraction web-based tool called SAGEmap xProfiler to compare EST pools from endothelial libraries and EST pools from non-endothelial libraries in order to identify novel endothelial specific genes. Schultz *et al.* (2000) used the tBLASTn search in association with a domain identification protocol in the SMART database, which contains signalling domains. Following a clustering method similar to Vasmatzis *et al.* (1998), the search predicted the existence of about a thousand new signalling proteins that awaits experimental validation.

The EST database is accelerating the discovery pace of new genes. Nevertheless, it should be pointed out that computational cloning cannot replace molecular biology, at least at this stage, but it offers a complementary approach to identifying new transcripts. The versatility of nucleotide sequence databases has been exploited to serve molecular biology not only in the discovery of new genes but also in detecting gene homologues, in predicting alternative splicing, gene polymorphisms and intron-exon boundaries as well as locating genes in chromosomal segments (reviewed by Pandley and Lewitter, 1999). Nevertheless, the computational predictions become meaningful only when they acquire experimental validation. For that reason it was necessary to investigate the regulation of expression and the functional role of VR-L in DRG.

CHAPTER 2

Investigating the functional role of VR-L

INTRODUCTION

IDENTIFICATION OF NEW MEMBERS OF THE VANILLOID FAMILY OF RECEPTORS

The cloning of the capsaicin receptor triggered an extensive search for other vanilloid receptors that might respond to capsaicin. Identification of other capsaicin-sensitive channels could account for the vanilloid responses observed *in vivo,* which do not conform totally to the pharmacological profile of VR1. A variety of cloning techniques was implemented and an increasing number of new members of the vanilloid family of receptors emerged. In the previous chapter the cloning of VR-L using bioinformatics methods was described. Useful insights into the putative function of VR-L might be provided by the function of other vanilloid related channels. For a summary of the new VR members cloned please refer to table 1.

OSM-9, an olfactory and mechanosensitive channel in *Caenorhabditis elegans*

C.elegans possesses two olfactory neurons designated AWA and AWC. The former uses G-protein coupled receptors for its signal transduction, while the latter mediates its responses via cyclic nucleotide-gated channels. Mutants were identified (Colbert *et al.,* 1997) that exhibited defective AWA odorant responses and normal AWC responses but with profound desensitisation. Nose-touch was also found to be defective as well as responses to osmotic changes, which are regulated by other sensory neurons. The gene responsible for these mutations was named *osm-9* and was found to have a secondary structure reminiscent of TRP channels, with 6 transmembrane domains and ankyrin repeats at the N terminus. It shares 27% amino acid identity with VR1. Although the gene is similar to a TRP homologue in *C.elegans*, it was not found to co-localise with it. The identification of *osm-9* serving such a divergent role from VR1, but overall sharing the same function i.e. the avoidance of noxious stimuli (osmotic, volatile and mechanical in the worm; heat, protons, capsaicin in vertebrates), provided strong evidence for the existence of other VR-like proteins.

VR.5'sv, an N-terminal splice variant of VR1

Schumacher *et al.* (2000a) screened a cDNA library constructed from adult rat DRG and trigeminal ganglia with a probe designed from the VR1 sequence. They identified a gene named VR.5'sv that diverges from VR1 in the N and C termini and shares 88%a.a. identity with the capsaicin receptor. In particular its sequence shares extensive stretches of identity with VR1 with a truncated intracellular N terminus, an in frame deletion corresponding to nucleotides 1121-1301 of VR1 and an additional 575bp sequence at its

C terminus. 5'-RACE reactions beginning from a common point in the VR1 and VR.5'sv sequences identified only VR1 and VR.5'sv in rat DRG, confirming the existence of two diverse genes. RT-PCR studies identified the expression of VR.5'sv in rat DRG, brain and peripheral blood mononuclear cells. Electrophysiological studies showed that this gene does not confer capsaicin, heat or proton sensitivity to host cells.

SIC, a stretch-inactivated channel

Suzuki *et al.* (1999) cloned a VR1 splice variant channel that is inhibited by stretch. Initially they performed degenerate PCR with primers based on the VR1 sequence. Northern blot analysis using the transcribed PCR product as a probe revealed its expression in liver and kidney. By performing RACE on a kidney cDNA library they cloned the full length cDNA, which was revealed to differ from VR1 on the C terminus while it lacked the N terminus and contained only one ankyrin repeat. On the protein level, it shares 90% a.a. identity with VR1. Electrophysiological studies showed that the channel's elicited inward currents and conductance were increased by exposure to hypertonic solution (causing cell shrinkage) and decreased by hypotonicity. These characteristics suggest the channel to be mechanosensitive and hence it was named stretch-inhibitable channel (SIC). Schumacher *et al.* (2000b) based on the fact that hypertonic stimuli are painful, examined the expression of SIC in sensory tissues. SIC expression was identified in small diameter DRG neurons and trigeminal ganglia.

VR-OAC, an osmotically activated channel

Liedtke *et al.* (2000) used EST sequences homologous to *osm9* and VR1 to screen a rat kidney library. They also screened a chicken inner ear library and a mouse hypothalamic library with probes generated from VR1 and *osm9* sequences. The search resulted in the identification of a novel gene in different species. The new gene is structurally similar to VR1 with 6 transmembrane domains, 3 ankyrin repeats and intracellular N and C termini and shares 51% a.a. identity with VR1 at the protein level. It is expressed in lung, kidney, spleen, testis and fat. *In situ* hybridisation revealed its expression in the brain, mainly in the circumventricular organs that lack the blood-brain barrier, in the median preoptic area that has been associated with the release of antidiuretic hormone and the choroid plexus that senses the pressure of the cerebrospinal fluid. It has also been found expressed in the inner ear and the large, mechanosensory trigeminal ganglia. The new channel was named vanilloid receptor-related osmotically activated channel (VR-OAC) and was found to be gated by

hypotonic conditions. VR1 agonists failed to activate the channel. Electrophysiological studies revealed that the channel allows an inward Ca^{2+} current in host cells, which triggers the release of Ca^{2+} from intracellular stores. Depolarisation or influx of other ions did not elicit the characteristic VR-OAC response, which shows that the initial Ca^{2+} entry is necessary in triggering release of intracellular Ca^{2+}.

Strotmann *et al.* (2000) cloned the same gene, which they named OTRP4. Additionally to the information presented by Liedtke *et al.* (2000) the Strotmann group also indicated that VR-OAC/OTRP4 is not excited by signals triggered by PLC activation. The channel activation did not lead to changes in cell volume. Like Liedtke, they reported the presence of extracellular calcium to be necessary in the channel activation, which agrees with the observation that regulation of cell volume under hypotonic conditions depends on extracellular Ca^{2+}.

VRL-2, an orphan vanilloid-like receptor

Delany *et al.* (2001) reported the cloning of VRL-2 from human kidney using bioinformatics tools. The novel vanilloid-like receptor shares 46% a.a. identity with the VR1 protein and is expressed in the epithelial cells of the trachea, kidney and salivary glands. At lower levels, it is also expressed in the brain, skeletal muscle, pancreas, prostate and bone marrow. Immunocytochemistry showed that it is not expressed in DRG neurons, but is prevalent in sympathetic and parasympathetic nerves. The secondary structure of the protein is similar to VR1 with 3 ankyrin repeats and 6 transmembrane domains. Heat, capsaicin and protons failed to activate the receptor.

ECaC, an epithelial calcium channel that participates in the trans-cellular Ca^{2+} transport in kidney cells

Hoenderop *et al.* (1999a) identified ECaC, an epithelial calcium channel, by injecting *Xenopus* oocytes with cRNA from a rabbit kidney library and monitoring $^{45}Ca^{2+}$ uptake. The identified clone is sharing 31% a.a. identity with VR1 and has a similar predicted topological structure. Northern blot analysis showed that ECaC is expressed in the small intestine, kidney and placenta and immunocytochemistry demonstrated its co-localisation with calbindin, a calcium-binding protein, in these tissues. Electrophysiological studies showed that ECaC functions as a calcium channel that is not blocked by L-type calcium channel antagonists or divalent cations that block voltage-gated calcium channels. Transepithelial calcium transport is important in regulating calcium homeostasis in the body, as the dietary calcium that is not absorbed by the intestinal tract or excreted in

urine is reabsorbed by kidney epithelial cells. The excess Ca^{2+} first crosses the apical membrane passively and then it binds to 1,25-dihydroxyvitamin D_3 dependent calcium-binding proteins (calbindins). Subsequently, the protein-calcium complex diffuses across the cytoplasm to the opposite side, where the Ca^{2+} is transported to a neighbouring cell via an ATPase and a Na^+-Ca^{2+} exchanger. The localisation of the ECaC protein and its pharmacological profile suggest that this channel participates in transepithelial Ca^{2+} transport. In support of this postulation, reducing the pH of the extracellular medium to 5.9 blocked the calcium current in ECaC injected oocytes, which can explain the hypercalciuria observed in patients with metabolic acidosis. Additionally, Hoenderop *et al.* (1999b) reported that ECaC is activated by hyperpolarisation, which is in agreement with previous findings that showed hyperpolarisation to activate Ca^{2+} influx in kidney epithelial cells. The current elicited is inward and Ca^{2+} selective. ECaC seems to possess a self-regulatory mechanism, as it does not allow Ca^{2+} influx in the presence of excess ion concentrations.

CaT1, a channel-like transporter that regulates Ca^{2+} influx in enterocytes

Peng *et al.* (1999) reported the cloning of CaT1, a transporter that mediates Ca^{2+} absorption in the gastrointestinal tract. They identified a clone from a rat duodenal cDNA library that induced $^{45}Ca^{2+}$ uptake in *Xenopus laevis* oocytes. The novel protein shares 31% identity with VR1. Unlike ECaC, CaT1 has 4 ankyrin repeats and different phosphorylation sites. Although it shares 75% amino acid identity with ECaC the N- and C-termini are distinctively different. CaT1 is expressed in small intestine, brain, thymus and adrenal gland. No signal was detected in the kidney where ECaC is expressed. The highest CaT1 signals were detected in the cecum, which is the site with the highest trans-cellular Ca^{2+} transfer in the rat intestine. The CaT1 expression was unaltered by 1,25 dihydroxyvitamin D_3 and calcium deficiency *in vivo*. Expression in *Xenopus* oocytes in the presence of Ca^{2+} showed the channel to elicit an inward current that constitutes of Ca^{2+} and monovalent cations and is voltage-dependent. Capsaicin or depletion of intracellular Ca^{2+} stores did not affect the current. Inability to record single channel conductance led to the hypothesis that CaT1 is a transporter and not a channel. Ca^{2+} seems to regulate CaT1 through a feedback mechanism, as prolonged exposure to Ca^{2+} blocks its permeation through the transporter. CaT1 showed higher

activity at alkaline pH, which might explain the hypercalcemia observed in peptic ulcer patients treated with antacids.

CaT-L, a Ca^{2+} transporter with a potential role in cell transformation

Wissenbach *et al.* (2001) cloned CaT-L by screening a placenta cDNA library using a TRP-like EST as a probe. CaT-L exhibits different tissue distribution from CaT1 and is 31% a.a. identical to the VR1 protein. It is expressed in placenta, pancreas, and salivary glands but not in kidney or the small intestine. Although CaT-L is not expressed in healthy prostate cells, it was detected in this tissue in a cancerous state during metastasis, indicating its possible role in cell transformation. Interestingly *trp-p8*, a trp-like channel (Tsavaler *et al.*, 2001), is over-expressed in prostate carcinomas and moderately expressed in other primary cancers. On the contrary, the expression of melastatin, a newly cloned TRP-like channel with 21% a.a. identity to VR1, is downregulated in metastatic melanomas (Duncan *et al.*, 1998). CaT-L is a constitutively open calcium channel. When its activity is recorded in response to hyperpolarisation, it shows a rapid and a slow inactivation, which prompted researchers (Niemeyer *et al.*, 2001) to investigate the existence of a possible feedback mechanism regulated by Ca^{2+}. Such a mechanism exists in other ion channels and it involves calmodulin, which binds to Ca^{2+} and inactivates further influx of the ion. The slow CaT-L inactivation was found to be calmodulin dependent. In high Ca^{2+} concentrations, calmodulin binds to CaT-L and inactivates the channel. This binding can be prevented by PKC phosphorylation of the channel, as the phosphorylation site lies within the calmodulin-binding site. CaT1 and ECaC contain a calmodulin-binding site but lack the phosphorylation site within, indicating that only CaT-L possesses this elegant mechanism for regulating the channel activity.

TRP12, a constitutively open channel expressed in kidney that might be osmotically regulated

Wissenbach *et al.* (2000) used bioinformatics tools to clone a vanilloid-related protein from mouse and human, that they named TRP12. The novel protein contains 6 transmembrane domains, 6 ankyrin-like repeats and shares 50% a.a. identity with VR1. The C terminus of TRP12 is highly similar to the SIC channel, while the latter shares the same N terminus as VR1. These similarities suggested that the three genes might be different splice variants of one gene. Northern blot analysis revealed a strong TRP12 signal in kidney, while fewer transcripts were identified in heart, brain, liver,

fibroblasts, aortic endothelial and epididymis cells. Heterologously expressed TRP12 seemed to express a constitutively open Ca^{2+} channel. Capsaicin, hypertonicity and depletion of intracellular Ca^{2+} stores had no effect on the channel, while decreasing the osmolarity of the extracellular medium resulted in elevating the Ca^{2+} current in 50% of transfected CHO and HEK cells. The possibility that the host cells variably express factors that regulate TRP12's response to hypotonicity needs to be investigated.

Investigating the VR-L function

The cloning of the capsaicin receptor led to the identification of more related proteins. Nevertheless, none of the novel proteins conferred capsaicin sensitivity to host cells. On the contrary, the new vanilloid-like channels exhibited a variety of phenotypes ranging from mechanosensation to sensing osmolarity changes and regulating Ca^{2+} transport. In the previous chapter the cloning of VR-L, another vanilloid related gene was described. VR-L shares 49% amino acid identity with VR1 and secondary structure analysis revealed that the two genes share the same topological structure. It is interesting to investigate whether VR-L is activated by vanilloids or by stimuli that trigger other members of the TRP family. Prior to investigating VR-L's function, it is necessary to study its tissue distribution, since it can provide useful clues to its function. Because VR-L's structure bears the signature of calcium channels, electrophysiological methods will be deployed to inquire into its function. Additionally, since the channel sequence contains many phosphorylation sites, it is important to examine whether VR-L's expression and function are under cellular control.

Table 1: Summary of new members of the vanilloid family of receptors

Name	%a.a. identity to VR1	Function
OSM-9	27	Olfanction, mechanosensation
VR.5'sv	88	Orphan
SIC	90	Activated in hypertonic conditions
VR-OAC	51	Activated in hypotonic conditions
VRL-2	46	Orphan
ECaC	31	Activated by hyperpolarisation, involved in Ca^{2+} transport in epithelial cells
CaT1	31	Probably a Ca^{2+} transporter involved in Ca^{2+} influx in enterocytes
CaT-L	21	Calmodulin-regulated Ca^{2+} transporter, important for cell differentiation
TRP12	50	Maybe mechanosensitive

CHAPTER 2

Investigating the functional role of VR-L

MATERIALS & METHODS

In addition to techniques described in Chapter 1, the following techniques were also used to perform the experiments described in this chapter.

2.1 Manufacturing Taq polymerase

Considering the number of PCR experiments that needed to be carried out, we decided it would be more cost effective to produce Taq polymerase in the lab. The only exception to the Taq used for the PCR reactions for the experiment described in section 2.5, where Pfu polymerase was deployed. A pTK1 plasmid encoding the full length Taq gene was utilised to express the enzyme in bacteria. All the materials used were purchased from Sigma unless stated differently.

The following solutions were prepared:

SUPERBROTH: 3.2% (w/v) tryptone, 2% (w/v) yeast extract, 0.5% (w/v) NaCl, adjusted to pH 7

SOLUTION A: 50mM Tris HCl pH7.9, 50mM dextrose, 1mM EDTA

SOLUTION B: 10mM Tris HCl, pH 7.9, 50mM KCl, 1mM EDTA, 0.5% (w/v) Tween 20, 0.5% (v/v) NP40

STORAGE BUFFER: 20mM Tris HCl pH8, 100mM KCl 1mM EDTA, 1mM DTT, 50% (v/v) glycerol, 0.5% (v/v) Tween 20, 0.5% (v/v) NP40

The following were also prepared or purchased: 0.1M IPTG, 50mg/ml kanamycin, LB plates with 50 μg/ml kanamycin, saturated ammonium sulphate, lysozyme in powder form, 30kDa and 300kDa cut-off filters from Millipore.

DAY 1

1) XL1 blue bacterial cells were transformed with the plasmid pTK1 (kanamycin resistant plasmid).

DAY 2

2) A colony was picked and was inoculated in a culture of 10ml Superbroth with 50 μg/ml kanamycin overnight at 37^0 C.

DAY 3

3) The starter culture was poured into 250ml of Superbroth with 50 μg/ml kanamycin and was left to grow at 37^0 C until OD600= 0.3-0.5.
4) IPTG was added to a final concentration of 2mM and the culture was left to grow 16-20 hours at 37^0 C until OD600~2.

DAY 4

From this point on all steps were carried out at 4^0 C.

5) The cells were centrifuged in a 250ml bottle (15min at 3.5K) and then the supernatant was discarded.
6) The bacterial pellet was resuspended in 10ml of solution A. 30mg lysozyme was mixed in by swirling to break the bacterial cell walls.
7) The solution was allowed to mix for 15min at room temperature and subsequently 10ml of solution B was added.
8) The solution was mixed well and was left to incubate in a 80^0C waterbath for 1 hour.
9) The solution was centrifuged at 12,000 rpm for 30min at 4^0 C and then the supernatant was filtered through a cotton plug.
10) An equal volume of saturated ammonium sulphate was added and vortexed in order to precipitate the proteins.
11) The solution was centrifuged at 12,000 rpm for 30min at 4^0 C and the liquid was discarded (the pellet and the floating precipitate were kept).
12) The pellet was washed with 20ml of 50% saturated ammonium sulphate in 20mM Tris HCl pH 8. The solution was centrifuged again and as much liquid as possible was removed.
13) The precipitate was resuspended in 3ml solution B and transferred in two 1.5ml eppendorf tubes.
14) The tubes were centrifuged at 14,000 rpm for 30min to remove any insoluble material (or longer if necessary) and the supernatant was transferred to a 15ml tube. Each pellet was washed again with another 1ml solution B and centrifuged to remove any insoluble material. All the supernatants were pooled together in the15ml tube.
15) The supernatant was poured in a 300kDa cut-off centricon filter and spun down at 4.5K at 4^0 C for 3 hours (or longer if necessary). The eluate was retained. The retentate was washed with 2ml solution B and spun down again. This eluate was retained as well.

DAY 5

16) The eluate was poured in a 30kDa cut-off filter and spun down at 4^0 C. The eluate was discarded. The final retentate was washed twice with 1.5ml solution B and was finally spun down to >200ul.
17) The retentate was resuspended with 2ml storage buffer that has been pre-equilibrated at -20C.

18) The Taq polymerase preparation was stored at -20°C in aliquots. In order to estimate the concentration of the enzyme a test PCR was carried out that compared the intensity of the signal with that obtained with a Taq of known concentration.

2.2 Primer sequences

The following primers (ordered from Sigma-Genosys) were used for PCR reactions in this chapter:

Cyclophilin- anneal. temp. 55-60^{0}C

Forward primer (5'-3'): ACCCCACCGTGTTCTTCGAC

Reverse primer (3'-5'): CATTTGCCATGGACAAGATG

CGRP (calcitonin gene related peptide) – anneal.temp. 55^{0}C

Forward primer (5'-3'): GGTGTGGTGAAGGACAAC

Reverse primer (3'-5'): CATAGGGAGAAGGGTTTC

VR1 (300bp product as seen in figure 2.8) - anneal.temp. 60^{0}C

Forward primer (5'-3'): GAACTCCTGCCTGGACCCTCC

Reverse primer (3'-5'): CATAGAGCCTCGGGGGCTTCTC

VR1 (400bp product as seen in figure 2.9)- anneal.temp. 60^{0}C

Forward primer (5'-3'): GATCGCAGGAGCATCTTCGAT

Reverse primer (3'-5'): CACCAAAGTAGAAGCCAGGCCT

VR-L (300bp product as seen in figure 2.2)- anneal.temp. 60^{0}C

Forward primer (5'-3'): TTTGCTGTAGCCCTAGTAAGC

Reverse primer (3'-5'): GACGTAGGTGAGGAGGACGTA

VR-L (400bp product as seen in figure 2.11)- anneal.temp. 60^{0}C

Forward primer (5'-3'): CTTTCAGGCTGGAGACTTCC

Reverse primer (3'-5'): TTGTCAATCTGCAGCAGCGGCATG

Primers for sequencing (anneal.temp. 50^{0}C):

T7: TAATACGACTCACTATAGGG

Sp6: ATTTAGGTGACACTATAGAA

Primers used for the insertion of the c-myc epitope in an extracellular loop of VR-L (the highlighted sequences indicate the epitope sequence. The PCR was performed at anneal.temp. 62^{0}C):

Primer A: GGCCACATTCTGATCCTGCTTG

Primer B:

AAGATCTTCCTCTGAGATGAGCTTTTGTTCATCTTCAGGGGCTTTGGGACTTC
G

Primer C:

GAACAAAAGCTCATCTCAGAGGAAGATCTTAACAACTCCACAGTGACGGAA
CAGCCC

Primer D: CTCAGATAAGGTGGGAAGAGTCTTC

2.3 Dorsal root ganglia culture

Coating of 35mm dishes

The 35mm dishes on which DRG cells were plated were coated with poly-lysine (Sigma), a polymer that can improve cohesion of the cells onto the dish. Poly-lysine was diluted in sterile distilled water to a final concentration of 10 µg/ml. Subsequently, 1ml solution was loaded on each 35mm dish to be coated and was left for 1 hour under the hood. The solution was then removed and the dishes were washed three times with sterile distilled water. The dishes were left to air-dry under the hood.

DRG extraction

Adult or newborn Wistar rats were euthanised by cervical dislocation and decapitation respectively. The skin was incised with a surgical scalpel and removed topically to reveal the spine. The spine was removed by disconnecting it from the rib cage with scissors. An incision was made along the spine and the spinal cord was removed using forceps. The incision was opened gently by applying pressure onto the incised vertebra and the remaining spinal nerves were cleared out. The dorsal root ganglia, positioned between the vertebra, were extracted using forceps and placed in sterile plates with 2ml medium (DMEM-GibcoBRL, 10% (v/v) fetal bovine serum-Sigma, 500units/ml penicillin and 500µg/ml Streptomycin-GibcoBRL). The axons were cleared of the cell bodies under the microscope using forceps and fine scissors.

DRG culture

1) The DRG neurons were pelleted after 3 min centrifugation at 1500rpm and subsequently treated with 0.125% (w/v) collagenase (Sigma) in medium for 2 hours at 37^0C in a humidified incubator in the presence of 5% CO_2.
2) After washing out the collagenase, the DRG were homogenised by using a flame polished Pasteur pipette. The homogenate was let to stratify in medium for 5 min

and the supernatant containing the cells was removed and centrifuged for 3min at 1500rpm.

3) The pellet was resuspended in medium and plated in dishes that had been coated with 10μg/ml poly-lysine and placed at 37^0C, 5%CO_2 in a humidified incubator.
4) The following day the medium was changed and the dishes were replenished with fresh medium containing 3.3μg/ml aphidicolin (Sigma), an antibiotic that inhibits the DNA polymerase α activity and therefore kills all mitotic cells e.g. Swann cells, fibroblasts.

Nerve growth factor treatment

For the experiment of VR1 and VR-L regulation of expression by NGF, dorsal root ganglia cells from adult rats were used. The cells were cultured for 7 days, changing the medium every 48 hours. 2.5S NGF (Promega) was used to treat cultures in a concentration of 50ng/ml and NGF antibody was used in concentration of 8μg/ml (from Dr. Helliwell, Novartis).

Capsaicin treatment

10 newborn Wistar rats were killed by decapitation and their DRG were extracted and cultured as described above (apart from being treated with collagenase for 45min instead of 2 hours). After 24 hours in culture, a dish with cells was treated with 3μM of capsaicin (Sigma) diluted in DMSO. The capsaicin-containing medium was washed out after 16 hours and the cells were removed from the culture by suspending them in denaturing solution (see RNA extraction, section 2.5).

2.4 NGF application in vivo

5 newborn Wistar rats were injected intraperitoneally with 2.5μg of 2.5S NGF (Promega) diluted in PBS, while 5 other newborn Wistar rats were injected only with the carrier PBS. After 4 hours, their DRG were removed and RNA extraction followed.

2.5 RNA extraction

a) from cultured dorsal root ganglia

1) A sterile tip attached to a pump was used to aspirate the medium from the culture dishes. Then, 0.3 ml of denaturing solution (see RNA extraction, Chapter1) were added to wash each dish about ten times by pipetting. Extra care was taken for the bottom of the dish not to be touched and no bubbles to be created.

2) All the washed cells from each dish was removed and was poured in an eppendorf tube. Another 0.3ml of denaturing solution were added with a fresh tip in each dish and the procedure was repeated. The RNA extraction was continued as described in Chapter 1, except a 40% reduction in the volume of all the solutions used subsequently (corresponding to a reduction in the volume of the denaturing solution used).

b) from tissues

100mg of tissue was weighed and placed into a glass homogeniser with 1 ml of denaturing solution. The tissue was homogenised with repeated strokes of the homogeniser's rod. It was then subjected to the same procedure for RNA extraction as described in Chapter 1.

2.6 Mammalian cell culture and transfection

HEK293 and COS7 (derived from CV-1, an African Green monkey kidney cell line, transformed by an origin defective mutant of SV40) cells were cultured as described in Chapter 1 for Jurkat cells without the presence of glutamate. For simplicity, we refer to these cells as HEK and COS respectively. These cells differ from Jurkat cells in that they are adhesive. In order to passage the cells when confluent, the following procedure was implemented:

1) The medium was aspirated and the cells were washed gently with 1X PBS.
2) The enzyme trypsin (Sigma), was added in a 1:5 dilution in PBS and the cells were transferred in a humidified incubator at 37^0C, 5% CO_2, for 1-2 min. The enzyme digested the cell processes resulting in detached cells.
3) Fresh medium was added to stop the reaction (the serum inhibits the enzymatic activity) and the cells were transferred in a falcon tube to be centrifuged for 5min at 1500g.
4) The supernatant was discarded and the cell pellet was resuspended in fresh medium. The cells were plated in a 1:5 ratio and were left in the incubator to grow.

HEK293 cells transfection with calcium phosphate

A calcium phosphate transfection kit from Clontech was purchased and used according to the manufacturer's instructions. The protocol is described here briefly:

1) For electrophysiological studies $2x10^5$ HEK293 cells were plated onto 35mm culture dishes.

2) The following day, 0.5-3 hours before transfection the medium was changed.
3) 100μl of a solution was prepared in an eppendorf tube containing 1μg of DNA to be transfected (Qiagen purified) with 0.1μg of GFP cDNA in pcDNA3 and 0.25M -containing calcium solution dissolved in sterile distilled water. This solution was dispensed in a dropwise fashion into a 15ml falcon tube containing 100μl of 2X HEPES-buffered saline while vortexing. The mixed solution was left to incubate at room temperature for 20 min for the DNA-salt complex to form.
4) The solution was vortexed gently and was added dropwise onto each culture plate. The plates were left in a humidified incubator at 37^0C with 5% CO_2 for 12 hours.
5) The following day the calcium phosphate-containing medium was removed and the plated were washed with 1X PBS pH7.4 (58mM Na_2HPO_4, 17mM NaH_2PO_4, 68mM NaCl). The cells were fed with fresh medium and recordings were performed from them 24 hours post-transfection.

COS7 cells transfection with liposomes

The SuperFect kit from Qiagen was used for lipofection, according to the following protocol:

1) 10^6 cells were plated onto 10cm culture dishes and incubated in a humidified incubator at 37^0C with 5% CO_2.
2) The following day, 10μg of the DNA of interest (prepared with the Qiagen miniprep method) was dissolved in TE pH7.4 (0.01M Tris-HCl, 10^{-3}M EDTA) with DMEM medium containing no serum or antibiotics (the serum and the antibiotics can interfere with the liposome-DNA formation).
3) 20μl of SuperFect transfection reagent were added in the DNA solution and mixed by vortexing. The sample was left to incubate at room temperature for 10min for the liposomes to take in the DNA.
4) In the meantime the cells were washed with 1X PBS.
5) The DNA solution was mixed with 5ml of medium containing serum and antibiotics by pipetting and was loaded onto the cells.
6) The cells were left for 2 hours in the incubator. Subsequently, the cells were washed with 1x PBS and fed with fresh medium. Fura-2 readings were performed 36 hours post-transfection.

2.7 Fura-2 fluorometry

Fura 2/AM (Calbiochem) is the cell permeable ester form of the dye fura-2, that is hydrolysed by cell esterases upon entrance in the cell and released in the cytoplasm. This dye is a Ca^{2+} indicator that changes excitation wavelength when bound to Ca^{2+}. In particular its excitation peak wavelength shifts from $\lambda=$340 to $\lambda=$380nm as more Ca^{2+} binds to it. For that reason it is practical for use in ratiometric fluorometry or imaging microscopy. While recording at $\lambda=$510nm emission, excitation of the sample switches from $\lambda=$340nm to $\lambda=$380nm in regular intervals. The peak of the fura-2 spectra is around $\lambda=$380nm when it is Ca^{2+}- free and $\lambda=$340nm when bound to 40μM of Ca^{2+}. The dissociation constant Kd of the dye can be affected by temperature, pH, ionic strength and possible interactions with cellular proteins. To eliminate variations due to these factors, ratiometric calibration is used, where the ratio of fluorescence intensities at wavelengths of different ion responses ($\lambda=$340nm and $\lambda=$380nm) is recorded. With this method additional variations are eliminated e.g. dye distribution, photobleaching and concentration, cell thickness etc. The calibration was achieved using the following equation (Grynkiewich *et al.*, 1985):

$$[Ca^{2+}]_i = K_D \times \frac{R - R_{min}}{R_{max} - R} \times \frac{S_0}{S_{max}}$$

Where $[Ca^{2+}]_i$ is the free Ca^{2+} concentration intracellularly, K_D the dissociation constant for the dye, R the fluorescence ratio of the two wavelengths, R_{min} the fluorescence ratio in zero Ca^{2+} conditions, R_{max} the fluorescence ratio in saturating Ca^{2+} conditions, S_0 the fluorescence at zero Ca^{2+} and S_{max} the fluorescence at saturating Ca^{2+} concentrations.

Fura 2/AM loading

1) the medium was aspirated from cultured transfected cells. The cells were rinsed with 1X PBS.
2) The cells were trypsinised as described in section 2.6. They were transferred in a falcon tube and centrifuged at 1,500g for 5 min.
3) $5x10^7$ cells were incubated in 4μM fura-2/AM for 45min in a 90% humidified incubator at 37^0C, 5% CO_2 with regular swirling to ensure an even dye distribution.
4) The cells were centrifuged for 5min at 1,500g and washed with 1X PBS. They were transferred back in the incubator and left for 10-15min.

5) The cells were centrifuged again and then resuspended in 0.5ml of PBS. Aggregates were disassociated with a 23G needle syringe. The cells were kept on ice to avoid ester extrusion from the cells and covered in foil to prevent photobleaching.
6) For the fluorometry, 50µl of cells were resuspended in a plastic cuvette with 2ml of Hanks buffer pH 7.4 without Ca^{2+} with continuous mixing by a magnetic rod.
7) A baseline of about 20nM intracellular Ca^{2+} was established for about 50sec and then Ca^{2+} was added to a final physiological concentration of 2mM. The establishment of a new baseline at about 60nM Ca_i^{2+} for 100sec, showed that Ca^{2+} diffused into the cells and was maintained in a constant concentration, proving that the cells were not leaky.
8) Stimuli were applied for about 100-200sec and ratiometric recordings were made. The cells were then solubilised with 0.5% (w/v) SDS in order to obtain R_{max}. The recordings were converted into changes of intracellular Ca^{2+} concentrations using the formula described above in a software programmed by Dr. T.Sihra (UCL). The results were plotted in Microsoft Excell.

Solutions

- To achieve drop of pH from 7.4 to 6, MES buffer was added in a final concentration of 50mM.
- 500µM capsaicin stock in DMSO was prepared and diluted to a final concentration of 1µM in Hanks buffer for the experiments.

2.8 Insertion of the c-myc epitope in an extracellular loop of theVR-L protein.

The following strategy was used:

1) Two separate PCR reactions were set up with primers A & B and C & D (figure 2.20), using >100ng of template and Pfu polymerase for 13 cycles. Using as few cycles as possible and Pfu polymerase, one can ensure the minimal incorporation of mistakes in the product. The PCR was performed as mentioned in Chapter 1 with annealing temperature at 60^0 C.
2) The PCR products were blunted with Klenow enzyme as follows: 1/10 of the sample volume of dNTPs were added in the PCR reaction together with 2.5 units of Klenow enzyme (Roche). The mixture was incubated at 37^0C for 30min to ensure overhangs filling.

3) The Klenow treated PCR products were analysed with gel electrophoresis and purified from the gel. The fragments were used as template for a PCR reaction using the primers A & D.
4) The PCR reaction was completed with 10min at 72^0C adding 1 unit of Taq polymerase in the case the PCR product would be cloned into a T- vector.
5) The PCR product was analysed with gel electrophoresis and purified from the gel.
6) The product was digested with the appropriate restriction enzymes and ligated in the appropriate construct.

2.9 *In vitro* transcription and translation

In vitro transcription and translation of constructs was achieved by using the TNT® Quick Coupled Transcription/Translation System from Promega. This kit performs eukaryotic *in vitro* translation directly from DNA by combining the RNA Polymerase, nucleotides, salts and RNasin® Ribonuclease Inhibitor with the reticulocyte lysate solution in a Master Mix. The manufacturer's protocol was followed which is described here briefly:

1) The TNT® Quick Master Mix was rapidly thawed by hand warming and placed on ice. The other components were thawed at room temperature and then stored on ice.
2) The following reaction components were assembled in a 1.5ml microcentrifuge tube and were gently mixed by pipetting:

TNT® Quick Master Mix:	40µl
[^{35}S]methionine (1,000Ci/mmol at 10mCi/ml):	2µl
DNA template(s) (0.5µg/µl):	2µl
Nuclease-Free Water to a final volume of	50µl

3) The reaction was incubated at 30°C for 60-90 minutes.
4) The results of translation were prepared to be analysed by SDS-PAGE. 2x SDS sample buffer was added to half of the reaction (the remainder of the reaction may be stored at -20°C). The tube was capped and heated at 100°C for 2 minutes to denature the proteins. Then an aliquot of the denatured sample was loaded onto a SDS-polyacrylamide gel or stored at -20°C.

5) The procedure for preparing a SDS-PAGE gel is described in detail in Chapter 3. The gel was subsequently stained with Coomassie blue as follows: a) the gel was dismantled from its cassette and placed in a container with 50% (v/v) methanol, 10% (v/v) acetic acid and 40% distilled water. The container was rocked gently onto a rotating platform for 10min at room temperature for the gel to be fixed. b) The fixer solution was replaced by a staining solution containing 0.2g Coomassie brilliant blue R-250 (Sigma) in 50ml acetic acid, 125ml of isopropanol and 325ml distilled water. The container was rocked for 30min at 50^0C. c) The solution was replaced by a destaining solution containing 10% (v/v) methanol and 7.5% (v/v) acetic acid in distilled water. The gel was left to destain in the rotating platform for 2 hours in the presence of tissue paper to absorb the extra stain. d) the gel was soaked in 7% (v/v) acetic acid, 7% (v/v) methanol and 1% (v/v) glycerol for 5min and was subsequently placed over Watman paper that was sitting on top of a vacuum gel drier. The gel was covered with cling film and was left to dry for 3 hours at 80^0C.
6) After drying, the gel formed a thin layer stuck onto the 3M Whatman paper (LabSales). It was then transferred into an autoradiography cassette with film (Sigma) laid on top of it. The film was left to expose overnight.
7) The following day the film was developed using Kodak developer and fixer (Sigma) according to the manufacturer's instructions: in a dark room, under red light the film was dipped into a tray containing developer using forceps for about 2 min until the signal was visible. It was then washed in running water for another 2 min before been transferred in a tray containing fixer. The film was fixed for 2 min until it became transparent and then it was washed in running water. The film was left to dry hanging in a drying cabinet.

2.9 Immunocytochemistry

PREPARATION

1) 2×10^5 cells were cultured on a poly-lysine coated coverslip in a 35mm dish and the following day they were transfected with 1 μg of DNA. After 24 hours, the cells were washed carefully 3 times with PBS.
2) The cells were fixed with 4% (w/v) paraformaldehyde pH7 (Sigma) for 20min at room temperature.
3) Subsequently, the cells were washed 3 times with PBS.

BLOCKING

1) PBS containing 0.1% (v/v) Triton-X (Sigma) was added for 10min to permeate the cells. Then the cells were washed once with PBS. For the experiment in this chapter, the cells were not permeabilised.
2) The cells were kept in 10% (v/v) goat serum (GibcoBRL) with 0.001% (v/v) Triton-X in PBS for one hour minimum in humid atmosphere to block unspecific binding. No Triton was used in this chapter's immunocytochemistry experiment.

ANTIBODIES

1) The primary antibody was added in the appropriate concentration (1:600 for polyclonal 200µg/µl anti-FLAG from Santa Cruz and 1:150 for 6µg/µl monoclonal anti-MYC from Sigma) for 1-2 hours at room temperature or at 4°C overnight.
2) The cells were washed carefully three times with PBS.
3) The secondary antibody was added in the appropriate concentration (1:600 for 1.5mg/ml anti-rabbit rhodamine and 1:200 for 1.5mg/ml anti-mouse fluorescein both purchased from Jackson ImmunoResearch Laboratory) and left for 30min in the dark.
4) The cells were washed 3 times with PBS.
5) Each coverslip was drained with paper and inverted onto a drop of cytofluor (glycerol/PBS solution) on a slide, trying to prevent the formation of bubbles. The edges of the coverslips were sealed with nail varnish and the slides were stored in the dark at 4^0C.

CHAPTER 2

Investigating the functional role of VR-L

EXPERIMENTAL RESULTS

2.1 Tissue distribution of VR-L

Following the cloning of VR-L, the new member of the vanilloid receptor family, further studies were undertaken to identify its function. Investigating the tissue distribution of a gene can provide an indication towards its function. The distribution of the VR-L transcript was examined by performing RT-PCR studies.

RNA from rat tissues was extracted and cDNA was synthesised using the same concentration of RNA for all the samples. Although, the starting RNA amount was the same across samples, the cDNA production can vary depending on the RNA and uncontrollable factors like the thickness of the eppendorf walls. In order to make sure that the RT-PCR was performed with the same cDNA amount across samples (normalisation), a PCR was carried out using primers for cyclophilin. Cyclophilin is a specific cyclosporin A-binding cytosolic protein, found to be abundant and highly conserved. During PCR, DNA amplifies exponentially until the reagents are depleted and then amplification reaches a plateau. The PCR was performed in the exponential phase of cyclophilin amplification (for details see figure 2.6, next section). Once the intensities of all bands were equalised by adjusting the cDNA concentrations across samples (figure 2.1A and 2.3A), a PCR was carried out using primers specific to VR-L (figures 2.2 and 2.3A). VR-L was found to be highly expressed in the spinal cord, nodose and dorsal root ganglia, in the lung, adrenal gland and ovaries. In lower amounts it was found to be expressed in brain, cerebellum, heart, thymus, spleen and testis. The widespread distribution of the gene was not unexpected, since the tBLASTn search that identified VR-L (Chapter 1) retrieved ESTs from libraries created from a variety of tissues. A control RT-PCR was performed (figures 2.1B, 2.3B) where no reverse transcriptase was included in the reaction, to ensure that the VR-L signal is not due to genomic DNA contamination during the RNA preparation. The cyclophilin primers were designed to cross an intron in the cyclophilin gene. Therefore, if there was genomic DNA in the sample, the intron would be amplified resulting in a band with a higher molecular weight than the band amplified from cyclophilin cDNA. Hence, these primers served as an additional control for genomic DNA contamination.

The experiment was performed n=4 times

Figure 2.1A: Normalisation of the tissue cDNA samples. The PCR was carried out (25 cycles) using primers for the cyclophilin gene. **Lane 1:** 100bp ladder, **Lane 2:** brain, **Lane 3:** cerebellum, **Lane 4:** spinal cord, **Lane 5:** nodose ganglia, **Lane 6:** dorsal root ganglia, **Lane 7:** heart, **Lane 8:** thymus, **Lane 9:** lung, **Lane 10:** liver, **Lane 11:** spleen, **Lane 12:** kidney, **Lane 13:** adrenal gland, **Lane 14:** muscle, **Lane 15:** urinary bladder

Figure 2.1B: Attempt to amplify the cyclophilin gene from a reverse transcription reaction where no reverse transcriptase had been added, controlling for genomic DNA contamination. The PCR reaction was performed as in figure 2.1A. The samples were loaded in the same order.

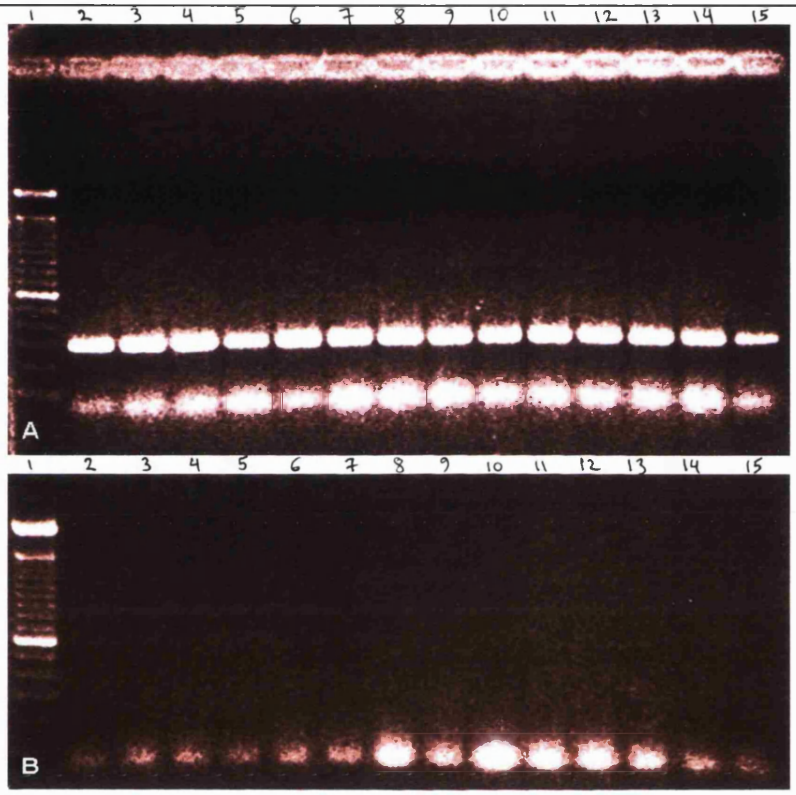

Figure 2.2: Tissue distribution of the VR-L gene (35 cycles). The samples were loaded in the same order as in figure 2.1.

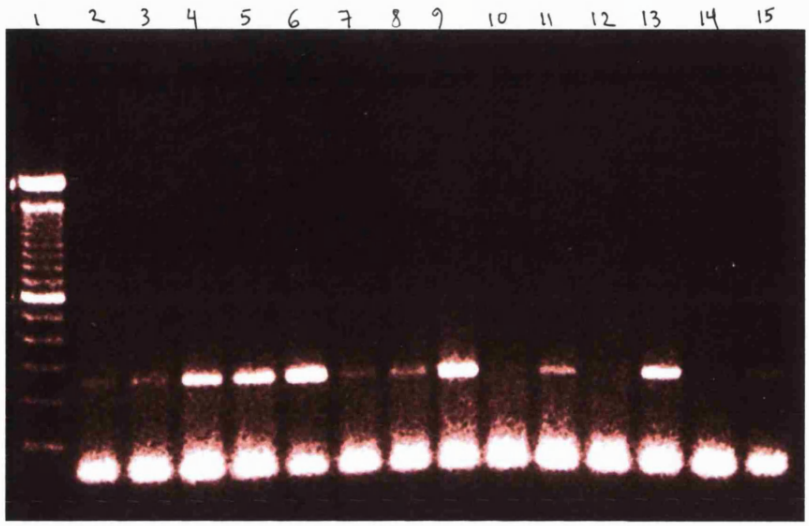

Figure 2.3A: Tissue distribution of VR-L (cont). **Lane 1:** testis (cyclophilin), **Lane 2:** ovaries (cyclophilin), **Lane 3:** 100bp ladder, **Lane 4:** testis (VR-L), **Lane 5:** ovaries (VR-L), Lane 6: negative control.

Figure 2.3B: Genomic DNA contamination control in the same RNA samples as the ones used in figure 2.3A (loaded in the same order).

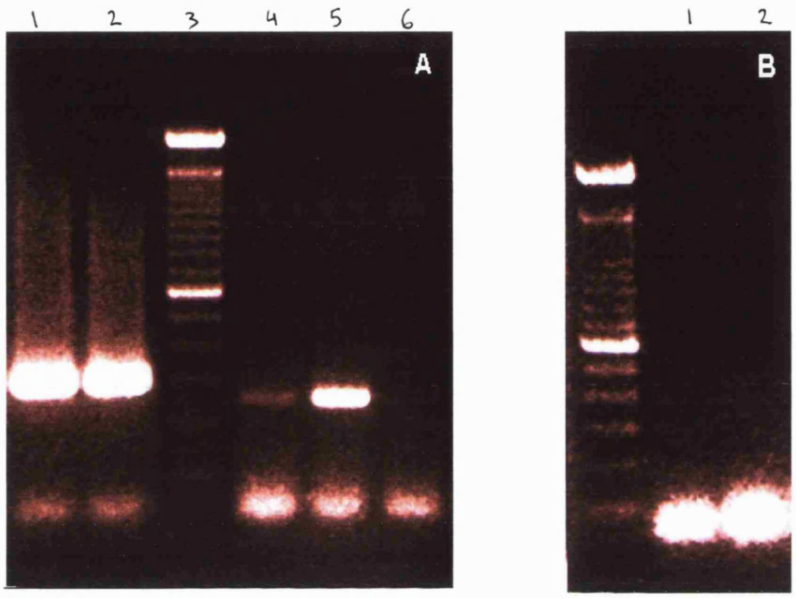

Since there is no genomic DNA contamination, the signals in figure 2.2 represent the VR-L transcript in the corresponding tissues. VR-L has a much broader tissue distribution than VR1 (Caterina *et al.*, 1997). It is expressed in the peripheral nervous system (nodose and dorsal root ganglia) but also in the central nervous system (brain, cerebellum, spinal cord) and in tissues of the immune system (thymus, lung, spleen, adrenal gland). Since VR-L mRNA is found in DRG, where its possible co-expression with VR1 might have interesting implications in the study of pain, further investigation of its expression in this tissue was necessary.

2.2 Regulation of VR1 and VR-L by Nerve Growth Factor.

The majority of the nociceptors that are sensitive to capsaicin also express trkA, the high affinity receptor for NGF . Winter *et al.* (1988) reported that capsaicin sensitivity of adult rat DRG neurons in culture is NGF dependent. Under inflammatory conditions, the concentration of NGF peripherally increases, it causes the degranulation of mast cells, which release more NGF, histamine and serotonin that subsequently sensitise the nociceptors (Shu and Mendell, 1999).

Considering that VR1 is expressed in trkA DRG neurons and that NGF can regulate the capsaicin response and expression of various genes, it was interesting to explore whether or not VR1 is regulated by NGF. Likewise, the role of NGF in inflammation and hyperalgesia together with the observation that VR-L is expressed in tissues of the nervous and the immune systems, led to the hypothesis that the VR-L gene might be regulated by this neurotrophin. A semi-quantitative RT-PCR approach was followed as described before (Boucher *et al.*, 2000a), where cDNA was synthesised from adult rat DRG neurons that had been cultured either in the presence of NGF or in its absence together with anti-NGF antibody. cDNA was also synthesised from neonatal rats that had been injected with NGF and control rats that had been injected with carrier solution. The concentrations of the differently treated samples were normalised using cyclophilin primers, as it was described in section 2.1. Primers for

CGRP were used as a positive control for the NGF treatment, as its expression is known to be upregulated by NGF (Lindsay *et al.*, 1989, Winston *et al.*, 2001). For the cultures, adult DRG were used since they do not depend on NGF for their survival. In this set-up anti-NGF antibody could be used to neutralise NGF in the medium without jeopardising the neurons' survival.

In order to examine the sensitivity of this approach, a preliminary experiment to quantify the dynamic range of RT-PCR as an assay system for the identification of differences in the transcript levels was carried out. The sensitivity of the system was tested by running different dilutions of a PCR reaction on a gel (figure 2.4). As it can be seen in this picture, the RT-PCR method is limited in recognising >2x difference in concentrations. The experiment was performed n=1time.

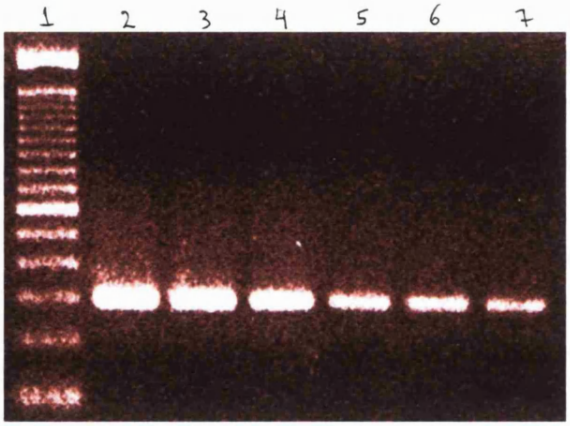

Figure 2.4: Sensitivity of RT-PCR in identifying differences in concentrations. All the samples run were amplifications of DRG cDNA using cyclophilin primers for 30 cycles.
Lane1: 100bp ladder
Lane 2: 50 µl PCR reaction
Lane 3: 25 µl PCR reaction (x2 dilution)
Lane 4: 12.5 µl PCR reaction (x4 dilution)
Lane 5: 8.3 µl PCR reaction (x6 dilution)
Lane 6: 6.25 µl PCR reaction (x8 dilution)
Lane 7: 5 µl PCR reaction (x10 dilution)

The DNA amplification in a PCR is exponential but is limited by the availability of the reagents and the activity of the DNA polymerase. As a result it reaches a plateau after a number of cycles, where the product has attained maximum amplification. Because the expression levels of genes differ and the semi-quantitative RT-PCR requires the amplification of two genes in the same tube, control RT-PCRs were run at different cycles in order to determine the point of saturation in the amplification of each gene studied (figure 2.5). The same amount of RNA was used to synthesise cDNA and the PCRs were carried out using the same amount of template.
The experiment was performed n≥10 times.

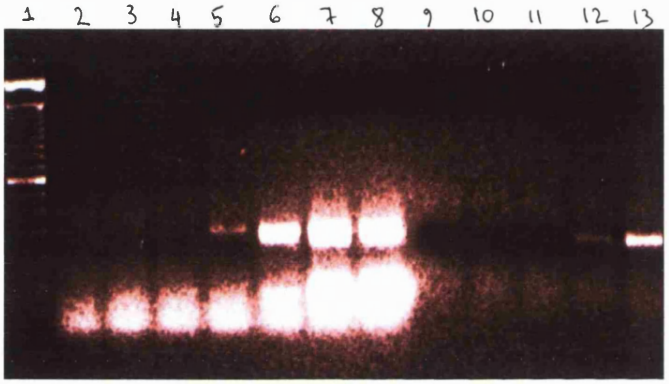

Figure 2.5: Determining the exponential amplification of VR1 and CGRP.
Lane 1: 100bp ladder
Lanes 2 to 8: amplification of VR1 in 10, 18, 20, 25, 30, 35 and 40 cycles
Lanes 9 to 13: amplification of CGRP in 10, 18, 20, 25, and 30 cycles

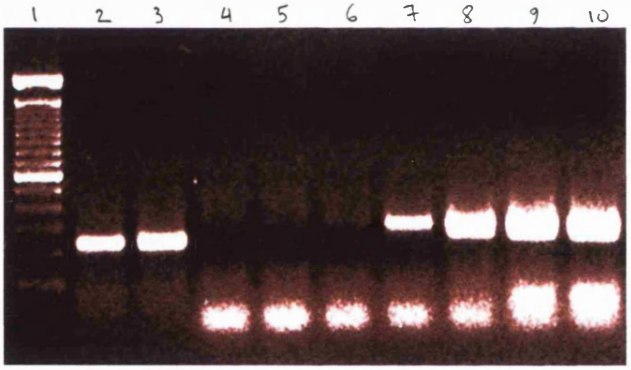

Figure 2.6: Determining the exponential amplification of CGRP (cont.) and cyclophilin
Lane 1: 100bp ladder
Lanes 2 to 3: amplification of CGRP in 35 and 40 cycles
Lanes 4 to 10: amplification of cyclophilin in 10, 18, 20, 25, 30, 35 and 40 cycles.

The number of cycles of exponential amplification was determined as follows for the different genes: 25 cycles for cyclophilin, 30 cycles for CGRP and 30 cycles for VR1. To normalise the cDNA amounts between the two differently treated samples (subjected to NGF and to anti-NGF antibody treatement) PCRs were run using the two different templates and the cyclophilin primers at 25 cycles (figure 2.7). Different volumes of template were used for each PCR. An example is given below. The experiment was performed n≥10 times.

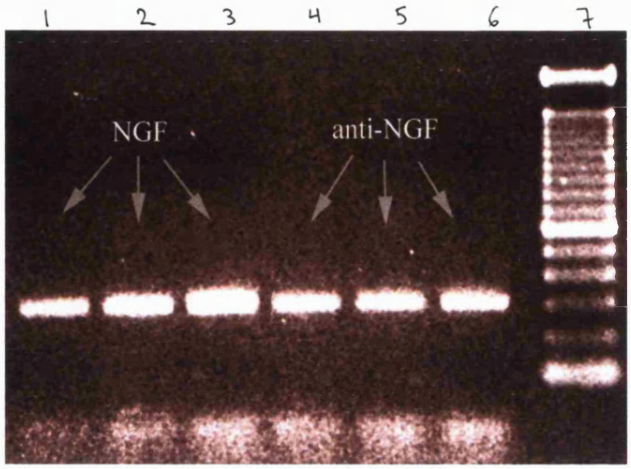

Figure 2.7: Normalisation of the cDNA amounts of the differently treated samples
Lane 1: PCR reaction with 2µl cDNA of NGF treated sample
Lane 2: PCR reaction with 2.5µl cDNA of NGF treated sample
Lane 3: PCR reaction with 3µl cDNA of NGF treated sample
Lane 4: PCR reaction with 2µl cDNA of anti-NGF treated sample
Lane 5: PCR reaction with 2.5µl cDNA of anti-NGF treated sample
Lane 6: PCR reaction with 3µl cDNA of anti-NGF treated sample
Lane 7: 100bp ladder. Normalisation was performed using cyclophilin primers.

For these particular samples, 2.5 µl cDNA of the NGF treated sample was normalised against 3 µl cDNA of the anti-NGF treated sample. Following normalisation of each set of samples, the semi-quantitative PCRs were carried out for VR1 and VR-L (figures 2.8 and 2.9).

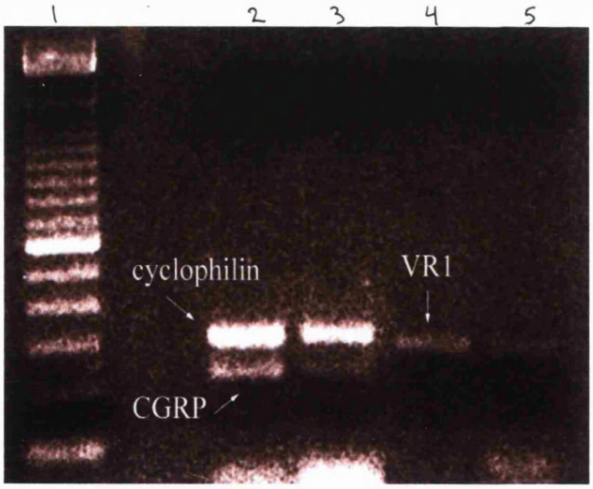

Figure 2.8: Upregulation of VR1 by NGF in cultured DRG
Lane 1: 100bp ladder
Lane 2: NGF treated sample. Cyclophilin amplification =25 cycles, CGRP=30 cycles
Lane 3: anti-NGF treated sample.
Lane 4: NGF treated sample. VR1 amplification = 30 cycles
Lane 5: anti-NGF treated sample.

The primers designed for VR1 did not allow co-amplification with cyclophilin in the same tube since the two bands were of similar size and thus not possible to be distinguished. New primers were designed for VR1 and the experiment was repeated (figure 2.9).

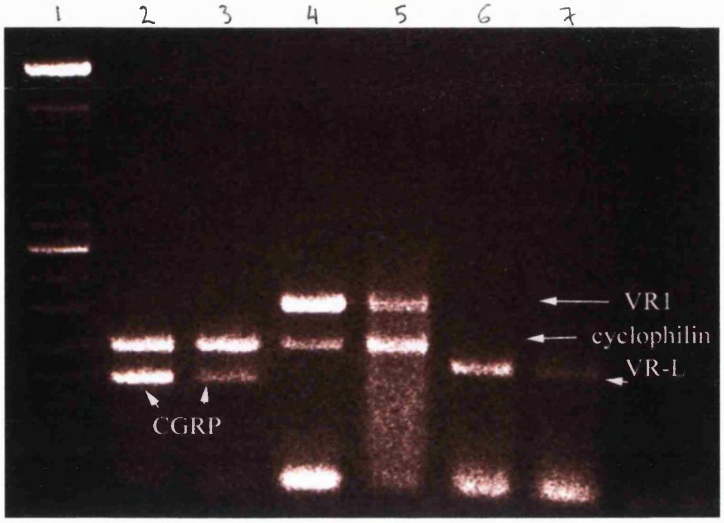

Figure 2.9: Upregulation of VR1 and VR-L by NGF in cultured DRG
Lane 1: 100bp ladder
Lane 2: NGF treated sample Cyclophilin amplification =25 cycles, CGRP=30 cycles
Lane 3: anti-NGF treated sample
Lane 4: NGF treated sample Cyclophilin = 25 cycles, VR1 = 35 cycles
Lane 5: anti-NGF treated sample
Lane 6: NGF treated sample. VR-L = 35 cycles
Lane 7: anti-NGF treated sample

The CGRP upregulation confirms the efficacy of the NGF treatment. The amplification time for VR1 was increased to 35 cycles, because competition with the cyclophilin primers was observed in control experiments. Both VR1 and VR-L show upregulation by NGF, albeit the size of the VR-L product did not allow co-amplification with cyclophilin. At the time of the experimentation only a small part of the VR-L gene had been sequenced and thus it was not possible to redesign the primers. In the meantime, the experiment was repeated with DRG cDNA from neonatal rats that had been injected with NGF (figure 2.10).

Figure 2.10: Upregulation of VR-L by NGF *in vivo*.
Lane 1: 100bp ladder
Lane 2: NGF treated sample. Cyclophilin amplification =25 cycles, CGRP=30 cycles
Lane 3: control sample (PBS injection)
Lane 4: NGF treated sample. VR-L amplification = 35 cycles
Lane 5: control sample (PBS injection)

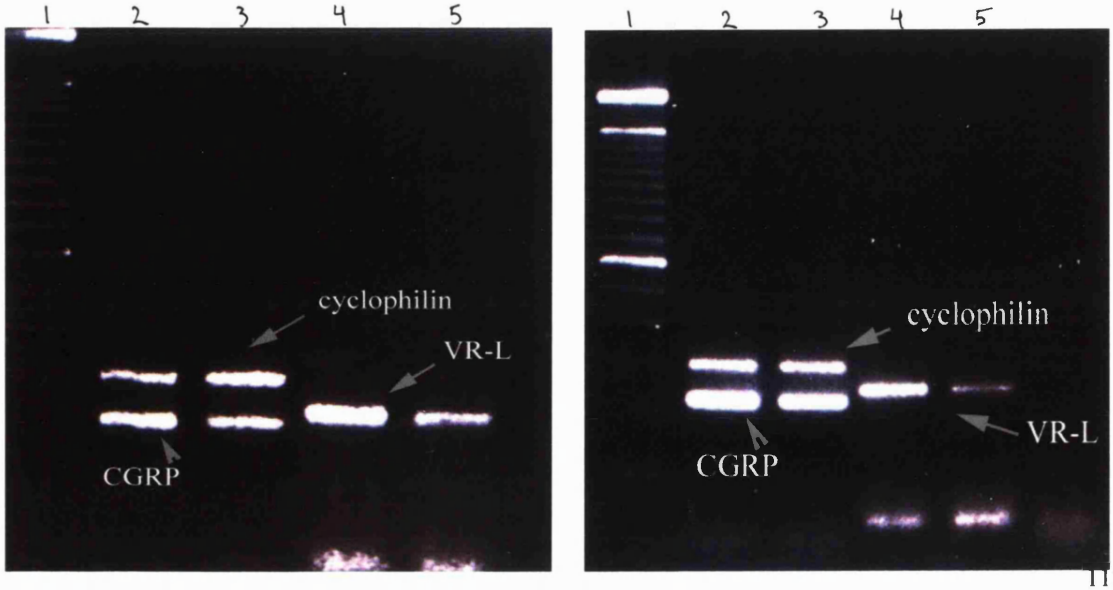

NGF upregulates VR-L *in vivo* in a similar manner to observed in cultures. Once the VR-L sequencing was completed, new primers were designed to allow co-amplification with cyclophilin in one tube using cDNA from NGF treated DRG cultures and DRG cDNA from NGF treated mice. (figures 2.11 and 2.12).

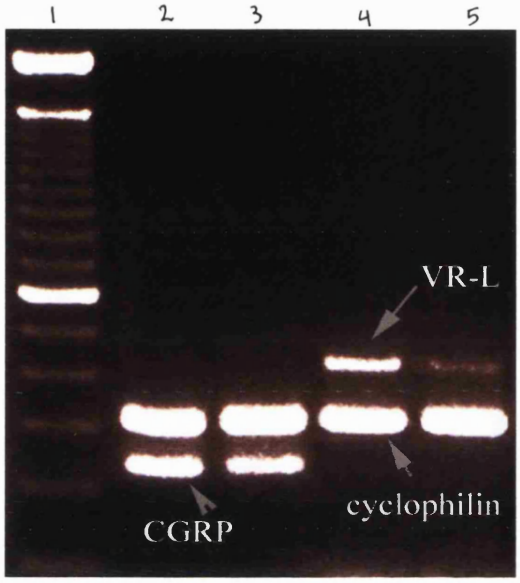

Figure 2.11: Up-regulation of VR-L by NGF in cultured DRG (adult rat)
Lane 1: 100bp ladder
Lane 2: NGF treated sample. Cyclophilin amplification =25 cycles, CGRP=30 cycles
Lane 3: anti-NGF treated sample
Lane 4: NGF treated sample. Cyclophilin= 25 cycles, VR-L= 35 cycles
Lane 5: anti-NGF treated sample

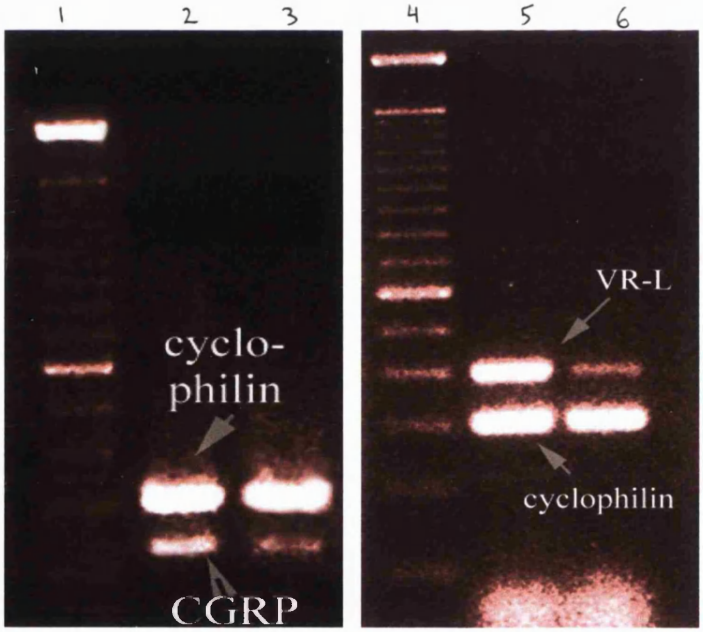

Figure 2.12: Up-regulation of VR-L by NGF *in vivo* (newborn rat)
Lane 1: 100bp ladder
Lane 2: NGF treated sample
Lane 3: control sample (PBS)
Lane 4: 100bp ladder
Lane 5: NGF treated sample
Lane 6: control sample (PBS)

In both cases of NGF application *in vivo* and *in vitro*, elevation of the VR-L mRNA levels was observed. The same upregulation was observed with two different sets of primers. In the presence of NGF the transcript upregulation was 3.2 times compared to the signal in the anti-NGF antibody sample (analysed by Metamorph Imaging System), while the VR1 upregulation was on average 2.6 times.
The experiment was performed n=5 times.

2.3 VR-L is expressed in capsaicin-insensitive dorsal root ganglia

Dorsal root ganglia comprise a heterologous population of neurons that can be distinguished by size, neurotrophin dependence, expression of markers and sensitivity to capsaicin. Capsaicin specifically excites the unmyelinated C polymodal and thinly myelinated Aδ nociceptors and thus it was not surprising to find VR1 to be specifically expressed in the small to medium size diameter neurons of dorsal root ganglia. Capsaicin in high concentrations has neurotoxic effects (Nagy *et al.*, 1980) on primary afferent nociceptors. Caterina *et al.* (1997) demonstrated that this specificity is a reflection of the specific expression of VR1, as non-neuronal cells transfected with VR1 and exposed to 3μM capsaicin for 7 hours exhibited necrotic death. The specific action of capsaicin on small diameter neurons was useful in determining whether or not VR-L is expressed in this group of dorsal root ganglia neurons. Cultures of adult rat DRG neurons were subjected to 3μM capsaicin overnight at 37^0 C in a humidified incubator. RNA was extracted and cDNA was synthesised from the capsaicin treated neurons as well as from control cultures. A semi-quantitative PCR was carried out, as described in section 2.2, where the cyclophilin amplification had been normalised between the capsaicin treated and the control DRG cultures. Primers for VR1 were used as a positive control for the efficacy of the capsaicin treatment.

The experiment was performed n=3 times.

Figure 2.13: Expression of VR-L in DRG neurons that do not respond to capsaicin
Lane1: 100 bp ladder
Lane 2: capsaicin treated culture (cyclophilin)
Lane 3: control culture (cyclophilin)
Lane 4: capsaicin treated culture (VR1-cyclophilin)
Lane 5: control culture (VR1-cyclophilin)
Lane 6: capsaicin treated culture (VR-L)
Lane 7: control culture (VR-L)
Lane 8 to 10: negative PCR controls for all sets of primers

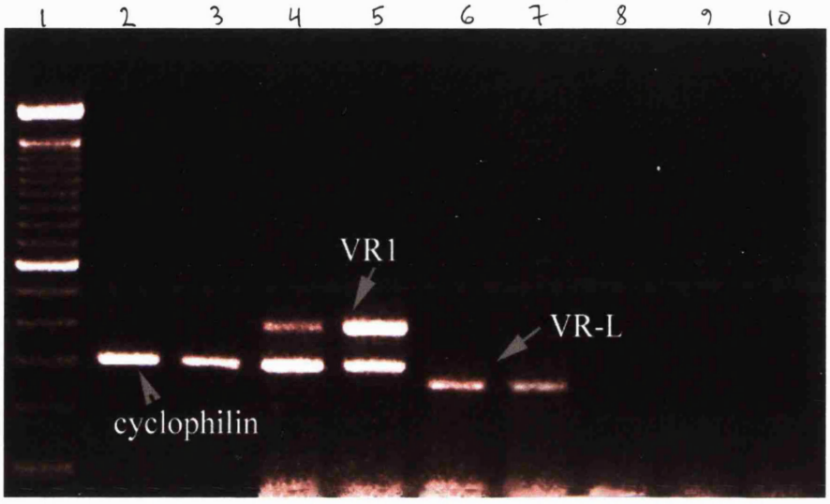

The VR1 expression levels were reduced with capsaicin treatment as expected, since high capsaicin concentrations have a neurotoxic effect and can diminish the number of VR1 expressing neurons. VR-L expression levels on the other hand remained unaltered, indicating that the VR-L mRNA presents little or no colocalisation with VR1. *In situ* hybridisation can provide more detailed information on the localisation of VR-L in DRG. Unfortunately, attempts to perform *in situ* hybridisation analysis for VR-L failed due to high background. Lack of time did not allow trial of many probes under different conditions. Nevertheless, the RT-PCR experiment on capsaicin-treated cultures shows that VR-L has a different expression pattern from VR1, which does not exclude colocalisation to a limited extent.

2.4 Functional studies: attempts to assign a role on VR-L

2.4.1 Fura-2 fluorometry

VR-L, a new member of the vanilloid receptor family was cloned using bioinformatics tools. RT-PCR studies showed that the novel protein is expressed in a variety of tissues of the immune and the nervous systems, including dorsal root ganglia. By performing semi-quantitative RT-PCR using capsaicin treated and control DRG cultures, it was established that VR-L is mainly expressed in the non-capsaicin-sensitive DRG population. *In vivo* and *in vitro* application of NGF resulted in elevating the VR-L transcript levels, indicating that VR-L like other receptors is under cellular control. These studies so far suggest that VR-L is a functional receptor, but its role has yet to be elucidated.

The structural topology and the resemblance of VR-L to the Transient Receptor Potential family of receptors are strong indications that VR-L is a calcium channel. Therefore an assay based on Ca^{2+} readout could be used to study the function of this receptor. The fluorometry method was favoured for its simplicity, its proven competence in studying Ca^{2+} signals, especially of TRP channels, and for its high throughput of data. COS7 cells were used that were transiently transfected with VR1 or VR-L and loaded with fura-2, a fluorescent dye that exhibits a shift in its excitation peak wavelength once bound to Ca^{2+}. Activation of a calcium channel will register as a fluorescence change when the fura-2 binds the incoming Ca^{2+}. In particular, when the free Ca^{2+} concentration is high (not bound to fura-2), the fluorescence emission (recorded at $\lambda =$ 510nm) is large at $\lambda =$ 340nm excitation, while for the same Ca^{2+}

concentration the fluorescence at 380nm excitation is low (captured at the same 510nm emission). The fluorescence recordings reverse when Ca^{2+} binds to fura-2 and thus free Ca^{2+} concentration is low i.e. the fluorescence is low at 340nm and high at 380nm. These excitation spectrum shifts can be converted to changes in intracellular Ca^{2+} (see Materials and Methods). Because the sample has the same optical characteristics when excited at two different wavelengths, the ratio of the intensities, rather than the absolute intensity values are calculated. This ratiometric approach allows for the cancellation of variations in illumination, dye loading, photobleaching, cell thickness etc. The cells were kept in suspension with the help of a magnetic rod in Hanks buffer pH 7.4 at room temperature without extracellular Ca^{2+}. Ca^{2+} was added during the measurement to a final concentration of 2mM. Achieving a new osmotic balance confirmed that the cells were not leaky and thus they were in a good condition to study the activation of a channel. Typical responses of transfected cells are shown below (figure 2.14):

Figure 2.14: Examples of responses of VR1, VR-L and untransfected COS7 cells to 1μM capsaicin and pH change from 7.4 to 6.

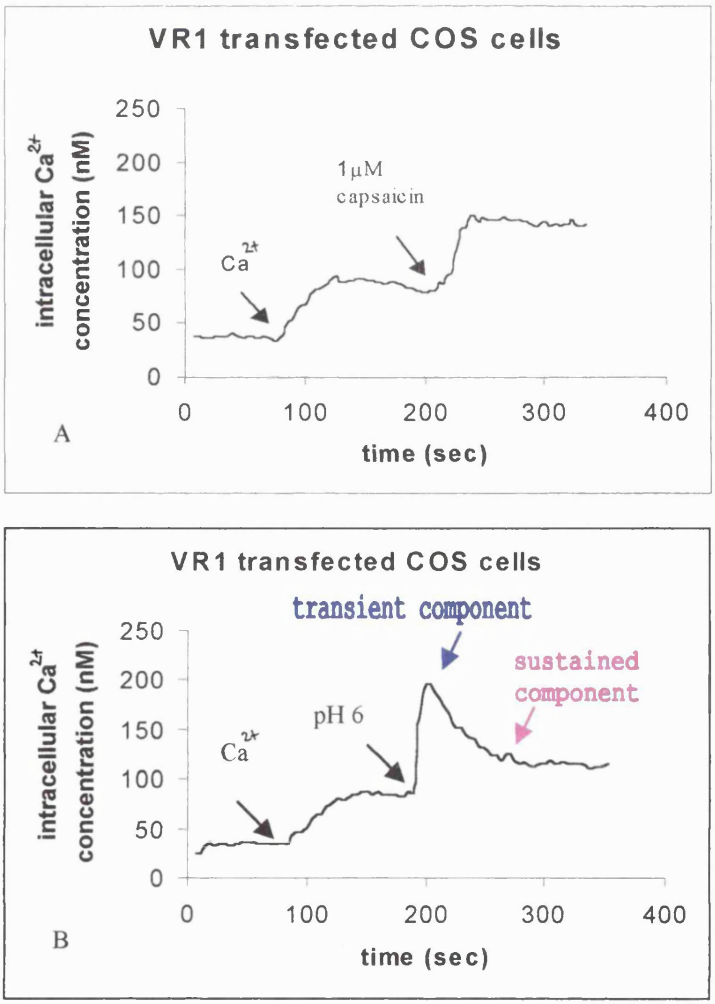

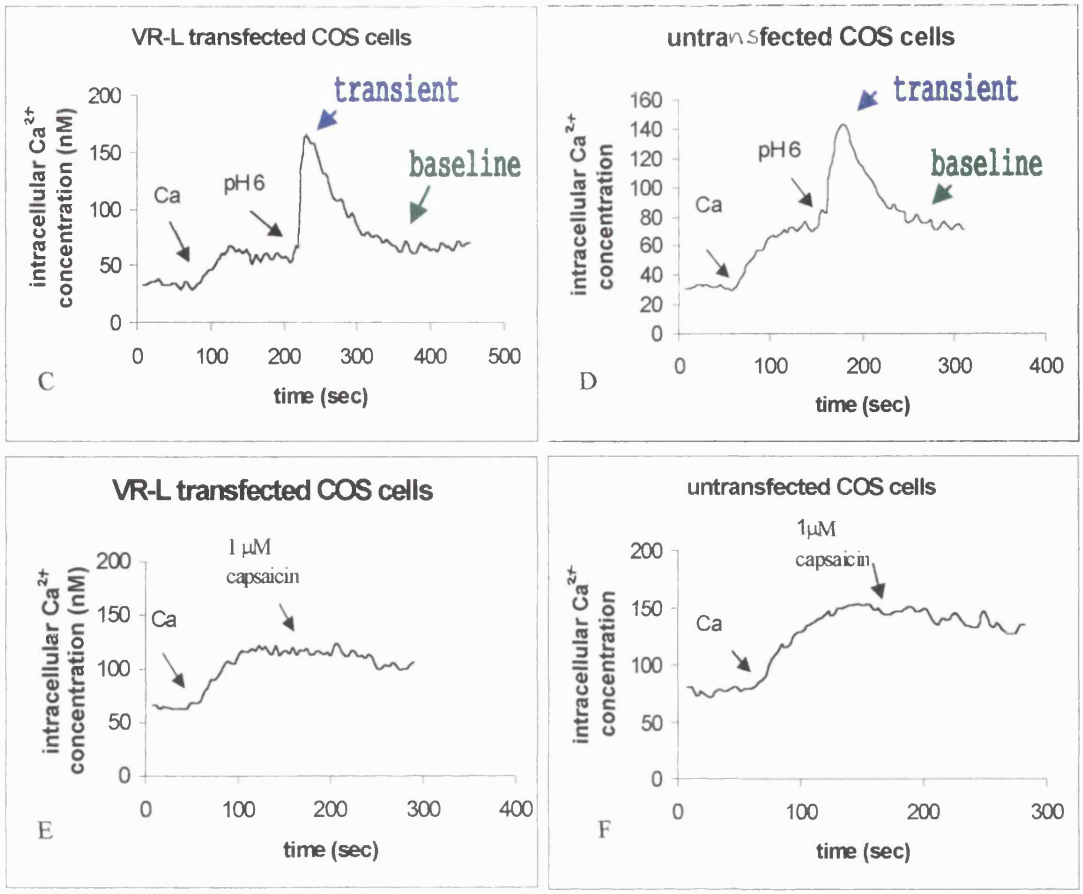

As it can be seen in figure 2.14, VR1 responds to capsaicin (panel A) while VR-L (panel E) and untransfected cells (panel F) do not. All the cells respond to pH decrease but with different potency. Additionally, the VR1 transfected cells exhibited a biphasic response to pH reduction, consisting of a transient and a sustained component (figure 2.14, panel B, blue and purple arrow respectively). VR-L (panel C) and untransfected cells (panel D) exhibited only the transient component (blue arrow) and then the current returned to baseline (green arrow). The results for capsaicin and pH responses were analysed statistically (figure 2.15).

Figure 2.15: Statistical analyses of VR1, VR-L transfected and naïve cells' responses

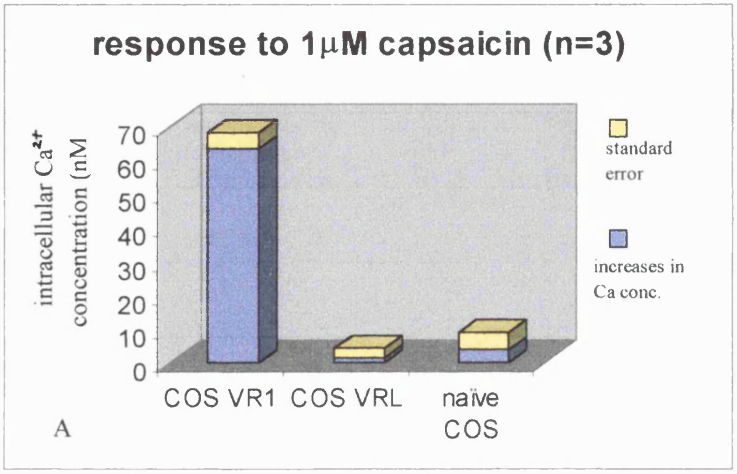

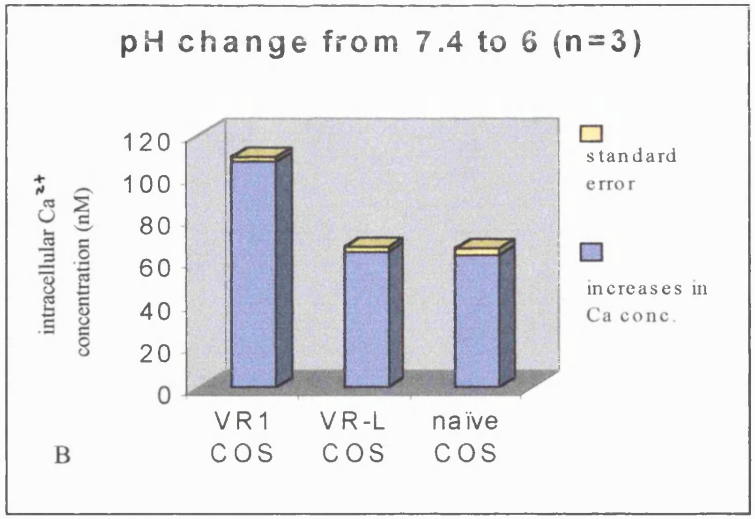

VR-L does not respond to capsaicin and pH decrease in a VR1 manner. It does not respond to capsaicin at all (figure 2.15A), while its response to pH change is similar to the one exhibited by untransfected COS cells (figure 2.15B). On the contrary, VR1 cells consistently responded to capsaicin and pH as expected (Tominaga *et al.*, 1998) eliciting an inward Ca^{2+} current that elevated the intracellular Ca^{2+} concentration almost x10 fold after capsaicin application (figure 2.15A) and roughly x2 fold after pH decrease compared to untransfected COS cells (figure 2.15B). The transient response (indicated by blue arrow in figure 2.14) exhibited by untransfected (panel D) and VR-L transfected cells (panel C) is reminiscent of an endogenous ASIC channel (acid-sensing ion channel) that responds to acidic environment with a transient current (Waldmann and Lazdunski, 1998). HEK293, COS7 and *Xenopus* oocytes have been found to express an endogenous proton-gated, rapidly inactivating, amiloride-sensitive membrane current that is probably encoded by a member of the ASIC family of channels (Cesare *et al.*, 1999b). Therefore, the transient component that is common between the VR1, VR-L and untransfected cells responses is due to an endogenous proton-gated channel, while the sustained component observed only in VR1 transfected cells that is clearly differentiated from baseline (figure 2.14B, purple arrow) is due to the capsaicin receptor.

An interesting observation (figures 2.16 and 2.17) that was made during the fura-2 recordings is that possibly the pH and capsaicin responses of VR1 cross-desensitise, in the same manner as heat and capsaicin responses (Tominaga *et al.*, 1998).

Figure 2.16: VR1 responses to 1μM capsaicin (A) and pH reduction from 7.4 to 6 (B).

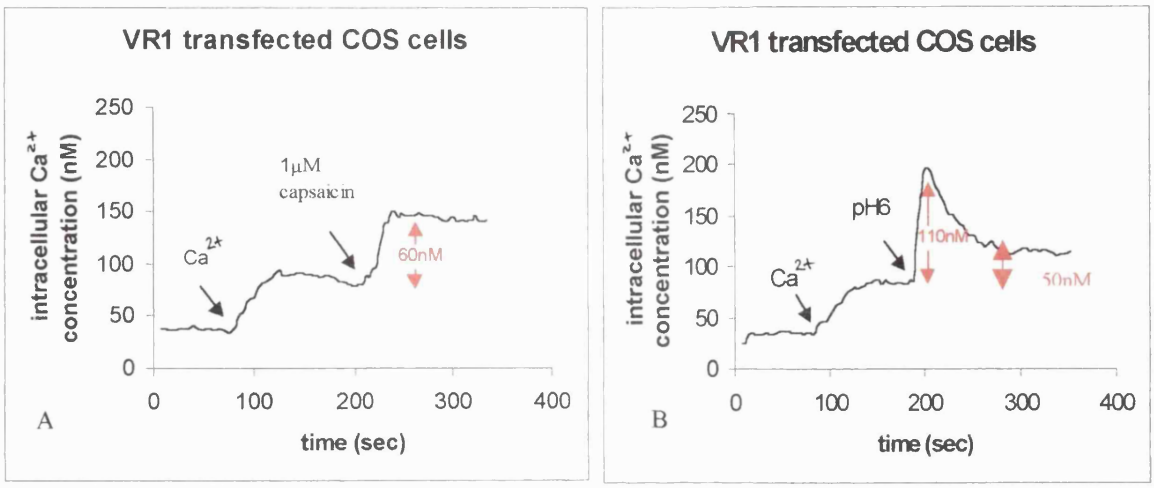

Figure 2.17: Co-application (A) or sequential application of 1μM capsaicin and pH reduction from 7.4 to 6 (B and C) in VR1 transfected COS7 cells.

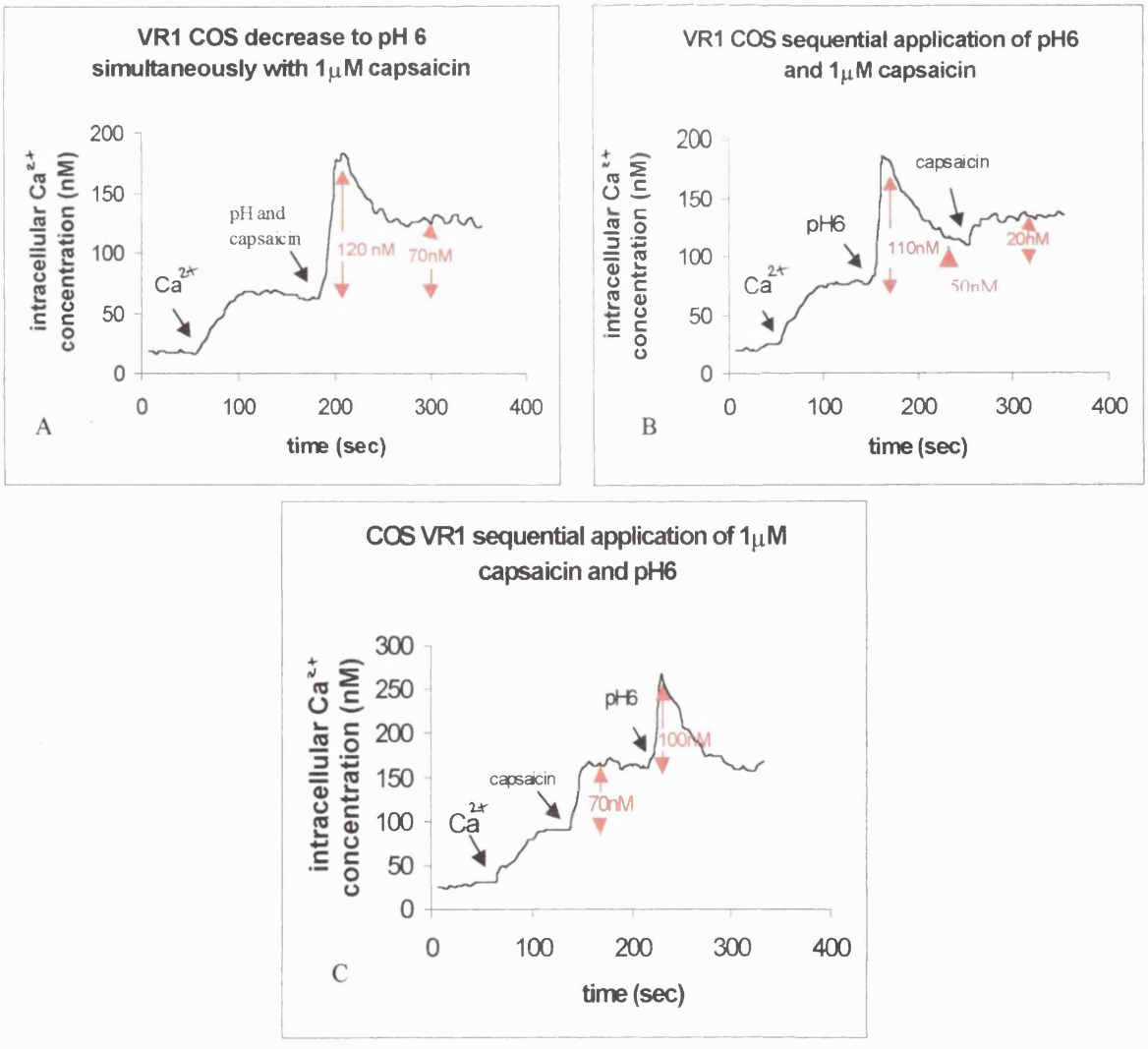

This preliminary data shows that pH change prior to capsaicin application (figure 2.17, panel B) desensitises the capsaicin evoked response (smaller intracellular Ca^{2+} concentration increase when compared with the single capsaicin application - figure 2.16 panel A). Likewise, application of capsaicin abolishes the sustained component of the pH response (figure 2.17 panel C) compared with single stimulation with protons (figure 2.16 panel B). Co-application of capsaicin and pH change (figure 2.17 panel A) seems to be synergistic. Nevertheless, one cannot postulate the existence of cross-desensitisation between capsaicin and pH responses, until this initial observation is supported by statistical analysis and repeated application of the stimuli.

2.4.2 Electrophysiological studies

Fluorometric studies showed that VR-L does not respond to capsaicin and protons. Since VR1 also responds to heat, it was interesting to examine whether heat activates VR-L. Heat experiments could not be conducted with the fluorometer, since it was not designed for such experiments. Dr. Cesare (UCL) kindly offered to examine heat responses using patch-clamp in an electrophysiological set-up that contained a heat exchanger with a rapid heating/cooling cycle. This devise could allow very rapid temperature changes (<20msec). Simultaneously with heat studies, the responses of VR1 and VR-L transfected cells to capsaicin and protons observed with fura-2 were confirmed. HEK293 cells were transfected with plasmids containing the genes of interest. The cells were also co-transfected with a plasmid containing GFP in a dilution 1:10 to the plasmid of interest. The elicited fluorescence allowed the identification of the transfected cells. Typical responses are shown below (figure 2.18).

Application of low pH (5.4) evoked a large but transient inward current in GFP(control) transfected and VR-L/GFP co-transfected cells. In VR1/GFP co-transfected cells, however, the evoked current was clearly larger and could be distinguished by a sustained component present throughout the application of the stimulus. As mentioned before (fluorometric studies section 2.4.1), the transient current is due to an endogenous proton responsive channel. Capsaicin application (500 nM) failed to evoke any response in GFP-transfected or VR-L/GFP co-transfected cells. VR1/GFP co-transfected cells, on

the other hand, show a large current that starts to recover after wash out, in agreement with Caterina *et al.* (1997).

Figure 2.18: Membrane inward currents measured at -60 mV evoked by fast application of high temperature 52°C (T), pH 5.4 (pH) and 500 nM capsaicin (caps) in HEK293 cells transfected with either GFP, GFP/VR-L or GFP/VR1.

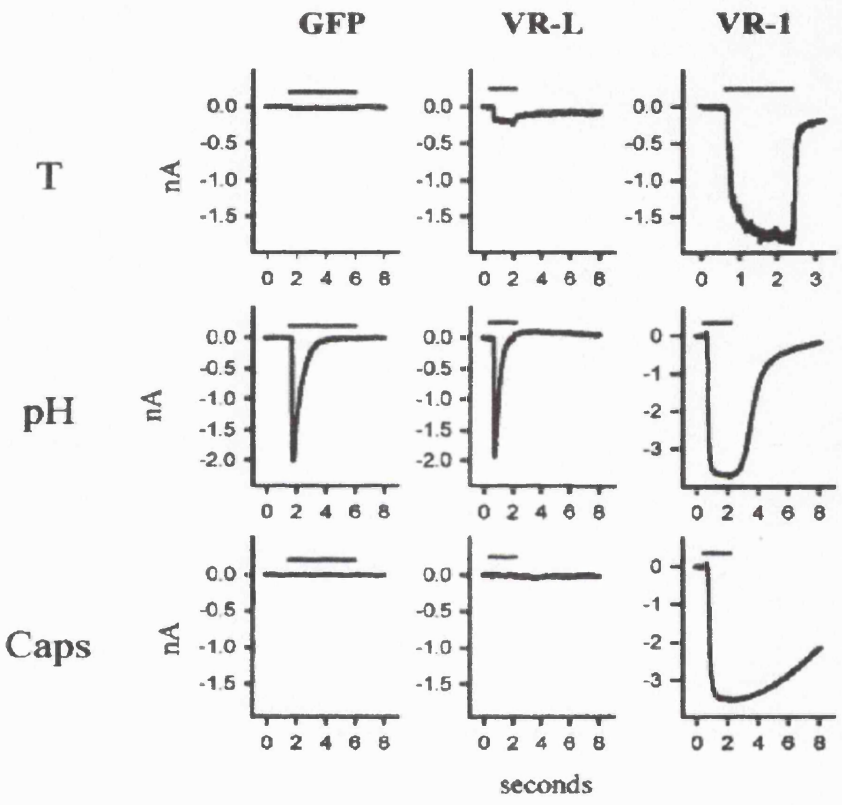

Brief pulses of heat (52°C) evoked fast activating inward currents in VR1/GFP co-transfected cells as reported before (Caterina *et al.*, 1997; Tominaga *et al.*, 1998). GFP-transfected and VR-L/GFP co-transfected cells both responded to heat with small currents of variable amplitude, probably due to a non-specific effect of heat on leakage currents. This effect can be particularly dramatic at temperatures higher than 53°C, that many times led to the disruption of the cell membrane. Dr. Wafford's group (Merck) repeated the electrophysiological experiments on VR1 and VR-L with heat, capsaicin and proton application. Their studies also included co-transfections of VR1 with VR-L to examine the possibility of a functional interaction between the two channels. A statistical representation of the results can be seen in figure 2.19.

Figure 2.19: Statistical analysis of high temperature 55^{0}C, pH 6.0 and 1μM capsaicin responses in HEK293 cells transfected with GFP, GFP/VR-L or GFP/VR1.

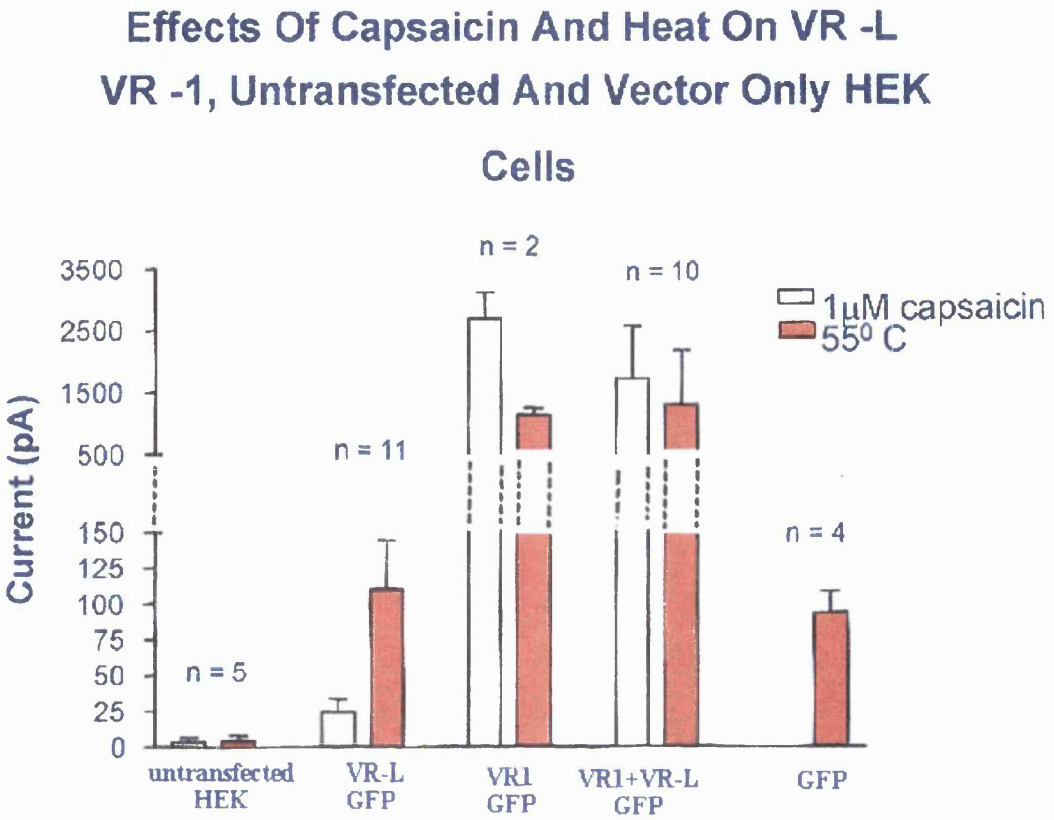

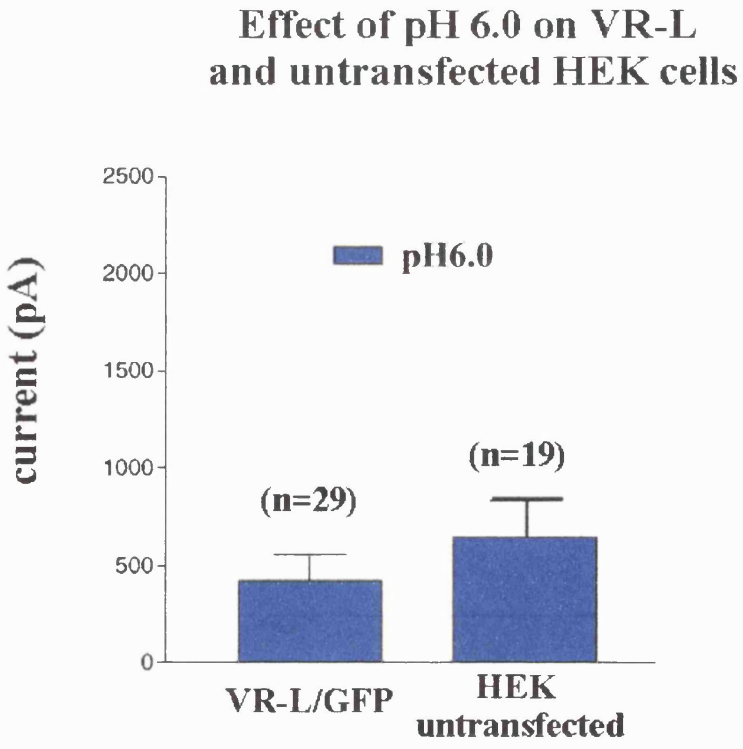

The statistical analysis confirmed that VR-L does not respond to acidic pH, capsaicin and heat. Additionally, when co-expressed with VR1, it does not alter the response of the capsaicin receptor to capsaicin or heat. Therefore it seems unlikely that VR-L has a synergistic or inhibitory effect on the VR1 function. Comparison of untransfected cells with vector transfected cells shows that transfection renders the membrane sensitive and the cells become leaky at high temperature. The small VR-L response to heat is hence non-specific and confirms our observation (figure 2.18) that non-physiological temperatures disrupt the cellular membrane.

In summary, fluorometric studies using fura-2 and patch-clamp studies showed that VR-L does not respond to capsaicin, heat and protons. VR-L resembles the TRP channels, of which a few members are store-operated i.e. they are activated by depletion of intracellular Ca^{2+} stores. Depletion of intracellular stores with thapsigargin (inhibitor of a sarcoplasmic/endoplasmic reticulum Ca^{2+}-ATPase) or with activation of an endogenous muscarinic receptor (G-protein coupled receptor) in VR-L transfected HEK293 cells showed that VR-L is not a store-operated channel (Dr. Delmas, UCL, personal communication). Because TRP3 and TRP6 are not store operated channels but are activated with diacylglycerol (Hofmann *et al.*, 1999), Dr. Delmas also examined the possible activation of VR-L by this second messenger. No current was identified upon application of a membrane permeable diacylglycerol analogue on VR-L transfected cells, indicating that this pathway does not activate VR-L. Finally, experiments contacted by Dr. Davis' group (personal communication, GlaxoSmithKline) showed that anandamide, a VR1 agonist, failed to activate VR-L.

2.5 VR-L is expressed on the cell membrane

Electrophysiological and fluorometric studies conducted by our group and collaborators showed that VR-L is not activated by capsaicin, heat, protons, depletion of intracellular stores, diacylglycerol and anandamide. Failing to identify the functional role of VR-L, the possibility that the protein does not reach the cell membrane to compose a functional channel was considered. In order to explore this possibility, an epitope was attached on the extracellular loop of the gene between the transmembrane domains 5 and 6. Subsequently, the protein expression was investigated with immunocytochemistry.

The *c-myc* epitope EQKLISEEDL was added after the aspartic acid at position 561 in the rat VR-L sequence, which is situated after transmembrane domain 5 and before the

pore loop (appendix 2.1). The epitope tagging was accomplished following a PCR strategy based on amplification of complementary templates (figures 2.20 and 2.21).

Figure 2.20: Epitope tagging PCR strategy

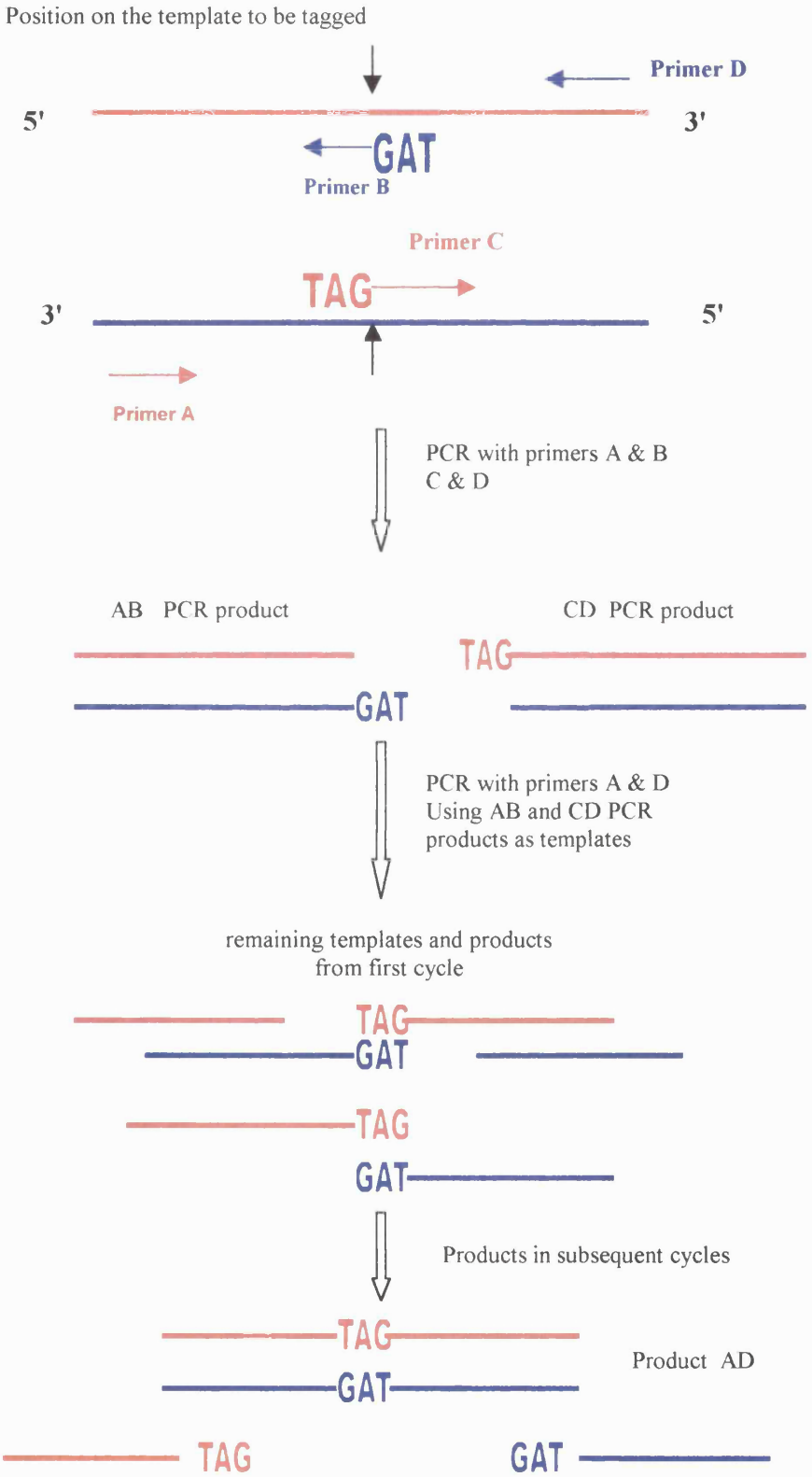

Subsequently the PCR product AD was digested with appropriate enzymes to be subcloned into the vector, digested with the same enzymes, that contained the original untagged sequence.

Figure 2.21: Subcloning the tagged gene sequence

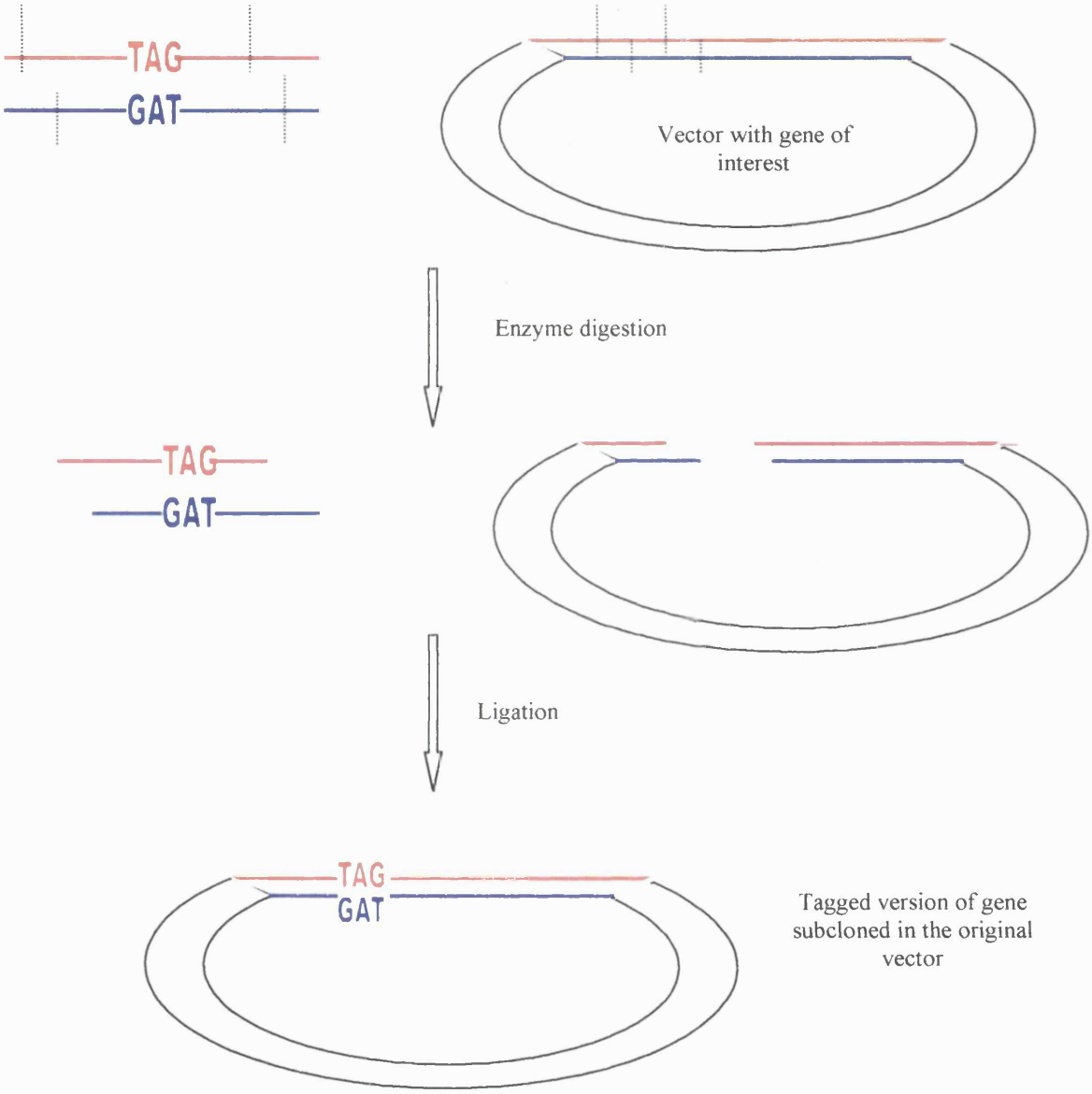

Primers equivalent to primers A and B (figure 2.20) were designed to amplify the rat VR-L region from nucleotide 1638 to 2040 (appendix 2.2). Primers equivalent to C and D amplified the VR-L region from nucleotide 2040 to 2501. For convenience the corresponding regions will be called AB (402bp product) and CD (462bp product). The PCR products amplified by the primers A&B and C&D are shown in figure 2.22.

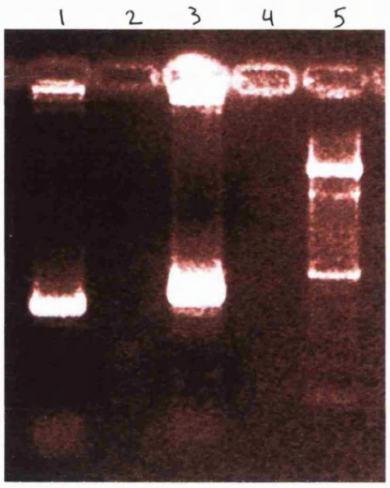

Figure 2.22: PCR amplification of AB and CD regions of rat VR-L

Lane 1: AB PCR product (~400bp expected)
Lane 3: CD PCR product (~ 460bp expected)
Lane 5: 100bp ladder

In order to achieve high fidelity of template amplification with as few mistakes as possible, the Pfu polymerase was used and the PCR was run for only 15 cycles. Before running the PCR samples on a gel, they were blunted using the Klenow enzyme. This treatment removed any base overhangs that might have been added at the product's 3' end by traces of Taq polymerase contained in the Pfu preparation. The PCR products AB and CD were extracted from the gel and purified, with the purpose of being employed as templates for a second PCR, giving rise to product AD (figure 2.20). The amplification of the rat VR-L nucleotide region 1637-2501 (AD product) was achieved with the *c-myc* epitope incorporated (figure 2.23).

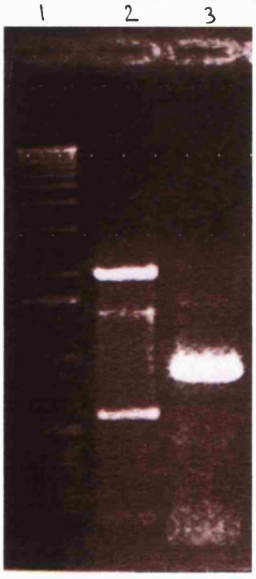

Figure 2.23: Amplification of the AD region of rat VR-L, incorporating the *c-myc* epitope

Lane 1: 1kb ladder
Lane 2: 100bp ladder
Lane 3: PCR product using fragments AB and CD as templates and the primers A and D (size expected: ~ 860bp)

The AD PCR product was purified from the gel and was digested (figure 2.25) with the enzymes NarI and Eco47III (strategy displayed in figure 2.21). The same enzymes were utilised to digest the rat VR-L sequence cloned in the vector pcDNAI (appendix 2.3, figure 2.24).

Figure 2.24: Digestion of rat VR-L in pcDNAI with NarI and Eco47III
Lane1: 1kb ladder
Lane2: digested rat VR-L (sizes expected: 6.7kb and 0.73bp)

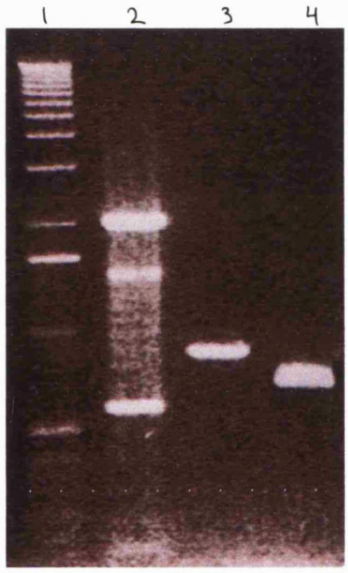

Figure 2.25: Digestion of PCR product AD with NarI and Eco47III

Lane1: 1kb ladder
Lane2: 100bp ladder
Lane3: undigested AD PCR product
Lane4: digested AD PCR product (size expected: ~ 0.73bp)

The digested vector (6.7kb) and the digested AD PCR product (0.73kb) were purified from the gel and they were subsequently ligated, following dephosphorylation of the vector. *E. coli* bacteria were transformed with the ligated DNA, colonies were selected on ampicillin LB plates and their plasmid DNA preparations were digested with NarI and Eco47III to confirm their identity. The plasmids that showed the correct digestion profile were sequenced to verify the incorporation of the *c-myc* epitope (appendix 2.4).

To confirm that the tagged VR-L gene can express a protein of the estimated size, a kit was used for *in vitro* transcription and translation of the construct. The mRNA is transcribed from the promoter prior to the gene (in this case T7) and translated incorporating radioactive methionine. The radioactive protein is run on a SDS-PAGE gel, which is subsequently dried onto paper and exposed on film, allowing the visualisation of the protein. The experiment was performed n=1 time.

Figure 2.26: *In vitro* transcription and translation of the original rat VR-L and of the rat VR-L with the *c-myc* epitope on the extracellular loop (rat VR-LmycX). The left side of the picture shows the Coomassie blue staining of the gel and the right side, the exposed film. The gel was loaded in the following order: protein molecular weight marker, rat VR-L, rat VR-LmycX, empty well, luciferase gene (positive control).

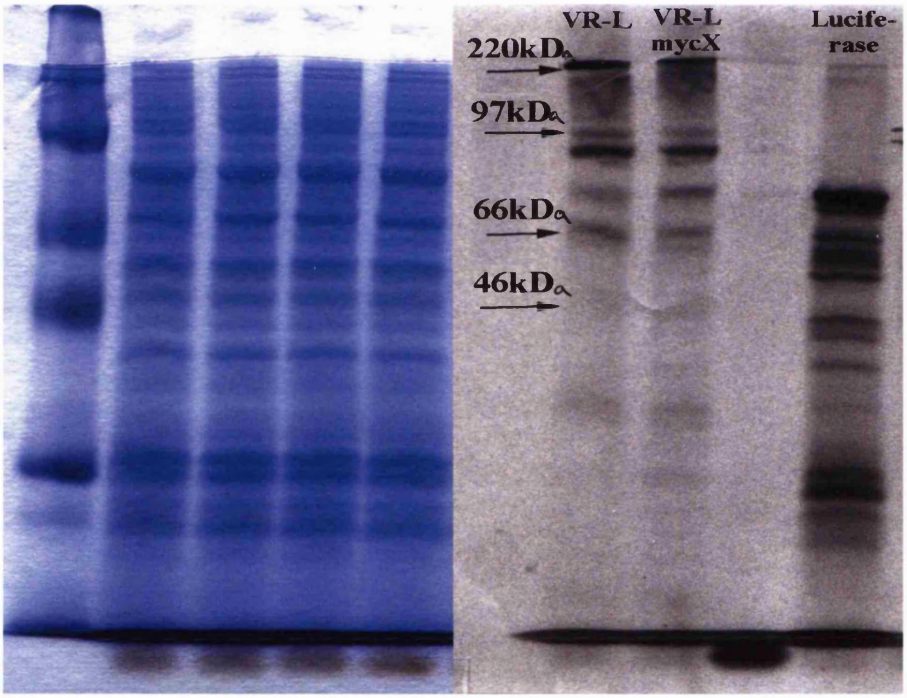

The construct rat VR-L mycX (VR-L with the *c-myc* epitope on the 3rd extracellular loop) expresses a protein of the expected size (~88kDa) as the original rat VR-L. The *c-myc* epitope insertion did not cause frameshift or insertion of an alternative initiation methionine or insertion of a stop codon. Hence, the tag did not interfere with the gene expression and the construct could be used for cell transfections. The construct was expressed in HEK293 cells. In order to ensure the transfer of the protein to the plasma membrane, the detection of the *c-myc* epitope was attempted with immunocytochemistry without permeabilising the cells (figure 2.27). If the protein had

reached the membrane and had incorporated in the lipid bilayer as ion channels do, then the *c-myc* epitope would be protruding from the cell surface and would be approachable by an antibody extracellularly. In that case, detection would be possible without permeabilising the cells. Permeabilisation is usually carried out to facilitate the antibody transfer inside a cell to detect an epitope intracellularly.
The experiment was performed n=1 times.

Figure 2.27: Detection of rat VR-L mycX with fluorescent immunocytochemistry on non-permeabilised HEK293 cells. Picture A: excitation of secondary FITC antibody that recognises the *c-myc* antibody. Picture B: visual field of picture A. Picture C: untransfected HEK 293 cells subjected to immunocytochemistry (negative control). Picture D: visual field of picture C.

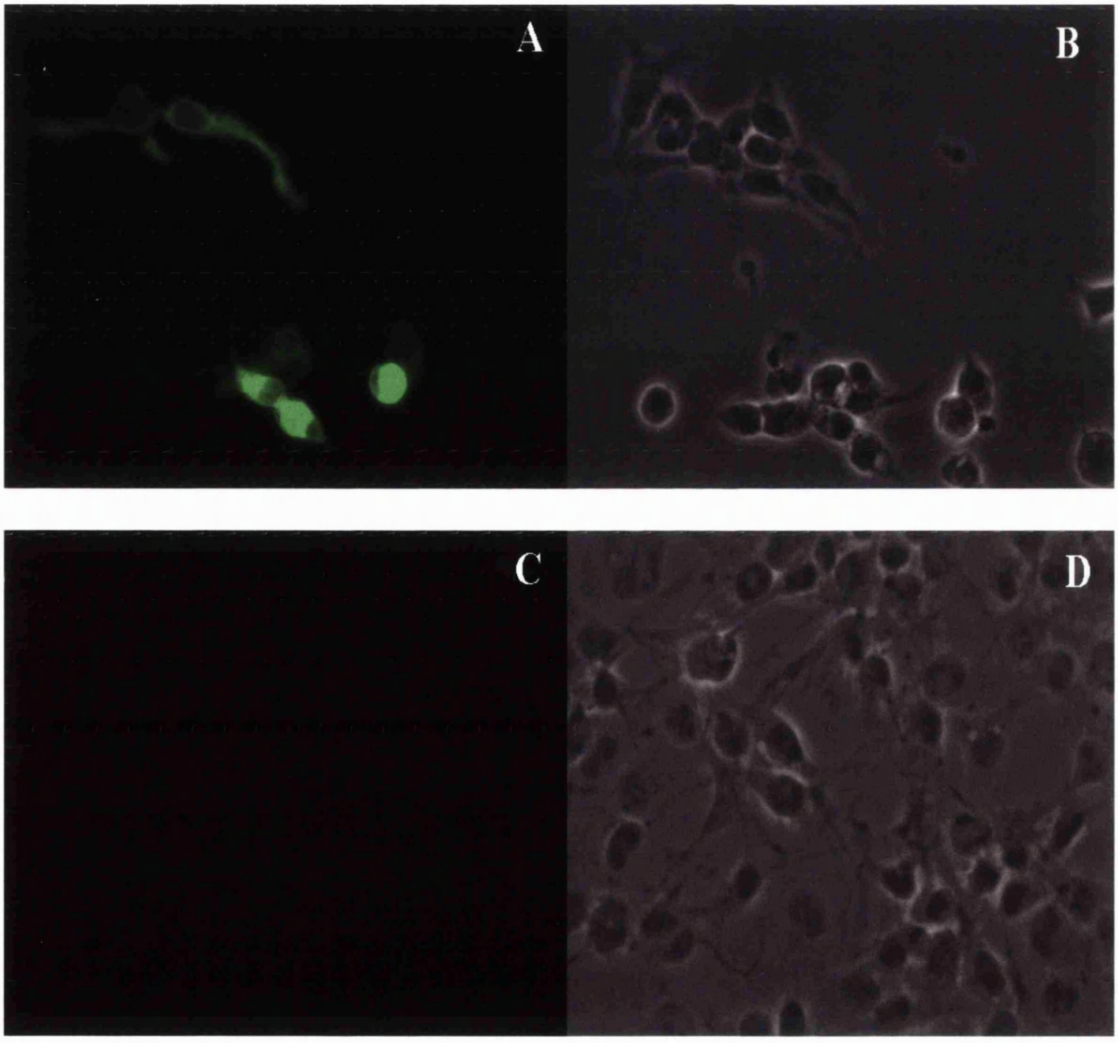

The rat VR-L mycX protein reaches the cell membrane, since the *c-myc* epitope on the extracellular loop of the protein is accessible to the *c-myc* antibody, without permeabilising the membrane. The negative control verified the authenticity of the

signal. Therefore, the channel protein was successfully processed and expressed on the cell membrane, suggesting that VR-L is a functional channel.

In summary, VR-L the novel member of the vanilloid receptor family is expressed in a variety of tissues mainly from the nervous and the immune system. RT-PCR studies using RNA from capsaicin-treated and control cultures showed that VR-L is expressed in the non-capsaicin sensitive DRG cell population. Semi-quantitative RT-PCR studies showed that the VR-L expression, like VR1's, is upregulated by NGF *in vivo* and *in vitro*. Therefore, VR-L like other receptors can be regulated by neurotrophins. Fluorometric and electrophysiological studies showed that VR-L is not activated by capsaicin, protons and heat and thus it is not a vanilloid receptor. Data produced by collaborators showed that VR-L is not a store-operated channel, is not activated by the VR1 agonist, anandamide, and does not share the TRP3 and TRP6 activation pathway. Since none of the known mechanisms that activate the TRP channel family succeeded in stimulating VR-L, the possibility that the protein does not form a functional channel was investigated. Detecting VR-L expression on the cell membrane via extracellular epitope recognition demonstrated that VR-L reaches the cell membrane. Further studies need to be carried out to assign a role on this novel vanilloid-like protein.

CHAPTER 2

Investigating the functional role of VR-L

DISCUSSION

VR-L tissue distribution

We cloned a new member of the vanilloid receptor family, sharing 49% amino acid identity with VR1 that we called Vanilloid-Receptor like Protein (VR-L). Before embarking on functional studies, the expression of the gene in different tissues was examined, as a gene's tissue distribution can reveal clues towards its function. By performing RT-PCR using RNA from rat tissues, the VR-L tissue distribution was established. The reason the RT-PCR method was used instead of Northern blotting is because it is more sensitive. Northern blotting failed to identify VR1 expression in the central nervous system (Caterina *et al.*, 1997), while immunocytochemistry and *in situ* hybridisation revealed VR1 expression in the rat and human brain (Mezey *et al.*, 2000). Since RT-PCR is less time consuming than *in situ* hybridisation, it was preferred for the initial characterisation.

Primarily, the cDNA samples were normalised using primers for cyclophilin, an abundant cytosolic protein (figure 2.1A). Once the cDNA amounts were equalised, a PCR was performed using primers for VR-L amplification (figures 2.2 and 2.3A). At the time this experiment was conducted, the VR-L cloning had not been completed and thus there was not enough sequence information to design primers that would allow co-amplification with cyclophilin in the same tube. For that reason the VR-L RT-PCR was performed separately from cyclophilin. VR-L expression was identified in high levels in spinal cord, dorsal root ganglia, nodose ganglia, lung, adrenal gland and ovaries (Garcia *et al.*, 1999). In more modest levels, VR-L was found to be expressed in the brain, cerebellum, heart, thymus, spleen, urinary bladder and testis. A control RT-PCR performed with no reverse transcriptase during the cDNA synthesis, showed that there was no genomic DNA contamination (figures 2.1B and 2.3B) and thus the PCR products were representative of the gene mRNA levels. The cyclophilin primers had been designed to cross an intron, providing an extra control for genomic DNA contamination. The VR-L expression pattern is strikingly different from the one exhibited by the capsaicin receptor. VR-L is expressed in a wide variety of tissues of mainly the nervous and the immune system. This result was not unexpected as the tBLASTn search that led to the cloning of VR-L, had retrieved EST entries from a variety of tissues such as endothelial cells, melanocytes, thymus, spleen, brain (table 1.1, Chapter 1).

The VR1 and VR-L transcripts are upregulated by the Nerve Growth Factor both *in vitro* and *in vivo.*

Winter *et al.* (1988) reported capsaicin sensitivity of adult rat DRG neurons in culture to be NGF-dependent. NGF deprivation led to the loss of the capsaicin induced currents in these neurons, which was reversible with the re-addition of the neurotrophin. This phenomenon is in agreement with the finding that sciatic nerve axotomy leads to the reduction of VR1 mRNA levels (Michael and Priestley, 1999), which is probably due to depletion of target tissue derived neurotrophic factors. During inflammation, the NGF concentration increases peripherally, which causes the mast cells to degranulate and release substances like histamine and NGF that sensitise sensory neurons and can cause hyperalgesia (reviewed by Shu and Mendell, 1999). These researchers reported that NGF also has a direct effect on VR1 by preventing tachyphylaxis during repeated capsaicin applications. Considering that VR1 is necessary in developing hyperalgesia (Caterina *et al.*, 2000, Davis *et al.*, 2000) it was not surprising to find that NGF, an inflammatory molecule, regulates its function.

The role of NGF in inflammation and hyperalgesia together with the observation that VR-L is expressed in tissues of the nervous and the immune systems led to studying its possible regulation by this neurotrophin. A semi-quantitative RT-PCR approach was followed as described before (Boucher *et al.*, 2000a). cDNA was synthesised from adult rat DRG neurons that had been cultured in the presence of NGF or anti-NGF antibodies (*in vitro* approach). For *in vivo* studies, cDNA was also synthesised from neonatal rats that had been injected with NGF and control rats that had been injected with carrier solution. Prior to comparing transcript levels in the different mRNA populations, it was necessary to establish the exponential amplification of the genes studied (figures 2.5 and 2.6). This was essential because during the polymerase chain reaction, the DNA amplification reaches a plateau due to reagents depletion, at which point the signals are saturated and cannot be compared since they appear to be of equal intensity. The concentrations of the treated samples were normalised using cyclophilin primers (figure 2.7). Primers for CGRP were used as a positive control for the NGF treatment as its expression is known to be upregulated by NGF (Lindsay *et al.*, 1989). For the cultures, adult DRG were used since they do not depend on NGF for their survival. In both cases of NGF application *in vivo* and *in vitro* (figures 2.9-2.12), elevation of the CGRP, VR1 and VR-L mRNA levels

was observed (Garcia *et al.*, 1999). The same upregulation was observed with two different sets of primers for both vanilloid genes. The observed VR1 upregulation by NGF is in agreement with the recent studies contacted by Winston *et al.* (2001) who also reported up-regulation of VR1 transcript levels by NGF in cultured DRG cells with Northern blot studies. Considering that a) NGF is retrogradely transported to the cell bodies in DRG where it can increase gene expression levels e.g. BDNF (Michael *et al.*, 1997) and that b) NGF has been shown to affect the function and expression of VR1, it was interesting to examine the possible effect of this neurotrophin on VR-L during inflammation and injury.

VR-L is expressed in the non-capsaicin-sensitive DRG population

Semi-quantitative RT-PCR studies showed VR-L expression in DRG neurons among other tissues. The upregulation of the gene's transcript levels by NGF led to a more detailed investigation of its expression in DRG. In the absence of an antibody against VR-L, an alternative method was deployed to study the VR-L expression. Because capsaicin has neurotoxic effects in large concentrations (>5μM), it can be used to eliminate the capsaicin-sensitive cells and thus distinguish them from the non-capsaicin-sensitive neuronal population. A semi-quantitative RT-PCR approach was followed where cDNA was synthesised from RNA harvested from capsaicin-treated and control DRG cultures. Amplification for the gene cyclophilin was used to normalise the samples. The VR1 mRNA levels were used as a positive control for the capsaicin treatment (figure 2.13 and also in Chapter 3 figure 3.2B). Capsaicin treatment (3μM, overnight) significantly reduced the VR1 transcript levels as expected, since the VR1 expressing cells respond to large capsaicin concentrations by a Ca^{2+} influx which leads to mitochondria vesiculation and cell lysis (Olah *et al.*, 2001b). Conversely, VR-L transcript levels were unaffected by capsaicin treatment. This indicates that the VR-L expressing cells did not undergo necrotic death due to the neurotoxic effect of capsaicin. This suggests that VR-L is not expressed in the same type of DRG neurons as VR1.

The neurotrophin study showed that VR-L mRNA levels are upregulated by NGF *in vivo* and *in vitro*. VR1 transcript upregulation by NGF was also observed, in agreement with Michael and Priestley (1999), who showed that 65% of trkA DRG cells also stain for VR1. Considering that VR-L is not expressed in the small, capsaicin sensitive DRG neurons, it seems unlikely that it co-expresses with trkA in a significant

proportion of cells to explain its direct upregulation by NGF. Unlike the VR1 upregulation that is triggered by NGF binding to trkA in the same neuron, the VR-L upregulation is probably a paracrine effect. The paracrine effect could be mediated by a neuropeptide released by small diameter neurons in response to NGF that subsequently affects VR-L expression in a different cell population. Since the NGF concentration is increased during inflammation, such an effect could have major physiological importance. An example of paracrine regulation was reported by Mantyh *et al.*, (1994) who showed the release of the neuropeptide Y by large diameter DRG neurons following injury. The researchers suggested a paracrine effect of this inhibitory neuropeptide released by large diameter neurons on small diameter neurons expressing NPY receptors that could lead to obstructing signalling of nociceptive information following peripheral injury. If VR-L is subject to paracrine regulation, it would be interesting to identify the molecule released by small diameter neurons that regulates the expression of the receptor.

An alternative possibility is that under adverse conditions, VR-L expression is not restricted to large diameter neurons only. For example, injury can evoke changes in gene expression patterns. Hudson *et al.* (2001) made the interesting observation that VR1 protein expression is higher in undamaged DRG after partial sciatic nerve section and L5 spinal nerve ligation. Furthermore, they detected increased VR1 expression in large A-fibre somata in the undamaged DRG. The finding of increased expression of a traditionally small diameter neuron gene in large diameter neurons after injury is not uncommon. SNS, a sodium channel expressed in small diameter DRG neurons, is found to be expressed in large, myelinated A fibres after L5 nerve section (Porreca *et al.*, 1999). Considering the alterations in gene expression patterns evoked by injury, one could postulate similar changes in VR-L expression during injury or inflammation. Analogous to inflammation, the change observed after nerve injury could be mediated by neurotrophins as well, since the distal damaged nerves undergo Wallerian degeneration leading to neurotrophin release from macrophages. Therefore, although VR-L is not traditionally expressed in small diameter neurons, the possibility that in adverse conditions its expression is triggered in small diameter neurons should be investigated.

Attempts to assign a functional role on VR-L

VR-L resembles TRP channels and VR1 in that it contains 6 transmembrane domains, ankyrin repeats and a putative pore loop. Since VR1 and the TRP channels allow the influx of calcium into the cell, one can postulate that VR-L is also a calcium channel. For that reason, a Ca^{2+} readout system was used for functional studies. The ratiometric dye fura-2 was used, that binds to Ca^{2+} and its excitation spectrum shifts from $\lambda=$ 340nm to $\lambda=$ 380nm as free Ca^{2+} decreases. When there is a lot of unbound Ca^{2+}, the fluorescence emission of the dye is high at $\lambda=$ 340nm and low at $\lambda=$ 380nm. When Ca^{2+} binds to the dye and there are few free Ca^{2+} ions, the fluorescence emission of the dye is low at $\lambda=$ 340nm and high at $\lambda=$ 380nm. COS7 cells were cultured and transfected with the genes of interest. Subsequently, the cells were harvested, were loaded with fura-2 and were kept in suspension in a fluorometer cuvette in the absence of Ca^{2+}. Addition of Ca^{2+} to the final concentration of 2mM (figure 2.14) evoked the passive diffusion of ions into the cells. Achieving a baseline in the Ca^{2+} readout, i.e. an osmotic balance, confirmed that the cells were not leaky and could be used for the fluorometer studies.

VR1 transfected cells were used as a positive control. These cells responded to capsaicin (figures 2.14 and 2.15) with an intracellular Ca^{2+} increase establishing the efficacy of the system. An interesting observation was that the increase of the intracellular Ca^{2+} concentration reached a plateau and it did not return to baseline. This is in disagreement with the electrophysiological recordings of VR1 (Caterina *et al.*, 1997), where the VR1 elicited currents exhibit tachyphylaxis. The difference between the two systems is that the patch clamp method records the current going through a channel on the membrane and thus monitors the activity of the channel, while fluorometric studies record changes in the intracellular Ca^{2+} concentration. Dedov and Roufogalis (2000) observed the same phenomenon in fluorometric studies of DRG neurons challenged with capsaicin. They observed that the intracellular Ca^{2+} concentration returned to baseline on average 15min after the capsaicin application, followed by medium change. Since the recordings presented in Chapter 2 were limited to about 3min post-application and the capsaicin solution was not washed out, full recovery of the intracellular Ca^{2+} concentration was not observed. Dedov and Roufogalis (2000) suggested that the delay in baseline recovery is due to Ca^{2+} buffering by mitochondria. When loads of Ca^{2+} enters the cell, the extra ions are accumulated by mitochondria, which are then released in the cytoplasm by a Na^{+} /Ca^{2+}

exchange mechanism on the mitochondrial membrane. Subsequently, the Ca^{2+} exits the cell via a plasma membrane Na^{+} /Ca^{2+} exchanger and an ATP-dependent Ca^{2+} pump. By using a mitochondrial uncoupler that releases the accumulated Ca^{2+} by dropping the mitochondrial membrane potential, the researchers showed that more Ca^{2+} enters the cell and is stored in mitochondria upon VR1 excitation than due to voltage-gated calcium channels. Additionally, the release of Ca^{2+} from mitochondria after capsaicin application is slower than after activation of voltage-gated calcium channels. The prolonged elevation of intracellular Ca^{2+} observed after capsaicin application might underlie the receptor desensitisation observed in repeated exposure to the irritant. The VR-L transfected cells and the control untransfected cells did not respond to capsaicin (figures 2.14 and 2.15). Therefore, VR-L does not function as a vanilloid receptor.

The VR1 transfected cells responded to a drop in pH from 7.4 to 6 as expected (Tominaga *et al.*, 1998). As seen in figures 2.14 and 2.15, VR-L and untransfected cells responded to protons but with a smaller increase in the intracellular Ca^{2+} concentration. Comparing the traces, one can see that the VR1 response to protons consists of two parts: an initial abrupt elevation of intracellular Ca^{2+} that rapidly inactivates followed by a prolonged plateau, which is higher than the baseline (figures 2.14 and 2.16B). The VR-L and the control cells exhibit the same abrupt elevation in intracellular Ca^{2+} that quickly recovers but they lack the sustained component observed in the VR1 response. This pattern is reminiscent of the patch clamp recordings on the VR1 receptor that showed a biphasic response (Tominaga *et al.*, 1998). The transient component of the response has been attributed to endogenous, amiloride-sensitive, proton-gated channels of the ASIC family of receptors. Cesare *et al.* (1999b) showed cell lines like HEK and COS cells to express an endogenous proton activated current that can be blocked by amiloride, suggesting an endogenous ASIC channel. It is possible that the transient elevation of Ca^{2+} observed in the fluorometric readings is due to the activation of an ASIC channel, while the sustained component observed only during VR1 activation is specific to the capsaicin receptor. Application of amiloride could confirm this hypothesis. Nevertheless, when comparing overall elevation of intracellular Ca^{2+} it is obvious that VR-L responded to protons exactly like untransfected cells, suggesting that protons do not activate the channel. Finally, figure 2.16 shows an interesting observation on the VR1 activation. Preliminary results show that protons and capsaicin cross-desensitise in a manner similar to the heat-capsaicin

cross-desensitisation observed in VR1 (Tominaga *et al.*, 1998). Protons and capsaicin seem to abolish each other's responses but when applied together they seem to work synergistically.

Electrophysiological recordings conducted by Dr. Cesare and Dr. Wafford's group confirmed the fluorometric results (Garcia *et al.*, 1999). Additionally, they carried out experiments with heat that were not possible with the fluorometer. Capsaicin, protons and heat-activated heterologously expressed VR1, while VR-L cells responded like control, mock-transfected cells (figures 2.18 and 2.19). Application of low pH 5.4 evoked only a transient current in the VR-L transfected cells as in control cells, that is due to an endogenous proton activated channel. Capsaicin did not elicit any response in these cells. Pulses of heat (52^0 C) on VR-L transfected cells resulted in small and variable amplitude currents that were also observed in control cells. In many experiments exposure to such high temperature resulted in the cell membrane disruption suggesting that the occasionally observed small currents were due to non-specific cell leakage. Comparison of untransfected cells and mock transfected cells revealed that the transfection itself rendered the cells sensitive to heat, causing current leakage at high temperatures (figure 2.19). Application of heat and capsaicin on cells co-expressing VR1 and VR-L elicited characteristic VR1 responses, indicating that VR-L does not affect the temperature and vanilloid sensitivity of the capsaicin receptor.

Fura-2 and electrophysiological studies showed that VR-L does not function like a vanilloid receptor, since it does not respond to capsaicin. Unlike VR1, it does not respond to protons and heat. Co-expression of VR-L with VR1 does not alter the vanilloid and heat sensitivity of the capsaicin receptor, suggesting that VR-L does not have an inhibitory or synergistic effect on VR1. Unfortunately, no studies on the effect of osmolarity on VR-L were conducted, but considering the widespread distribution of the gene in tissues not associated with such a function, it is highly unlikely that osmotic changes activate VR-L. Therefore, the function of VR-L remains elusive to this point.

VR-L is a functional receptor?

Application of noxious stimuli like heat, capsaicin and protons that activate nociceptors failed to activate VR-L. Although VR-L is expressed in nociceptors, it might not respond directly to noxious stimuli but have a different role e.g. in the development of the nociceptor. Alternatively, VR-L might be a pseudogene that is not expressed. To test

this possibility, a *c-myc* epitope was placed on the extracellular loop between transmembrane domains 5 and 6 of VR-L and followed its expression on the plasma membrane of host cells with immunocytochemistry. The immunocytochemistry was performed without permeabilising the cells, so that the antibody could reach the epitope only when it is placed extracellularly i.e. the protein is expressed on the plasma membrane.

The construct was engineered via a PCR method based on amplification of complementary templates (figure 2.20). Briefly, two VR-L PCR products were generated that contained complementary sequences of the *c-myc* epitope at their 3' terminals. One of the PCR products corresponded to a short region of the VR-L sequence prior to the tag insertion point and the other PCR product contained the VR-L sequence after the tag insertion point. By using these two PCR products as template for a second PCR reaction, a product was obtained that contained a short region of VR-L with the *c-myc* tag inserted. By employing cloning methods this region was used to substitute the corresponding "wild-type" sequence in the VR-L gene. *In vitro* transcription and translation confirmed that the construct expressed the right size protein, indicating that no frameshift occurred during the cloning manipulations and that the insertion of the tag did not interfere with the protein production. The *c-myc* tagged construct was used to transiently transfect HEK293 cells. Immunocytochemistry proceeded without cell permeabilisation, using an anti-*c-myc* monoclonal primary antibody and a secondary anti-mouse FITC antibody. Fluorescence was detected in *c-myc* tagged VR-L-transfected cells, indicating that VR-L reached the plasma membrane. Untransfected cells did not exhibit any fluorescence, which confirmed that the *c-myc* signal was authentic.

Studies on VR-L conducted by other labs

Caterina *et al.* (1999) reported the cloning of rat VR-L by PCR from a brain cDNA library and human VR-L from a myeloid cell line using EST based primers. Their human VR-L clone is identical to the one cloned by our group. The researchers conducted similar functional experiments to the ones described in this chapter and they established that VR-L is not activated by capsaicin or protons. The tissue distribution was investigated by Northern blot analysis, which rendered results identical to the semi-quantitative RT-PCR analysis. In contrast to the electrophysiological results

presented in this chapter, the researchers detected heat activation of VR-L expressed in *Xenopus* oocytes and HEK cells. The current was elicited only in temperatures exceeding 53^0C. Immunocytochemistry data revealed the co-expression of the receptor with CGRP in dorsal root ganglia but not with substance P or lectin IB4. Additionally, VR-L co-localised with RT97, a marker for myelinated neurons. Most of the VR-L staining neurons exhibited the morphology of large diameter neurons. The immunocytochemistry pattern and the heat sensitivity recorded by this group, led to the postulation that VR-L is expressed in medium to large diameter Aδ mechano- and heat-sensitive type I neurons that are lightly myelinated and have a heat response threshold of ~53^0C. Neither our group nor collaborators (Dr. Wafford's group at Merck and Dr. Davis group at Glaxo-SmithKline) ever recorded heat-sensitive currents from VR-L transfected host cells. In most cases, exposure to high heat caused rupture of the cell membrane making it impossible to obtain consistent recordings. Moreover, as shown in figure 2.19 transfection rendered the cells susceptible to heat applications, which caused leakage currents. A closer look at the electrophysiological recordings presented by Caterina *et al.* (1999) shows that VR-L transfected HEK cells were activated by heat at 53^0 C only after 20-30sec of application. The duration of the stimulus application to produce an effect is unusually long, especially for such a noxious stimulus. On the contrary, Aδ neurons respond to 53^0 C within 1 sec. Finally, the wide distribution of VR-L in tissues where exposure to high heat is not encountered physiologically e.g. lymphocytes, contradicts with the assignment of a high heat sensor role to the channel.

Kanzaki *et al.* (1999) cloned the mouse homologue of VR-L for the purpose of studying the effect of Insulin-like Growth factor I (IGF-I) in stimulating Ca^{2+} entry during cell growth. The scientific interest of this group lies on CD20, a cell surface protein that functions as a calcium channel. IGF-I accelerates the cell cycle in cells expressing CD20 ectopically, indicating the role of this protein in cell progression (Kanzaki *et al.*, 1997). These researchers cloned the mouse homologue of VR-L, by using degenerate primers based on the CD20 sequence and a mouse cell line (Balb/c 3T3), that has been shown to respond to IGF-I, as template. The receptor cloned was named GRC for Growth factor Regulated Channel because it was found to respond to IGF-I when expressed in CHO host cells (that endogenously contain the IGF-I receptor) under serum-free conditions. Immunocytochemistry studies showed the receptor to be expressed intracellularly under quiescent conditions. But when IGF-I was added, the receptor translocated to the plasma membrane and an inward Ca^{2+} current was

elicited. The translocation effect was found to be mediated by PI3 kinase, which suggests VR-L to be phosphorylated following the IGF-I receptor activation. The channel's translocation was replicated with the addition of PDGF or foetal bovine serum but not EGF. Apart from lymphocytes, endothelial cells are also known to respond to IGF-I with a Ca^{2+} influx (Munaron and Pla, 1995). Since VR-L is expressed in both types of tissue it would be interesting to examine if it is the calcium channel that underlies this phenomenon.

In summary, VR-L was found to be expressed in a variety of tissues of mainly the immune and nervous systems. Semi-quantitative RT-PCR studies showed that the channel's mRNA levels are upregulated by NGF in a similar manner to VR1. By using DRG cultures treated with a neurotoxic capsaicin concentration, it was established that VR-L is expressed in the non-capsaicin sensitive DRG population, which is in agreement with the immunocytochemistry studies conducted by Caterina *et al.* (1999). Fluorometric and electrophysiological studies showed that VR-L does not respond to the noxious stimuli that activate nociceptors. Immunocytochemistry studies targeting a *c-myc* epitope expressed on an extracellular loop of VR-L confirmed that the channel reaches the plasma membrane.

Proposed experiments

a) on the possible role of VR-L in inflammation

The VR-L upregulation by NGF *in vivo* and *in vitro* suggests possible changes in the expression pattern of this gene during inflammation, since the concentration of NGF increases in inflammation. Preliminary studies suggest that VR-L transcripts are upregulated during inflammation (Dr. Treanor from Amgen, personal communication). It would be interesting to examine if other types of cells e.g. small diameter DRG neurons start expressing VR-L following peripheral inflammation or whether its expression is restricted in large diameter neurons only. If that is the case, it would be challenging to identify the factor released by small diameter neurons that regulates the VR-L expression and to determine the potential role of this mechanism in relaying nociceptive information. By using *in situ* hybridisation and immunocytochemistry to compare VR-L expression in the DRG of normal and inflamed animals, it is possible to investigate whether the gene expression is induced in a different cell population during inflammation. In case the localisation of VR-L expression is not altered during

inflammation, real-time PCR, semi-quantitative PCR or the RNA protection method could be used to examine if there is transcript upregulation. If a difference were established in the VR-L expression during inflammation, it would be interesting to examine the mediator of this change. Since the studies presented in this chapter indicate that NGF upregulates the VR-L transcripts, it would be intriguing to study the receptor in NGF over-expressing mice (Albers *et al.*, 1994).

It is necessary to carry out a more detailed characterisation of VR-L expression in DRG than the one published (Caterina *et al.*, 1999). It would be useful to examine VR-L co-localisation with other neurotrophins and their receptors that might regulate its function. BDNF plays a role in nociception, mechanosensation and maintenance of sensory neurons (reviewed by Boucher *et al.*, 2000b). The BDNF mRNA is normally expressed in small diameter neurons and co-localises with the trkA receptor. NGF application upregulates BDNF in small diameter trkA expressing DRG neurons (Michael *et al.*, 1997). Additionally, peripherally increased NGF during inflammation induces the *de novo* BDNF expression in large diameter neurons (Mannion *et al.*, 1999). Michael *et al.* (1999) also reported that axotomy evokes BDNF expression in large diameter neurons. The findings that 1) both BDNF and VR-L are upregulated by NGF 2) VR-L is expressed in large diameter neurons and 3) BDNF expression is induced in large diameter neurons during inflammation and nerve injury, leads to the possibility that VR-L function is regulated by neurotrophins and might have a role in inflammation.

Another finding that suggests the study of VR-L in the context of inflammation was that VR1 and VR-L are expressed in the third and fifth cortical layers of the brain (Mezey *et al.*, 2000). This was not unexpected as the fifth layer sends axons to the brainstem and the spinal cord, which are important in the transmission of nociceptive information and layer 3 is important in the establishment of thalamocortical connections that participate in the ascending pain pathways. The stromal cell-derived factor-1α (SDF-1α), a chemokine, is also expressed in layer 5 (Tham *et al.*, 2001). This factor has been implicated in the development of the cortex and in haematopoesis (Zou *et al.*, 1998) but also in the migration of T cells in sites of inflammation (Nanki *et al.*, 2000). Recently, CXCR4 the receptor for SDF-1α was found to be expressed in DRG neurons and to co-localise with VR1 and substance P (Oh *et al.*, 2001). This group showed that SDF-1α and other chemokines can evoke inward Ca^{2+} currents in DRG neurons and also

cause allodynia as determined by punctate mechanical stimulation. Considering the role of SDF-1α in inflammation and its co-localisation with VR1 and VR-L in relays of nociceptive information, it is enticing to postulate a role of VR-L in pain perception during inflammation.

b) on determining whether IGF-I regulates the VR-L function in DRG

According to Kanzaki *et al.* (1999), the mouse homologue of VR-L translocates to the plasma membrane subsequently to IGF-I receptor activation by IGF-I (insulin-like growth factor I) and elicits a Ca^{2+} current. The phenomenon was found to be mediated by PI_3 kinase, which suggests that IGF-I receptor stimulation leads to the phosphorylation of the mouse VR-L through PKC activation, which triggers the receptor translocation. PDGF and foetal bovine serum had the same effect on VR-L, suggesting that the translocation is not specific to IGF-I receptor activation. It would be interesting to examine whether these growth factors have the same effect on VR-L in DRG. To test this possibility, the VR-L expression could be examined by immunocytochemistry in DRG neurons cultured in serum deprived media and in serum containing IGF-I or other growth factors. Considering that IGF-I can compensate for NGF withdrawal in neonatal DRGs (Russell *et al.*, 1998), one could examine whether NGF can cause translocation of VR-L from intracellular compartments to the plasma membrane.

Despite the fact that VR-L does not respond directly to noxious stimuli, the possibility that it has a role in nociception is not excluded. Since the receptor's function in DRG neurons has not been elucidated so far, the generation of VR-L knock-out mice is eagerly anticipated. VR-L might play a role in regulating the function of other receptors. VR.5'sv, a splice-variant of VR1 with no detectable phenotype, was found to act as a dominant-negative modulator of the VR1 function (Dr. Schumacher, personal communication). Although we detected no change in the capsaicin and heat sensitivity of VR1 when co-expressed with VR-L, it is possible that VR-L undertakes its role under specific conditions e.g. inflammation. Therefore, examining possible functional interactions between VR-L and other receptors might provide an insight into the role of VR-L.

CHAPTER 3

Interactions between vanilloid receptors and members of the Transient Receptor Potential family of receptors

INTRODUCTION

The Transient Receptor Potential family of receptors emerged from phototransduction studies in Drosophila

VR-L and VR1 share on average 20% identity at the amino acid level with channels of the Transient Receptor Potential (TRP) family. The capsaicin receptor and the vanilloid-like receptors that were subsequently cloned exhibit the same topological structure as TRP channels, encompassing 6 transmembrane domains with a putative pore between transmembrane domains 5 and 6, intracellular termini and ankyrin repeats at the N-terminus.

The first member of the TRP family to be cloned was *trp*, a Drosophila mutant with a hindered photoreceptor signalling mechanism. In the fruitfly, the phototransduction process begins with the light inducing a current in photoreceptors by activating rhodopsin. Subsequently, phospholipase C (PLC) is activated, through a G protein coupled to rhodopsin, that generates diacylglycerol (DAG) and inositol triphosphate (IP3). The generation of IP3 causes a biphasic photoreceptor response, consisting of a transient increase in membrane conductance that is selective for Ca^{2+} and can be blocked by La^{2+} and a less Ca^{2+}-selective sustained current that is insensitive to La^{2+}. The *trp* mutants lack the Ca^{2+}-selective transient response. Montell *et al.* (1985) cloned the gene responsible for this mutation and they named it *trp* for transient receptor potential. The *trp* channel was found to resemble voltage-sensitive calcium channels with calmodulin binding sites, suggesting regulation by Ca^{2+}, 6 transmembrane domains and ankyrin repeats that link it to the cytoskeleton; albeit it lacks the specific charged residues of voltage-gated Ca^{2+} channels. Phillips *et al.* (1992) cloned Drosophila cDNAs containing calmodulin-binding sites. One of the genes identified was found to be very similar to *trp* and it was named *trpl* (transient receptor potential-like).

TRP channels and capacitative Ca^{2+} entry

The biphasic response of photoreceptors to light is reminiscent of the capacitative Ca^{2+} entry mechanism or store-operated Ca^{2+} entry. Based on a series of experiments indicating the role of IP3 in Ca^{2+} signalling, Putney (1986) suggested that the capacitative Ca^{2+} entry (CCE) model where IP3, generated as a result of PLC activation, stimulates the IP3 receptor on intracellular Ca^{2+} stores and causes their depletion of Ca^{2+}. The emptying of the stores triggers the influx of extracellular Ca^{2+} through the plasma membrane via an unknown mechanism, which refills the stores. Thapsigargin can generate CCE without inducing the production of IP3, by

inhibiting a Ca^{2+} pump on intracellular stores and thus causing the leak of Ca^{2+} from the stores. Nevertheless, store depletion is not a prerequisite for capacitative Ca^{2+} entry. Fasolato *et al.* (1993) described the activation of CCE channels in macrophages in response to PLC stimulation, in the presence of heparin that blocks IP3 receptors and thus Ca^{2+} depletion from IP3 sensitive stores. The *trp* and *trpl* channels were examined for their role in CCE via heterologous expression in the insect cell line SF9. Vaca *et al.* (1994) demonstrated that *trp* transfected cells respond to thapsigargin and to bradykinin when co-transfected with the bradykinin receptor with an inward current reversing at +40mV. The current elicited is Ca^{2+}-selective but loses its selectivity when cations are not present and it can be blocked by Mg^{2+} and La^{2+}. Hu *et al.* (1994) showed that *trpl* expressed in a cell line is insensitive to thapsigargin and encodes a constitutively open channel that allows the influx of a nonselective current reversing at 0mV. The current can be augmented by the activation of G protein-coupled receptors. Sinkins *et al.* (1996) used chimeras of *trp* and *trpl* to demonstrate that the C- termini of the proteins regulate the channel activity e.g. activation by store depletion or G protein-coupled receptor activation, while the N-termini specify the ion selectivity of the channel. Although the *trp* channel is activated by thapsigargin-induced store depletion it cannot account for the endogenous current (I_{CRAC}) observed during capacitative Ca^{2+} entry in a variety of tissues (reviewed by Putney and McKay, 1999). In mast cells, I_{CRAC} is a very small (fA range), strongly inward current showing high selectivity for Ca^{2+}. In endothelial cells I_{CRAC} is equally selective for Ca^{2+} and Ba^{2+} and demonstrates detectable single channel events (2-10pS). In pancreatic cells, I_{CRAC} is not blocked by La^{2+}, which usually blocks Ca^{2+} channels and is not selective for Ca^{2+}. Therefore, the I_{CRAC} current cannot be entirely attributed to the *trp* channel, but it is possible that this channel participates in the mechanism that generates the store-operated current by interacting with other proteins.

The mammalian TRP homologues

The cloning of the Drosophila TRP channels led to a pursuit for the identification of the mammalian homologues that might play a role in Ca^{2+} signalling. The TRP family of receptors expanded rapidly to include numerous members that Clapham *et al.* (2001) recently proposed to segregate in three groups according to sequence homology. These groups were denoted short, long and osm-9-like TRP channels. The osm-9-like group

comprises three subfamilies that have been described in chapter 2: a) VR1 and VR-L b) OTRPC4/VROAC, c) ECaC, CaT1 and CaT-L. Interestingly, CaT1 was found to gate a current with many of the physical properties of I_{CRAC} (Yue *et al.*, 2001). It is Ca^{2+}-selective, inwardly rectifying at hyperpolarising potentials, it is blocked by La^{2+}, it loses its selectivity when divalent cations are not present and has single channel conductance to Na^{+} at 60pS. But unlike the I_{CRAC} current, CaT1 was activated by store depletion only when it was expressed in low concentrations indicating that probably additional regulating proteins are needed to form the I_{CRAC} channel.

The long TRP group consists of four subfamilies: a) melastatin and KIAA1616, b) TRP-PLIK and ChaK2, c) TRPC7 and Trp-p8 and d) Mtr1 and FLJ20041. As it was mentioned in chapter 2, melastatin is associated with cancer and it was found to be downregulated in metastatic melanomas. KIAA1616 and FLJ20041 were identified in sequencing projects and their function is unknown. TRP-PLIK was cloned by Runnels *et al.* (2001) on the basis of its interaction with PLC-β_1. The channel elicits a non-selective, outwardly rectifying current with single channel conductance of ~100pS. The channel also contains a kinase domain in its C terminus that autophosphorylates the protein and regulates the channel's activity. ChaK2 is 60% identical with TRP-PLIK at the protein level and its function remains unknown. It was cloned by Ryazanov *et al.* (1999) in a database-mining project that aimed at identifying alpha-kinases, a novel class of kinases with unique motifs that phosphorylate residues in α helices. TRPC7 (Nagamine *et al.*, 1998) is expressed in the brain in high levels. It elicits a nonselective current with conductance of 60pS that can be regulated by ADP-ribose. Trp-p8 is highly expressed in prostate tissue and is upregulated in a cancerous state, while Mtr1 (Prawitt *et al.*, 2000) is associated with the Beckwith-Wiedelmann syndrome, which imputes high susceptibility to cancer development.

The short group of TRP channels consists of four subfamilies: a) TRPC1, b) TRPC4 and TRPC5, c) TRPC3, TRPC6, TRPC7 and d) TRPC2. These channels are also denoted TRP1-7. Wes *et al.* (1995) cloned the first mammalian TRP homologue, which was named TRPC1, by screening human genomic and cDNA libraries with an EST sequence homologous to *trp*. In the same year, Zhu *et al.* cloned *Htrp-1*, another human *trp* homologue, that is a splice variant of TRPC1, lacking a stretch of amino acids at the beginning of the gene. Sinkins *et al.* (1998) recorded TRPC1 currents that were constitutively expressed, could be blocked by La^{3+} and were not affected by

thapsigargin or IP3 treatment. Zitt *et al.* (1996) cloned another human splice variant of TRPC1, called TRPC1A that is identical to *Htrp-1,* but lacks about 40 amino acids at the N terminus. TRPC1A gates a current induced by thapsigargin and IP3 application and can be blocked by Gd^{2+}.

Okada *et al.* (1998) cloned the mouse TRPC4 that can be activated by stimulation of G protein-coupled receptors and by receptors with tyrosine kinase activity (Schaefer *et al.,* 2000). The bovine TRPC4 (Philipp *et al.,* 1996) was found to be sensitive to store depletion, gating a current very similar to the endothelial I_{CRAC} with high cation selectivity and permeability to Ba^{2+}. Okada *et al.* (1998) and Philipp *et al.* (1998) cloned the mouse and rabbit TRPC5 respectively. Okada reported that the mouse TRPC5 expression augmented Ca^{2+} entry induced by ATP, while Philipp (1998) reported the rabbit TRPC5 current to be activated by thapsigargin. Both TRPC4 and TRPC5 contain a PDZ domain, that other TRP receptors lack. These domains can bind to the carboxyl end of other proteins, which are important in protein scaffolding on the plasma membrane. Tang *et al.* (2000) reported that other proteins with PDZ domains e.g. PLC-β1 and proteins associated with the cytoskeleton co-immunoprecipitate with TRPC4 and TRPC5. In 2001 the same group reported that all TRP channels contain a domain that interacts with IP3 receptors and calmodulin with different affinity. Sossey-Alaoui *et al.* (1999) reported the expression of TRPC5 in foetal and adult brain and identified single nucleotide variations of this gene associated with developmental neurological conditions.

TRPC3, TRPC6 and TRPC7 form non-selective cation channels that rectify in both directions and are not affected by thapsigargin treatment. Zhu *et al.* (1996) described the cloning of human TRPC3. Zitt *et al.* (1997) reported TRPC3 to be constitutively active. Although it is not store-operated, it is gating currents that amplify in response to thapsigargin and stimulation of G protein-coupled receptors (Zhu *et al.,*1998). The latter currents are blocked by PLC inhibitors, suggesting TRPC3 to be stimulated by PLC activation. Activation of the trkB receptor by BDNF in pontine neurons led to PLC stimulation, which induced Ca^{2+} influx. By conducting electrophysiological studies using TRPC3 antibodies and inhibitors in isolated neurons or heterologous expression systems, TRPC3 was found to gate part of the BDNF-induced Ca^{2+} current (Li *et al.,* 1999). Additionally, TRPC3 was found to co-immunoprecipitate with trkB. Diacylglycerol can activate TRPC3 and TRPC6 independently of PKC (Hofmann *et al.,*

1999), which is reminiscent of the TRP and TRPL activation by polyunsaturated fatty acids (Chyb *et al.*, 1999). Kiselyov and Muallem (1999) reported the interaction of TRPC3 with IP3 receptors, which results in the TRPC3 regulation by IP3. These researchers proposed that in a heterologous overexpression system the exceeding TRPC3 protein is not coupled to endogenous IP3 receptors, rendering it susceptible to regulation by diacylglycerol and other fatty acids. The murine TRP6 (Boulay *et al.*, 1997) is insensitive to thapsigargin-induced store depletion but it can be activated by G protein-coupled receptor stimulation. In agreement with this, the mouse TRP6 was recently found to be activated by alpha(1)-adrenoreceptor stimulation (Inoue *et al.*, 2001), implying a role for this channel in the sympathetic nervous system. TRPC7 is constitutively expressed and its activity is enhanced by ATP and diacylglycerol (Okada *et al.*, 1999), while it is not affected by thapsigargin induced store depletion.

The rat TRPC2 is specifically expressed in the vomeronasal organ, indicating its possible function in pheromone signalling (Liman *et al.*, 1999). The mouse TRPC2 is store operated (Vannier *et al.*, 1999), as it can be activated by thapsigargin application or G protein-coupled receptor activation. It was also found to play a role in Ca^{2+} influx in the sperm during fertilisation (Jungnickel *et al.*, 2001). In particular, antibodies against TRPC2 inhibited the acrosome reaction (release of enzymes by sperm processes when in contact with the egg) that can be induced by thapsigargin or physiologically by glycoproteins in the egg's zona pellucida. The human TRPC2 is probably a pseudogene as it contains stop codons in the reading frame (Zhu *et al.*, 1996). Zhu and colleagues (1996) examined whether TRP channels are indeed capacitative Ca^{2+} entry channels or they facilitate Ca^{2+} entry via an unrelated mechanism. They addressed this question by transfecting antisense fragments of murine TRP channels in a mouse fibroblast cell line that exhibits endogenous CCE. The blockade of CCE in this cell line established the importance of TRP channels in capacitative Ca^{2+} entry. The TRP channels are summarised in table 1.

The TRP channels form heteromultimers

Xu *et al.* (1997) reported that *trp* and *trpl* co-immunoprecipitate. As mentioned before, *trp* is store operated and its activity can be inhibited by La^{3+}, while *trpl* is constitutively active, gating a large outwardly rectifying current. Co-expression of the two channels rendered a heteromultimeric channel that exhibits a combination of the parental phenotypes i.e. it is store-operated, it gates an outwardly rectifying current that was smaller than the one gated by *trpl*, is Ca^{2+} selective and insensitive to

Yeast two - hybrid studies, column binding assays and co-immunoprecipitation experiments showed that the two channels interact via their N-termini. Co-transfection of *trp* with constructs containing only the N-termini of *trp* or *trpl* decreased *trp* activity, acting as dominant negative modulators. *Trp* and *trpl* constructs were generated substituting the pore region with a region from the *Shaker B* type of K^+ channels. The constructs completely abolished wild type *trp* and *trpl* activity showing that these channels form homomultimers and heteromultimers. The current gated by the *trp-trpl* channel has many of the light-induced current characteristics observed in Drosophila photoreceptors that cannot be attributed to each of the channels individually. *Trp* mutants though exhibit a residual light-induced response that cannot be due to *trp-trpl* channels or *trpl* alone. This finding prompted Xu *et al.* (2000) to look for a remaining component of the trp-related phototransduction mechanism. They identified TRPγ, which is related to *trp* and *trpl* exhibiting the same topological structure. Co-immunoprecipitation experiments showed that the new channel interacts with *trp* and also with *trpl* with higher affinity. TRPγ alone gates a non-selective, constitutively active current, while when expressed with *trpl* as a fusion protein, the resulting channel was not constitutively open but could be activated by PLC, following G protein coupled receptor stimulation. TRPγ suppresses *trpl* activity *in vitro* in a heterologous expression system and also *in vivo* as shown by creating transgenic Drosophila flies expressing the N terminus of TRPγ in a *trp* mutant background.

Xu *et al.* (1997) also reported that the human TRPC1 and TRPC3 co-immunoprecipitate. Wu *et al.* (2000) observed that transfection of antisense human TRPC1 and TRPC3 constructs in HEK cells that endogenously express these two channels, inhibited capacitative Ca^{2+} entry to a larger extent than antisense TRPC3 alone. These results further support the idea that TRP1 and TRPC3 channels interact and indicate that they probably form a store-operated channel. Recently, Strubing *et al.* (2001) identified TRPC1 interactions with TRPC4 and TRPC5 in the rat brain. The novel channel created by TRPC1 and TRPC5 is not affected by thapsigargin but can be stimulated by G protein-coupled receptor activation. The current elicited exhibits small inward conductances at negative potentials and strong outward rectification at positive potentials, whereas TRPC5 alone shows inward currents. The I-V relations of the TRPC1-TRPC5 heteromultimer are reminiscent of NMDA receptors, but unlike the latter receptors the TRPC1-TRPC5 current is not affected by Mg^{2+}.

Do vanilloid receptors form heteromultimers?

Considering that the vanilloid receptors resemble TRP channels, it would not be unreasonable to postulate possible interactions between vanilloid receptors or between vanilloid receptors and TRP channels. Preliminary data supports this possibility, as VR1 can form homomultimers (Kedei *et al.*, 2001) and VR.5'sv was found to act as a dominant negative modulator on VR1 (Dr. Schumacher, personal communication). TRP-VR or VR-VR interactions could result in channels with novel phenotypes that could explain the heterogeneity of vanilloid responses observed *in vivo* that cannot be solely explained by VR1 activity. Additionally, interactions between VR-L and other channels could confer a role to this orphan receptor. For these reasons, the possible interactions between VR1, VR-L and TRP channels were examined in this chapter using co-immunoprecipitation studies.

Table 1: Summary of the TRP channel characteristics.

Name	Store-operated	Induced by thapsigargin	Induced by G-protein activation	Blocked by La^{2+}	Notes	Ca^{2+} – selective current
trp	+	+	+	+		+, inward
trpl	-	-	augmented	-		+, inward
CaT1	+			+		+, inward
melastatin					Downregulated in melanomas	
KIAA1616 FLJ20041					Unknown function	
TRP-PLIK						-, outward
Chak2					Unknown function	
TRPC7					Expressed in brain	-
Trp-p8, Mtrp1					Associated with cancer	
VR1,VR-L, VR-OAC, ECaC, CaTL	-	-	-	-		+, inward
TRPC1		-	-	+		
TRPC1A		+	+		Blocked by Gd^{2+}	+, inward
TRPC4					Characteristics depend on species	
TRPC5					Characteristics depend on species	
TRPC3	-	augmented	augmented		Involved in BDNF current, activated by DAG	-
TRPC6		-	+		Activated by DAG	-
TRPC7		-			Activity enhanced by DAG and ATP	-
TRPC2	+	+	+		Fertilisation, pheromone signalling	

CHAPTER 3

Interactions between vanilloid receptors and members of the Transient Receptor Potential family of receptors

MATERIALS & METHODS

In addition to methods already described in Chapters 1 and 2, the following methods were used in this chapter.

3.1 Primer sequences

The detection of the TRP channels in DRG by PCR was carried out using Taq polymerase, whereas the constructs' formation was accomplished using Pfu polymerase. The following oligonucleotides were ordered from Sigma-Genosys.

- **TRP primers**

TRP1 (βsubtype) anneal.temp: 65^{0}C

Forward primer (5'-3'): TCTGGCGTCTCCTCCTCCTCCC

Reverse primer (3'-5'): CGCAGAACACAGCGTGCATTCACAGCC

TRP1 (α&β) anneal.temp: 65^{0}C

Forward primer (5'-3'): GGGAAATTTCTAGGAATGTTCCTTCTT

Reverse primer (3'-5'): CTCATGATTTGCTATCAGCTGG

TRP2 anneal.temp: 65^{0}C

Forward primer (5'-3'): GCCTCCGGATGGCGCCAGCATCC

Reverse primer (3'-5'): CTAGCCCTTGGTCTCCAGATCTTCCC

TRP3 anneal.temp: 57^{0}C

Forward primer (5'-3'): ATTCATAGAGAACATTGGCTATGTC

Reverse primer (3'-5'): CTGTCATCCTCGATTTCTTGGTAT

TRP4 anneal.temp: 55^{0}C

Forward primer (5'-3'): ATGGCTCAGTTCTATTACAAACG

Reverse primer (3'-5'): GCACCTGCTTCTCTCCGCTGGG

TRP5 anneal.temp: 55^{0}C

Forward primer (5'-3'): AAGGCCCGGCATGAATTCACG

Reverse primer (3'-5'): GCTGGTAGGAGTTGTTCATCATGGCA

TRP6 anneal.temp: 57^{0}C

Forward primer (5'-3'): GTTTTAAGACTCTGTTCTGGG

Reverse primer (3'-5'): CGCATCATCCTCAATTTCCTGGAATGAAC

•Construct primers

VR1 FLAG/MYC anneal.temp: 65^{0}C

KpnI site FLAG epitope

Forward primer (5'-3'):GGGGTACCCCATGGACTACAAGGACGACGATGACAAG GAACAACGGGCTAGCTTAGACT

KpnI site c-myc epitope

Forward primer (5'-3'): GGGGTACCCCATGGAACAAAAGCTCATCTCAGAGGAA GATCTTGAACAACGGGCTAGCTTAGAC

Reverse primer (3'-5'): GCGCTTCTTGCTCCTCTGCAGGAAGGGCA

Human VR-L FLAG anneal.temp: 65^{0}C

HindIII FLAG epitope

Forward primer (5'-3'): AAAAGCTTTATGGACTACAAGGACGACGATGACAAGA CCTCACCCTCCAGC

Reverse primer (3'-5'): GCGCTGTGGCCTCGGTAATAGTC

Rat VR-L FLAG/MYC anneal.temp: 65^{0}C

SacII FLAG epitope

Forward primer (5'-3'): CCCCGCGGGATGGACTACAAGGACGACGATGACAAGA CTTCAGCCTCCAGC

SacII c-myc epitope

Forward primer (3'-5'): CCCCGCGGGATGGAACAAAAGCTCATCTCAGAGGAAG ATCTTA CTTCAGCCTCCAGC

Reverse primer (3'-5'): TCTGCAGCAGCGGCATGATGCAG

Human TRP1 MYC anneal. temp: 65^{0}C

HindIII KpnI c-myc epitope

Forward primer (5'-3'): AAGCTTGGTACCACCATGATGGAACAAAAGCTCATCTC AGAGGAAGATCTTGCGGCCCTGTACCCG

Reverse primer (3'-5'): TCAGCACTAAGTTCAAATGCTCTCAGAATTGG

Human TRP3 FLAG/MYC anneal temp: 65^{0}C

Forward primer A (5'-3'): GCGCTGCTTCGCGATGTACGGGC

FLAG epitope

Reverse primer B (3'-5'): CTTGTCATCGTCGTCCTTGTAGTCCATGGACCTAATC AGTAGCAACGATAAAAC

c-myc epitope

Reverse primer B (3'-5'): AAGATCTTCCTCTGAGATGAGCTTTTGTTCCATGGAC CTAATCAGTAGCAACGATAAAAC

FLAG epitope

Forward primer C (5'-3'): GACTACAAGGACGACGATGACAAGGAGGGAAGCCC ATCCCTGAGACGCATGACA

c-myc epitope

Forward primer C (5'-3'): GAACAAAAGCTCATCTCAGAGGAAGATCTTGAGGGA AGCCCATCC

Reverse primer (3'-5'): CCACAGCCAGCTGCAGCGCGTTC

Mouse TRP6 MYC anneal. temp: 65^{0}C

EcoRI c-myc epitope

Forward primer (5'-3'): TAGGAATTCCACCATGGAACAAAAGCTCATCTCAGAG GAAGATCTTAGCCAGAGCCCGAGG

Reverse primer (3'-5'): GCACAATTTCATATTCCTGGCAATGTGCAGCG

3.2 Immunoprecipitation

The following solutions were prepared. The materials used were from Sigma unless otherwise stated.

Lysis buffer: 50mM Tris-Cl pH7.5, 150mM NaCl, 5mM EDTA, 5mM EGTA in distilled sterile water. The pH of the buffer was set to 7.4 and then 1ml Triton X-100 (1% (v/v) final) was added. The solution was kept at 4^{0}C.

Protease inhibitors used in 1ml of lysis buffer: 6µl of 1.5mg/ml aprotinin (final 10µg/ml), 0.5µl of 10mg/ml leupeptin – Peptide Institute Inc. (final 5µg/ml), 0.1µl of 10mg/ml antipain – Peptide Institute Inc. (final 1µg/ml), 0.2µl of 5mg/ml pepstatin A - Peptide Institute Inc (final 1µg/ml), 5µl of 0.2M PMSF (500µM final).

Phosphatase inhibitors used in 1ml of lysis buffer: 10µl of 0.1M Na^+ pyrophosphate (1mM final), 10µl of 0.1M Na orthovanadate (1mM final), 100µl of 0.5M NaF (50mM final)

TBS/Triton pH 7.6: 20mM of Tris base, 137mM of NaCl. The pH was adjusted with 1M HCl

Method

1) 1-2 x10^6 HEK or COS cells were cultured in a 10cm dish and the following day transfected with 7µg of DNA (calcium phosphate method or SuperFect respectively).
2) After 24 hours, the cells were scraped off the dish with a sterile cell scraper (BDH) and they were transferred into a sterile falcon to be centrifuged at 1500g for 5min.
3) The pellet was washed once in 1xPBS with no Ca^{2+}, Mg^{2+} and then centrifuged at 1500g for 5min.
4) The pellet was resuspended in 1ml buffer (865µl lysis buffer 1% (v/v) Triton-X with 135µl protease/phosphatase inhibitors) and was transferred to an eppendorf and vortexed well. It was left on a roller at 4^0 C for 1hour.
5) The solution was then centrifuged at 14,000 rpm for 15min at 4^0 C. 1ml of the clarified supernatant containing the cytosolic and membrane proteins was retained. To ensure that most of the proteins were released, the pellet (containing non-lysed cells and nuclei) was resuspended in 1ml of lysis buffer and loaded on a SDS-PAGE gel. 50µl of the supernatant was loaded as a crude homogenate to control for the expression of the transfected DNA. Another 50 µl aliquot was used for a Bradford assay.
6) The lysate was precleared with 50µl of 50% (w/v) slurry Sepharose protein A (Amersham) or Sepharose protein G (Santa Cruz). It was vortexed well and left on a roller at 4^0 C for 10min. Afterwards, it was centrifuged on a microfuge for 1min top speed and the supernatant was transferred in a fresh eppendorf tube.
7) 4-5µg of primary polyclonal anti-FLAG or monoclonal anti-c-myc antibodies were added and the samples were incubated on a roller either overnight at 4^0 C or for 2-3 hours at room temperature.
8) 50µl of 50% (w/v) slurry Sepharose protein A/G was added directly to the lysate and vortexed well. The tube was left to incubate on a roller at 4^0 C for 2 hours.
9) The solution was centrifuged for 1min on a microfuge at top speed. The resulting pellet was washed 5 times with 1ml cold TBS, 0.1% (v/v) Triton-X pH7.5 (no inhibitors) after good vortexing. Extra attention was paid not to remove any beads.

10) The final wash was removed as much as possible. 50µl of 2x sample buffer was added and vortexed well. The tube was kept at 95-100^0 C for 5min and then cooled down on ice. It was centrifuged for a few seconds on a microfuge at top speed and the supernatant was carefully removed and transferred to a new tube. The sample was frozen at –20^{0}C until ready to load on a SDS-PAGE gel.

3.3 Bradford Assay

To prepare the Bradford reagent (Sigma) for use, 20ml of Bradford reagent were mixed with 80ml of sterile distilled water and stored at room temperature. A stock of 10mg/ml BSA (Sigma) was also prepared. 50 µl of BSA 10mg/ml were mixed with 950ml distilled water giving a final concentration of 0.5 µg/µl BSA. The following amounts of 0.5 µg/µl BSA were added in separate eppendorf tubes: 5µl (2.5µg), 10µl (5 µg), 20µl (10 µg), 30µl (15 µg) and 40µl (20 µg). A blank tube was also included to be used for zeroing the spectrophotometer. To each tube 10µl of lysis buffer and 1ml of Bradford reagent stock were added and vortexed well. The O.D. readings of these samples were taken at λ= 595nm and a linear graph was generated with the concentration of BSA on the x-axis and the corresponding O.D. on the y-axis. An example of such a graph is shown:

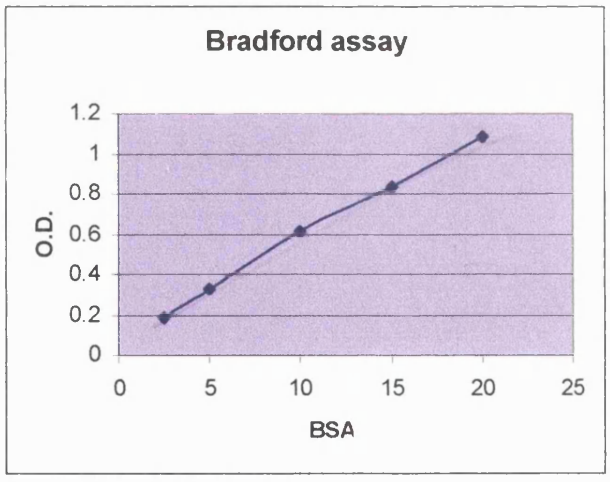

BSA (µg)	O.D$_{\lambda=595nm}$ reading
2.5	0.183
5	0.325
10	0.609
15	0.840
20	1.087

To prepare the protein samples:

10µl of protein sample (that resulted from cell lysis prior to immunoprecipitation) were added in an eppendorf tube with 1ml of the diluted Bradford reagent. Also a 4x dilution of the protein sample was prepared in case the sample was too concentrated: 5µl protein sample mixed with 15µl of lysis buffer. The O.D. of the sample was taken at λ= 595nm. By consulting the graph prepared from the BSA standards, the concentration of the protein sample was determined. By finding the value on the x-axis that corresponds

to the O.D. value (y axis) of the sample, it is possible to estimate the amount and thus the concentration of the sample.

3.4 Separation of cytosol from plasma and vacuole membranes for immunoprecipitation

1) 1-2 x10^6 eukaryotic cells (HEK293 or COS7) were cultured on a 10cm dish and the following day transfected with 7μg of DNA (calcium phosphate method or SuperFect).
2) After 24 hours, the cells were scraped using a cell scraper and were transferred into a sterile falcon. The tube was centrifuged at 1500g for 5min.
3) The cells were washed once in 1xPBS with no Ca^{2+}, Mg^{2+} and spun down at 1500g for 5min.
4) The pellet was resuspended in 2ml of lysis buffer (for immunoprecipitation) containing no detergent and salt.
5) A glass homogeniser was used to break the cells, with 40 strokes approximately. The cells were centrifuged at 1000g for 5min at 4^0 C. The supernatant was kept (membranes and cytosol with 50-100nm vesicles), while the pellet was discarded (containing the nuclei and unbroken cells).

To separate the cytosol from the membranes:

6) The supernatant was ultracentrifuged at 4^0 C at 100,000g for 1hour. The new supernatant (cytosol) was removed and a Bradford assay was performed.

7) The pellet (containing the membranes) that resulted from the ultracentrifugation was resuspended in 0.5ml 1% (v/v) Triton lysis buffer and was left to incubate on a roller at 4^0C for 1hour for the membrane proteins to be released. Afterwards, it was centrifuged for 10min at 4^0C, top speed. The supernatant containing the membrane proteins was saved and a Bradford assay was performed.

3.5 Treatment with peptide-N-glycosidase F (PNGase F)

Adjustments were made to the manufacturer's protocol (Roche) to suit the experimental conditions.

a) PNGaseF enzyme treatment of crude protein lysate

1) 25 µl of protein lysate was mixed with SDS to a final concentration of 0.5% (v/v) and β-mercaptoethanol to 3% (v/v) final concentration in order to denature the protein. The solution was heated for 5min at 100^{0}C.
2) The sample was cooled down and mixed with buffer containing $NaHPO_4$ (250mM final), EDTA (50mM final) at pH7.5 and Triton-X to 1% (v/v) final concentration. The non-ionic detergent was added in 5 fold excess to SDS to prevent inactivation of the enzyme by SDS. It was taken care not to exceed the 1% (v/v) Triton-X final concentration, so as not interfere with the electrophoretic separation of the protein.
3) The sample was vortexed well and mixed with 5 units of PNGaseF and protease inhibitors. The mixture was left for 16 hours in a 37^0 C waterbath. It was subsequently mixed with SDS buffer, heated for 5 min at 100^{0}C and analysed on a SDS-PAGE gel.

a) PNGaseF enzyme treatment of immunoprecipitated protein attached onto protein A or G Sepharose

1) The immunoprecipitated protein on beads was mixed with SDS (0.3% (v/v) final) and β-mercaptoethanol (0.2% (v/v) final) and heated up for 5min at 100^{0}C to release the protein.
2) The sample was cooled down and centrifuged on a benchtop to bring down the condensation. The supernatant was removed and transferred to an eppendorf tube. Steps 2-3 of protocol (a) were followed as described above.

3.6 SDS-PAGE gel

The following solutions were prepared using materials from Sigma.

2X Sample SDS buffer: To prepare the 2x sample buffer for loading protein samples on a SDS-PAGE gel, the following reagents were used: 100 mM TrisHCl pH 6.8, 4% (w/v) SDS, 0.2% (w/v) bromophenol blue and 20% (v/v) glycerol. The solution can be kept at -20°C. Before use, 100mM DTT needs to be added.

8.5% Stacking Gel: 0.4M Tris-HCl pH8.8, 0.1% (w/v) SDS, 8.5% (v/v) of 1:20 acrylamide/bis acrylamide, 0.03% (w/v) ammonium persulphate, 0.06% (v/v) TEMEM.

Top Gel: 0.125M Tris-HCl pH 6.8, 0.1% (w/v) SDS, 5% (v/v) of 1:20 acrylamide/bis acrylamide, 0.05% (w/v) ammonium persulphate, 0.1% (v/v) TEMED.

10X Laemmli buffer pH 8.3: 25mM Tris base, 192mM glycine, 1% (w/v) SDS.

The tank was set as follows:

1) Two glass plates, the spacers and comb were cleaned with running water, without any detergents. They were subsequently wiped with a tissue soaked in ethanol. The glasses were clamped together with the spacers in between, leaving a 1-2mm gap at the bottom.
2) The rubber seal was placed onto the bottom of the pouring tray. The glass plates were fitted on top of the tray creating a seal. The stacking gel was prepared and poured slowly, avoiding bubbles. The gel was poured until reaching 1 cm below the level of the comb. 1ml of distilled water was poured to prevent oxygen from diffusing into the gel and thus inhibit polymerisation. The gel was left to polymerise for 1 hour.
3) Once the gel was set, the over-laid water was poured off and the top of the gel was washed 2-3 times with water to remove any un-polymerised acrylamide. The gel was left on its side to drain onto tissue.
4) The top gel was prepared and poured immediately. It was left to polymerise for 1 hour.
5) Once the gel was set, the comb was carefully removed. The glass plates with the gel were carefully removed from the tray and placed into the tank. The wells were rinsed with 1X Laemmli buffer. Buffer was also poured in the bottom chamber and any bubbles that can cause resistance to the electric current were removed.
6) The samples were slowly loaded avoiding bubbles. 10µl of Full Range Rainbow Marker (Amersham) were also loaded.
7) The top chamber was placed on top of the gel and was filled with buffer. The gel was run overnight at 7mA.

3.7 Protein gel to membrane transfer

Transfer buffer: 20% (v/v) methanol in 1X Laemmli buffer

1) The blotting cassette was laid with 3 sheets of 3M Whatman paper (LabSales), wet with transfer buffer. Creases and bubbles were removed by pressuring a pipette horizontally on top of them.
2) A piece of pre-wet Hybond-ECL membrane, the size of the gel, was gently placed onto the Whatman paper, avoiding any creases and bubbles.
3) The gel was dismantled and placed gently over the membrane, removing any bubbles with pressure. The position of the markers was marked onto the membrane. The wells of the gel were removed with a scalpel. The gel was then wet with transfer buffer.

4) Three wet 3M Whatman paper sheets were placed on top of the gel, removing any bubbles by rolling a pipette over them. The cassette was closed and placed in the tank with the membrane facing towards the positive electrode. The tank was run at 28V for 3 hours.
5) To ensure complete transfer of the proteins onto the membrane, the gel was stained with Ponceau solution.

3.8 Western blot and detection with ECL

The following solutions were prepared using materials from Sigma:

Blocking buffer: 5% (w/v) marvel in TBS pH 7.6 (2.4g of Tris base, 8g of NaCl in 1l of distilled water, pH adjusted with HCl).

Wash buffer: 0.1% (v/v) Tween 20 in TBS.

Antibody buffer: 1% (w/v) Marvel, 0.1% (v/v) Tween 20 in TBS.

The antibody concentrations used had been optimised by dot blotting (probing serial dilutions of the antigen dried onto Hybond-ECL membrane with serial dilutions of the antibodies).

1) The membrane was removed from the cassette and incubated in blocking buffer with shaking for 45 min to block any non-specific binding sites.
2) The membrane was transferred in a sterile plastic bag with antibody buffer containing 1:1500 polyclonal anti-FLAG antibody (Santa Cruz 200µg/µl) or 1:300 monoclonal anti-*c-myc* antibody (Sigma 6µg/µl) or 1:200 anti-VR-L polyclonal antibody (Alpha Diagnostic Intl. Inc. 1µg/µl). The bag was placed onto a rotating platform for 1 hour at room temperature.
3) The membrane was washed three times with wash buffer for 10min each time, shaking onto the platform.
4) The membrane was transferred in a fresh plastic bag containing antibody buffer with 1:1500 anti-rabbit or anti-mouse immunoglobulin horseradish-linked whole antibody (Amersham). It was left shaking on the platform for 1 hour at room temperature.
5) The membrane was washed three times in wash buffer, shaking 10 min each time.
6) Equal volumes of detection solution 1 and 2 (Amersham) were mixed and poured over the membrane. The membrane was left to incubate for 1 min.
7) The excess liquid was dried off onto paper and the membrane was wrapped in cling film, smoothing out any bubbles and creases. It was then placed on top of a film that had been laid in an autoradiography cassette. The film was left to expose for 1 min

and it was developed as described in Chapter 2, Materials and Methods section. If the signal was weak, another film was exposed for longer.

3.9 Membrane stripping

In cases where the membrane needed to be reprobed with other antibodies, the following procedure was implemented:

1) The membrane was submerged in stripping buffer (100mM 2-mercaptoethanol, 2% (w/v) sodium dodecyl sulphate, 62.5mM Tris-HCl pH6.7) and incubated at 50^0C for 15 min with occasional agitation. The temperature and the time were empirically set.
2) The membrane was washed twice for 10min in TBS buffer at room temperature using large volume of wash buffer. The membrane was incubated with the ECL detection reagents and exposed to film to ensure complete removal of the antibodies.
3) The membrane was blocked by immersion in 5% (w/v) blocking buffer (marvel in TBS) for 1 hour at room temperature.
4) The immunodetection was performed as described above.

3.10 Adaptor construction

The oligonucleotides (Sigma-Genosys) ordered for the formation of the adaptors were the following:

Forward primer (5'-3'): GGCCGCCGCGGT

Reverse primer (3'-5'): CTAGACCGCGGC

a) Oligonucleotide phosphorylation

The primers were phosphorylated in order to facilitate their cloning into the vector as follows: 2μg of each oligonucleotide was mixed in an eppendorf with 10X buffer (500mM Tris-HCl, 100mM $MgCl_2$, 1mM EDTA, 50mM dithiothreitol, 1mM spermidine pH 8.2), ATP (Roche) to a final concentration of 10mM and 1 unit of T4 kinase (Roche). The reaction mixture was left to incubate for 1 hour in a 37^0C waterbath.

b) Phenol-chloroform extraction

1) Equals volumes of phenol and chloroform (Sigma) were added into the eppendorf and vortexed to remove the enzyme. The sample was left on ice for 2 minutes and then centrifuged for 2 min on a benchtop.
2) The supernatant was transferred in a fresh eppendorf and re-extracted with an equal volume of chloroform.

3) The oligonucleotides were precipitated with adding 1/10 of the volume 3M sodium acetate pH5.2 (Sigma) and 2.5 volumes ethanol. The sample was left at -20^0C for 1 hour.
4) The eppendorf tube was spun down for 20min at 4^0C and the pellet was then washed with 70% ethanol to remove excess salt. After drying in a vacuum, the pellet was resuspended in 10μl of sterile distilled water.

c) Adaptor formation

In an eppendorf tube 5μl of each phosphorylated oligonucleotide were added and mixed together with Tris-HCℓ pH7.5 in a final concentration of 0.03M. The reaction was heated at 65^0C for 5 min and then it was left at room temperature overnight. This allowed the reaction to cool down slowly and the complementary primers to form a duplex that would be subsequently ligated into the pcDNA3 vector.

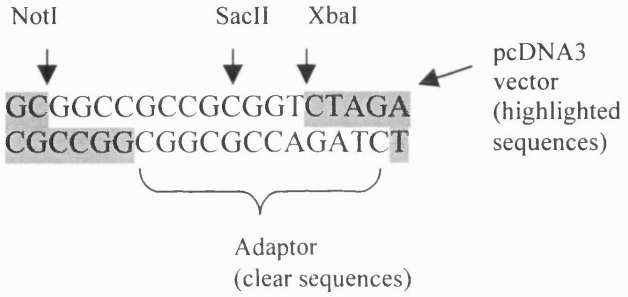

3.11 Production of the CHO stable cell line expressing rat VR-L/FLAG

a) GENETICIN® (G418 Sulphate) Selective Antibiotic Dose Response Curve

The CHO (Chinese Hamster Ovary) cells were cultured the same way as HEK293 and COS7 cells (chapter 2). In order to produce the cell line, it was first necessary to establish the optimum concentration of the antibiotic geneticin-G418 sulphate (GibcoBRL) to use for selecting the stable clones. The conditions should be stringent enough to allow only the survival of the right clones without producing toxic effects. For that reason, CHO cells were cultured with different concentrations of geneticin and the antibiotic dose-response curve was determined.

1) The geneticin selective antibiotic was dissolved in PBS at a concentration of 100 mg/ml (active substance) and filtered using a 0.22 μm filter.
2) Fifteen 35mm dishes were prepared by adding geneticin selective antibiotic to the growth medium in a range from 100-1500 μg/ml in 100 μg increments.
3) Cells were plated in about 20% confluency and the dishes were incubated in a humidified CO_2 atmosphere at 37^0 C.

4) The medium was changed every two days.
5) At 14 days, the supernatant was aspirated and the dishes were washed with PBS. The cells were stained with 0.5% (w/v) methylene blue and 50% (v/v) methanol for 20 minutes.
6) The plates were scored by calculating percentage of survival: the percentage of survival in the presence of each dilution of geneticin versus the percentage of survival in the absence of geneticin.
7) A dose response curve was generated by plotting the percentage of survival on the y axis versus the concentration of geneticin selective antibiotic in µg/ml on the x axis. The concentration used for selection should be the lowest one that killed all the cells. In our experiment the concentration established was 1mg/ml.

b) Selection of stable clones

A variation of the method described in Short Protocols in Molecular Biology (unit 9.5) was used to create the stable cell line.

1) 10^6 CHO cells were plated onto a 10cm dish. The following day the cells were transfected with 10µg of rat VR-L/FLAG DNA in pcDNA3 using the lipofection method.
2) The cells were harvested 36 hours later and plated in about 20% confluency in the presence of 1mg/ml geneticin. The medium was changed every 2 days and the cells were cultured for 2 weeks.
3) The cells were transferred in a 6 well plate. During this period, colonies had formed, stemming from the first resistant clones. In order to harvest these colonies, the medium was aspirated and sterile rings, cut from pipette tips, were stuck on each well, using sterile grease.
4) The colony enclosed in each ring was washed with PBS and subjected to trypsin treatment for 1-2 min. Fresh medium was added and the detached cells were pipetted out of the ring and into a well in a 24 well dish with 0.5ml medium.
5) After 2 hours, when the cells got attached onto the surface of the dish, the medium was changed. The following day geneticin was added.
6) Once the cells were confluent, they were passaged into 6 well plates in the presence of geneticin.
7) The selection was continued until confluency. The cells were then transferred into 10cm dishes and kept under selection until they became confluent. At this point, the cells were passaged and continued being cultured, while at the same time frozen stocks of each clone was prepared. The clones were analysed by Western blotting.

CHAPTER 3

Interactions between vanilloid receptors and members of the Transient Receptor Potential family of receptors

EXPERIMENTAL RESULTS

3.1 Expression of Transient Receptor Potential channels in dorsal root ganglia

Considering that members of the transient receptor potential family (TRP) of channels form heteromultimers, the possibility that vanilloid receptors interact with each other or with TRP channels was investigated. Prior to conducting experiments on protein interactions, it was necessary to verify the expression of TRP channels in the dorsal root ganglia. Since a subset of DRG neurons are nociceptors, any interaction between vanilloid receptors and other channels might have important implications in the study of pain.

TRP channels were detected with a RT-PCR study using rat cDNA from cultured DRG neurons that had been subjected to 3μM capsaicin treatment and control cultures (figure 3.2). This way, it was possible to inquire into the expression of TRP transcripts in the tissue of interest and to gather preliminary data regarding whether or not they are located in small, capsaicin-sensitive DRG neurons. Primers were designed from published rat TRP DNA sequences, that had been aligned to identify unique regions for each gene (accession numbers: AF061873, AF061255, AF136401, AF061875, AB008889, AF061876 and AF061877). Initially, control RT-PCR reactions for cyclophilin amplification were carried out to ensure the quality of the cDNA synthesised. Additionally, the TRP primers were tried in reactions containing tissue cDNA that these TRP channels were cloned from (figure 3.1).

Figure 3.1: Expression of TRP channels in rat tissues (control PCR). **Picture A:**Lane1: 100bp ladder. Lanes 2-4: cyclophilin amplification in rat brain, heart and adrenal gland. Lane 5: TRP1 β variant in rat heart (464bp). Lane 6: TRP2 in rat brain (288bp). Lane 7: TRP3 in rat heart (92bp). Lane 8: TRP4 in rat brain (386bp). Lane 9: TRP5 in rat adrenal gland (118bp). Lane 10: TRP6 in rat heart (195bp).
Lane 11: 100bp ladder. **Picture B:** Lane 1: 100bp ladder. Lane 2: cyclophilin amplification in rat heart. Lane 3: TRP1(α and β) in rat heart.

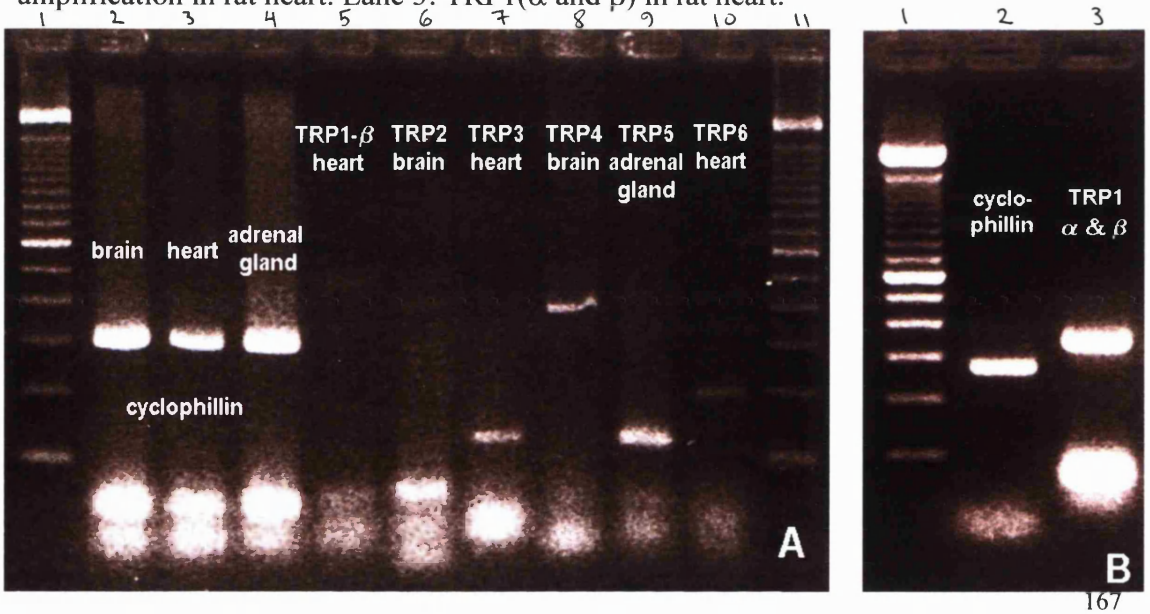

Figure 3.2: Expression of TRP channels in normalised capsaicin treated and control rat DRG cultures. The marks (+) and (-) denote 3μM capsaicin overnight treatment and control culture respectively.

Picture A

Lane 1:100bp ladder. Lane 2: TRP1-β in DRG

Picture B

Lane 1: 100bp ladder. Lanes 2 and 3 (positive control for capsaicin treatment): VR1 and cyclophilin amplification in capsaicin treated and control culture. Lanes 4 and 5: VR-L and cyclophilin amplification. Lanes 6 and 7(positive control for capsaicin treatment): CGRP and cyclophilin amplification. Lanes 8 and 9: TRP1 (α and β variants) and cyclophilin amplification.

Picture C

Lane 1: 100bp ladder. Lanes 2 and 3: TRP2 and cyclophilin amplification in capsaicin treated and control culture. Lanes 4 and 5: TRP3 and cyclophilin amplification. Lanes 6 and 7: TRP4 and cyclophilin amplification. Lanes 8 and 9: TRP5 and cyclophilin amplification. Lanes 10 and 11: TRP6 and cyclophilin amplification.

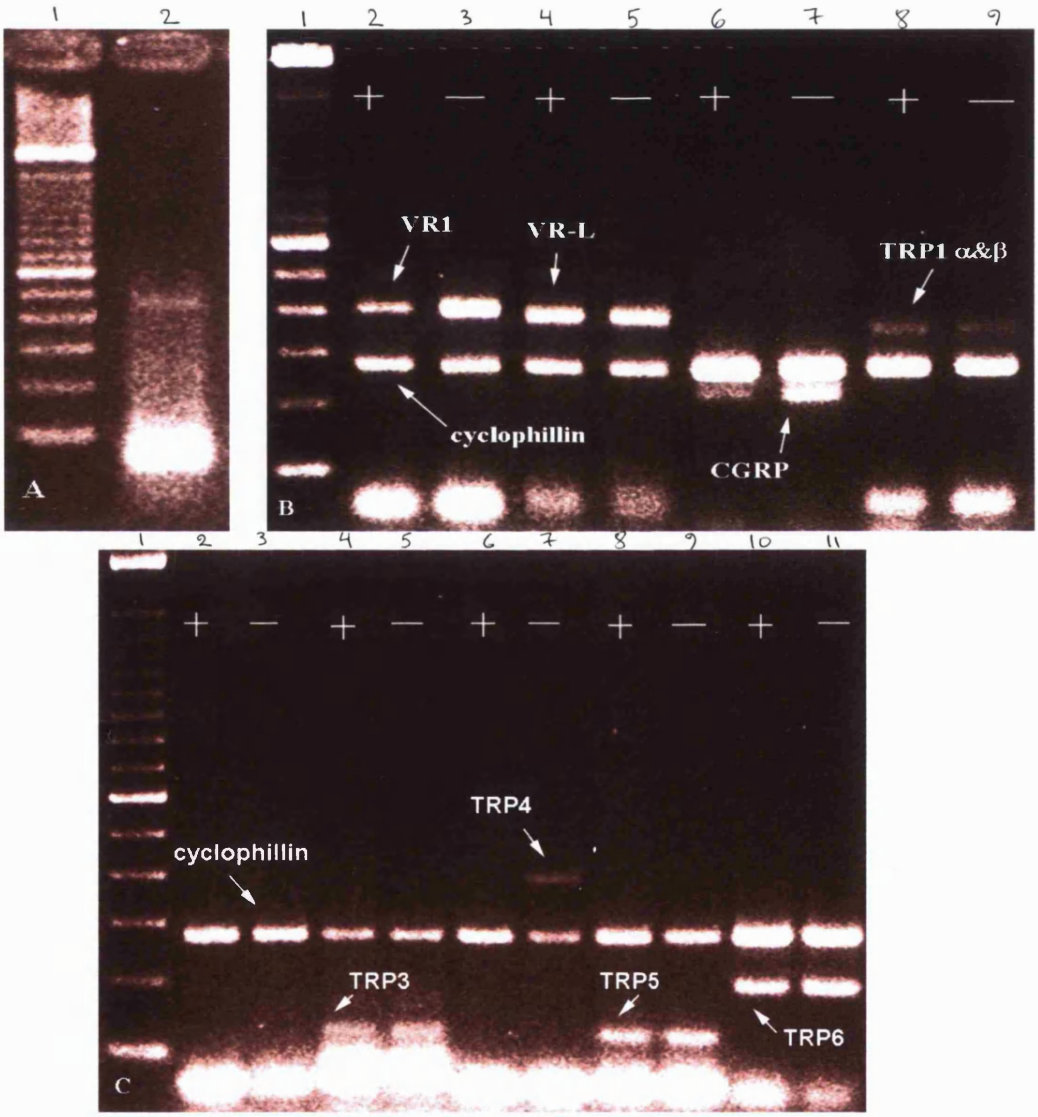

Two isoforms have been reported for the rat TRP1: TRP1α and the splice variant TRP1β, which lacks a stretch of amino acids at the N terminus (Wang *et al.*, 1999).

Since the expression of the β variant of TRP1 was found to be low in the control heart tissue (figure 3.1A) and DRG neurons (figure 3.2A), primers were designed to cross the common region between the two TRP1 variants α and β (figures 3.1B and 3.2B). TRP2 is specifically expressed in the vomeronasal organ and hence it was not possible to control for its expression. Amplification from brain cDNA was attempted but failed (figure 3.1A), probably due to the low concentration of the signal, since it is only expressed in the vomeronasal organ. The rest of the TRP channels were amplified from cDNAs of the tissues they were cloned from (figure 3.1A), confirming the primers' functionality. TRP2 was not found in DRG neurons, unlike the rest of the TRP channels. With the exception of TRP4, the TRP1-6 mRNA levels were not affected by capsaicin treatment. The TRP4 transcript presented dramatic decrease after capsaicin administration, suggesting co-localisation with VR1 to a large extent. The limited expression of VR1 and CGRP in the capsaicin treated culture, confirmed the effectiveness of the capsaicin application. The experiment was performed n=3 times.

3.2 Addition of epitopes on vanilloid and TRP channels

In order to explore possible interactions between vanilloid and TRP channels, it was necessary to construct epitope tagged versions of the genes, as it was not possible to acquire antibodies against the encoded proteins. The commonly used FLAG and c-myc epitopes were selected and was added at the respective N-termini of the proteins, after the initiation methionine. Previous studies (Xu *et al.*, 1997) had shown that addition of epitopes at this site does not interfere with expression of TRP proteins. The protein tagging was carried out following the PCR strategy described in figures 2.20 and 2.21 (Chapter 2) or the more simple PCR method described below.

Figure 3.3 : PCR strategy for addition of epitope tags. R.E. site : restriction enzyme site. The forward primer was designed to contain certain elements in the following order: restriction enzyme site, initiation methionine, epitope, and region of complementarity to the gene of interest.

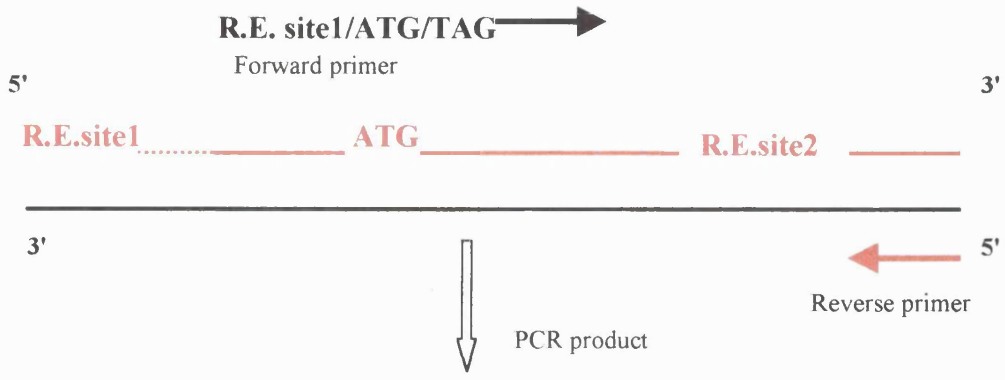

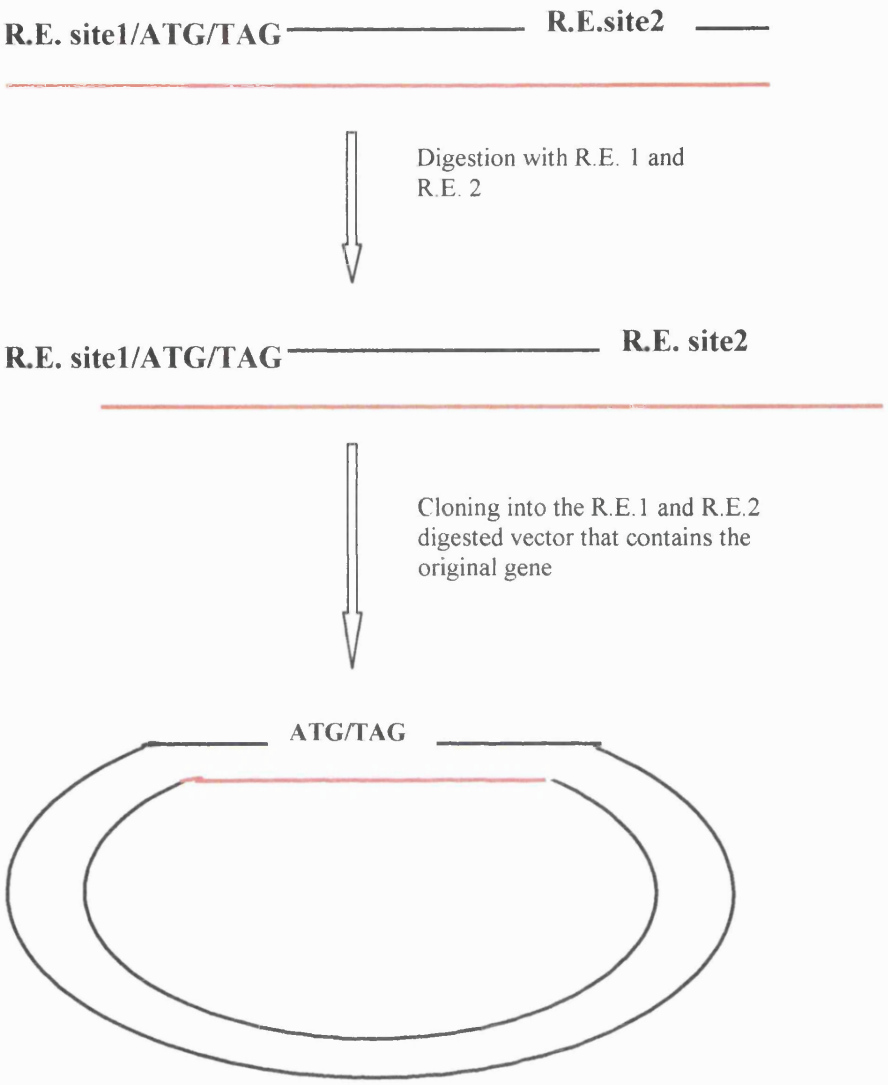

Unfortunately it was not possible to acquire the cDNAs of all the TRP channels identified in DRG neurons. Human TRP1, human TRP3 and human TRP6 were a generous gift from Dr. Delmas and the bovine flag tagged TRP4 was a gift from Dr. Schilling. The epitope insertion in each construct is described below.

Rat VR1-FLAG/MYC construct

The forward primer for tagging VR1 contained at its 5' end a KpnI site. The reverse primer was designed to cross the BsmBI site at the original VR1 sequence (appendix 3.2a). The resulting PCR product of about 430bp could then be digested (rendering a 330bp fragment) and subcloned into the pcDNA3-VR1 sequence that had been pre-digested with KpnI-BsmBI (figure 3.4). Since the process is the same for tagging with either FLAG or c-myc, only the results of the c-myc construct are shown.

Figure 3.4: Addition of the c-myc epitope on VR1 with PCR. Picture A: Lane 1: 100bp ladder. Lane 2: 430bp PCR product. Picture B: Lane 1: 100bp ladder. Lane 2: PCR product digested with KpnI and BsmBI. Picture C: Lane 1: 1kb ladder. Lane 2: undigested VR1 gene in pcDNA3 vector. Lane 3: VR1 in pcDNA3 digested with KpnI and BsmBI (bands expected: 7.8kb and 0.3kb).

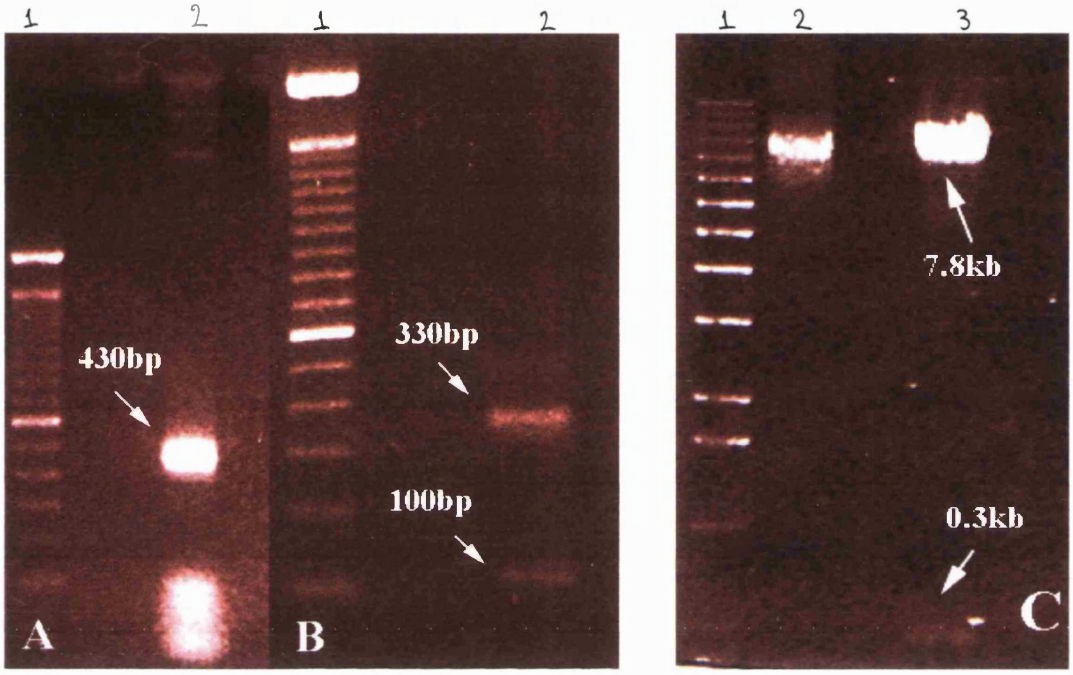

The VR1 digested gene in the pcDNA3 vector was purified from the gel and dephosphorylated, in order to be ligated to the digested PCR product. *E.coli* cells were transformed with the ligated DNA and plasmid preparations from selected colonies were carried out. The correct insertion of the c-myc epitope was demonstrated with DNA sequencing (appendix 3.1).

Human VR-L FLAG construct

The forward primer for FLAG insertion in human VR-L with PCR was designed to include a HindIII site on its N end, before the initiation methionine and the epitope. This site, which resides in the multiple cloning site of the vector pcDNA3 where human VR-L is cloned into (7.9kb total size), was later used to subclone the tagged version of the gene. The reverse primer was designed to cross a VR-L region that contains the enzyme BfrI. The resulting PCR product was approximately 500bp and after digestion with HindIII and BfrI gave a fragment of about 380bp (appendix 3.2b). The original human VRL-pcDNA3 construct was digested with HindIII and BfrI in order to be ligated to the FLAG tagged version (figure3.5).

Figure 3.5: Insertion of FLAG epitope with PCR in human VR-L. Picture A: Lane 2: 1kb ladder. Lane 1: digestion of human VR-L in pcDNA3 with HindIII and BfrI. Picture B: Lane 1: 500bp PCR product. Lane 2: 100bp ladder. Picture C: Lane 1: 1kb ladder. Lane 2: digestion of the T vector subcloned PCR product with HindIII and BfrI. Lane 3: 100bp ladder.

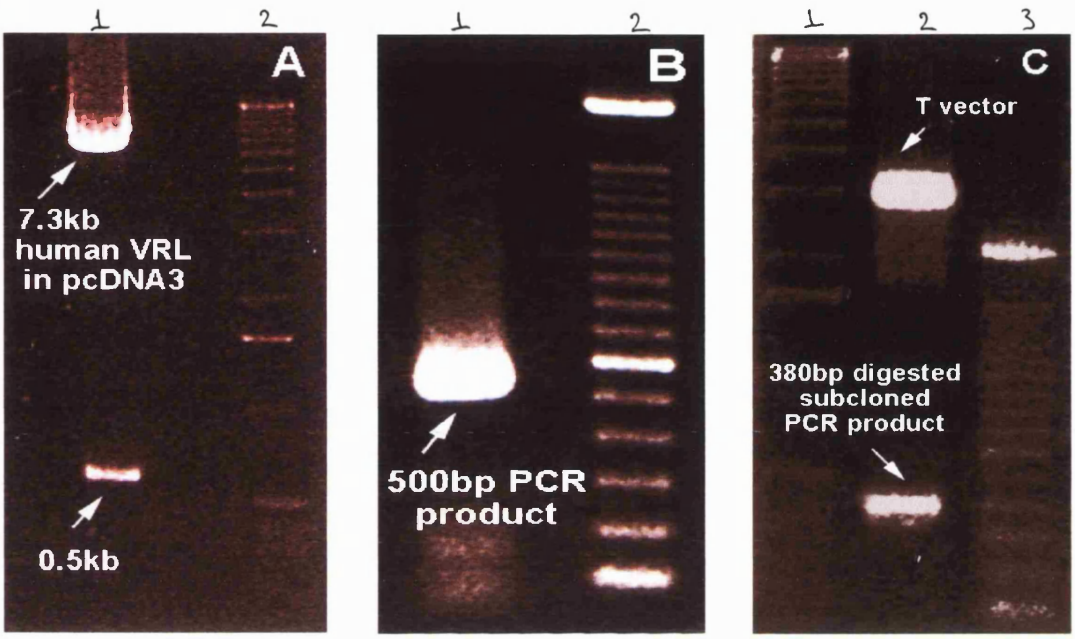

The PCR product was subcloned into T vector to ensure a reserve of the FLAG version of the gene, in order to troubleshoot failed ligations. The correct insertion of the FLAG epitope into human VR-L was confirmed with DNA sequencing (appendix 3.1).

Rat VR-L FLAG/MYC construct

Two versions of the rat VR-L gene, cloned into pcDNAI vector, were produced with the FLAG or c-myc epitope. The forward primer was designed to contain a SacII site prior to the initiation methionine and the epitope. The reverse primer was designed from a region about 450bp downstream the initiation ATG (appendix 3.2c). The resulting PCR product was digested with SacII and SmaI to generate a 280bp fragment that was consequently cloned into the SacII-SmaI digested pcDNAI-rat VRL sequence (figure 3.6). Since the same PCR method for tagging was used in both rat VR-L constructs, only the c-myc epitope insertion is shown.

Figure 3.6: Insertion of the c-myc epitope into the rat VR-L gene. Picture A: Lane 1: 1kb ladder. Lane 2: SacII-SmaI digested rat VR-L/pcDNAI. Picture B: Lane 1: 100bp ladder. Lane 2: 420bp PCR product. Picture C: Lane 1: SacII-SmaI digested PCR product. Lane 2: 100bp ladder.

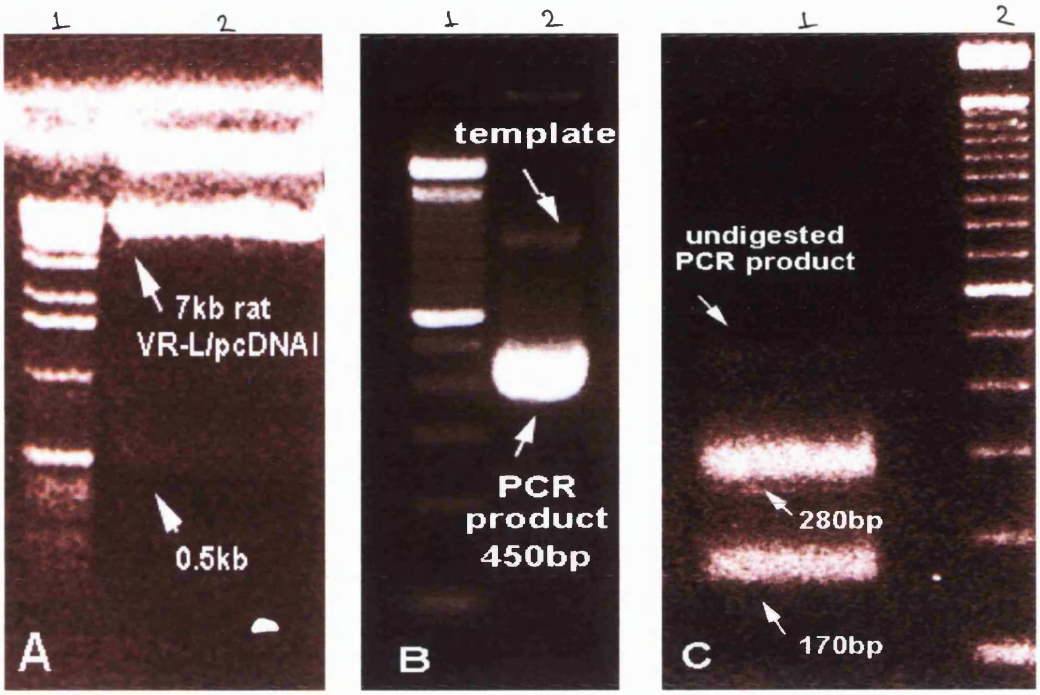

The 280bp-digested PCR fragment was ligated into the SacII-SmaI digested 7kb vector/rat VR-L fragment to create the c-myc tagged version of the gene. DNA preparations from transformed bacteria colonies were analysed with diagnostic restriction enzyme digestions and DNA sequencing (appendix 3.1).

Human TRP1-MYC construct

The forward primer for the human TRP1-MYC construct contained a KpnI site at its 5' end. The reverse primer was designed to start amplification at 625bp downstream of the initiation methionine (appendix 3.2d) and cross a ClaI site. The template for the PCR was TRPC1A, the splice variant of human TRP1 (Zitt *et al.*, 1996) in pcDNA3 vector, that when digested with KpnI and ClaI rendered two fragments of about 9.7kb and 0.95kb. The 625bp PCR product was digested with the two enzymes to produce a 540bp fragment, that was subsequently ligated to the 9.7kb digested vector fragment (figure 3.7).

Figure 3.7: Insertion of c-myc epitope in human TRP1. Picture A Lane 1: 1kb ladder. Lane 2: 100bp ladder. Lane 3: KpnI-ClaI digested human TRP1/pcDNA3. Picture B Lane 1: 625bp PCR fragment. Lane 2: 100bp ladder. Picture C Lane 1: 540bp digested PCR product. Lane 2: 100bp ladder.

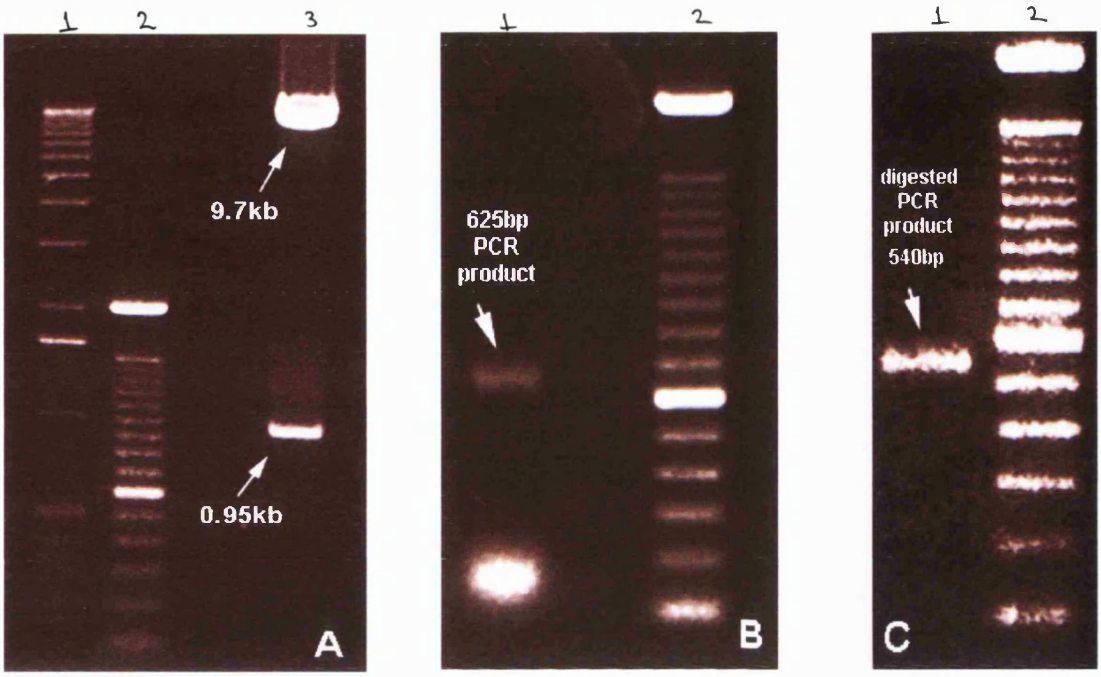

The correct insertion of the c-myc epitope was verified with DNA sequencing (appendix 3.1)

Human TRP3 FLAG/MYC construct

The forward primer for this construct was designed to contain a MfeI site prior to the initiation methionine and the epitope. The reverse primer was designed from a region 260bp after the initiation methionine, crossing a SacII site. The two restriction enzyme sites were later used to subclone the PCR product into the digested human TRP3/pcDNA3 (figure 3.8), resulting in the epitope-tagged TRP3 gene (appendix 3.2e). The cloning strategy leading to the addition of the FLAG epitope is shown in figure 2.20 and 2.21.

Figure 3.8: Insertion of FLAG epitope in human TRP3. Picture A Lane 1: AB PCR product. Lane 2: CD PCR product. Lane 3: 100bp ladder. Picture B Lane 1: 100bp ladder. Lane 2: AD PCR product. Picture C Lane 1: 100bp ladder. Lane 2: MfeI-SacII digested AD PCR product. Picture D Lane 1: 1kb ladder. Lane 2: MfeI-SacII digested human TRP3/pcDNA3.

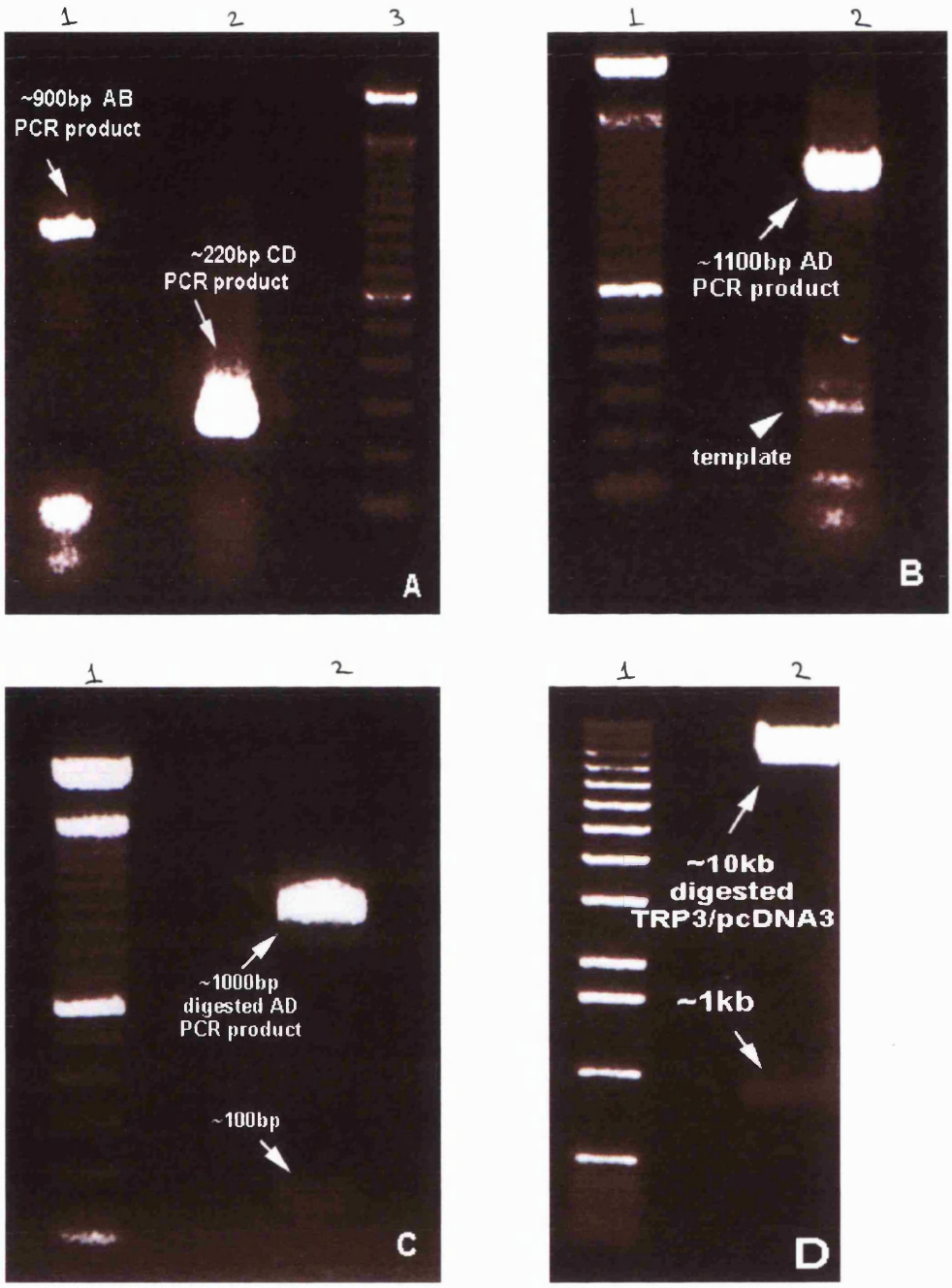

The correct insertion of the FLAG epitope was established with DNA sequencing (appendix 3.1).

Mouse TRP6-MYC construct

The forward primer for this construct was designed to contain an EcoRI site at its N' end. The reverse primer was designed about 700bp downstream the initiation methionine, crossing a XhoI site. The 700bp PCR product, when cut with EcoRI and XhoI rendered a 500bp fragment approximately (figure 3.9) that was ligated into the original gene containing vector pvSport (appendix 3.2f).

Figure 3.9: Insertion of the c-myc epitope into mouse TRP6. Picture A Lane 1: 1kb ladder. Lane 2: 100bp ladder. Lane 3: EcoRI-XhoI digested mouse TRP6/pvSport. Picture B Lane 1: 100bp ladder. Lane 2: ~700bp PCR product. Picture C Lane 1: 100bp ladder. Lane 2: EcoRI-XhoI digested PCR product.

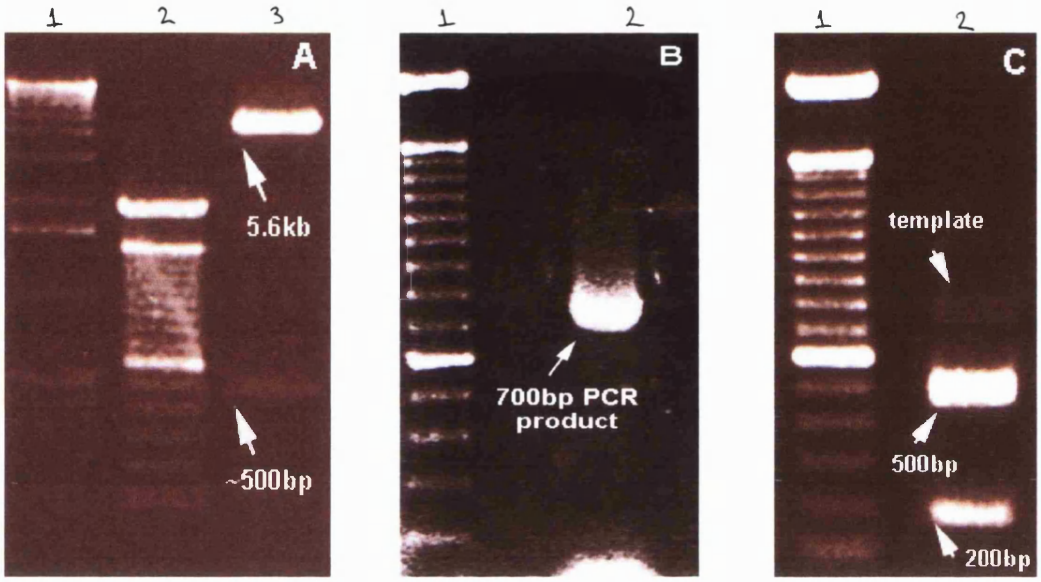

DNA preparations from successfully transformed ligations were analysed with restriction enzyme digestion and sequencing (appendix 3.1).

The successful reconstruction of the restriction enzyme sites at the points of ligation was validated with DNA sequencing and diagnostic digestions. DNA sequencing also verified that no mistakes were introduced into the gene sequence. An example of diagnostic digestions is given below (figure 3.10).

Figure 3.10: Diagnostic restriction enzyme digestions of the VR and TRP constructs.
Picture A: Lane 1: undigested mouse TRP6-MYC. Lane 2: 1kb ladder. Lane 3: mouse TRP6-MYC digested with EcoRI. Lane 4: mouse TRP6-MYC digested with XhoI
Picture B: Lane 1: 1kb ladder. Lane 2: undigested human VRL-FLAG. Lane 3: human VRL-FLAG digested with HindIII and BfrI.
Picture C: Lane 1: 1kb ladder. Lane 2: undigested VR1-FLAG. Lane 3: VR1-FLAG digested with KpnI. Lane 4: VR1-FLAG digested with BsmBI. Lane 6: undigested rat VRL-FLAG. Lane 7: rat VRL-FLAG digested with SacII. Lane 8: rat VRL-FLAG digested with SmaI.
Picture D: Lane 1: 1kb ladder. Lane 2: VR1-MYC digested with KpnI. Lane 3: rat VRL-MYC digested with SacII. Lane 4: rat VRL-MYC digested with SmaI.
Picture E: Lane 1: 1kb ladder. Lane 2: undigested human TRP1. Lane 3: human TRP1 digested with KpnI. Lane 4: human TRP1 digested with ClaI. Lane 6: undigested human TRP3-FLAG. Lane 7: human TRP3-FLAG digested with SacII. Lane 8: human TRP3-FLAG digested with MfeI. Lane 9: human TRP3-MYC digested with SacII. Lane 10: human TRP3-MYC digested with MfeI

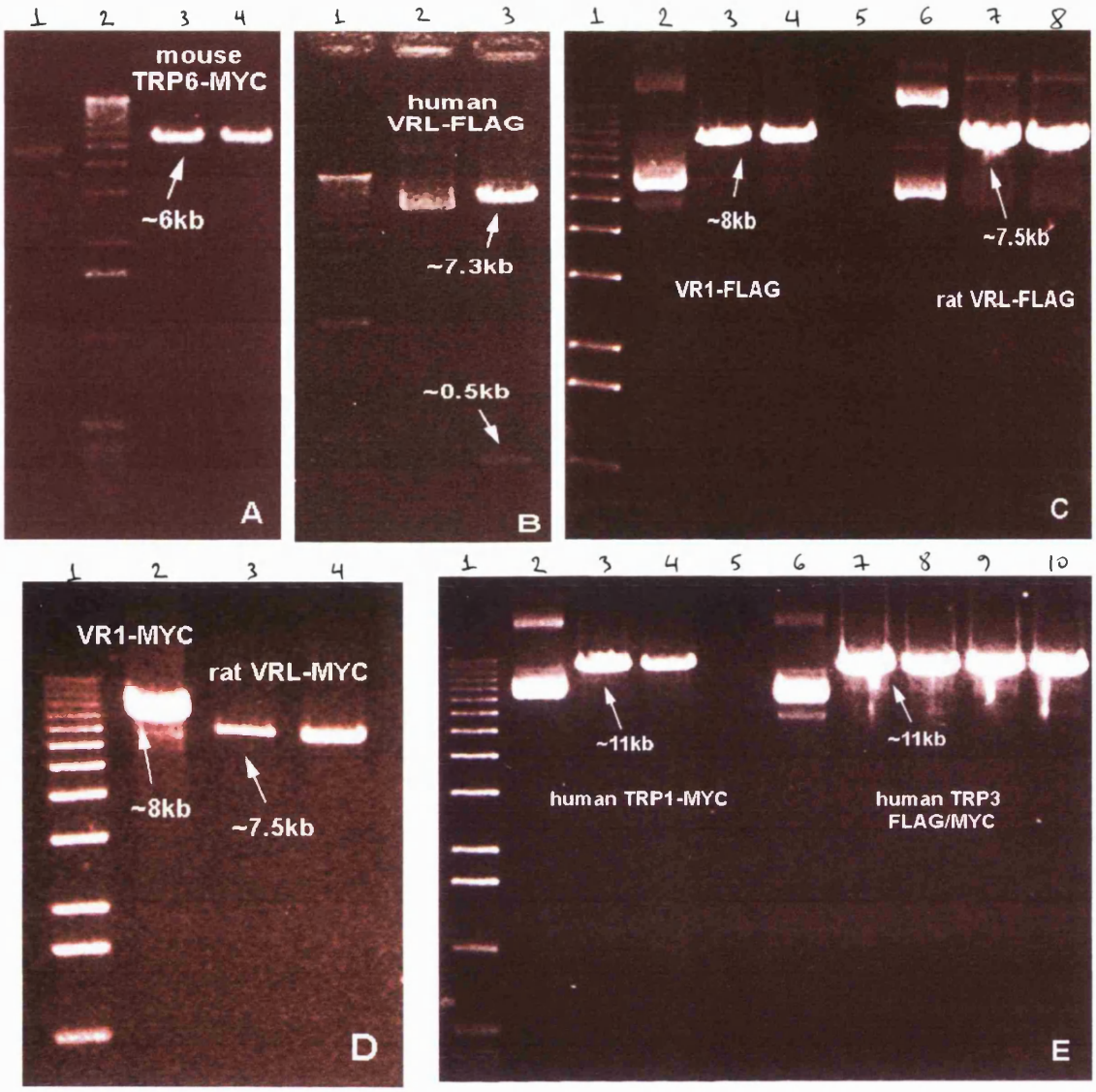

To further substantiate the correct re-assembly of the restriction enzyme sites and the correct insertion of the epitopes without disrupting the open reading frame, the constructs were transcribed and translated *in vitro* incorporating radioactive methionine to examine whether they would produce proteins of the expected size (figure 3.11). The radioactive products of the *in vitro* protein production were subject to a SDS-PAGE and the results were analysed with autoradiography.

Figure 3.11: *In vitro* transcription and translation of VR and TRP constructs.
Picture A: Coomassie blue staining of SDS-PAGE gel and exposed film. The gel had been loaded in the following order: protein molecular weight marker, VR1 (97kDa), human VRL (89kDa), rat VRL (88kDa), human TRP1 (88kDa), mouse TRP6 in pvSport (108kDa), mTRP6 in pcDNA3 (108kDa), VR1-FLAG (97kDa), human VRL-FLAG (89kDa), rat VRL-FLAG (88kDa), rat VRL-MYC (88kDa), human TRP1-MYC (100kDa), mouse TRP6-MYC in pvSport (108kDa), mouse TRP6 in pcDNA3 (108kDa), bovine TRP4-FLAG in pcDNA3 (114kDa).

Picture B: Coomassie blue staining of the SDS-PAGE gel and exposed film. The gel had been loaded in the following order: human TRP3 (102kD), VR1 (97kD), protein molecular weight marker, human TRP3-FLAG (102kD), human TRP3-MYC (102kD), VR1-MYC (97kD). The experiment was performed n=1 time.

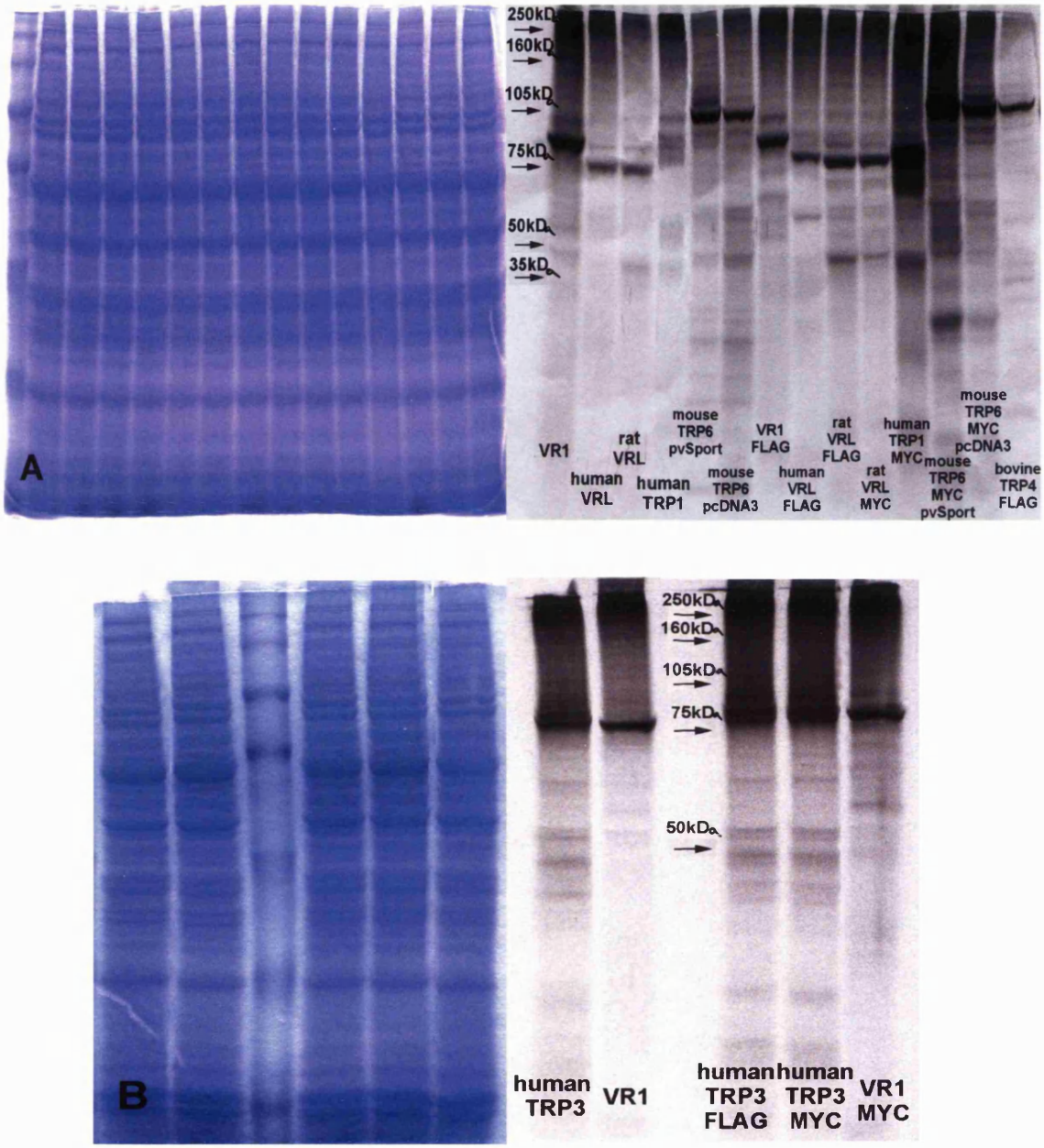

The mouse TRP6 has been subcloned into pcDNA3, in order to examine its expression levels in comparison to pvSport. This was necessary since we had no experience with the latter vector. The bovine TRP4-FLAG was a kind gift from Dr Schielling. The construct human TRP1-MYC appears to yield a higher *in vitro* protein production than the untagged human TRP1. Most probably this is due to the inclusion of a Kozak sequence prior to the initiation methionine in the tagged construct. All the constructs rendered proteins of the right size, however since it was an *in vitro* experiment,

immunocytochemistry was also performed to examine the protein expression *in vivo*. HEK293 cells were transfected with the constructs individually and their epitopes were detected with anti-FLAG and *anti-c-myc* antibodies via fluorescent secondary antibodies (figure 3.12). The experiment was performed n=3 times.

Figure 3.12: Immunocytochemistry of VR and TRP constructs in HEK293 cells. The visual field and fluorescent pictures resulting from the excitation of the secondary antibodies are shown. Pictures A and B have been taken from untransfected cells subjected to the same protocol with the anti-FLAG and anti-*c-myc* (negative control).

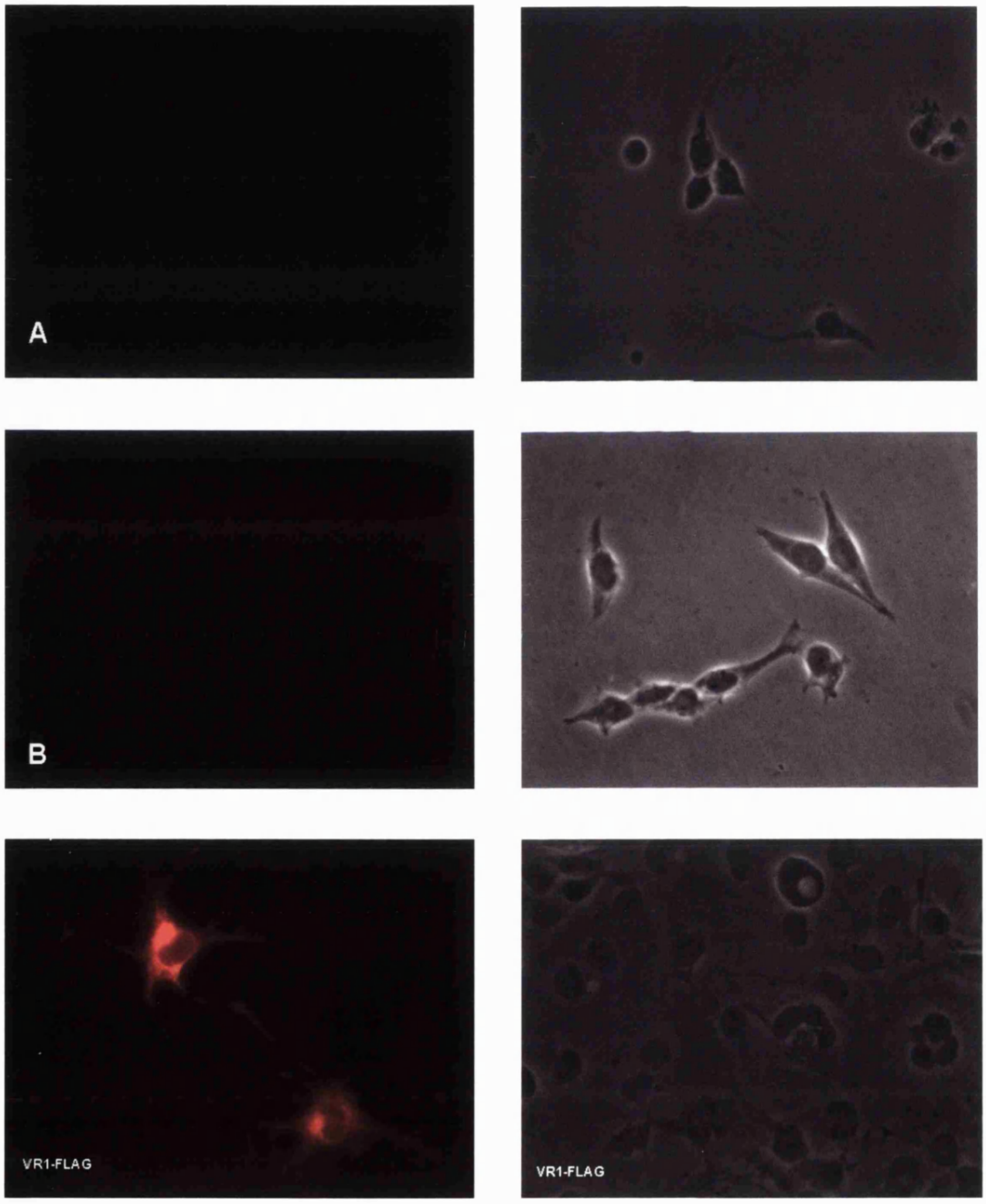

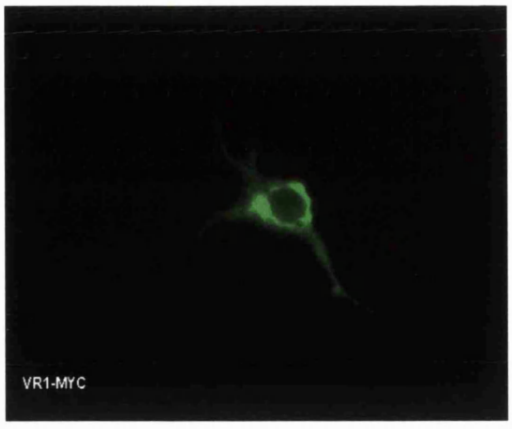
VR1-MYC

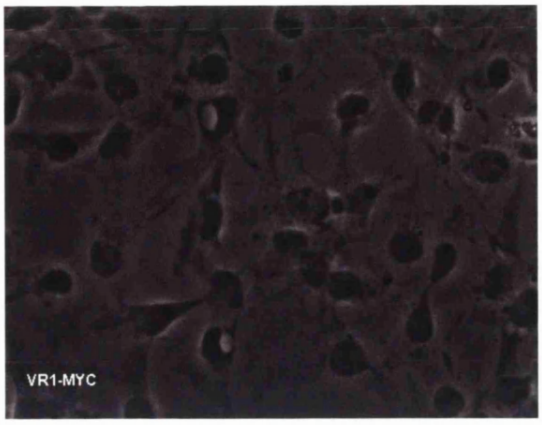
VR1-MYC

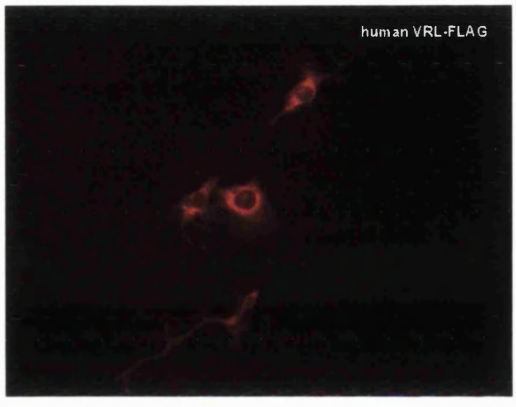
human VRL-FLAG

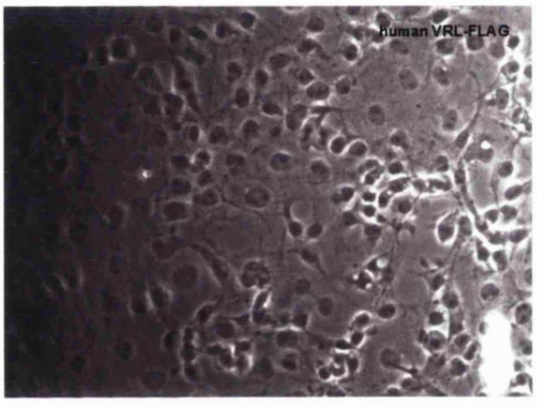
human VRL-FLAG


rat VRL-FLAG

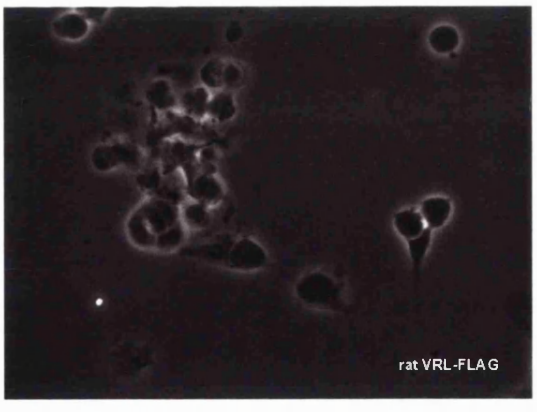
rat VRL-FLAG

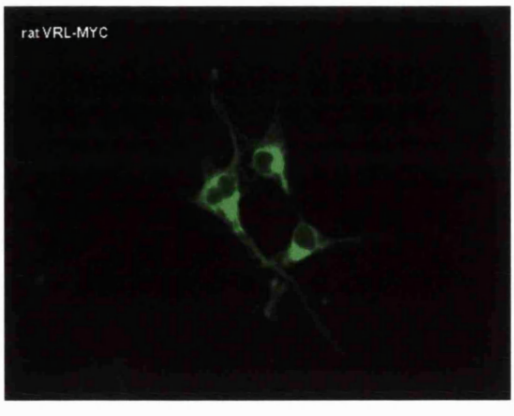
rat VRL-MYC

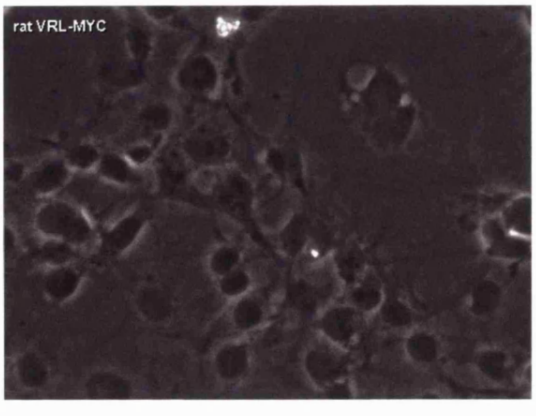
rat VRL-MYC


human TRP1-MYC

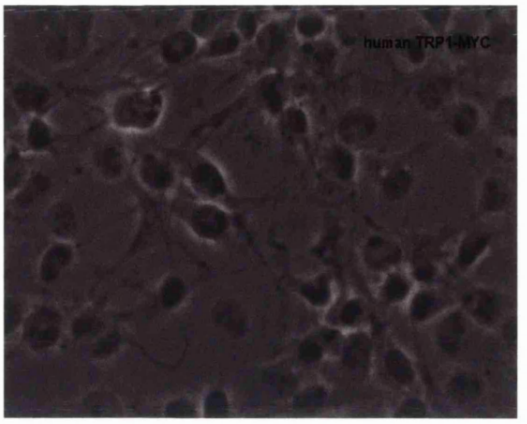
human TRP1-MYC


human TRP3-FLAG

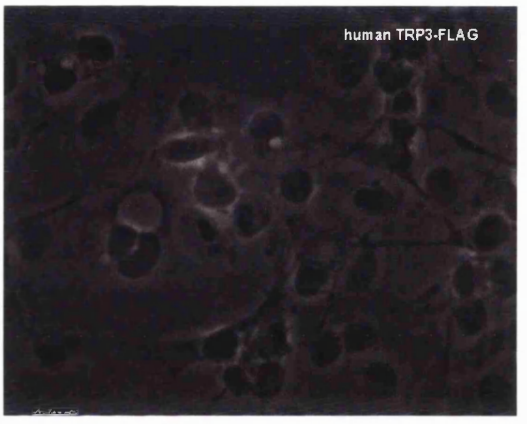
human TRP3-FLAG

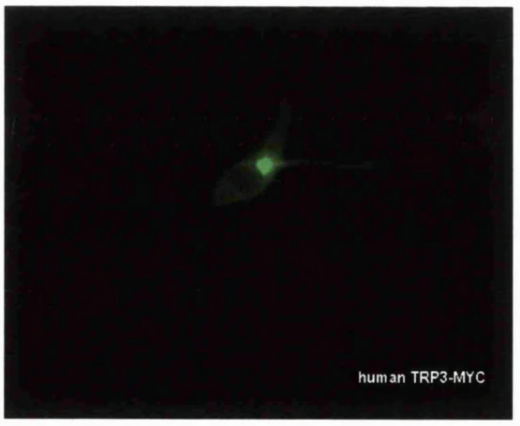
human TRP3-MYC

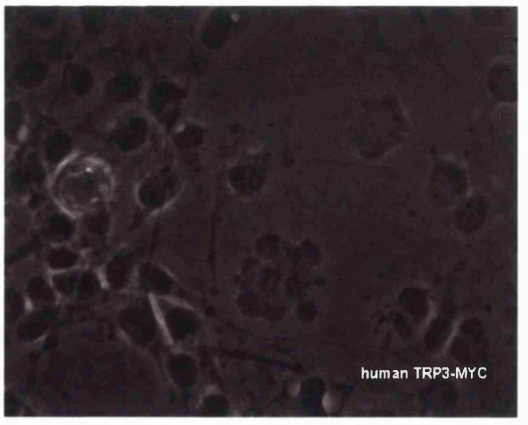
human TRP3-MYC

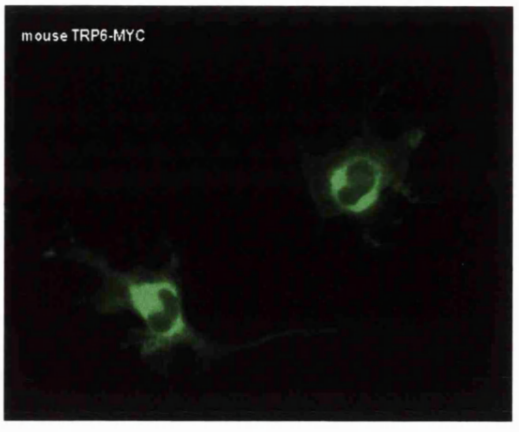
mouse TRP6-MYC

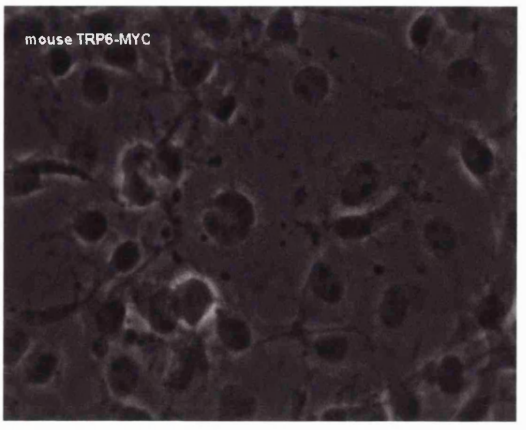
mouse TRP6-MYC

The successful immunocytochemistry verified the expression of the proteins and the insertion of the epitopes at sites accessible to the antibodies. Moreover, the functionality of the constructs was tested electrophysiologically by using patch-clamp in transfected HEK293 cells. This was possible only for the VR1 constructs via capsaicin stimulation (figure 3.13). We observed that the epitope addition did not alter the VR1 current characteristics, compared to control (figure 3.13A). Application of capsaicin throughout the recording induced an inward current exhibiting tachyphylaxis. Unfortunately, we did not have the set-up for recording TRP responses, but we relied on the fact that functional TRP constructs with epitopes at the same site as ours had been made before (Xu *et al.*, 1997). The experiment was performed n=1 time.

Figure 3.13: Patch-clamp recordings from HEK293 cells transfected with VR1 constructs in the presence of 3μM capsaicin for 6 sec. Picture A: current from a VR1 transfected cell (positive control). Picture B: current from a VR1-FLAG transfected cell. Picture C: current from a VR1-MYC transfected cell.

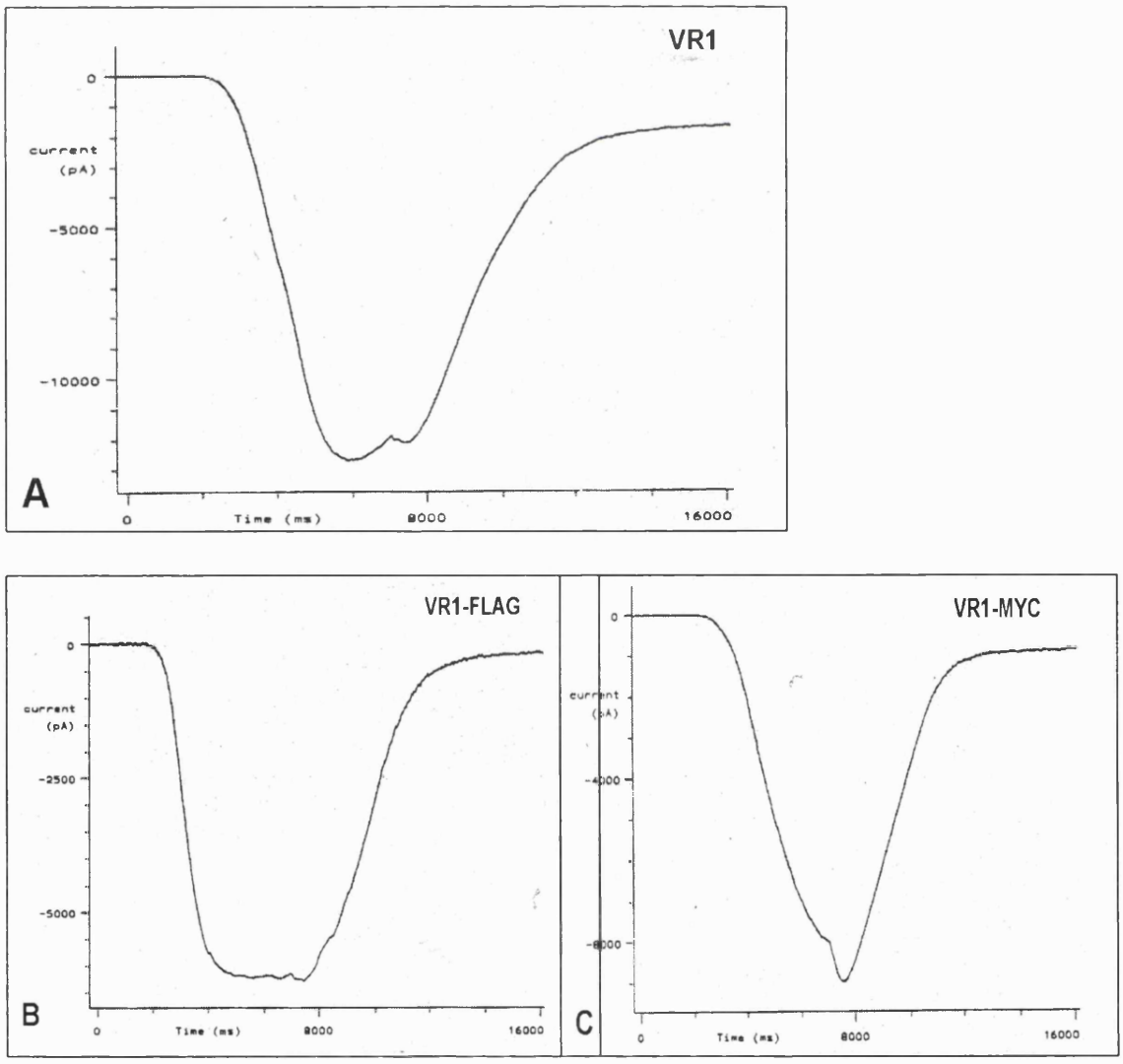

In summary, the expression of TRP channels was established in DRG neurons by using RT-PCR. Additionally, examination of the TRP channels expression in capsaicin treated DRG cultures demonstrated that TRP4 transcripts are located to a large extent in the VR1 expressing neuronal population, while the rest of the TRP channels are probably found in a mixed population (capsaicin-sensitive and capsaicin-insensitive). The fact that TRP channels can form heteromultimers and the identification of their expression in DRG led to the hypothesis that maybe TRP channels interact with the topologically similar members of the vanilloid receptors. Since no antibodies against TRP channels and vanilloid receptors were available, epitopes were inserted in the corresponding cDNAs. The correct epitope insertion was confirmed with diagnostic digestions, DNA sequencing and *in vitro* transcription and translation of the constructs. The functionality of the epitopes and the *in vivo* protein expression was verified with immunocytochemistry in cells transfected with the constructs. Additionally, the VR1 constructs were assayed electrophysiologically. Subsequently, these constructs were used in co-immunoprecipitation studies to study any possible interactions between TRP and vanilloid receptors.

3.3 VR and TRP channels co-immunoprecipitation experiments

3.3a Immunoprecipitation of the rat VR-L protein

Following the insertion of epitopes in vanilloid and TRP channels, it was necessary to establish the immunoprecipitation conditions, prior to embarking on co-immunoprecipitation experiments. Although immunocytochemistry experiments proved the protein expression *in vivo*, it was necessary to examine whether the antibodies could recognise the epitopes in cell lysates and whether they would be functional in western blots. The construct rat VR-L/FLAG was used to transfect COS7 cells. 36 hours post-transfection, the cells were harvested and solubilised with the non-ionic detergent Triton X-100. A polyclonal antibody against the epitope FLAG was used to precipitate the tagged protein from the cell lysate in conjunction with protein A coated beads. The precipitated protein was analysed by SDS-PAGE immunoblotting (figure 3.14A). Together with the precipitate an aliquot of the crude protein lysate was analysed to ensure protein detection in case the immunoprecipitation failed. The peroxidase catalyses the oxidation of luminol and results in the emission of light, which indirectly allows the visualisation of the

precipitated protein with exposure to autoradiography. The precipitate was also probed with anti-VR-L antibody (figure 3.14B).

Figure 3.14 (A): Autoradiography of Western blot of rat VR-L/FLAG protein probed with anti-FLAG antibody. Lane 1: immunoprecipitated protein from lysate of VR-L/FLAG transfected cells with anti-FLAG antibody. Lane 2: precipitate from untransfected cell lysate. Lane 3: crude transfected cell lysate. Lane 4: protein molecular weight marker. The experiment was performed n=4 times.
Figure 3.14 (B): Autoradiography of the same Western blot of rat VR-L/FLAG protein as picture A, probed with anti-VR-L antibody. (n=2) Lane 5: same amount of immunoprecipitated protein from same lysate as picture A, lane 1. Lane 6: precipitate from untransfected cell lysate. Protein amounts were determined by performing Bradford assay.

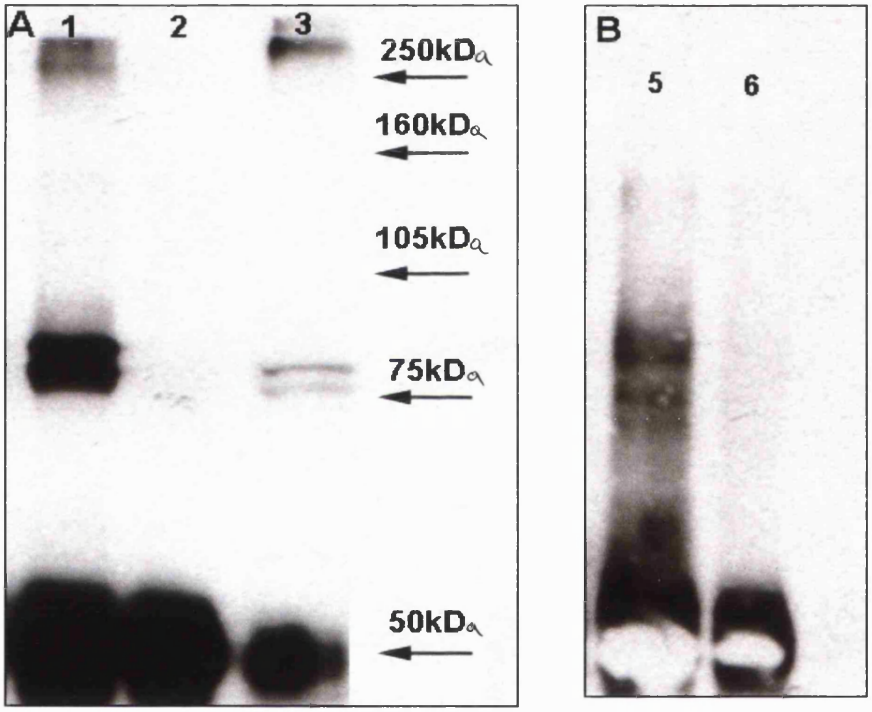

The rat VR-L/FLAG protein was detected as a douplet in the range between 75kDa and 105kDa, after probing with anti-FLAG antibody. The douplet was confirmed to be VR-L as it was also detected with the anti-VR-L antibody. No protein was detected with either antibody in the untransfected cell lysate, establishing the antibody specificity. The crude cell lysate exhibited the same douplet in a slightly lower molecular weight due to different salt concentration compared to the precipitates. The intense bands at 50kDa are the heavy chains of the anti-FLAG polyclonal antibody, which was run together with the precipitate. The light chains of the antibody, that run lower, are not shown, as the membrane had been cut at about 50kDa. The SDS-PAGE gel was also stained with

Ponceau solution, to ensure that complete protein transfer onto the membrane took place. Since the anti-FLAG antibody exhibits higher specificity for the epitope than the anti-VR-L antibody for the VR-L protein, the former was used for the immunoprecipitation experiments.

3.3b Investigating the nature of the rat VR-L protein

VR-L was expected to immunoprecipitate as a protein of 88kDa. The protein detected was in the right size range but appeared as a douplet. Prior to investigating what this duplex represents, the size of each band was calculated from the distance they migrated in the gel. By plotting the log of each of the marker's protein mass versus the distance they have travelled along the gel, the following graph was obtained:

Figure 3.15: Log of protein mass versus the log of distance covered by each of the protein markers.

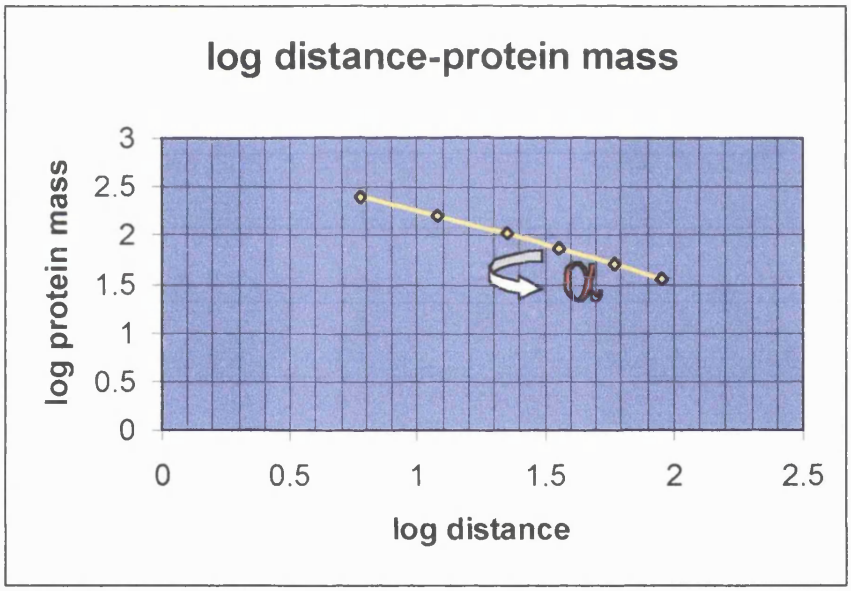

The line obtained by joining all the data points can be described by the formula $y = \alpha * x$, where y = log protein mass, x = log distance and α = the tangential angle. By calculating α from the given data points and by measuring the distance covered by the two bands of the douplet one can estimate their protein mass. Considering that the estimated α is 0.77 and the distance covered by the higher and lower VR-L bands is 30mm and 33mm respectively, one can calculate that the two bands differ about 10kDa in mass. In some blots, a third higher band was also observed which differs about 10-15kDa from the higher band of the douplet (see blot below, figure 3.16A). VR-L was

predicted to contain many glycosylation and myristylation sites, thus we considered the possibility the higher VR-L bands to represent the processed forms of the protein. In order to rule out the possibility that these modifications are cell-line specific, the VR-L/FLAG protein was also expressed in HEK293 cells (figure 3.14A). Simultaneously, we examined the likelihood of the two bands being by-products of protease activity, by performing immunoprecipitation in the presence and absence of protease inhibitors (figure 3.16B). Finally, rat VR-L/FLAG was immunoprecipitated with non-immune IgG to ensure the specificity of the anti-FLAG signal (figure 3.16C).
The experiment was performed n=1time.

Figure 3.16. Picture A: expression of rat VR-L/FLAG in HEK293 and COS7 cells. Picture B: expression of rat VR-L/FLAG in HEK293 and COS7 cells in the presence and absence of protease inhibitors. Picture C: immunoprecipitation with non-immune IgG and without antibody in rat VR-L/FLAG transfected cells.

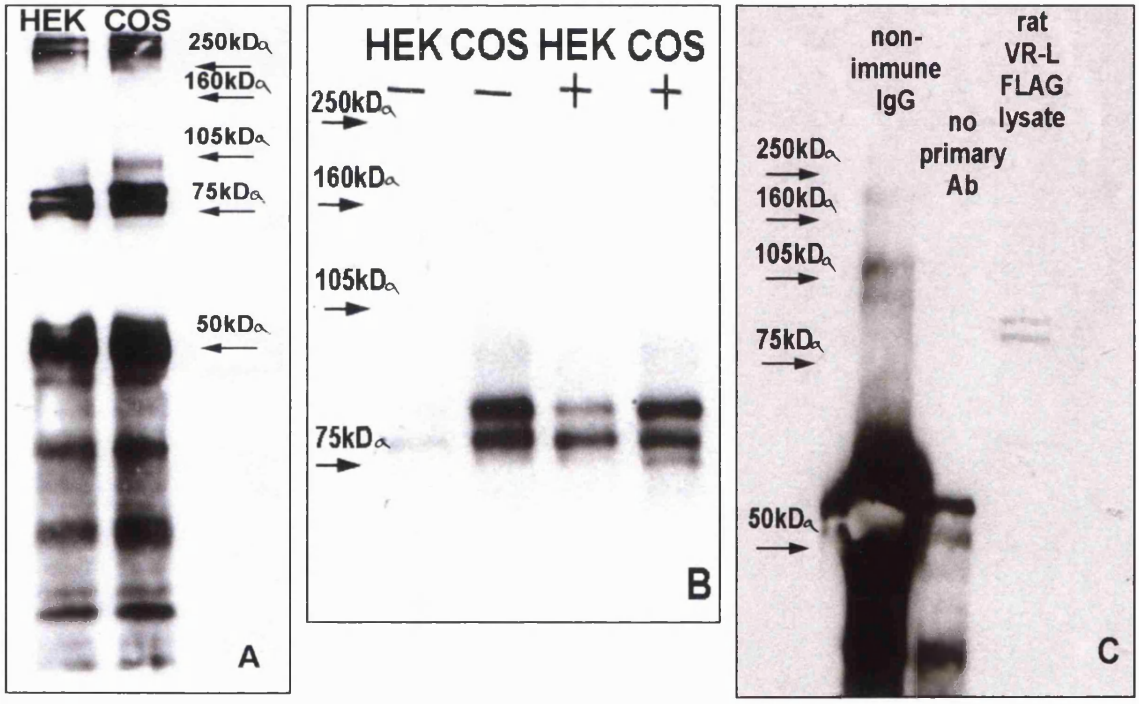

The expression of rat VR-L in a different mammalian cells line did not alter the appearance of the protein douplet.Additionally, it was established that the douplet is not a by-product of protease activity, since the absence of protease inhibitors in the lysis buffer did not change the VR-L signal on the blot. The douplet is specifically recognised by the anti-FLAG antibody as it was proven by the lack of recognition by the non-

immune IgG. Bands in this blot around 105kDa are non-specific as they do not correspond to the expected protein molecular weight for VR-L.

The immunoprecipitations were performed from whole cell lysates and hence the VR-L signal depicts the protein in both the cytoplasm and the plasma membrane. In order to examine whether the two VR-L bands represent the cytoplasmic form of the protein and a mature version incorporated in the plasma membrane, the membrane and cytoplasm lysates of VR-L/FLAG transfected HEK293 and COS7 cells were separated and immunoprecipitations were performed from them (figure 3.17).

Figure 3.17: Anti-FLAG western blot of VR-L/FLAG protein immunoprecipitations from membrane and cytoplasmic preparations of transfected HEK293 and COS7 cells. Lane 1: immunoprecipitation from membrane preparation of transfected HEK293 cells. Lane 2: immunoprecipitation from membrane preparation of transfected COS7 cells. Lane 3: molecular weight protein marker. Lane 4: immunoprecipitation from cytoplasmic preparation of transfected HEK293 cells. Lane 5: immunoprecipitation from cytoplasmic preparation of transfected COS7 cells.

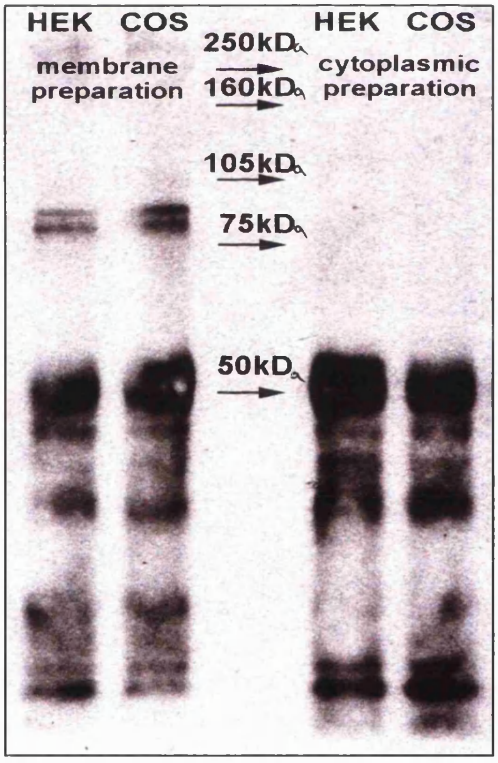

Although no signal was detected in the cytoplasm, probably due to a diluted preparation, both bands were detected in the membrane. Therefore the doublet does not represent the cytoplasm and membrane form of the protein.
The experiment was performed n=2times.

Zhu *et al.* (1998) and Vannier *et al.* (1998) reported the detection of multiple bands in immunoprecipitated human TRP3 protein, very similar to the ones seen in the VR-L/FLAG western blots. The analysis performed on human TRP3 revealed that this protein is N-glycosylated and the multiple bands represent the protein at different stages of maturation. Heterologous expression systems, especially COS cells, are notorious for being able to synthesise only a fraction of the mature protein (Sadeghi *et al.*, 1997). Computational analysis of the VR-L protein demonstrated the existence of one N-glycosylation site (chapter 1, part 1d). This indication and the fact that VR-L belongs to the family of Transient Receptor Potential channels, led to the investigation of N-glycosylation in VR-L. HEK293 and COS7 cells were transfected with the rat VR-L/FLAG construct and immunoprecipitations were performed. Crude lysates and precipitates were subjected to incubation with PNGase F, an enzyme that cleaves all types of asparagine bound N-glycans (figure 3.18). The resulting proteins were analysed with SDS-PAGE electrophoresis. The experiment was performed n=2 times.

Figure 3.18: PNGaseF treatment of crude lysates and immunoprecipitates from rat VR-L/FLAG transfected HEK293 cells. Lane 1: crude lysate treated with PNGaseF. Lane 2: untreated crude lysate. Lane 3: immunoprecipitate treated with PNGaseF. Lane 4: untreated immunoprecipitate. The (+) and (-) indicate the presence or absence of enzyme treatment. The red arrows and the corresponding numbers indicate the observed bands.

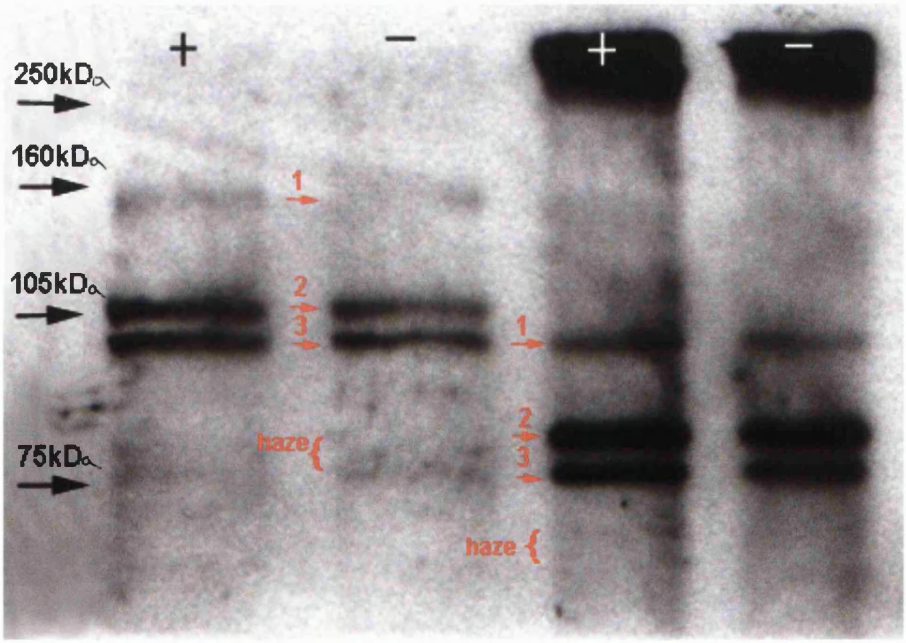

No obvious change was observed between the enzyme treated and untreated samples in the experiment of figure 3.18 and repetitions of the experiment. Unfortunately, no

control confirming the enzyme's functionality was available. Nevertheless, the possibility of VR-L being digested by other glycosidases remains. Additionally, one may speculate the different band sizes of VR-L to represent myristoylated and unprocessed forms of the protein. Unfortunately, due to time limitations no further experiments were carried out to examine myristoylation or digestion by other glycosidases.

3.3c Co-immunoprecipitation of VR and TRP proteins

Prior to performing co-immunoprecipitation experiments with TRP and VR channels, a control co-immunoprecipitation was executed using rat VR-L/FLAG and rat VR-L/MYC constructs. TRP and VR channels are similar topologically to K^+ channels that are known to form tetramers (Doyle *et al.*, 1998), thus it is possible that VR-L subunits assemble in a similar way. The two VR-L constructs were used to transfect COS7 cells in a 1:1 ratio. The lysate was subjected to immunoprecipitation with anti-*c-myc* antibodies and was analysed with blotting with anti-FLAG antibody (figure 3.19A) and anti-*c-myc* antibody (figure 3.19B). Co-immunoprecipitations were carried out in the presence and absence of phosphotase inhibitors in case the interactions depend on the phosphorylation state of the proteins (figure 3.19A, lanes 1 and 2). Co-immunoprecipitations were attempted from mixed cell lysates individually expressing each VR-L construct (figure 3.19A, lane 5). Any interactions detected from the latter sample would show that the proteins have non-specific affinity for each other and thus the interaction would not have functional significance. Control immunoprecipitations were also performed from cells transfected with a single construct (figure 3.19A lane 3, figure 3.19B lane 1) or with no construct (figure 3.19A lane 4).
The experiment was performed n=5 times.

Figure 3.19: Co-immunoprecipitation of rat VR-L/FLAG and VR-L/MYC proteins. **Picture A**, lane 1: anti-*c-myc* immunoprecipitation of VR-L/FLAG and VR-L/MYC co-transfected cells in the presence (+) of phosphotase inhibitors. Lane 2: anti-*c-myc* immunoprecipitation of VR-L/FLAG and VR-L/MYC co-transfected cells in the absence (-) of phosphotase inhibitors. Lane 3: crude lysate of rat VR-L/FLAG and VR-L/MYC mixed cells. Lane 4: untransfected cell lysate. Lane 5:anti-*c-myc* immunoprecipitation from lysate of mixed single transfected VR-L FLAG/MYC cell populations. The blot was performed with anti-FLAG.
Picture B, lane 1: crude rat VR-L/MYC lysate. Lane 2: anti-*c-myc* immunoprecipitation of rat VR-L/MYC and rat VR-L/FLAG co-transfected cells. Lane 3: lysate of mixed single transfected VR-L FLAG/MYC cell populations. Blotting with anti-*c-myc*.

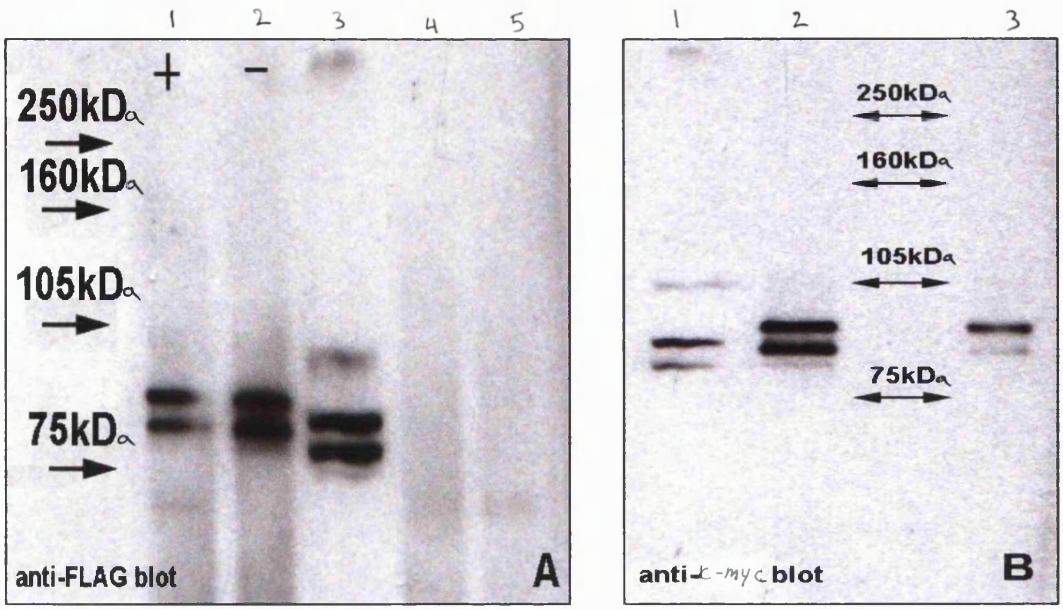

The specificity of the antibody was confirmed by the absence of signal in non-transfected cells. Blotting with both antibodies showed that the co-transfection was successful. Co-immunoprecipitation of VR-L/FLAG with VR-L/MYC was achieved and was proven to be independent of phosphorylation as the inclusion of phosphatase inhibitors did not affect the protein interaction. The interaction was confirmed to be authentic, since an attempt to perform co-immunoprecipitation from mixed lysates of single transfected cells failed. All the VR and TRP constructs were subjected to single immunoprecipitation, before attempting to carry out co-immunoprecipitations (figure 3.20). The membranes were blotted with the appropriate antibody against the epitopes.

Figure 3.20: Immunoprecipitations of VR and TRP constructs. **Picture A**, lane 1: VR1/FLAG (97kDa). Lane 2: human VR-L/FLAG (89kDa). Lane 3: human TRP3/FLAG (102kDa). Lane 4: bovine TRP4/FLAG (114kDa).**Picture B** lane 1: VR1/MYC (89kDa), Lane 2: rat VR-L/MYC (88kDa). Lane 3: human TRP1/MYC (100kDa). Lane 4: human TRP3/MYC (102kDa). Lane 5: mouse TRP6/MYC (108kDa).

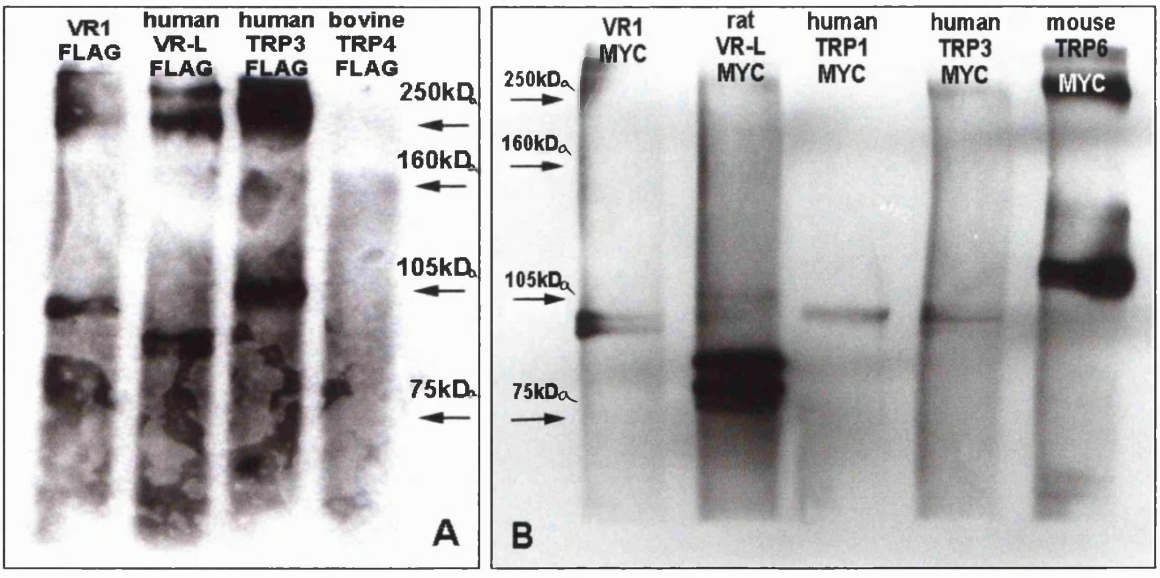

Proteins of the expected sizes were acquired, except from the bovine TRP4/FLAG construct that did not render any protein in repeated attempts for immunoprecipitation. Despite expressing a protein of the expected size in an *in vitro* transcription and translation system (figure 3.11), no protein was detected with immunocytochemistry or immunoprecipitation. Additionally it was observed that VR1 and many of the TRP proteins manifested multiple bands like rat VR-L.

Subsequently, co-immunoprecipitations were performed (figure 3.21). VR1 and VR-L were attempted to co-immunoprecipitate with each other and with TRP3 and TRP6. Unfortunately, co-immunoprecipitations with TRP1 failed as the protein expression for this construct was not consistent. A Kozak sequence had been added prior to the ATG in this construct that might have changed its expression pattern. The immunoprecipitations were performed with the anti-FLAG antibody and the westerns with the anti-*c-myc* antibody.

The membranes were also stripped and blotted with the immunoprecipitation antibody to ensure detectable levels of expression of the transfected genes. The experiment was performed n=1 time .

Figure 3.21: Co-immunoprecipitations of VR and TRP proteins. **Picture A:** western blot with anti-c-myc of the following co-immunoprecipitations, performed with anti-FLAG. Lane 1:co-immunoprecipitation from VR1/FLAG and VR1/MYC co-transfected cells. Lane 2: co-immunoprecipitation from VR1/FLAG and rat VR-L/MYC co-transfected cells. Lane 3: co-immunoprecipitation from VR1/FLAG and human TRP3/MYC co-transfected cells. Lane 4: co-immunoprecipitation from VR1/FLAG and mouse TRP6/MYC co-transfected cells. Lane 5: protein marker. Lane 6: co-immunoprecipitation from human VR-L/FLAG and human TRP3/MYC co-transfected cells. **Picture B:** stripped membrane of picture A and western blot with anti-FLAG.
Picture C: western blot with anti-c-myc of the following co-immunoprecipitations, performed with anti-FLAG. Lane 1: co-immunoprecipitation from VR1/FLAG and VR1/MYC co-transfected cells. Lane 2: co-immunoprecipitation from VR1/FLAG and rat VR-L/MYC co-transfected cells. Lane 3: co-immunoprecipitation from human VR-L/FLAG and rat VR-L/MYC co-transfected cells. Lane 4: co-immunoprecipitation from rat VR-L/FLAG and mouse TRP6/MYC co-transfected cells. Lane 5: co-immunoprecipitation from rat VR-L/FLAG and rat VR-L/MYC co-transfected cells. **Picture D:** stripped membrane of picture C and western blot with anti-FLAG.

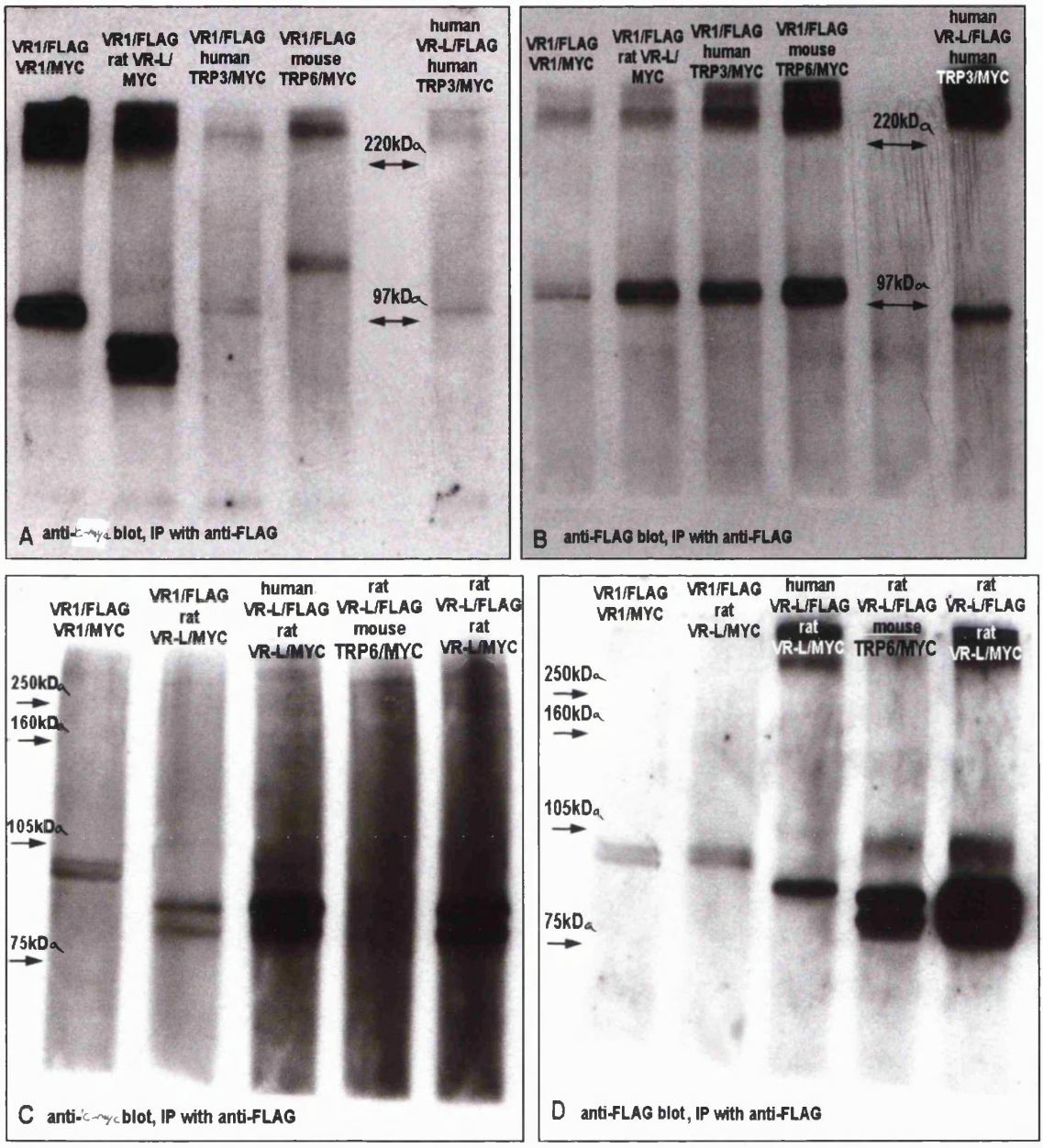

VR1 and VR-L were found to form homomultimers but also to interact with each other. Interaction between the human and the rat VR-L was detected, suggesting that the interaction can be conserved across the species. VR1 was also found to interact with TRP3 and TRP6, while VR-L was found to interact only with TRP3. To support the immunoprecipitation results, a negative control was performed, where co-immunoprecipitations were carried out from lysates of mixed single transfected cell populations (figure 3.22).

(n=1)

Figure 3.22: Negative control for protein interactions. Cells were transfected with one construct at a time. Their lysates were mixed and co-immunoprecipitations with anti-FLAG were performed from them. The samples were run on a SDS-PAGE gel and analysed with western blot with anti-*c-myc* antibody. Lane 1: immunoprecipitation from VR1/MYC transfected cells (control). Lane 2: immunoprecipitation from rat VR-L/FLAG and rat VR-L/MYC mixed lysates. Lane 3: immunoprecipitation from rat VR-L/FLAG and mouse TRP6/MYC mixed lysates. Lane 4: immunoprecipitation from human VR-L/FLAG and human TRP3/MYC mixed lysates. Lane 5: immunoprecipitation from VR1/FLAG and mouse TRP6/MYC mixed lysates. Lane 6: immunoprecipitation from VR1/FLAG and human TRP3/MYC mixed lysates. Lane 7: immunoprecipitation from VR1/FLAG and rat VR-L/MYC mixed lysates. Lane 8: immunoprecipitation from VR1/FLAG and VR1/MYC mixed lysates.

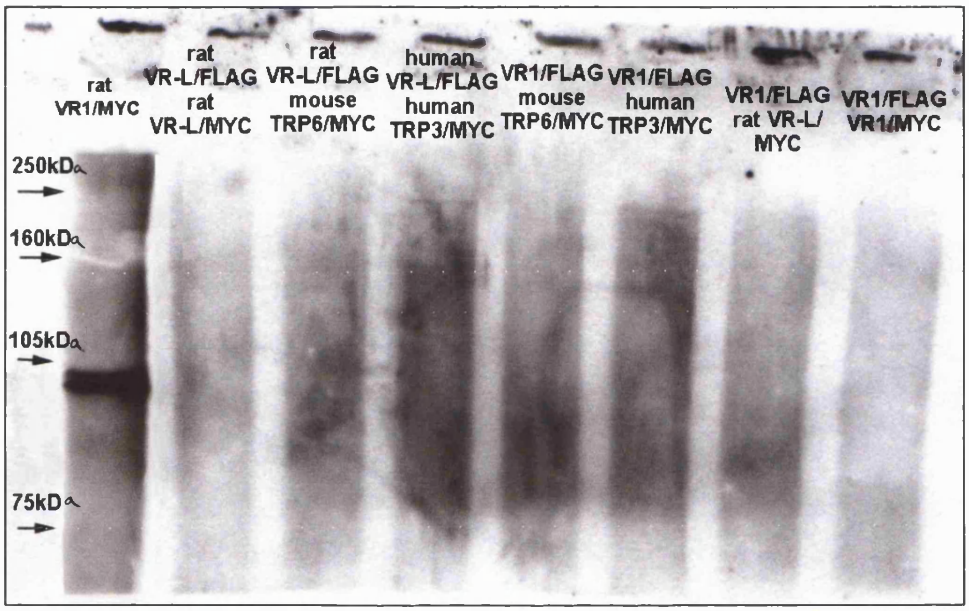

The absence of non-specific interactions between mixed lysates from singly transfected cells confirmed that the interactions shown in figure 3.21 are specific. Unfortunately, it was not possible to acquire VR and TRP cDNAs from the same species, but the fact that the human VR-L/rat VR-L interaction was maintained, conferred confidence in the possibility that an inter-species VR-TRP interaction would be tolerated.

3.4 Construction of a rat VR-L stable cell line

The question to be addressed, following the identification of the VR-VR and the VR-TRP interactions, is what is the functional significance of these interactions. In order to investigate the role of these protein heteromultimers, it is necessary to co-express the VR and TRP genes in a heterologous system and employ electrophysiological methods for functional analysis. To facilitate such experiments, it is convenient to have a stable cell line that expresses one of the genes of interest. The cell line can then be transiently

transfected with other genes and study the functional importance of their interaction with the endogenous gene.

Since collaborators have constructed a VR1 stable cell line (Dr. Wafford's group, Merck), we decided to create a VR-L stable cell line. CHO cells were chosen because they contain the IGF receptor, the activation of which, according to Kanzaki *et al.* (1999), leads to the translocation of VR-L from the cytoplasm to the cell membrane. The pcDNA3 vector contains the selection marker neomycin, which confers resistance to the antibiotic geneticin. The rat VR-L/FLAG construct was chosen for the production of the cell line, as the VR1 cell line was made with the rat vanilloid receptor. The rat VR-L/FLAG cDNA had been cloned into pcDNAI, which does not contain the neomycin gene. For that reason, it was necessary to subclone the construct into pcDNA3. Rat VR-L/pcDNAI (see appendix 3.2c) was digested with SacII and XbaI in order to remove the cDNA (figure 3.23A). The pcDNA3 vector was digested with NotI and XbaI and dephosphorylated (figure 3.23A). A NotI-SacII-XbaI adaptor was designed, phosphorylated and ligated to the digested vector (figure 3.23B) in order to introduce the SacII site into pcDNA3 (appendix 3.2g).

Figure 3.23: Insertion of a SacII site into pcDNA3. Picture A, lane 1: 1kb ladder. Lane 2: pcDNA3 digested with NotI and XbaI (expected size: 5.5kb). Lane 3: rat VR-L/FLAG in pcDNAI cut with SacII and XbaI (expected size: 4.8kB vector and 2.7 kb cDNA). Picture B, lane 1: 1kb ladder. Lane 2: uncut pcDNA3 with SacII inserted. Lane 3: pcDNA3-SacII digested with SacII (expected size 5.5 kb).

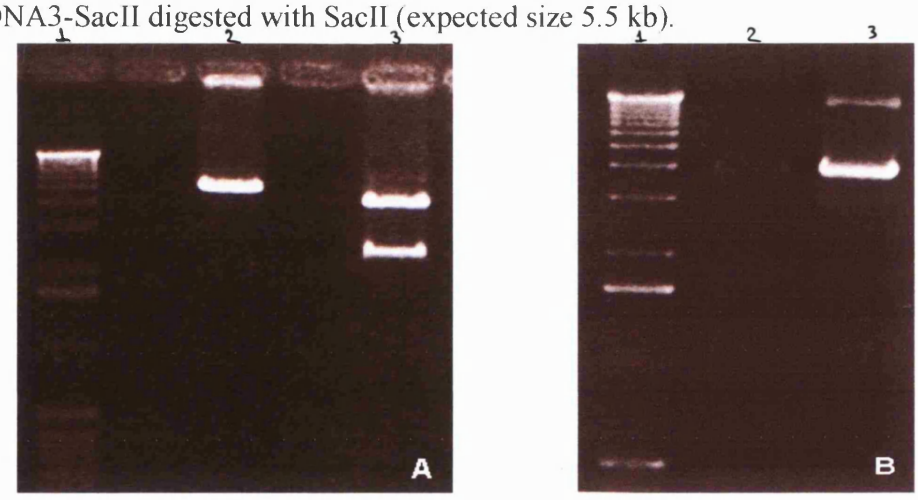

The pcDNA3 vector with the newly inserted SacII site was digested with SacII and XbaI and subsequently ligated to the SacII-XbaI digested rat VR-L cDNA. The correct insertion of rat VR-L/FLAG into pcDNA3 was confirmed with digestion (figure 3.24), *in vitro* transcription and translation (figure 3.25) and sequencing (appendix 3.3). The

digestion of the construct produced the right size band, which along with the sequencing indicated the successful subcloning of rat VR-L/FLAG into pcDNA3. *In vitro* synthesis of the correct size protein showed that the subcloning procedure did not interfere with the gene's coding region.

Figure 3.24: Diagnostic digestion of the rat VR-L/FLAG construct in pcDNA3. Lane 1: 1kb ladder. Lane 2: undigested rat VR-L/FLAG in pcDNA3. Lane 3: rat VR-L/FLAG in pcDNA3 digested with SacII (expected size: 8.2kb).

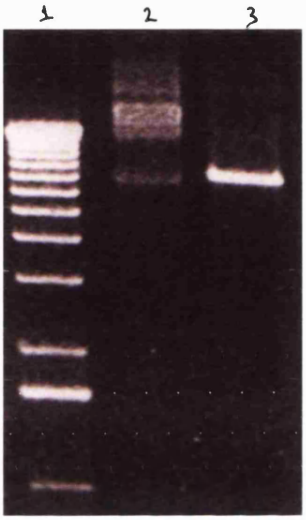

Figure 3.25: *In vitro* transcription and translation of the rat VR-L/FLAG construct in pcDNA3. Lanes1-3: coomassie blue staining of the SDS-PAGE gel. Lanes 4-6: exposure on film. The gel was loaded in the following order: Lanes1/4: rat VR-L in pcDNA1. Lanes 2/5: molecular weight protein marker. Lanes 3/6: rat VR-L/FLAG in pcDNA3(n=1).

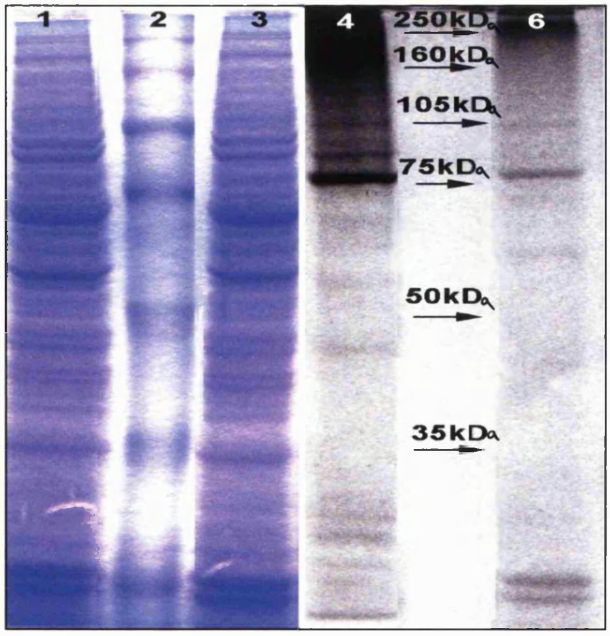

Prior to using this construct for the generation of the cell line, the right dose of the antibiotic geneticin (the antibiotic marker expressed in the vector) for the experiment was established. This was necessary because if the geneticin concentration were too low, CHO cells would survive without incorporating the construct into their genome. On the other hand if the concentration were too high, it would be toxic even onto the desirable cells. For that reason, CHO cells were plated in the concentration that would be used for the cell line construction (10-20% confluent) and were subjected to different concentrations of geneticin in the range of 100-1200 μg/ml over a period of 2 weeks. After this time, the live cells were stained with methylene blue and the percentage of surviving cells in the presence of each dilution of geneticin versus the percentage of survival in the absence of the drug was calculated, generating a geneticin response curve (figure 3.26).

Figure 3.26: Plot of percentage of CHO cell survival versus increasing concentrations of geneticin after the period of 2 weeks.

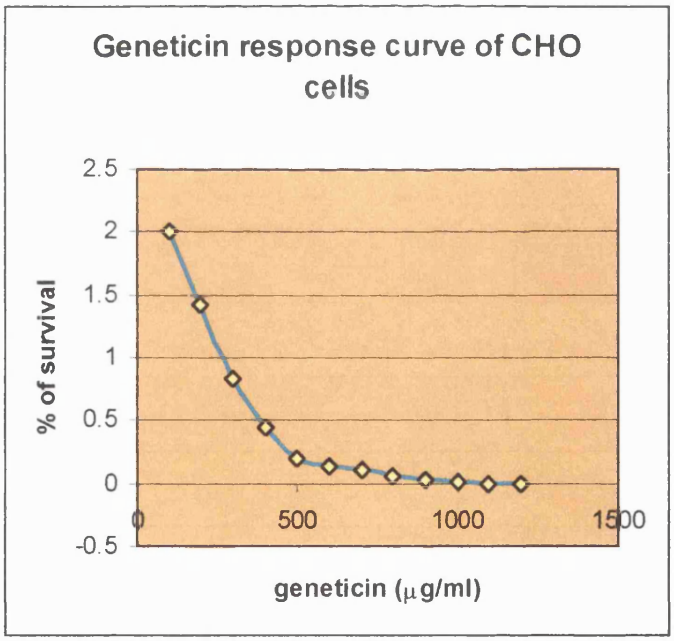

It should be pointed out that this curve is specific to this particular cell and drug batch and the cell confluency. These parameters were maintained stable during the production of the cell line. 1000 μg/ml was the chosen geneticin concentration as it was the one which allowed the fewest cells to survive before causing a toxic effect on the whole cell population. CHO cells were transfected with the construct, were plated at low concentration (~10-20%) and were subjected to the chosen geneticin dose for two weeks. During this period most cells died and the surviving cells formed colonies

around them as they proliferated. Ten colonies were harvested, expanded and analysed by western blotting using anti-FLAG antibodies. One colony that showed relatively high expression levels of the rat VR-L protein was maintained to propagate the cell line. The stable incorporation of the rat VR-L/FLAG construct in the genome of the CHO cells was confirmed with immunoprecipitation with the anti-FLAG antibody and was compared to transient expression of the construct in naive cells (figure 3.27).

Figure 3.27: Western blot analysis of the rat VR-L/FLAG CHO cell line. Lane 1: immunoprecipitation from transiently transfected CHO cells with rat VR-L/FLAG in pcDNA3. Lane 2: immunoprecipitation from the CHO cell line. Lane 3: immunoprecipitation from untransfected CHO cells.

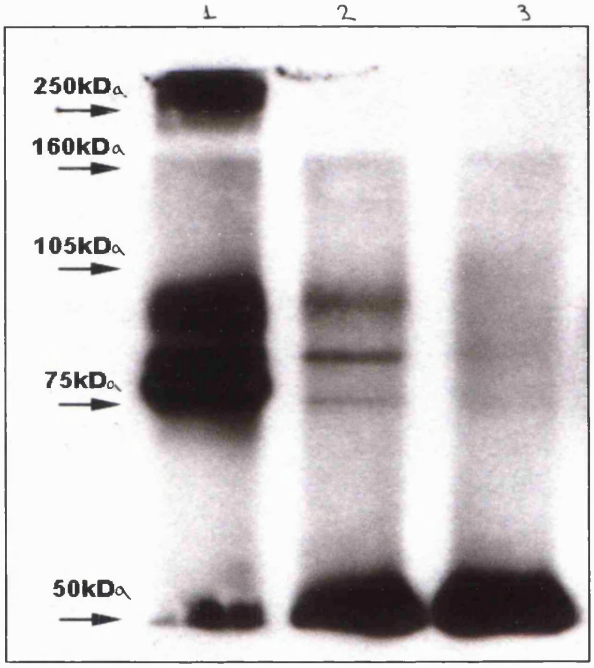

The CHO cell line expresses the right size VR-L/FLAG protein. The expression level is much lower compared to the one observed in the transient transfection, as expected since the latter results in protein over-expression. The experiment was performed n=3 times.

In summary, the expression of TRP channels in DRG neurons was established using RT-PCR analysis. Additionally, semi-quantitative RT-PCR using cDNA from capsaicin treated and control cultures suggested that TRP4 colocalises to a large extent with VR1. Considering that the vanilloid receptors are similar to the TRP channels, which can heteromultimerise, the possibility of interactions between vanilloid and TRP channels was explored by co-immunoprecipitation experiments. In the absence of appropriate antibodies, epitopes were added on VR and TRP genes and the immunoprecipitation experiments were carried out using antibodies against the epitopes. VR-L was found to

immunoprecipitate as a douplet protein. This douplet formation is not due to inadequate protein processing by the host cells, to digestion by proteases or to differential protein configuration according to its localisation in the cell. The douplet was not affected by PNGase F induced deglycosylation. VR1 and VR-L were found to form homomultimers and heteromultimers. Furthermore, co-immunoprecipitation experiments showed VR1 to interact with TRP3 and TRP6, while VR-L interacted only with TRP3. In order to study the functional role of these interactions a stable VR-L cell line was generated in CHO cells. The cell line can subsequently serve as a useful tool in functional studies to elucidate the role of VR-L and the importance of interactions among vanilloid receptors as well as between vanilloid and transient receptor potential channels.

CHAPTER 3

Interactions between vanilloid receptors and members of the Transient Receptor Potential family of receptors

DISCUSSION

TRP channels are expressed in DRG neurons

Spurred by the finding that TRP channels interact to form heteromultimers, the possibility that vanilloid receptors interact with each other or with members of the TRP channel family was investigated in this chapter. Initially the expression of TRP channels in DRG neurons was examined since there was no relevant preliminary data. RT-PCR studies were conducted to inquire into the TRP transcript synthesis in nociceptors. Published rat TRP sequences were aligned and unique regions for each gene were identified. Primers were designed from these regions and they were tested with cDNA from tissues the TRP sequences were cloned from. Cyclophilin amplification (figure 3.1A) confirmed the quality of the cDNA synthesised from rat brain, heart and adrenal gland. TRP3, TRP4, TRP5 and TRP6 were successfully amplified from cDNA of the tissues of origin (figure 3.1A and 3.1B) and DRG neurons (figure 3.2B and 3.2C). Two isoforms have been published for TRP1: TRP1α and the splice variant TRP1β. Because TRP1β was identified in low levels in heart and DRG cDNA (figures 3.1A and 3.2A), primers were designed that identified both isoforms. TRP2 transcripts were not identified in DRG neurons with RT-PCR. This result was not unexpected as Liman *et al.* (1999) reported the specific expression of TRP2 in neurons of the vomeronasal organ in the rat.

The expression of TRP channels in DRG neurons was examined in capsaicin treated and control cultures that had been normalised using cyclophilin amplification. To control for the efficacy of the capsaicin treatment, the expression of VR1, VR-L and CGRP was examined in the two DRG populations. VR1 and CGRP transcript levels were downregulated in the capsaicin treated population as expected since large capsaicin concentrations exert a neurotoxic effect on small diameter neurons. On the other hand, the VR-L transcript levels were not affected since VR-L is expressed in the capsaicin insensitive DRG neurons (Garcia *et al.*, 1999, Caterina *et al.*, 1999). Expression of TRP1, TRP3, TRP5 and TRP6 did not seem to be affected by the capsaicin treatment indicating that these genes are mainly expressed in capsaicin insensitive neurons. The size of the TRP3 and TRP5 PCR products was close to the primer dimers making it difficult to distinguish any subtle changes in the transcript levels. Unfortunately it was not possible to design primers amplifying larger gene regions, without compromising their specificity. Interestingly, the TRP4 mRNA levels depict a considerable decrease in the capsaicin treated DRG sample, suggesting this gene to be specifically expressed in the small diameter neurons. This finding together with the reported ability of TRP4 to

heteromultimerise (Strubing *et al.*, 2001) make TRP4 a good candidate for interacting with VR1.

Insertion of epitope tags in TRP and vanilloid channels

Co-immunoprecipitation studies were deployed to study any possible interactions between TRP channels and vanilloid receptors. Unfortunately, it was not possible to obtain the cDNAs for all the TRP channels. The genes used in this study were VR1, VR-L, TRP1, TRP3 and TRP6. Because no antibodies were available for the encoded proteins, epitope tagged versions of these genes were constructed using PCR. The FLAG and c-myc epitopes were chosen, as they are traditionally used for tagging proteins and there are well-characterised antibodies against them used in co-immunoprecipitation studies (Hawkins *et al.*, 1999). The correct epitope insertion and subcloning was confirmed with restriction enzyme digestions (figure 3.10) and DNA sequencing (appendix 3.1). The constructs were tested for their ability to synthesise protein by using *in vitro* transcription and translation in the presence of radioactive methionine. The synthesised proteins were analysed with SDS-PAGE electrophoresis and autoradiography (figure 3.11). All the constructs rendered proteins of the expected size. Because TRP1 was found to express low levels of protein, a Kozak sequence was added prior to its ATG site during the epitope insertion. This led to an increase in the protein production as can be seen in figure 3.11. Additionally a flag tagged version of the bovine TRP4 gene was acquired from Dr. Schilling, which gave the right size protein.

The expression of the epitopes was tested by immunocytochemistry in transfected HEK293 cells (figure 3.12). Fluorescence associated with the epitopes' expression was identified in the cytoplasm and the plasma membrane for all the constructs tested, indicating that the constructs synthesise protein *in vivo* and the antibodies can recognise the epitopes in the sites they have been inserted. Unfortunately, repeated attempts to identify TRP4-FLAG expression with immunocytochemistry failed, suggesting that either the protein is not expressed *in vivo* or that the epitope is not accessible. Possibly the former hypothesis is true since according to Dr. Schilling it was not possible to record currents from this construct. The functionality of the VR1 constructs was tested using patch-clamp in transfected cells (figure 3.13B and 3.13C). Application of capsaicin caused inward currents of the same amplitude and inactivation as the untagged VR1, suggesting that insertion of the epitopes did not change the characteristics of the channel.

VR-L immunoprecipitates as a protein doublet that reaches the plasma membrane

Prior to carrying out co-immunoprecipitation experiments to investigate TRP-vanilloid receptor interactions, the conditions for single immunoprecipitations were established. The FLAG tagged version of VR-L was successfully immunoprecipitated with anti-FLAG antibody from a lysate of transfected COS7 cells (figure 3.14A). The antibody recognised a doupletprotein around 80-90kDa, which is the protein size expected for VR-L. The two proteins migrated closely together on the gel and they were confirmed to be VR-L by using an anti-VR-L polyclonal antibody (figure 3.14B). By measuring the migration distance of the douplet on the gel and comparing it to the protein marker, the size difference between the two bands was estimated to be about 10kDa. Immunoprecipitations in the presence and absence of protease inhibitors showed that this douplet is not a result of protein degradation (figure 3.16B). Additionally, the two VR-L bands did not result from a cell line's inability to process the VR-L protein, as the same douplet was immunoprecipitated from lysates of different cell lines (figure 3.16A). Attempts to immunoprecipitate VR-L with non-immune immunoglobulins failed, showing that the anti-FLAG antibody specifically recognised the flag tagged VR-L protein. The rest of the constructs, with the exception of TRP4-FLAG, were successfully immunoprecipitated with the appropriate antibodies (figure 3.20). Since TRP4 expression had not been detected with immunocytochemistry and electrophysiology, it was concluded that this construct was problematic. Sequencing of the TRP4-FLAG terminals revealed that no untranslated regions had been included in the construct, which could have hindered the gene expression as the untranslated regions often contain important signals for the localisation of the mRNA to specific cellular compartments where it can be translated.

The finding that VR-L immunoprecipitates as a douplet protein prompted the examination of the douplet localisation in the cell. Immunoprecipitations of the flag tagged VR-L protein were attempted from membrane and cytoplasm preparations of transfected cells (figure 3.17). The VR-L douplet was identified in the membrane preparations. The protein was not identified in the cytoplasm preparation, although immunocytochemistry studies showed VR-L expression in the cytoplasm (figure 3.12). This is probably due to a diluted signal since the cytoplasm extracts were prepared in large volumes (10ml). Zhu *et al.* (1998) and Vannier *et al.* (1998) reported that the TRP3 protein is manifested as multiple bands in western blots with two bands

prevailing, similarly to the douplet depicted by VR-L. These researchers found the TRP3 bands to be susceptible to endoglycosidase H and peptide N-glycosidase F treatments, indicating that these bands represent glycosylated forms of the protein. Since N-glycosylation is the most common form of protein glycosylation and because it has been observed in members of the TRP family, the possibility that the VR-L douplet depicts the protein at different stages of maturation was considered. FLAG tagged VR-L protein lysate and immunoprecipitate from transfected HEK cells were subjected to peptide N-glycosidase F treatment and the result was analysed in a SDS-PAGE gel followed by autoradiography (figure 3.18). No difference in the signal was noticeable between the control and treated samples, suggesting that the douplet does not represent differentially processed protein. The haze observed at about 75kDa is probably the result of partial protein degradation, while the signal detected beyond 250kDa (also evident in other gels) is probably non-denatured protein that remained in the gel's wells. Interestingly, a band at about 160kDa was observed in addition to the expected douplet at about 80kDa. This band can either represent a glycosylated form of the protein or protein dimer that was not denatured.

The fact that the PNGase F treatment did not alter the VR-L signal does not rule out the possibility that VR-L is glycosylated. Unfortunately there was no control available to test the enzyme's efficacy and the incubation conditions. PNGase F requires the use of detergents to denature the 3D protein structure, that will allow the enzyme to access the cleavage site and hydrolyse the bond between the asparagine and the oligosaccharide. Nevertheless, the detergents inactivate the enzyme, which can be prevented by the use of Triton X-100. Endoglycosidase H, which cleaves between two N-acetylglucosamine residues in the core of the oligosaccharide, can be used instead since it does not require detergent and cannot be inactivated by it. Taking into consideration that Kanzaki *et al.* (1999) reported the mouse VR-L homologue to be sensitive to tunicamycin, a glycosylation inhibitor, reinforces the hypothesis that the VR-L douplet represents the protein at different maturation stages.

VR1 and VR-L form homomultimers

In order to examine whether VR-L forms homomultimers, different tagged versions of rat VR-L (VR-L/FLAG and VR-L/MYC) were co-transfected in HEK293 cells and immunoprecipitations were carried out with the anti-*c-myc* antibody, followed by western blot with the anti-FLAG antibody (figure 3.19). Signal detection with the anti-

FLAG antibody suggests that when the VR-L/MYC protein was immunoprecipitated with the anti-*c-myc* antibody, it also co-immunoprecipitated VR-L/FLAG. This result indicates that VR-L/FLAG and VR-L/MYC associated to form multimers. The antibodies specifically recognise the corresponding epitopes as confirmed by membrane stripping and reprobing performed in later experiments (figure 3.20) and by the fact that no signal was observed in untransfected cells. The homomultimer formation is not dependent on the phosphorylation state of the protein, since inclusion of phosphatase inhibitors in the lysates did not alter the result. Both constructs had been successfully transfected as confirmed by single immunoprecipitations. Attempts to co-immunoprecipitate the two VR-L constructs from mixed lysates of cells transfected with one construct each failed, showing that the interaction between the two VR-L proteins is not a result of non-specific affinity.

Similarly, VR1/FLAG and VR1/MYC were found to co-immunoprecipitate (figure 3.21) indicating that VR1 forms homomultimers. This finding is in agreement with Kedei *et al.* (2001), who reported that VR1 forms homomultimers and predominantly tetramers. The researchers co-immunoprecipitated differently tagged forms of VR1, establishing that VR1 forms homomultimers. Subsequently, they examined the migration of VR1 in native gels from lysates of transfected COS7 cells and from DRG membranes. VR1 migrated mainly as a tetramer, although dimers and trimers were also detected. Chemical cross-linking resulted in the formation of VR1 complexes, verifying the protein's ability to form multimers. Interestingly, addition of VR1 agonists in cells transfected with VR1 resulted in the endogenous cross-linking of the protein in tetramers.

VR1 and VR-L form heteromultimers with each other and with members of the TRP family of channels.

Since members of the TRP family are known to form heteromultimers, the possibility that VR1 and VR-L interact with each other and with TRP channels was examined by co-immunoprecipitations. Anti-FLAG antibody co-immunoprecipitated rat VR1/FLAG and rat VR-L/MYC from transfected cells (figure 3.21A and 3.21C). This result showed that VR1 can interact with VR-L to form heteromultimers. Interaction of the vanilloid receptors with TRP channels was also tested using anti-FLAG antibody to immunoprecipitate one protein and anti-*c-myc* to detect any interacting protein with western blot. VR1 was found to

interact and co-immunoprecipitate with TRP3 and TRP6, while VR-L was found to interact with TRP3. The TRP1 construct was not used in these experiments due to difficulty in achieving consistent protein expression. Stripping the membrane and reprobing with anti-FLAG to detect the immunoprecipitated protein (figures 3.21B and 3.21D) confirmed that the transfections were successful. Although the interactions detected were not between proteins of the same species, a control interaction between human VR-L/FLAG and rat VR-L/MYC showed that the interactions can be conserved across species. Attempts to co-immunoprecipitate proteins from mixed lysates instead of co-transfected lysates failed (figure 3.22), proving that the identified interactions are specific.

The interaction observed between VR1 and VR-L is stronger than the one observed between VR and TRP channels. This could be due to the fact that the vanilloid receptors tested were from the same species and are more closely related to each other than to TRP proteins. Another factor that could affect the intensity of the signal is the ratio of the cDNAs transfected. For this experiment 1:1 ratio was used. It is possible that the heteromultimers formed consisted of an unequal ratio of proteins i.e. three subunits of TRP proteins could be required to interact with one VR subunit to form a channel. Therefore, by altering the amounts of the proteins co-expressed, stronger interactions could be favoured. The interaction between VR1 and VR-L was observed in two experiments, while the VR-TRP interactions were observed in only one, due to lack of antibodies for repeating the experiments. Unfortunately the commercial production of the polyclonal anti-FLAG antibody used in these experiments was discontinued. Due to the lack of time required to set up the conditions for a new batch of antibody from a different company, the experiments were not repeated.

Generation of a VR-L stable cell line

Following the identification of the protein interactions, it is necessary to decipher their functional significance. TRP proteins are known to cluster in heteromultimers resulting in the generation of channels with new characteristics (Xu *et al.*, 1997, Strubing *et al.*, 2001). The formation of new channels by vanilloid and TRP channels could contribute to the complex pharmacology of vanilloid responses observed *in vivo* (see Chapter 1) that cannot be solely attributed to VR1. Furthermore, such interactions could possibly assign a functional role to the orphan receptor VR-L. Although co-expression of VR-L with VR1 did not change the VR1 receptor responses to heat and capsaicin (Chapter 2,

figure 2.19), it is possible for VR-L to be regulating another aspect of the capsaicin receptor function e.g. in thermal hyperalgesia or inflammation.

VR.5'sv (Dr. Schumacher personal communication) and a pore mutant of VR1 (Oxford *et al.*, 2000) have been found to regulate VR1 in a dominant negative fashion, showing that vanilloid receptors can form heteromultimers with functional implications. Therefore, careful functional analysis is needed to identify the role of the interactions between VR1 and VR-L and between the vanilloid and TRP channels. In order to facilitate functional experiments that require co-expression of vanilloid and other channels, a VR-L stable cell line was generated. The rat VR-L/FLAG construct was subcloned into a vector that confers resistance to geneticin. The new construct was transfected in CHO cells and was subjected to sustained selection with the antibiotic geneticin. A resistant colony was identified, expanded and analysed for expressing the FLAG epitope and thus the VR-L protein (figure 3.27). Western blot analysis identified the VR-L doublet, proving that the CHO cell line is stably expressing the VR-L/FLAG protein. Subsequently, this cell line can be used in functional studies of vanilloid and TRP channels interactions.

Proposed experiments

a) Biochemical studies

The co-immunoprecipitation experiments described in this chapter provide interesting information on the subunit interactions that might take place *in vivo* and result in novel channels. Initially, it would be necessary to repeat the experiments and also include more TRP channels in the study, preferentially of the same species as the vanilloid receptors. Different ratios of transfected genes should be used to examine whether the recombinant channels consist of an unequal subunit composition. The analysis of the multimers in native gels could elucidate their nature i.e. if they favour dimer, trimer, tetramer or other configuration. In order to study the subunit stoichiometry in VR1 and VR-L homomultimers as well as in VR-TRP heteromultimers more analytically, the methods of sucrose density gradient centrifugation and gel filtration could be deployed, that have been traditionally used to study channel composition. In the former method protein lysates are sedimented by centrifugation through a steep sucrose gradient in a tube. The proteins move along the tube until they reach a point where their surroundings have equal sedimentation velocity. As a result, protein multimers can be separated according to their buoyant density and separated in fractions. In the method of gel filtration, different

protein sizes can be separated if passed through a column containing porous matrix and collected in fractions. Large molecules that cannot pass through the pores flow out more rapidly, while smaller molecules are retained by the matrix.

Experiments should be conducted to examine in which tissues the VR-TRP interactions take place *in vivo.* Existing data on the distribution of each gene could provide clues as to which tissues these interactions could have functional significance. Co-immunoprecipitations from native tissues could be carried out. The results could be replicated in a yeast-two hybrid system and in column binding assays. The VR1-VR-L interaction presents special interest as the pharmacological profile of VR1 cannot account for all vanilloid responses observed *in vivo* and no clear role for VR-L has been identified. Although VR1 and VR-L probably do not colocalise in rat DRG neurons (figure 2.13, 3.2), it is worth investigating an *in vivo* interaction between the two channels in brain and spinal cord tissue, where they have both been identified. Interestingly, preliminary experiments show the colocalisation of VR1 with VR-L in human DRG (Dr. Davis Glaxo-SmithKline, personal communication), providing the first insight into an *in vivo* interaction between the two channels. Considering that VR1 and TRP channels can be glycosylated (Kedei *et al.*, 2001, Zhu *et al.*, 1998), it would be interesting to examine whether VR-L exists in a N-glycosylated form in native tissues. Although the deglycosylation experiments described in this chapter suggested VR-L not to be glycosylated, these experiments should be repeated in a range of incubation conditions using VR1 as a control. Putative glycosylation sites on VR-L could also be mutated and the mutant constructs could be analysed on SDS-PAGE gels and compared with the wild-type protein.

b) functional analysis of interactions

The functional significance of the interactions identified between VR1 and VR-L as well as between vanilloid and TRP channels could be deciphered by generating double knockout animals. But in the absence of such animals, electrophysiological studies could be carried out to address the function of the heteromultimers. The VR-L stable cell line generated (figure 3.27) could be used for transfections with TRP channels to carry out recordings using protocols for capacitative Ca^{2+} entry studies i.e. Ca^{2+} store depletion with thapsigargin, activation of G protein coupled receptors. The same experiments could be conducted with VR1 in order to investigate any possible changes in the TRP channel phenotype or in the capsaicin receptor function i.e. responses to

heat, capsaicin and protons. Since application of VR1 agonists in VR1 transfected cells was found to induce the formation of a VR1 tetramer (Kedei *et al.*, 2001), it would be interesting to examine if any particular conditions favour the formation of heteromultimers between VR1 and VR-L or TRP channels. For example, since NGF causes the upregulation of VR-L (Chapter 2, figures 2.9, 2.10, 2.11, 2.12) it would be intriguing to examine whether VR1-VR-L heteromultimer formation is favoured during inflammation, where the NGF concentration increases. Moreover, taking into consideration the finding that the mouse VR-L homologue translocates in response to IGF-I (Kanzaki *et al.*, 1999), it would be interesting to examine the effect of this trophic factor in the VR1-VR-L heteromultimer.

VR1 was identified to interact with TRP3 and TRP6. Considering that these TRP channels can be activated by diacylglycerol (Hofmann *et al.*, 1999), it would be challenging to examine whether VR-TRP heteromultimers can be activated by this second messenger. Since diacylglycerol is generated following the activation of G protein coupled receptors such as the bradykinin receptor, whose ligand is released during inflammation and sensitises nociceptors (reviewed by Perl, 1996), a VR-TRP channel could play a role in the transduction of pain related information. TRP4 was found to be predominantly expressed in the capsaicin-sensitive DRG population (figure 3.2C), making it a good candidate for interacting with VR1. Although it was not possible to carry out co-immunoprecipitations for VR1 and TRP4, a functional interaction between the two channels is worth investigating. Clues that point towards an interplay between the two receptors include the regulation of VR1 activity by NGF (Shu and Mendell, 1999, Chuang *et al.*, 2001) and the TRP4 activation following stimulation of trk receptors (Schaefer *et al.*, 2000). Similarly, VR-L was found to interact with TRP3. Since the latter can be activated by BDNF via PLC stimulation (Li *et al.*, 1999), it would be interesting to examine whether the VR-L-TRP3 heteromultimer is indirectly activated by BDNF or other neurotrophins. The possibility that the VR-TRP interactions represent an elegant way to introduce functional complexity in the process of nociception without generating new proteins remains to be examined.

Concluding remarks

In this thesis the cloning of a member of the vanilloid family of receptors using bioinformatics tools is described. The novel receptor was cloned from Jurkat cells, a human leukemic T lymphocyte cell line and was named Vanilloid Receptor-like Protein (VR-L). VR-L shares the same topological structure with VR1 and TRP channels and exhibits 49% identity with the rat capsaicin receptor. The VR-L transcript was identified in a wide range of tissues, differentiating it from the specifically expressed VR1. Semi-quantitative RT-PCR analysis showed VR-L to be expressed in the capsaicin-insensitive DRG population and its transcript levels to be regulated by NGF *in vivo* and *in vitro*. Electrophysiological and fluorometric studies showed that unlike VR1, capsaicin, heat and protons do not activate VR-L. Immunocytochemistry studies using a tagged VR-L construct showed the protein to be expressed on the cell membrane, indicating that VR-L is transported to the plasma membrane successfully.

Although VR-L is the most closely related member of the TRP superfamily to the capsaicin receptor, it does not behave as a vanilloid receptor. Failing to identify its functional role, we considered the possibility that VR-L plays an indirect role by regulating the activity of VR1 or other TRP channels. This hypothesis was based on the following facts: 1) TRP channels form heteromultimers generating novel channels, 2) VR.5'sv, an N-terminal splice variant of VR1 and a VR1 pore mutant interact with the capsaicin receptor and repress its activity and 3) the pharmacological profile of VR1 cannot account for all the vanilloid responses observed *in vivo*, indicating that there are more vanilloid receptors to be cloned. Initially, the expression of TRP channels in DRG neurons was examined using RT-PCR. Capsaicin treatment showed that with the exception of TRP4, TRP1, TRP3, TRP5 and TRP6 are predominantly expressed in the capsaicin-insensitive neurons. Therefore, TRP channels exist in DRG and hence there is the possibility of VR-TRP interactions. In order to investigate possible interactions, epitope tagged version of VR and TRP genes were generated. These constructs were used in co-immunoprecipitation studies, which showed VR1 and VR-L to form homomultimers and also heteromultimers with each other. Additionally, there is the indication that VR-L interacts with TRP3 and VR1 with TRP3 and TRP6. A VR-L stable cell line was generated to study the functional importance of the interactions identified.

Considering the following facts, a possible role of VR-L in inflammation was proposed: 1) VR-L is expressed in tissues of the immune and the nervous system, 2) VR-L mRNA levels are regulated by NGF, 3) VR-L can interact with VR1, a receptor involved in the transduction of nociceptive information and 4) during nerve injury *de novo* VR1 expression is identified in large diameter neurons, where VR-L is normally expressed. Although heterologous expression studies showed VR-L not to directly respond to noxious stimuli, the conclusion of this thesis is that VR-L could play a role in pain perception, particularly during inflammation.

CHAPTER 1

In silico cloning of VR-L, a new member of the vanilloid receptor family

APPENDIX

Appendix 1.1: tblastn search results, as in 21 February 1998,using the VR1 amino acid sequence as a query. Only the entries with P up to 10^{-5} are shown.

Sequences producing High-scoring Segment pairs:		Reading frame	High Score	Probability P(N)	N
gb|W44731.1|W44731	zb98d02.s1 Soares_parathyroid_tumor_NbHP..+2		216	2.5e-51	3
gb|AA476107.1|AA476107	vh17b08.r1 Soares_mammary_gland_NbMM.....+1		239	7.1e-47	3
gb|W38665.1|W38665	zb98d02.r1 Soares_parathyroid_tumor_NbHP..-1		162	1.6e-40	4
gb|AA139413.1|AA139413	mq35a11.r1 Barstead MPLRB1 Mus muscu.....+1		303	2.4e-38	2
gb|AA304033.1|AA304033	EST16729 Aorta endothelial cells, TN.....+1		202	2.6e-34	2
gb|W82502.1|W82502	mf04g06.r1 Soares mouse p3NMF19.5 Mus mu..+2		222	3.4e-32	3
gb|N23395|N23395	yx83e12.s1 Homo sapiens cDNA clo.....+3		127	1.2e-31	5
gb|AA281349.1|AA281349	zs94g12.s1 NCI_CGAP_GCB1 Homo sapien.....+3		283	6.7e-31	1
gb|AA236416.1|AA236416	zr54h04.r1 Soares_NhHMPu_S1 Homo sap.....+1		259	4.0e-30	2
gb|W92895|W92895	zh80h02.r1 Soares fetal liver sp.....+1		122	4.8e-28	3
gb|AA741232.1|AA741232	ny96a11.s1 NCI_CGAP_GCB1 Homo sapien.....-2		231	1.9e-25	2
gb|H20025.1|H20025	yn55e02.s1 Soares adult brain N2b5HB55Y ..-1		231	2.2e-25	2
gb|AA461295.1|AA461295	zx65a01.s1 Soares_total_fetus_Nb2HF8.....-3		231	2.3e-25	2
gb|AA357145.1|AA357145	EST65829 Jurkat T-cells III Homo sap.....+2		152	1.4e-24	3
gb|AA321554.1|AA321554	EST24046 CCRF-CEM cells, cyclohexami.....+2		233	6.0e-24	1
gb|H51393|H51393	yo30f10.s1 Homo sapiens cDNA clo.....-3		198	2.5e-22	2
gb|AA768829|AA768829	nz64g08.s1 NCI_CGAP_GCB1 Homo sa.....-3		203	1.5e-21	2
gb|AA236417|AA236417	zr54h04.s1 Soares NhHMPu S1 Homo.....-3		203	1.8e-21	2
gb|T12251.1|T12251	A468F Heart Homo sapiens cDNA clone A468..+3		211	1.1e-20	1
gb|N26729|N26729	yx62c11.s1 Homo sapiens cDNA clo.....-3		204	5.9e-20	1
gb|H50364|H50364	yo29h05.s1 Homo sapiens cDNA clo.....-3		198	4.0e-19	1
gb|W53556|W53556	md55c08.r1 Soares mouse embryo N.....+3		188	9.2e-18	1
gb|H21490|H21490	yn76c11.s1 Homo sapiens cDNA clo.....-2		185	2.7e-17	1
gb|H49060|H49060	yo21f05.s1 Homo sapiens cDNA clo.....-1		152	5.6e-15	2
gb|N21167|N21167	yx47e06.s1 Homo sapiens cDNA clo.....-1		112	9.5e-15	2
gb|N35179|N35179	yx83e12.r1 Homo sapiens cDNA clo.....-1		139	1.6e-13	2
gb|AA015295|AA015295	mh14e11.r1 Soares mouse placenta.....+1		156	3.7e-13	1
gb|H27879|H27879	yn79h03.s1 Homo sapiens cDNA clo.....-2		124	4.4e-12	2
gb|AA281348|AA281348	zs94g12.r1 NCI_CGAP_GCB1 Homo sa.....-2		144	3.4e-10	1
gb|AA274980|AA274980	va94f07.r1 Soares mouse 3NME12 5.....+2		132	4.5e-09	1
gb|AA078617|AA078617	7PO7E06 Chromosome 7 placental c.....+2		80	3.1e-07	2
gb|N24224|N24224	yx21g11.r1 Homo sapiens cDNA clo.....+1		121	3.2e-07	1
gb|AA144832|AA144832	mr69d04.r1 Stratagene mouse test.....+1		64	2.9e-05	2
dbj|C45219|C45219	C.elegans cDNA clone yk390d4 : 5.....+3		65	0.0016	3

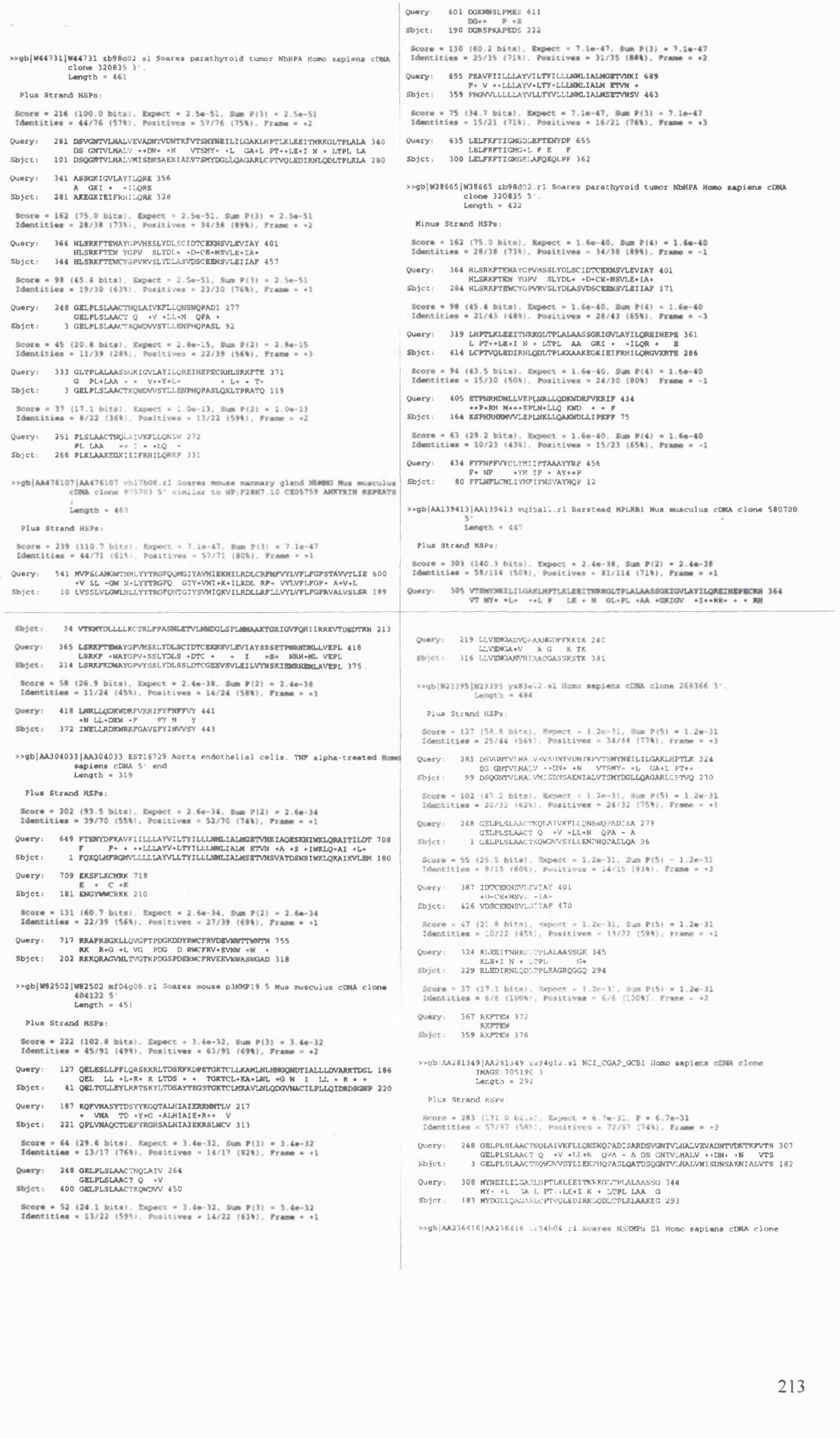

>gb|W44731|W44731 zb98d02.s1 Soares parathyroid tumor NbHPA Homo sapiens cDNA clone 320835 3'.
Length = 461

Plus Strand HSPs:

Score = 216 (100.0 bits), Expect = 2.5e-51, Sum P(3) = 2.5e-51
Identities = 44/76 (57%), Positives = 57/76 (75%), Frame = +2

Query: 281 DSVGNTVLHALVEVADNTVDNTKFVTSMYNEILILGAKLHPTLKLEEITNRKGLTPLALA 340
DS GNTVLHALV ++DN+ +N VTSMY+ +L GA+L PT++LE+I N + LTPL LA
Sbjct: 101 DSQGNTVLHALVMISDNSAENIALVTSMYDGLLQAGARLCPTVQLEDIRNLQDLTPLKLA 280

Query: 341 ASSGKIGVLAYILQREIHEPECRHLSRKFTE 371
A GKI + +ILQRE
Sbjct: 281 AKEGKIEIFRHILQREP 328

Score = 162 (75.0 bits), Expect = 2.5e-51, Sum P(3) = 2.5e-51
Identities = 28/38 (73%), Positives = 34/38 (89%), Frame = +2

Query: 364 HLSRKFTEWAYGPVHSSLYDLSCIDTCEKNSVLEVIAY 401
HLSRKFTEW YGPV SLYDL+ +D+CE+NSVLE+IA+
Sbjct: 344 HLSRKFTEWCYGPVRVSLYDLASVDSCEENSVLEIIAF 457

Score = 98 (45.4 bits), Expect = 2.5e-51, Sum P(3) = 2.5e-51
Identities = 19/30 (63%), Positives = 23/30 (76%), Frame = +3

Query: 248 GELPLSLAACTNQLAIVKFLLQNSWQPADI 277
GELPLSLAACT Q +V +LL+N QPA +
Sbjct: 3 GELPLSLAACTKQWDVVSYLLENPHQPASL 92

Score = 45 (20.8 bits), Expect = 2.8e-15, Sum P(2) = 2.8e-15
Identities = 11/39 (28%), Positives = 22/39 (56%), Frame = +3

Query: 333 GLTPLALAASSGKIGVLAYILQREIHEPECRHLSRKFTE 371
G PL+LAA + + V++Y+L+ + L+ + T+
Sbjct: 3 GELPLSLAACTKQWDVVSYLLENPHQPASLQXLTPRATQ 119

Score = 37 (17.1 bits), Expect = 1.0e-13, Sum P(2) = 1.0e-13
Identities = 8/22 (36%), Positives = 13/22 (59%), Frame = +2

Query: 251 PLSLAACTNQLAIVKFLLQNSW 272
PL LAA ++ I + +LQ +
Sbjct: 266 PLKLAAKEGKIEIFRHILQREP 331

>gb|AA476107|AA476107 vh17b08.r1 Soares mouse mammary gland NbMMG Mus musculus cDNA clone 875703 5' similar to WP:F28H7.10 CE05759 ANKYRIN REPEATS ;
Length = 463

Plus Strand HSPs:

Score = 239 (110.7 bits), Expect = 7.1e-47, Sum P(3) = 7.1e-47
Identities = 44/71 (61%), Positives = 57/71 (80%), Frame = +1

Query: 541 MVPSLAMGWTNMLYYTRGFQQMGIYAVMIEKMILRDLCRFMFVYLVFLFGFSTAVVTLIE 600
+V SL +GW N+LYYTRGFQ GIY+VMI+K+ILRDL RF+ VYLVFLFGF+ A+V+L
Sbjct: 10 LVSSLVLGWLNLLYYTRGFQHTGIYSVMIQKVILRDLLRFLLVYLVFLPGFAVALVSLSR 189

Query: 601 DGKNNSLPMES 611
DG++ P +S
Sbjct: 190 DGRSPKAPEDS 222

Score = 130 (60.2 bits), Expect = 7.1e-47, Sum P(3) = 7.1e-47
Identities = 25/35 (71%), Positives = 31/35 (88%), Frame = +2

Query: 655 FKAVFIILLLAYVILTYILLLNMLIALMGETVNKI 689
F+ V ++LLLAYV+LTY+LLLNMLIALM ETVN +
Sbjct: 359 FRGVVLLLLLAYVLLTYVLLLNMLIALMSETVNSV 463

Score = 75 (34.7 bits), Expect = 7.1e-47, Sum P(3) = 7.1e-47
Identities = 15/21 (71%), Positives = 16/21 (76%), Frame = +3

Query: 635 LELFKFTIGMGDLEFTENYDF 655
LELFKFTIGMG+L F E F
Sbjct: 300 LELFKFTIGMGELAPQEQLPF 362

>gb|W38665|W38665 zb98d02.r1 Soares parathyroid tumor NbHPA Homo sapiens cDNA clone 320835 5'.
Length = 422

Minus Strand HSPs:

Score = 162 (75.0 bits), Expect = 1.6e-40, Sum P(4) = 1.6e-40
Identities = 28/38 (73%), Positives = 34/38 (89%), Frame = -1

Query: 364 HLSRKFTEWAYGPVHSSLYDLSCIDTCEKNSVLEVIAY 401
HLSRKFTEW YGPV SLYDL+ +D+CE+NSVLE+IA+
Sbjct: 284 HLSRKFTEWCYGPVRVSLYDLASVDSCEENSVLEIIAF 171

Score = 98 (45.4 bits), Expect = 1.6e-40, Sum P(4) = 1.6e-40
Identities = 21/43 (48%), Positives = 28/43 (65%), Frame = -3

Query: 319 LHPTLKLEEITNRKGLTPLALAASSGKIGVLAYILQREIHEPE 361
L PT++LE+I N + LTPL AA GKI + +ILQR + E
Sbjct: 414 LCPTVQLEDIRNLQDLTPLKXAAKEGKIEIFRHILQRGVXRTE 286

Score = 94 (43.5 bits), Expect = 1.6e-40, Sum P(4) = 1.6e-40
Identities = 15/30 (50%), Positives = 24/30 (80%) Frame = -1

Query: 405 ETPNRMDMLLVEPLNRLLQDMWDRFVKRIF 434
++P+RH M+++EPLN+LLQ KWD + + F
Sbjct: 164 KSPHRHRMVVLEPLNKLLQAAWDLLIPKFF 75

Score = 63 (29.2 bits), Expect = 1.6e-40, Sum P(4) = 1.6e-40
Identities = 10/23 (43%), Positives = 15/23 (65%), Frame = -1

Query: 434 FYFNFFVYCLYMIIPTAAAYYRP 456
F+ NF +YM IP + AY++P
Sbjct: 80 FFLNFLCNLIYMFIPNSVAYHQP 12

>gb|AA139413|AA139413 mq35a11.r1 Barstead MPLRB1 Mus musculus cDNA clone 580700 5'
Length = 447

Plus Strand HSPs:

Score = 303 (140.3 bits), Expect = 2.4e-38, Sum P(2) = 2.4e-38
Identities = 58/114 (50%), Positives = 81/114 (71%), Frame = +1

Query: 305 VTSMYNEILILGAKLHPTLKLEEITNRKGLTPLALAASSGKIGVLAYILQREIHEPECRH 364
VT MY+ +L+ ++L P LE + N GL+PL +AA +GKIGV +I++RE+ + + RH

Sbjct: 34 VTKMYDLLLLKCSRLFPASNLETVLMNDGLSPLMMAAKTGKIGVFQHIIRREVTDEDTRH 213

Query: 365 LSRKFTEWAYGPVHSSLYDLSCIDTCEKNSVLEVIAYSSSETPNRMDMLLVEPL 418
LSRKF +WAYGPV+SSLYDLS +DTC + + I +S+ NRH+ML VEPL
Sbjct: 214 LSRKFKDWAYGPVYSSLYDLSSLDTCGEEVSVLEILVYMSKIEMRHEMLAVEPL 375

Score = 58 (26.9 bits), Expect = 2.4e-38, Sum P(2) = 2.4e-38
Identities = 11/24 (45%), Positives = 14/24 (58%), Frame = +3

Query: 418 LWRLLQDKWDRFVKRIFYFNFFVY 441
+N LL+DKW +F FY N Y
Sbjct: 372 IWELLRDKWRKFGAVSFYINVVSY 443

>gb|AA304033|AA304033 EST16729 Aorta endothelial cells, TNF alpha-treated Homo sapiens cDNA 5' end
Length = 319

Plus Strand HSPs:

Score = 202 (93.5 bits), Expect = 2.6e-34, Sum P(2) = 2.6e-34
Identities = 39/70 (55%), Positives = 52/70 (74%), Frame = +1

Query: 649 FTENYDFKAVFIILLLAYVILTYILLLNMLIALMGETVNKIAQESKQNIWKLQRAITILDT 708
F F+ + ++LLLAYV+LTYILLLNMLIALM ETVN +A +S +IWKLQ+AI +L+
Sbjct: 1 FQXQLNFRGMVLLLLLAYVLLTYILLLNMLIALMSETVNSVATDSWSIWKLQKAIKVLEM 180

Query: 709 EKSFLKCMRK 718
E + C +K
Sbjct: 181 ENGYWWCRKK 210

Score = 131 (60.7 bits), Expect = 2.6e-34, Sum P(2) = 2.6e-34
Identities = 22/39 (56%), Positives = 27/39 (69%), Frame = +1

Query: 717 RKAFRSGKLLQVGFTPDGKDDYRWCFRVDEVWWTTWNTN 755
RK R+G +L VG PDG D RWCFRV+EVNW +W +
Sbjct: 202 RKKQRAGVMLTVGTKPDGSPDERWCFRVEEVNWASWGAD 318

>gb|W82502|W82502 mf04g06.r1 Soares mouse p1NMF19.5 Mus musculus cDNA clone 404122 5'
Length = 451

Plus Strand HSPs:

Score = 222 (102.8 bits), Expect = 3.4e-32, Sum P(3) = 3.4e-32
Identities = 45/91 (49%), Positives = 63/91 (69%), Frame = +2

Query: 127 QELESLLPFLQRSKKRLTDSRFKDPETGKTCLLKAMLNLHNGQNDTIALLLDVARKTDSL 186
QEL LL +L+R+ K LTDS + + TGKTCL+KA+LNL +G N I LL + R + +
Sbjct: 41 QELTGLLEYLRRTSKYLTDSAYTEGSTGKTCLMKAVLNLQDGVNACILPLLQIDRDSGMP 220

Query: 187 KQFVMASYTDSYYKGQTALHIAIERRMNTLV 217
+ VMA TD +Y+G +ALHIAIE+R+ V
Sbjct: 221 QPLVNAQCTDEFYRGHSALHIAIEKRSLMCV 313

Score = 64 (29.6 bits), Expect = 3.4e-32, Sum P(3) = 3.4e-32
Identities = 13/17 (76%), Positives = 14/17 (82%), Frame = +1

Query: 248 GELPLSLAACTNQLAIV 264
GELPLSLAACT Q +V
Sbjct: 400 GELPLSLAACTKQWDVV 450

Score = 52 (24.1 bits), Expect = 3.4e-32, Sum P(3) = 3.4e-32
Identities = 13/22 (59%), Positives = 14/22 (63%), Frame = +1

Query: 219 LLVENGADVQAAANGDFFKKTK 240
LLVENGA+V A G K TK
Sbjct: 316 LLVENGANVHIRACGASSKSTK 381

>gb|N23395|N23395 yx83e12.s1 Homo sapiens cDNA clone 268366 3'.
Length = 484

Plus Strand HSPs:

Score = 127 (58.8 bits), Expect = 1.2e-31, Sum P(5) = 1.2e-31
Identities = 25/44 (56%), Positives = 34/44 (77%), Frame = +3

Query: 281 DSVGNTVLHALVEVADNTVDNTKFVTSMYNEILILGAKLHPTLK 324
DS GNTVLHALV ++DN+ +N VTSMY+ +L GA+L PT++
Sbjct: 99 DSQGNTVLHALVMISDNSAENIALVTSMYDGLLQAGARLCPTVQ 230

Score = 102 (47.2 bits), Expect = 1.2e-31, Sum P(5) = 1.2e-31
Identities = 20/32 (62%), Positives = 24/32 (75%), Frame = +1

Query: 248 GELPLSLAACTNQLAIVKFLLQNSWQPADISA 279
GELPLSLAACT Q +V +LL+N QPA + A
Sbjct: 1 GELPLSLAACTKQWDVVSYLLENPHQPASLQA 96

Score = 55 (25.5 bits), Expect = 1.2e-31, Sum P(5) = 1.2e-31
Identities = 9/15 (60%), Positives = 14/15 (93%), Frame = +3

Query: 387 IDVCEKNSVLEVIAY 401
+D+CE+NSVL +IA+
Sbjct: 426 VDSCEENSVLEIIAF 470

Score = 47 (21.8 bits), Expect = 1.2e-31, Sum P(5) = 1.2e-31
Identities = 10/22 (45%), Positives = 13/22 (59%), Frame = +1

Query: 324 KLREITNRKGLTPLALAASSGK 345
KLE+I N + LTPL G+
Sbjct: 229 KLEDIRNLQDLTPLKAGRQGGQ 294

Score = 37 (17.1 bits), Expect = 1.2e-31, Sum P(5) = 1.2e-31
Identities = 6/6 (100%), Positives = 6/6 (100%), Frame = +2

Query: 367 RKFTEW 372
RKFTEW
Sbjct: 359 RKFTEW 376

>gb|AA281349|AA281349 xa94g12.s1 NCI_CGAP_GCB1 Homo sapiens cDNA clone IMAGE:705190 3
Length = 294

Plus Strand HSPs:

Score = 283 (131.0 bits), Expect = 6.7e-31, P = 6.7e-31
Identities = 57/97 (58%), Positives = 72/97 (74%), Frame = +3

Query: 248 GELPLSLAACTNQLAIVKFLLQNSWQPADISARDSVGNTVLHALVEVADNTVDKTKFVTS 307
GELPLSLAACT Q +V +LL+N QPA + A DS GNTVLHALV ++DN+ +N VTS
Sbjct: 3 GELPLSLAACTKQWDVVSYLLENPHQPASLQATDSQGNTVLHALVMISDNSAENIALVTS 182

Query: 308 MYNEILILGAKLHPTLKLEEITNRKGLTPLALAASSG 344
MY+ +L GA+L PT++LE+I K + LTPL LAA G
Sbjct: 183 MYDGLLQAGARLCPTVQLEDIRNLQDLTPLKLAAKEG 293

>gb|AA236416|AA236416 zc54h04.r1 Soares NbHMPu S1 Homo sapiens cDNA clone

667255 5'
Length = 431

Plus Strand HSPs:

Score = 259 (119.9 bits), Expect = 4.0e-30, Sum P(2) = 4.0e-30
Identities = 53/105 (50%), Positives = 73/105 (69%), Frame = +1

Query: 127 QKLESLLPFLQRSKKRLTDSEFKDPETGKTCLLKAMLNLHNGQNDTIALLLDVARKTDSL 186
++L L +L ++ K LTDSE+ + TGKTCL+KA+LNL +G N I LL + R + +
Sbjct: 115 EDLAGLPEYLSKTSKYLTDSEYTEGSTGKTCLMKAVLNLKDGVNACILPLLQIDRDGGNP 294

Query: 187 KQFVNASYTDSYYKGQTALHIAIERNNMTLVTLLVENGADVQAAA 231
+ VNA TD YY+G +ALHIAIE+R+~ V LLVENGA+V A A
Sbjct: 295 QPLVNAQCTDDYYRGHSALHIAIEKRSLQCVKLLVENGANVHARA 429

Score = 43 (19.9 bits), Expect = 4.0e-30, Sum P(2) = 4.0e-30
Identities = 8/29 (27%), Positives = 15/29 (51%), Frame = +2

Query: 95 RPSSQDSVSAGEKPPRLYDRRSIFDAVAQ 123
+P A + P +DR +F+AV++
Sbjct: 20 QPQLPKGTGASQPDPNRFDRDRLFNAVSR 106

>>gb|W92895|W92895 zh80h02.r1 Soares fetal liver spleen 1NFLS 81 Homo sapiens cDNA clone 418419 5'
Length = 432

Plus Strand HSPs:

Score = 122 (56.5 bits), Expect = 4.8e-28, Sum P(3) = 4.8e-28
Identities = 21/35 (60%), Positives = 28/35 (80%), Frame = +1

Query: 537 YVASMVPSLAMGWFNMLYYTRGFQQMGIYAVMIEK 571
Y+ +V +L +GW N+LYYTRGFQ GIY+VMI+K
Sbjct: 22 YLPLLVSALVLGWLNLLYYTRGFQHTGIYSVMIQK 126

Score = 97 (44.9 bits), Expect = 4.8e-28, Sum P(3) = 4.8e-28
Identities = 20/23 (86%), Positives = 23/23 (100%), Frame = +3

Query: 660 IILLLAYVILTYILLLNMLIALM 682
++LLLAYV+LTYILLLNMLIALM
Sbjct: 339 LLLLLAYVLLTYILLLNMLIALM 407

Score = 89 (41.2 bits), Expect = 4.8e-28, Sum P(3) = 4.8e-28
Identities = 17/35 (48%), Positives = 21/35 (60%), Frame = +2

Query: 624 GWSYNSLYSTCLELPKFTIGMGDLEFTENYDFKAV 658
G Y + LELPKFTIGMG+L F E F+ +
Sbjct: 230 GAQYRGILEASLELPKFTIGMGELAFQEQLHFRGM 334

>>gb|AA741232|AA741232 ny96a11.s1 NCI_CGAP_GCB1 Homo sapiens cDNA clone IMAGE:1286108 similar to contains Alu repetitive element; Length = 454

Minus Strand HSPs:

Score = 231 (107.0 bits), Expect = 1.9e-25, Sum P(2) = 1.9e-25
Identities = 47/106 (44%), Positives = 69/106 (65%), Frame = -2

Query: 104 AGEKPPRLYDRRSIFDAVAQSNCQELESLLPFLQRSKKRLTDSEFKDPETGKTCLLKAML 163
A + P +DR +F+AV++ ++L L +L ++ K LTDSE+ + TGKTCL+KA+L
Sbjct: 318 ASQPDPNRFDRDRLFNAVSRGVPEDLAGLPEYLSKTSKYLTDSEYTEGSTGKTCLMKAVL 139

Query: 164 NLHNGQNDTIALLLDVARKTDSLKQFVNASYTDSYYKGQTALHIAI 209
NL +G N I LL + R + + VNA TD YY+G +ALHIAI
Sbjct: 138 NLKDGVNACILPLLQIDRDSGNPQPLVNAQCTDDYYRGHSALHIAI 1

Score = 37 (17.1 bits), Expect = 1.9e-25, Sum P(2) = 1.9e-25
Identities = 9/23 (39%), Positives = 9/23 (39%), Frame = -1

Query: 86 RPGDGPASVRPSSQDSVSAGEKP 108
RP D P SAG KP
Sbjct: 364 RPSDKSQPQLPKGNRCQSAGSKP 296

>>gb|H20025|H20025 yn55e02.s1 Homo sapiens cDNA clone 172346 3' similar to contains Alu repetitive element;; Length = 408

Minus Strand HSPs:

Score = 231 (107.0 bits), Expect = 2.2e-25, Sum P(2) = 2.2e-25
Identities = 47/106 (44%), Positives = 69/106 (65%), Frame = -1

Query: 104 AGEKPPRLYDRRSIFDAVAQSNCQELESLLPFLQRSKKRLTDSEFKDPETGKTCLLKAML 163
A + P +DR +F+AV++ ++L L +L ++ K LTDSE+ + TGKTCL+KA+L
Sbjct: 318 ASQPDPNRFDRDRLFNAVSRGVPEDLAGLPEYLSKTSKYLTDSEYTEGSTGKTCLMKAVL 139

Query: 164 NLHNGQNDTIALLLDVARKTDSLKQFVNASYTDSYYKGQTALHIAI 209
NL +G N I LL + R + + VNA TD YY+G +ALHIAI
Sbjct: 138 NLKDGVNACILPLLQIDRDSGNPQPLVNAQCTDDYYRGHSALHIAI 1

Score = 37 (17.1 bits), Expect = 2.2e-25, Sum P(2) = 2.2e-25
Identities = 9/23 (39%), Positives = 9/23 (39%), Frame = -3

Query: 86 RPGDGPASVRPSSQDSVSAGEKP 108
RP D P SAG KP
Sbjct: 364 RPSDKSQPQLPKGNRCQSAGSKP 296

>>gb|AA461295|AA461295 zx65a01.s1 Soares total fetus Nb2HF8 9w Homo sapiens cDNA clone 796296 3' similar to contains Alu repetitive element; Length = 383

Minus Strand HSPs:

Score = 231 (107.0 bits), Expect = 2.3e-25, Sum P(2) = 2.3e-25
Identities = 47/106 (44%), Positives = 69/106 (65%), Frame = -3

Query: 104 AGEKPPRLYDRRSIFDAVAQSNCQELRSLLPFLQRSKKRLTDSEFKDPETGKTCLLKAML 163
A + P +DR +F+AV++ ++L L +L ++ K LTDSE+ + TGKTCL+KA+L
Sbjct: 318 ASQPDPNRFDRDRLFNAVSRGVPEDLAGLPEYLSKTSKYLTDSEYTEGSTGKTCLMKAVL 139

Query: 164 NLHNGQNDTIALLLDVARKTDSLKQFVNASYTDSYYKGQTALHIAI 209
NL +G N I LL + R + + VNA TD YY+G +ALHIAI
Sbjct: 138 NLKDGVNACILPLLQIDRDSGNPQPLVNAQCTDDYYRGHSALHIAI 1

Score = 37 (17.1 bits), Expect = 2.3e-25, Sum P(2) = 2.3e-25
Identities = 9/23 (39%), Positives = 9/23 (39%), Frame = -2

Query: 86 RPGDGPASVRPSSQDSVSAGEKP 108
RP D P SAG KP
Sbjct: 364 RPSDKSQPQLPKGNRCQSAGSKP 296

>>gb|AA357145|AA357145 EST65829 Jurkat T-cells III Homo sapiens cDNA 5' end
Length = 299

Plus Strand HSPs:

Score = 152 (70.4 bits), Expect = 1.4e-24, Sum P(3) = 1.4e-24
Identities = 27/38 (71%), Positives = 32/38 (84%), Frame = +2

Query: 364 HLSRKPTEWAYGPVRSSLYDLSCIDTCEKNSVLEVIAY 401
HLSRKPTEW YGPV SLYDL+ D+C +NSVLE+IA+
Sbjct: 14 HLSRKPTEWCYGPVRVSLYDLASKDSCKENSVLEIIAF 127

Score = 66 (30.6 bits), Expect = 1.4e-24, Sum P(3) = 1.4e-24
Identities = 11/19 (57%), Positives = 18/19 (94%), Frame = +2

Query: 405 ETPNRHDMLLVSPLNRLLQ 423
++P+RH M+++EPLN+LLQ
Sbjct: 134 KSPHRHRMVVLKPLNKLLQ 190

Score = 66 (30.6 bits), Expect = 1.4e-24, Sum P(3) = 1.4e-24
Identities = 11/23 (47%), Positives = 15/23 (65%), Frame = +3

Query: 434 FYFMFFVYCLYKIIFTAAAYYRP 456
F+ NF +YK IF A AY++P
Sbjct: 219 FFLNFLCNLIYKFIFNAVAYHQP 287

>>gb|AA321554|AA321554 EST24046 CCRF-CEM cells, cyclohexamide treated I Homo sapiens cDNA 5' end
Length = 323

Plus Strand HSPs:

Score = 233 (107.9 bits), Expect = 6.0e-24, P = 6.0e-24
Identities = 46/65 (70%), Positives = 52/65 (80%), Frame = +2

Query: 774 SFSLRSSRVSGRNWKNFALVPLLRDASTRDRRATQQEEVQLKHTTGSLKPEDAEVFKDSM 833
SFSLRS RVSGR+WKNFALVPLLR+AS R R + Q KEV L+ ++GSLKPEDAEVFK
Sbjct: 2 SFSLRSSRVSGRHWKNFALVPLLKEASKRDQRQSAQPEEVYLRQFSGSLKPEDAEVFKSPA 181

Query: 834 VPGEK 838
GEK
Sbjct: 182 ASGEK 196

>>gb|HS1393|HS1393 yo30f10.s1 Homo sapiens cDNA clone 179467 3' similar to contains Alu repetitive element;; Length = 401

Minus Strand HSPs:

Score = 198 (91.7 bits), Expect = 2.5e-22, Sum P(2) = 2.5e-22
Identities = 40/83 (48%), Positives = 56/83 (67%), Frame = -3

Query: 127 QELESLLPFLQRSKKRLTDSEFKDPETGKTCLLKAMLNLHNGQNDTIALLLDVARKTDSL 186
++L L +L ++ K LTDSE+ + TGKTCL+KA+LNL +G N I LL + R + +
Sbjct: 249 EDLAGLPEYLSKTSKYLTDSEYTEGSTGKTCLMKAVLNLKDGVNACILPLLQIDRDSGNP 70

Query: 187 KQFVNASYTDSYYKGQTALHIAI 209
+ VNA TD YY+G +ALHIAI
Sbjct: 69 QPLVNAQCTDDYYRGHSALHIAI 1

Score = 48 (22.2 bits), Expect = 2.5e-22, Sum P(2) = 2.5e-22
Identities = 9/21 (42%), Positives = 13/21 (61%), Frame = -2

Query: 87 PGDGPASVRPSSQDSVSAGRK 107
PG+GP + DS +S S E+
Sbjct: 391 PGEGPXNSXXSE*RSTSSTTER 329

Query: 164 NLHNGQNDTIALLLDVARKTDSLKQFVNASYTDSYYKGQTALHIAI 209
NL +G N I LL + R + + VNA TD YY+G +ALHIAI
Sbjct: 138 NLKDGVNACILPLLQIDRDSGNPQPLVNAQCTDDYYRGHSALHIAI 1

Score = 37 (17.1 bits), Expect = 1.9e-25, Sum P(2) = 1.9e-25
Identities = 9/23 (39%), Positives = 9/23 (39%), Frame = -1

Query: 86 RPGDGPASVRPSSQDSVSAGEKP 108
RP D P SAG KP
Sbjct: 364 RPSDKSQPQLPKGNRCQSAGSKP 296

>>gb|H20025|H20025 yn55e02.s1 Homo sapiens cDNA clone 172346 3' similar to contains Alu repetitive element;; Length = 408

Minus Strand HSPs:

Score = 231 (107.0 bits), Expect = 2.2e-25, Sum P(2) = 2.2e-25
Identities = 47/106 (44%), Positives = 69/106 (65%), Frame = -1

Query: 104 AGEKPPRLYDRRSIFDAVAQSNCQELESLLPFLQRSKKRLTDSEFKDPETGKTCLLKAML 163
A + P +DR +F+AV++ ++L L +L ++ K LTDSE+ + TGKTCL+KA+L
Sbjct: 318 ASQPDPNRFDRDRLFNAVSRGVPEDLAGLPEYLSKTSKYLTDSEYTEGSTGKTCLMKAVL 139

Query: 164 NLHNGQNDTIALLLDVARKTDSLKQFVNASYTDSYYKGQTALHIAI 209
NL +G N I LL + R + + VNA TD YY+G +ALHIAI
Sbjct: 138 NLKDGVNACILPLLQIDRDSGNPQPLVNAQCTDDYYRGHSALHIAI 1

Score = 37 (17.1 bits), Expect = 2.2e-25, Sum P(2) = 2.2e-25
Identities = 9/23 (39%), Positives = 9/23 (39%), Frame = -3

Query: 86 RPGDGPASVRPSSQDSVSAGEKP 108
RP D P SAG KP
Sbjct: 364 RPSDKSQPQLPKGNRCQSAGSKP 296

>>gb|AA461295|AA461295 zx65a01.s1 Soares total fetus Nb2HF8 9w Homo sapiens cDNA clone 796296 3' similar to contains Alu repetitive element; Length = 383

Minus Strand HSPs:

Score = 231 (107.0 bits), Expect = 2.3e-25, Sum P(2) = 2.3e-25
Identities = 47/106 (44%), Positives = 69/106 (65%), Frame = -3

Query: 104 AGEKPPRLYDRRSIFDAVAQSNCQELRSLLPFLQRSKKRLTDSEFKDPETGKTCLLKAML 163
A + P +DR +F+AV++ ++L L +L ++ K LTDSE+ + TGKTCL+KA+L
Sbjct: 318 ASQPDPNRFDRDRLFNAVSRGVPEDLAGLPEYLSKTSKYLTDSEYTEGSTGKTCLMKAVL 139

Query: 164 NLHNGQNDTIALLLDVARKTDSLKQFVNASYTDSYYKGQTALHIAI 209
NL +G N I LL + R + + VNA TD YY+G +ALHIAI
Sbjct: 138 NLKDGVNACILPLLQIDRDSGNPQPLVNAQCTDDYYRGHSALHIAI 1

Score = 37 (17.1 bits), Expect = 2.3e-25, Sum P(2) = 2.3e-25
Identities = 9/23 (39%), Positives = 9/23 (39%), Frame = -2

Query: 86 RPGDGPASVRPSSQDSVSAGEKP 108
RP D P SAG KP
Sbjct: 364 RPSDKSQPQLPKGNRCQSAGSKP 296

>>gb|AA357145|AA357145 EST65829 Jurkat T-cells III Homo sapiens cDNA 5' end
Length = 299

Plus Strand HSPs:

Score = 152 (70.4 bits), Expect = 1.4e-24, Sum P(3) = 1.4e-24
Identities = 27/38 (71%), Positives = 32/38 (84%), Frame = +2

Query: 364 HLSRKPTEWAYGPVRSSLYDLSCIDTCEKNSVLEVIAY 401
HLSRKPTEW YGPV SLYDL+ D+C +NSVLE+IA+
Sbjct: 14 HLSRKPTEWCYGPVRVSLYDLASKDSCKENSVLEIIAF 127

Score = 66 (30.6 bits), Expect = 1.4e-24, Sum P(3) = 1.4e-24
Identities = 11/19 (57%), Positives = 18/19 (94%), Frame = +2

Query: 405 ETPNRHDMLLVSPLNRLLQ 423
++P+RH M+++EPLN+LLQ
Sbjct: 134 KSPHRHRMVVLKPLNKLLQ 190

Score = 66 (30.6 bits), Expect = 1.4e-24, Sum P(3) = 1.4e-24
Identities = 11/23 (47%), Positives = 15/23 (65%), Frame = +3

Query: 434 FYFMFFVYCLYKIIFTAAAYYRP 456
F+ NF +YK IF A AY++P
Sbjct: 219 FFLNFLCNLIYKFIFNAVAYHQP 287

>>gb|AA321554|AA321554 EST24046 CCRF-CEM cells, cyclohexamide treated I Homo sapiens cDNA 5' end
Length = 323

Plus Strand HSPs:

Score = 233 (107.9 bits), Expect = 6.0e-24, P = 6.0e-24
Identities = 46/65 (70%), Positives = 52/65 (80%), Frame = +2

Query: 774 SFSLRSSRVSGRNWKNFALVPLLRDASTRDRRATQQEEVQLKHTTGSLKPEDAEVFKDSM 833
SFSLRS RVSGR+WKNFALVPLLR+AS R R + Q KEV L+ ++GSLKPEDAEVFK
Sbjct: 2 SFSLRSSRVSGRHWKNFALVPLLKEASKRDQRQSAQPEEVYLRQFSGSLKPEDAEVFKSPA 181

Query: 834 VPGEK 838
GEK
Sbjct: 182 ASGEK 196

>>gb|HS1393|HS1393 yo30f10.s1 Homo sapiens cDNA clone 179467 3' similar to contains Alu repetitive element;; Length = 401

Minus Strand HSPs:

Score = 198 (91.7 bits), Expect = 2.5e-22, Sum P(2) = 2.5e-22
Identities = 40/83 (48%), Positives = 56/83 (67%), Frame = -3

Query: 127 QELESLLPFLQRSKKRLTDSEFKDPETGKTCLLKAMLNLHNGQNDTIALLLDVARKTDSL 186
++L L +L ++ K LTDSE+ + TGKTCL+KA+LNL +G N I LL + R + +
Sbjct: 249 EDLAGLPEYLSKTSKYLTDSEYTEGSTGKTCLMKAVLNLKDGVNACILPLLQIDRDSGNP 70

Query: 187 KQFVNASYTDSYYKGQTALHIAI 209
+ VNA TD YY+G +ALHIAI
Sbjct: 69 QPLVNAQCTDDYYRGHSALHIAI 1

Score = 48 (22.2 bits), Expect = 2.5e-22, Sum P(2) = 2.5e-22
Identities = 9/21 (42%), Positives = 13/21 (61%), Frame = -2

Query: 87 PGDGPASVRPSSQDSVSAGRK 107
PG+GP + DS +S S E+
Sbjct: 391 PGEGPXNSXXSE*RSTSSTTER 329

>>gb|AA768829|AA768829 nz64g08.s1 NCI_CGAP_GCB1 Homo sapiens cDNA clone IMAGE:1300286 similar to contains Alu repetitive element; Length = 430

Minus Strand HSPs:

Score = 203 (94.0 bits), Expect = 1.6e-21, Sum P(2) = 1.6e-21
Identities = 41/100 (41%), Positives = 63/100 (63%), Frame = -3

Query: 104 AGEKPPRLYDRRSIFDAVAQSNCQELESLLPFLQRSKKRLTDSEFKDPETGKTCLLKAML 163
A + P +DR +F+AV++ ++L L +L ++ K LTDSE+ + TGKTCL+KA+L
Sbjct: 317 ASQPDPNRFDRDRLFNAVSRGVPEDLAGLPEYLSKTSKYLTDSEYTEGSTGKTCLMKAVL 138

Query: 164 NLHNGQNDTIALLLDVARKTDSLKQFVNASYTDSYYKGQT 203
NL +G N I LL + R + + VNA TD YY+G +
Sbjct: 137 NLKDGVNACILPLLQIDRDSGNPQPLVNAQCTDDYYRGHS 18

Score = 37 (17.1 bits), Expect = 1.5e-21, Sum P(2) = 1.5e-21
Identities = 9/23 (39%), Positives = 9/23 (39%), Frame = -2

Query: 86 RPGDGPASVRPSSQDSVSAGEKP 108
RP D P SAG KP
Sbjct: 363 RPSDKSQPQLPKGNRCQSAGSKP 295

>>gb|AA236417|AA236417 zr54h04.s1 Soares NhHMPu S1 Homo sapiens cDNA clone 667255 3'
Length = 370

Minus Strand HSPs:

Score = 203 (94.0 bits), Expect = 1.8e-21, Sum P(2) = 1.8e-21
Identities = 41/100 (41%), Positives = 63/100 (63%), Frame = -3

Query: 104 AGEKPPRLYDRRSIFDAVAQSNCQELESLLPFLQRSKKRLTDSEFKDPETGKTCLLKAML 163
A + P +DR +F+AV++ ++L L +L ++ K LTDSE+ + TGKTCL+KA+L
Sbjct: 317 ASQPDPNRFDRDRLFKAVSRGVPEDLAGLPEYLSKTSKYLTDSEYTEGSTGKTCLMKAVL 138

Query: 164 NLHNGQNDTIALLLDVARKTDSLKQFVNASYTDSYYKGQT 203
NL +G N I LL + R + + VNA TD YY+G +
Sbjct: 137 NLKDGVNACILPLLQIDRDSGNPQPLVNAQCTDDYYRGHS 18

Score = 37 (17.1 bits), Expect = 1.8e-21, Sum P(2) = 1.8e-21
Identities = 9/23 (39%), Positives = 9/23 (39%), Frame = -2

Query: 86 RPGDGPASVRPSSQDSVSAGEKP 108
RP D P SAG KP
Sbjct: 363 RPSDKSQPQLPKGNRCQSAGSKP 295

>>gb|T12251|T12251 A468F Homo sapiens cDNA clone A468.
Length = 220

Plus Strand HSPs:

Score = 211 (97.7 bits), Expect = 1.1e-20, P = 1.1e-20
Identities = 42/69 (60%), Positives = 51/69 (73%), Frame = +3

Query: 624 GWSYNSLYSTCLELPKFTIGMGDLEFTENYDFKAVPIILLLAYVILTYILLLNMLIALMD 683
G Y + LELPKFTIGMG+L F E F+ + ++LLLAYV+LTYILLLNMLIALM
Sbjct: 12 GAQYRGILVASLELPKFTIGMGELAFQEQLHFRGMVLLLLAYVLLTYILLLNMLIALMS 191

Query: 684 ETVNKIAQE 692
ETVN +A +

```
Sbjct:   192 ETVNSVATD 218


>>gb|W26729|W26729 yx62c11.s1 Homo sapiens cDNA clone 266324 3'.
            Length = 374

  Minus Strand HSPs:

 Score = 204 (94.5 bits), Expect = 5.9e-20, P = 5.9e-20
 Identities = 42/91 (46%), Positives = 61/91 (67%), Frame = -3

Query:   119 DAVAQSNCQELESLLPFLQRSKKRLTDSEFKDPETGKTCLLKAMLNLHNGQNDTIALLLD 178
             +AV++   ++L  L  +L ++ K LTDSE+ +  TGKTCL+KA+LNL +G N  I  LL
Sbjct:   273 MAVSRGVPEDLAGLPEYLSKTSKYLTDSEYTEGSTGKTCLMKAVLNLKDGVNAXILPLLQ 94

Query:   179 VARKTDSLKQFVNASYTDSYYKGQTALHIAI 209
             + R + + +  VNA  TD YY+G +ALHIAI
Sbjct:    93 IDRDSGNPQPLVNAQCTDDYYRGHSALHIAI 1


>>gb|H50364|H50364 yo29h05.s1 Homo sapiens cDNA clone 179385 3'.
            Length = 386

  Minus Strand HSPs:

 Score = 198 (91.7 bits), Expect = 4.0e-19, P = 4.0e-19
 Identities = 40/83 (48%), Positives = 56/83 (67%), Frame = -3

Query:   127 QELESLLPFLQRSKKRLTDSEFKDPETGKTCLLKAMLNLHNGQNDTIALLLDVARKTDSL 186
             ++L  L  +L ++ K LTDSE+ +  TGKTCL+KA+LNL +G N  I  LL + R + +
Sbjct:   249 EDLAGLPEYLSKTSKYLTDSEYTEGSTGKTCLMKAVLNLKDGVNACILPLLQIDRDSGNP 70

Query:   187 KQFVNASYTDSYYKGQTALHIAI 209
             +  VNA  TD YY+G +ALHIAI
Sbjct:    69 QPLVNAQCTDDYYRGHSALHIAI 1


>>gb|W53556|W53556 md55c08.r1 Soares mouse embryo NbME13.5 14.5 Mus musculus
            cDNA clone 372302 5'.
            Length = 416

  Plus Strand HSPs:

 Score = 188 (87.1 bits), Expect = 9.2e-18, P = 9.2e-18
 Identities = 35/64 (54%), Positives = 49/64 (76%), Frame = +3

Query:   110 RLYDRRSIPDAVAQSNCQELESLLPFLQRSKKRLTDSEFKDPETGKTCLLKAMLNLHNGQ 169
             +++R  +FD V++ +  +L+ LL FL   KKRLTD EF++P TGKTCL KA+LNL NG+
Sbjct:   222 KVFNRPILFDIVSRGSTADLDGLLSFLLTHKKRLTDSEFRRPSTGKTCLPKALLNLSNGR 401

Query:   170 NDTI 173
             NDTI
Sbjct:   402 NDTI 413


>>gb|H21490|H21490 ym76c11.s1 Homo sapiens cDNA clone 174356 3' similar to
            contains Alu repetitive element;.
            Length = 379

  Minus Strand HSPs:

 Score = 185 (85.7 bits), Expect = 2.7e-17, P = 2.7e-17
 Identities = 38/72 (52%), Positives = 49/72 (68%), Frame = -2

Query:   138 RSKKRLTDSEFKDPETGKTCLLKAMLNLHNGQNDTIALLLDVARKTDSLKQFVNASYTDS 197
```

```
Query:   687 WKIAQESKNIWKLQRAIT 704
             N +A +S +IWKLQ+AI+
Sbjct:   431 NXVATDSWSIWKLQRAIS 378


>>gb|AA015295|AA015295 nh14e11.r1 Soares mouse placenta 4NbMP13.5 14.5 Mus
            musculus cDNA clone 442508 5'
            Length = 310

  Plus Strand HSPs:

 Score = 156 (72.2 bits), Expect = 3.7e-13, P = 3.7e-13
 Identities = 27/55 (49%), Positives = 35/55 (63%), Frame = +1

Query:   709 EKSFLKCKRKAFRSGKLLQVGFTPDGKDDYRWCFRVDEVNWTTWNTNVGIINEDP 763
             E  +  C RK  R+G+LL+VG   DG  D RWCFRV+EVNW  W   +  ++EDP
Sbjct:     1 EMGYWWCRRKRHRAGRLLKVGTKGDGIPDERWCFRVEEVNWAAWEKTLPTLSEDP 165


>>gb|H27879|H27879 yn79h03.s1 Homo sapiens cDNA clone 174677 3' similar to
            contains Alu repetitive element;.
            Length = 354

  Minus Strand HSPs:

 Score = 124 (57.4 bits), Expect = 4.4e-12, Sum P(2) = 4.4e-12
 Identities = 25/51 (49%), Positives = 34/51 (66%), Frame = -2

Query:   153 TGKTCLLKAMLNLHNGQNDTIALLLDVARKTDSLKQFVNASYTDSYYKGQT 203
             TGKTCL+KA+LNL +G N  I  LL + R + +  VNA  TD YY+G +
Sbjct:   170 TGKTCLMKAVLNLKDGVNACILPLLQIDRDSGNPQPLVNAQCTDDYYRGHS 18

 Score = 48 (22.2 bits), Expect = 4.4e-12, Sum P(2) = 4.4e-12
 Identities = 9/24 (37%), Positives = 16/24 (66%), Frame = -1

Query:   127 QELESLLPFLQRSKKRLTDSEFKD 150
             ++L  L  +L ++ K LTDSE+ +
Sbjct:   249 EDLAGLPEYLSKTSKYLTDSEYTE 178


>>gb|AA281348|AA281348 zs94g12.r1 NCI_CGAP_GCB1 Homo sapiens cDNA clone
            IMAGE:705190 5'
            Length = 424

  Minus Strand HSPs:

 Score = 144 (66.7 bits), Expect = 3.4e-10, P = 3.4e-10
 Identities = 25/47 (53%), Positives = 31/47 (65%), Frame = -2

Query:   717 RKAFRSGKLLQVGFTPDGKDDYRWCFRVDEVNWTTWNTNVGIINEDP 763
             RK  R+G +L VG   PDG  D RWCFRV+EVNW +W   +  + EDP
Sbjct:   381 RKKQRAGVXLTVGTKPDGSPDERWCFRVEEVNWASWEQTLPTLCEDP 241


>>gb|AA274980|AA274980 va94f07.r1 Soares mouse 3NME12 5 Mus musculus cDNA clone
            747109 5'
            Length = 334

  Plus Strand HSPs:

 Score = 132 (61.1 bits), Expect = 4.5e-09, P = 4.5e-09
 Identities = 22/42 (52%), Positives = 29/42 (69%), Frame = +2

Query:   722 SGKLLQVGFTPDGKDDYRWCFRVDEVNWTTWNTNVGIINEDP 763
             +G+LL+VG   DG  D RWCFRV+EVNW  W   +  ++EDP
```

```
             R  K LTDSE+ +  TGKTCL+KA+LNL +G N  I  LL + R + +  VNA  TD
Sbjct:   216 RPSKYLTDSEYTEGSTGKTCLMKAVLNLKDGVNACILPLLQIDRDSGNPQPLVNAQCTDD 37

Query:   198 YYKGQTALHIAI 209
             YY+G +ALHIAI
Sbjct:    36 YYRGHSALHIAI 1


>>gb|H49060|H49060 yo21f05.s1 Homo sapiens cDNA clone 178593 3' similar to
            contains Alu repetitive element;.
            Length = 357

  Minus Strand HSPs:

 Score = 152 (70.4 bits), Expect = 5.6e-15, Sum P(2) = 5.6e-15
 Identities = 31/57 (54%), Positives = 40/57 (70%), Frame = -1

Query:   153 TGKTCLLKAMLNLHNGQNDTIALLLDVARKTDSLKQFVNASYTDSYYKGQTALHIAI 209
             TGKTCL+KA+LNL +G N  I  LL + R + +  VNA  TD YY+G +ALHIAI
Sbjct:   171 TGKTCLMKAVLNLKDGVNACILPLLQIDRDSGNPQPLVNAQCTDDYYRGHSALHIAI 1

 Score = 41 (19.0 bits), Expect = 5.7e-15, Sum P(2) = 5.7e-15
 Identities = 7/16 (43%), Positives = 12/16 (75%), Frame = -3

Query:   135 PLQRSKKRLTDSEFKD 150
             +L ++ K LTDSE+ +
Sbjct:   226 YLSKTSKYLTDSEYTE 179


>>gb|N21167|N21167 yx47e06.s1 Homo sapiens cDNA clone 264898 3' similar to
            contains Alu repetitive element;.
            Length = 401

  Minus Strand HSPs:

 Score = 112 (51.9 bits), Expect = 9.5e-15, Sum P(2) = 9.5e-15
 Identities = 21/42 (50%), Positives = 31/42 (73%), Frame = -1

Query:   127 QELESLLPFLQRSKKRLTDSEFKDPETGKTCLLKAMLNLHNG 168
             ++L  L  +L ++ K LTDSE+ +  TGKTCL+KA+LNL +G
Sbjct:   251 EDLAGLPEYLSKTSKYLTDSEYTEGSTGKTCLMKAVLNLKDG 126

 Score = 79 (36.6 bits), Expect = 9.5e-15, Sum P(2) = 9.5e-15
 Identities = 18/44 (40%), Positives = 23/44 (52%), Frame = -2

Query:   165 LHNGQNDTIALLLDVARKTDSLKQFVNASYTDSYYKGQTALHIA 208
             L    N  I  LL + R + +  VNA  TD YY+G   LHIA
Sbjct:   136 LRTESNACILPLLQIDRDSGNPQPLVNAQCTDDYYRGHEPLHIA 5


>>gb|N35179|N35179 yx83e12.r1 Homo sapiens cDNA clone 268366 5'.
            Length = 433

  Minus Strand HSPs:

 Score = 139 (64.4 bits), Expect = 1.6e-13, Sum P(2) = 1.6e-13
 Identities = 24/46 (52%), Positives = 30/46 (65%), Frame = -1

Query:   718 KAFRSGKLLQVGFTPDGKDDYRWCFRVDEVNWTTWNTNVGIINEDP 763
             K  R+G +L VG   PDG  D RWCFRV+EVNW +W   +  + EDP
Sbjct:   340 KKQRAGVMLKVGTKTDGSPDERWCFRVEEVNWASWEQTLPTLCEDP 203

 Score = 55 (25.5 bits), Expect = 1.6e-13, Sum P(2) = 1.6e-13
 Identities = 10/18 (55%), Positives = 15/18 (83%), Frame = -3

Query:   135 PLQRSKKRLTDSEFKDPE 152
             PL ++ K LTDSE+ +PE
Sbjct:   226 PLSKTSKYLTDSEYTEPE 173
```

```
Sbjct:    14 AGRLLKVGTKGDGIPDERWCFRVEEVNWAAWEKTLPTLSEDP 139


>>gb|AA078617|AA078617 7P07E06 Chromosome 7 Placental cDNA Library Homo sapiens
            cDNA clone 7P07E06
            Length = 227

  Plus Strand HSPs:

 Score = 80 (37.0 bits), Expect = 3.1e-07, Sum P(2) = 3.1e-07
 Identities = 14/23 (60%), Positives = 19/23 (82%), Frame = +2

Query:   367 RKPTEWAYGPVRSSLYDLSCIDT 389
             RK T-W YGP+ S+LYDL+ ID+
Sbjct:   137 RKHTQWTYGPLTSTLYDLTEIDS 205

 Score = 58 (26.9 bits), Expect = 3.1e-07, Sum P(2) = 3.1e-07
 Identities = 11/34 (32%), Positives = 19/34 (55%), Frame = +2

Query:   325 LEEITNRKGLTPLAIAASSGKIGVLAYILQREIN 358
             L+  + N +GLTP  LA   Q   +++Q+  H
Sbjct:    44 LDLVPNHQGLTPFKLAGVEGDTVMFQHLMQKRKH 145


>>gb|N24224|N24224 yx21g11.r1 Homo sapiens cDNA clone 262436 5'.
            Length = 326

  Plus Strand HSPs:

 Score = 121 (56.0 bits), Expect = 3.2e-07, P = 3.2e-07
 Identities = 28/83 (33%), Positives = 43/83 (51%), Frame = +1

Query:   405 ETPNRHDKLLVEPLNRLLQDKWDRFVKRIFYFNFFVYCLYMIIFTAAAYYRPVEGLPPYK 464
             ++P RH M-++EPLN+LLQ KWD  + + F          I    A +   ++
Sbjct:    37 KSPXRHRMVVLEPLNKLLQAKWDLLIPKFFLNFLCKLXYMPIFTAVAYHQPTLKEQAAPH 216

Query:   465 LKNTVGDYFRVTGEILSVSGGVY 487
             LK  VG+  -TG IL + GG+Y
Sbjct:   217 LKAEVGNSMLLTGHILILLGGIY 285


>>gb|AA144832|AA144832 mr69d04.r1 Stratagene mouse testis (#937308) Mus musculus
            cDNA clone 602695 5'
            Length = 262

  Plus Strand HSPs:

 Score = 64 (29.6 bits), Expect = 2.9e-05, Sum P(2) = 2.9e-05
 Identities = 14/27 (51%), Positives = 19/27 (70%), Frame = +1

Query:   200 KGQTALHIAIERRNMTLVTLLVENGAD 226
             KG+TALH A    N  +V LL++ GAD
Sbjct:    76 KGRTALHFASCMGNDQIVQLLLDHGAD 156

 Score = 59 (27.3 bits), Expect = 2.9e-05, Sum P(2) = 2.9e-05
 Identities = 11/22 (50%), Positives = 15/22 (68%), Frame = +1

Query:   248 GELPLSLAACTNQLAIVKFLLQ 269
             G  PL LAACTN + ++  LL+
Sbjct:   178 GNTPLHLAACTNHVPVITTLLR 243

 Score = 42 (19.4 bits), Expect = 0.68, Sum P(2) = 0.49
 Identities = 8/15 (53%), Positives = 11/15 (73%), Frame = +1

Query:   275 ADISARDSVGNTVLH 289
```

```
            AD + +D +GNT LH
Sbjct:   151 ADPNQQDGLGNTPLH 195

 Score = 40 (18.5 bits), Expect = 1.5, Sum P(2) = 0.79
 Identities = 9/22 (40%), Positives = 14/22 (63%), Frame = +1

Query:   333 GLTPLALAASSGKIGVLAYILQ 354
            G TPL LAA +  + V+  +L+
Sbjct:   178 GNTPLHLAACTNHVPVITTLLR 243


>>dbj|C45219|C45219 C.elegans cDNA clone yk390d4 : 5' end, single read
            Length = 360

  Plus Strand HSPs:

 Score = 65 (30.1 bits), Expect = 0.0017, Sum P(3) = 0.0017
 Identities = 14/29 (48%), Positives = 18/29 (62%), Frame = +3

Query:   203 TALHIAIERRNMTLVTLLVENGADVQAAA 231
            T LH+A    N  +  LL+ENGA  +AAA
Sbjct:    96 TPLHVAAHYNNDKVAMLLLENGASAKAAA 182

 Score = 48 (22.2 bits), Expect = 0.0016, Sum P(3) = 0.0016
 Identities = 12/27 (44%), Positives = 14/27 (51%), Frame = +1

Query:   248 GELPLSLAACTNQLAIVKFLLQNSWQP 274
            G  PL +AA  NQ+ I   LLQ    P
Sbjct:   190 GYTPLHIAAXKNQMEIASTLLQFKADP 270

 Score = 41 (19.0 bits), Expect = 5.9, Sum P(2) = 1.0
 Identities = 8/22 (36%), Positives = 14/22 (63%), Frame = +1

Query:   333 GLTPLALAASSGKIGVLAYILQ 354
            G TPL +AA   +  + + +LQ
Sbjct:   190 GYTPLHIAAXKNQMEIASTLLQ 255

 Score = 40 (18.5 bits), Expect = 0.0016, Sum P(3) = 0.0016
 Identities = 8/15 (53%), Positives = 10/15 (66%), Frame = +1

Query:   330 NRKGLTPLALAASSG 344
            +R G TPL L+A  G
Sbjct:   280 SRAGFTPLHLSAQEG 324


>>gb|AA479879|AA479879 zw44a01.s1 Soares total fetus Nb2HF8 9w Homo sapiens cDNA
            clone 772872 3' similar to TR:G1161922 G1161922 P19 PROTEIN. [1] ;
            Length = 250

  Minus Strand HSPs:

 Score = 43 (19.9 bits), Expect = 0.0047, Sum P(3) = 0.0047
 Identities = 10/24 (41%), Positives = 15/24 (62%), Frame = -1

Query:   205 LHIAIERRNMTLVTLLVENGADVQ 228
            +H A      +  + +LVE+GADVQ
Sbjct:   230 VHDAARTGFLDTLKVLVEHGADVQ 167

 Score = 43 (19.9 bits), Expect = 0.0047, Sum P(3) = 0.0047
 Identities = 10/24 (41%), Positives = 12/24 (50%), Frame = -1

Query:   248 GELPLSLAACTNQLAIVKFLLQNS 271
            G LP+ LA      A+V FL   S
Sbjct:   151 GALPIHLAVQEGHTAVVSFLAAES 80
```

Appendix 1.2: the pGEM-T easy vector used for subcloning PCR products (information provided by Promega)

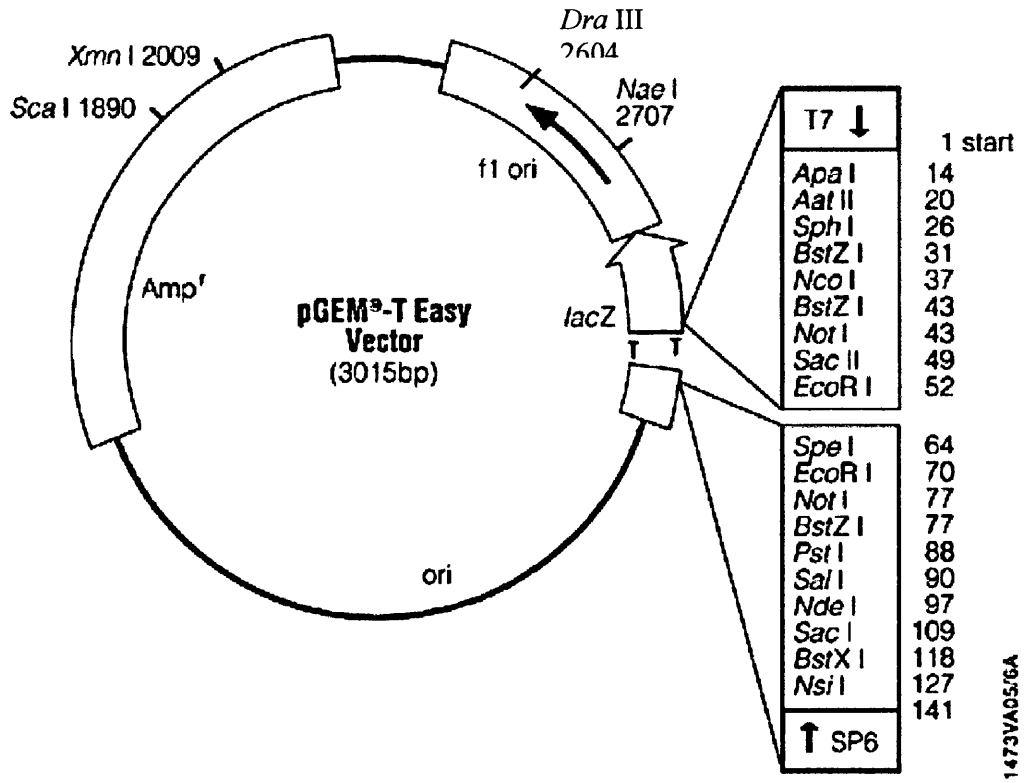

The pGEM-T Easy Vector System is a convenient system for the cloning of PCR products. The vector is prepared by cutting the pGEM®-T Easy Vector with *Eco*R V and adding a 3′ terminal thymidine to both ends. These single 3′-T overhangs at the insertion site greatly improve the efficiency of ligation of a PCR product into the plasmid by preventing recircularization of the vector and providing a compatible overhang for PCR products generated by certain thermostable polymerases. These polymerases often add a single deoxyadenosine, in a template-independent fashion, to the 3′-ends of the amplified fragments.
The high copy number pGEM-T Easy Vector contains T7 and SP6 RNA polymerase promoters flanking a multiple cloning region within the alpha-peptide coding region of the enzyme beta-galactosidase. Insertional inactivation of the alpha-peptide allows recombinant clones to be directly identified by color screening on indicator plates.
The pGEM-T Easy Vector multiple cloning region is flanked by recognition sites for the restriction enzymes *Eco*R I, *Bst*Z I and *Not* I, thus providing three single-enzyme digestions for release of the insert. Alternatively, a double-digestion may be used to release the insert from either vector. The pGEM-T Easy Vector also contains the origin of replication of the filamentous phage f1 for the preparation of single-stranded DNA (ssDNA).

Appendix 1.3: 5'UTR-429bp of VR-L sequence (considering the first nucleotide of UTR as number 1). The sequencing has been repeated twice and the nucleotides confirmed. Primers used to confirm sequence: UTR, Met, J13

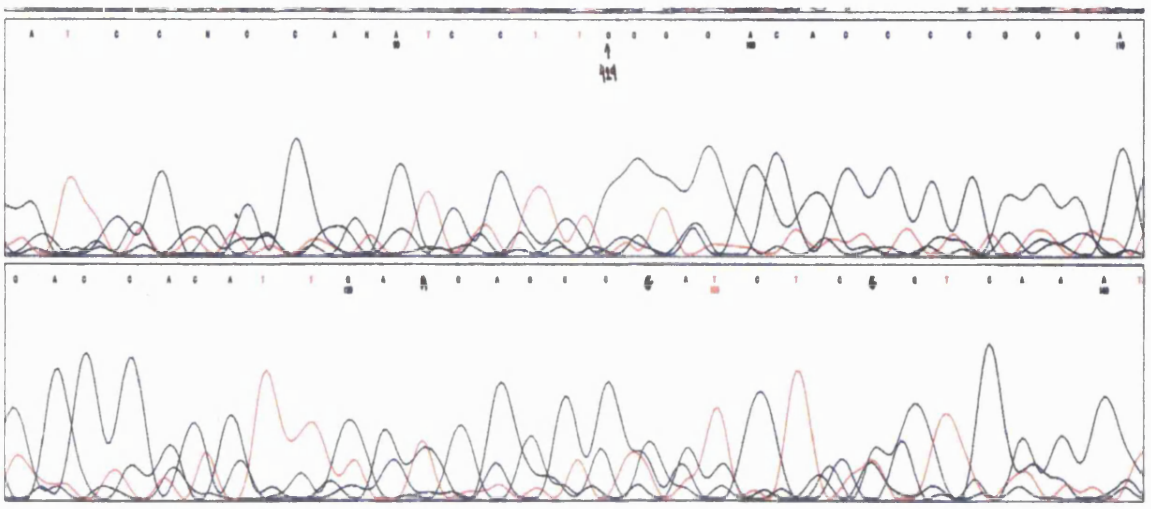

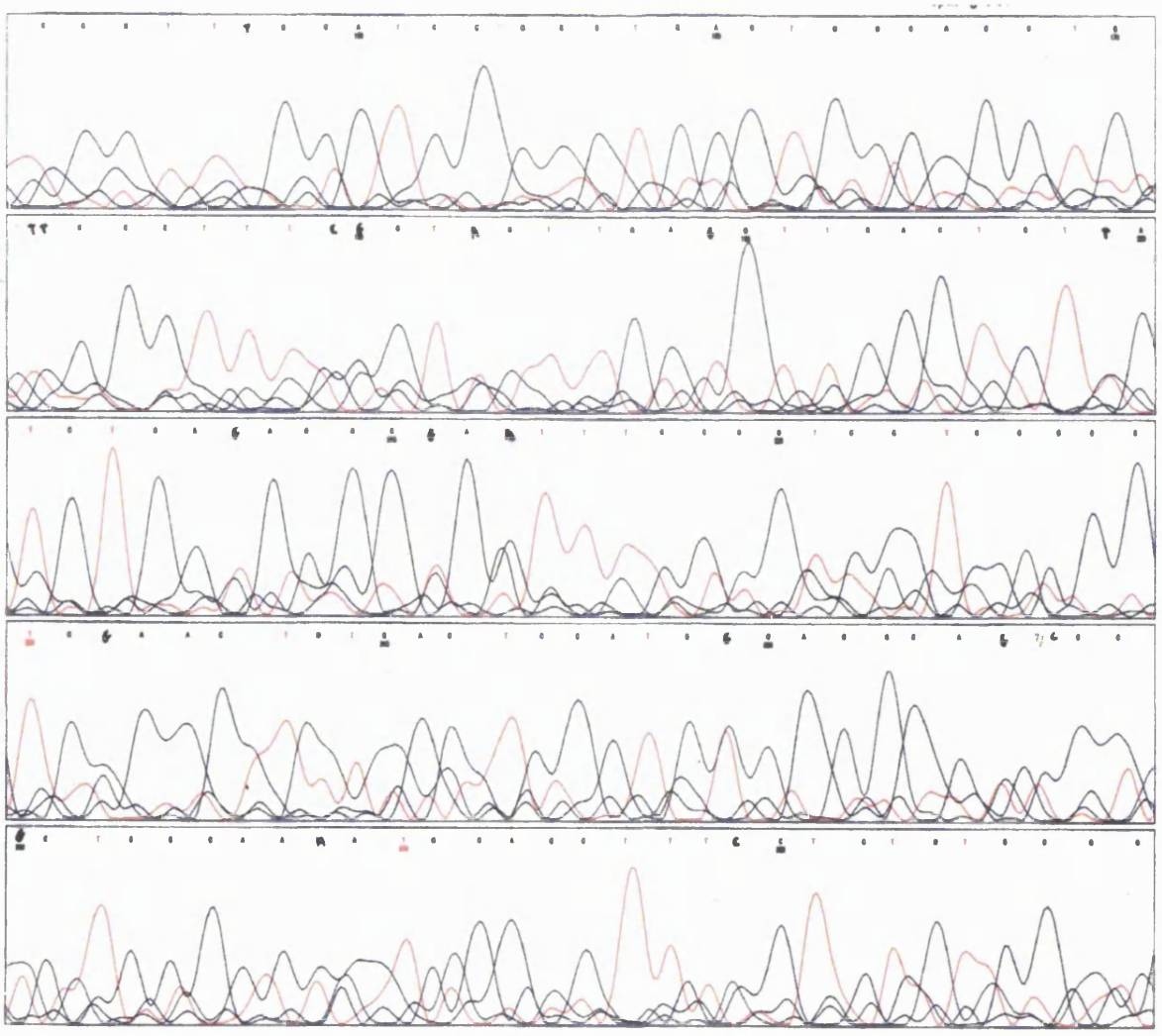

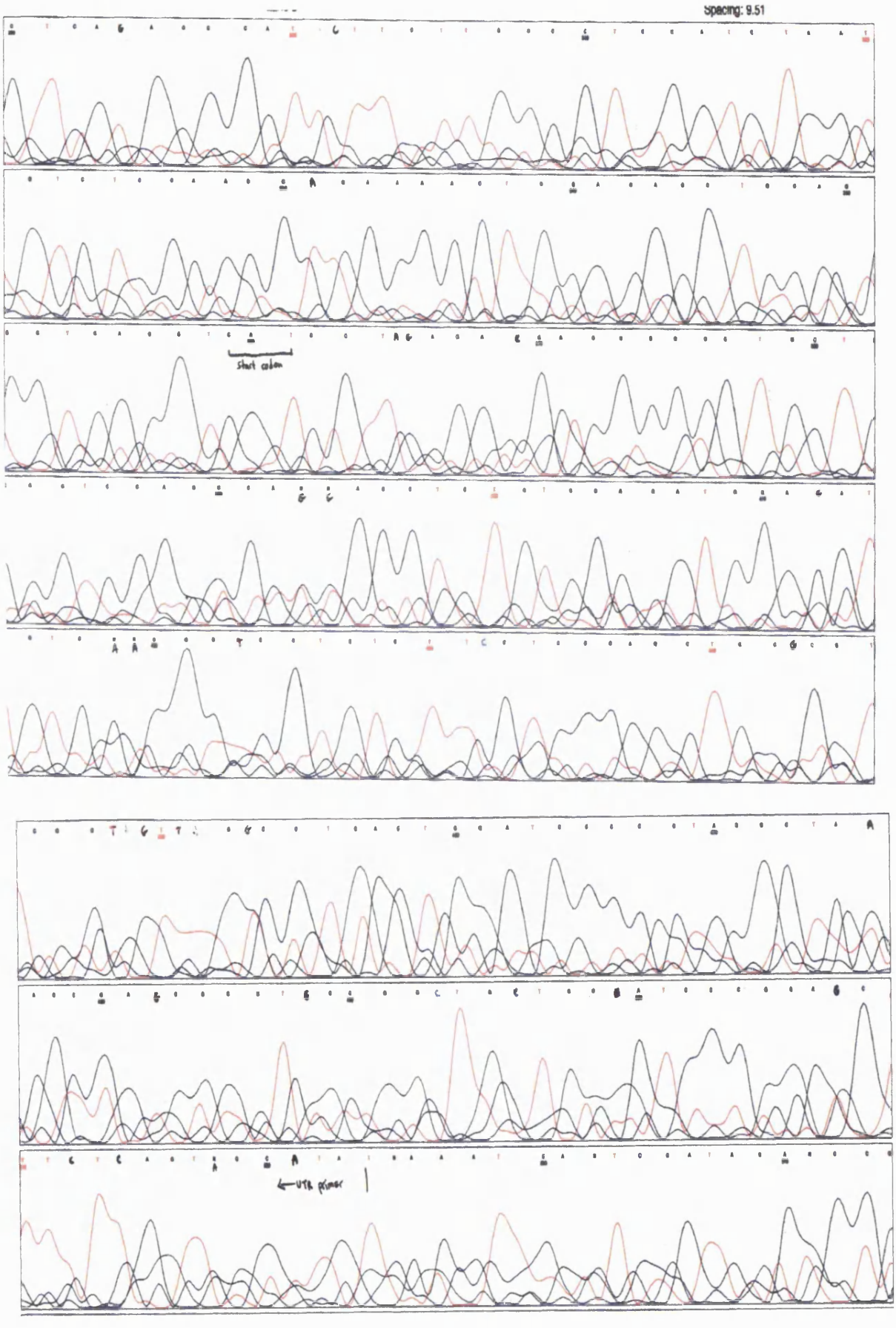
Spacing: 9.51
Start codon
←UTR primer

Appendix 1.3: 336-851bp of VR-L sequence. Primers used: J11, J12, J13

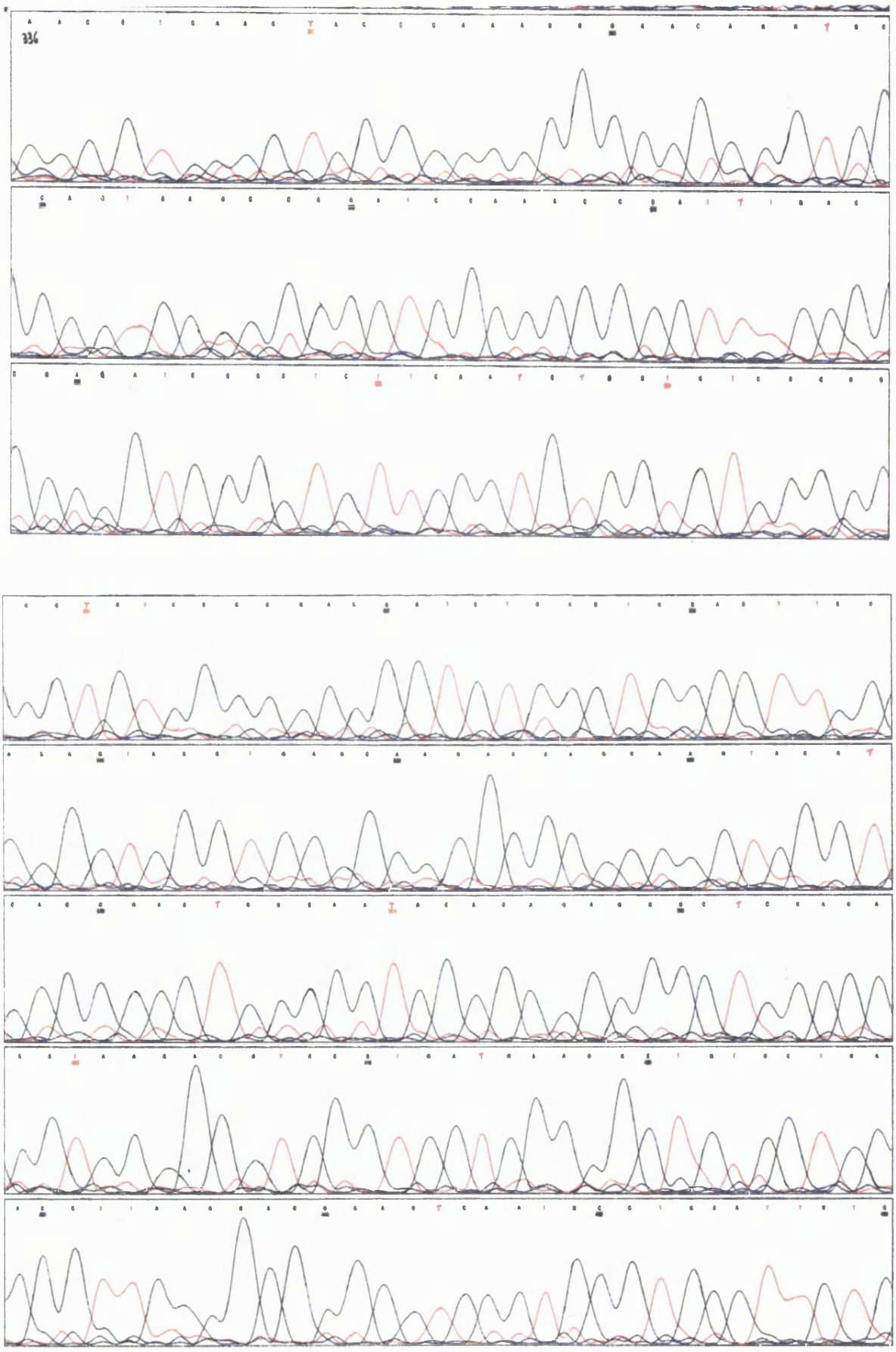

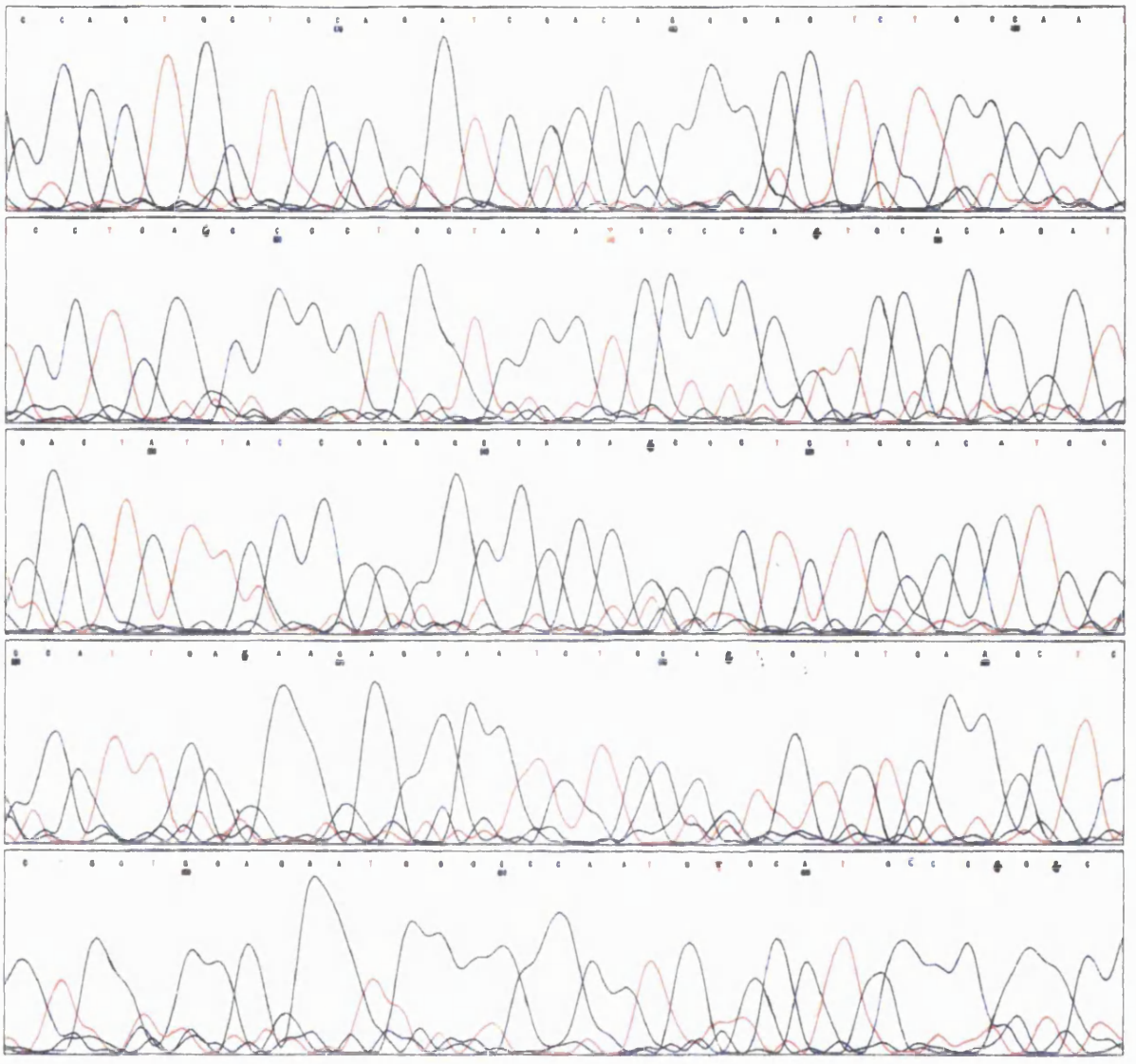

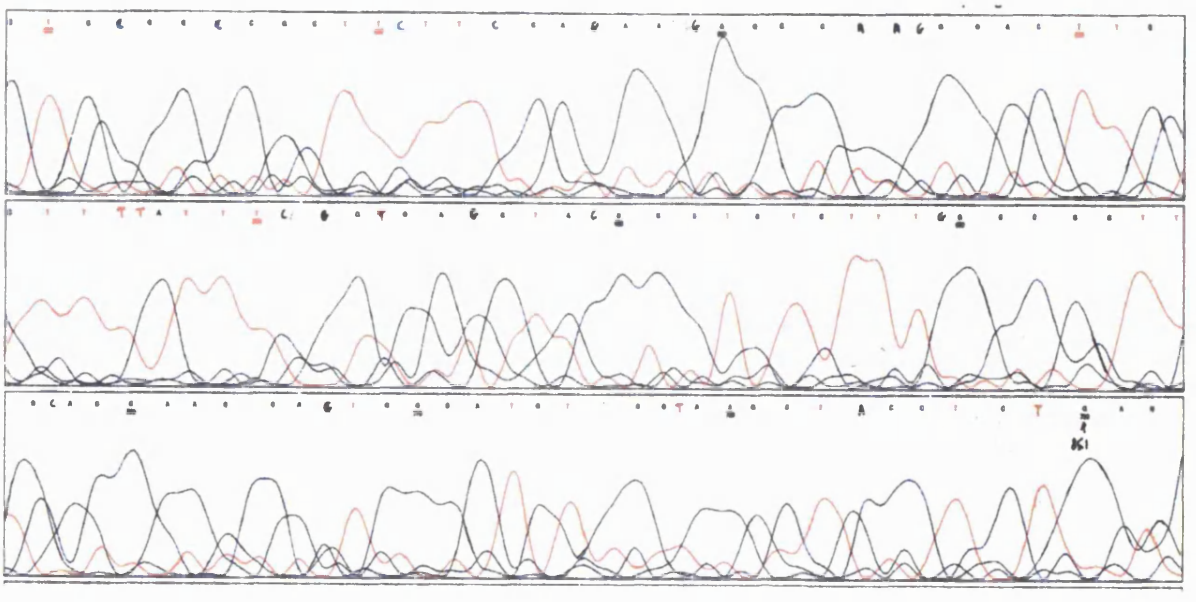

Appendix 1.3: 852-1371bp of VR-L sequence. Primers used: J1,J2,J3

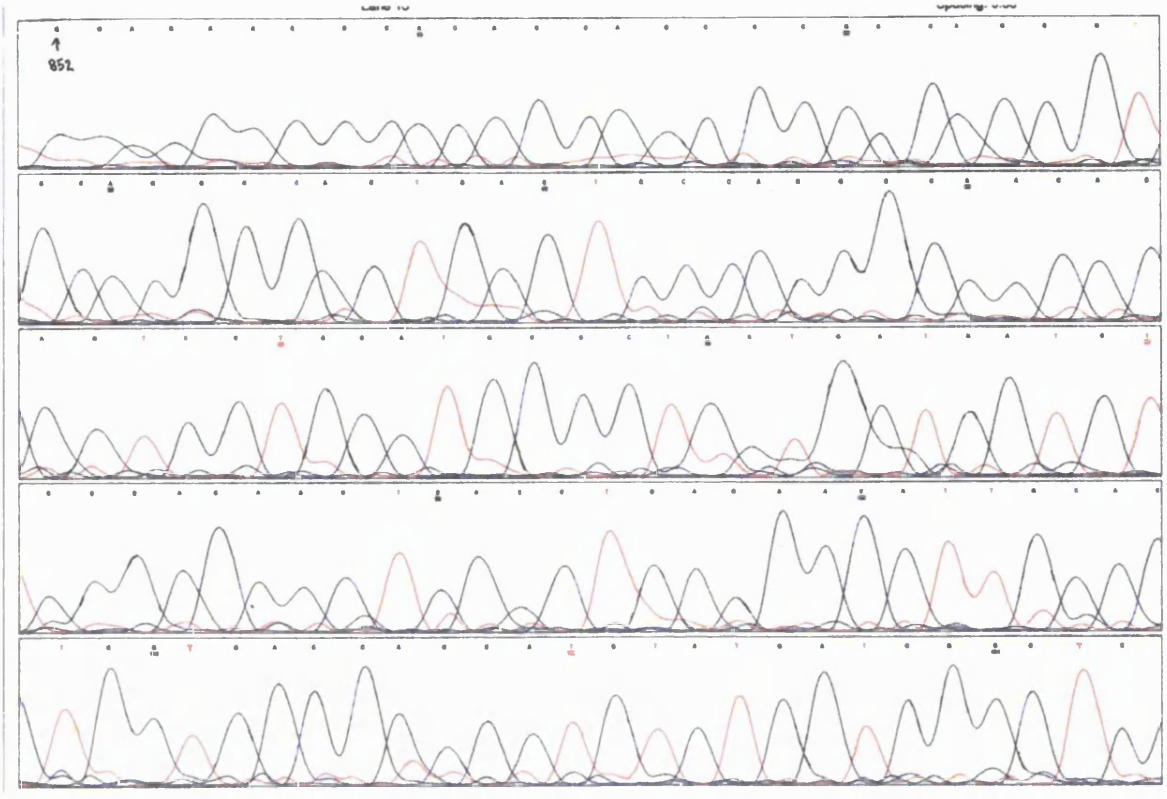

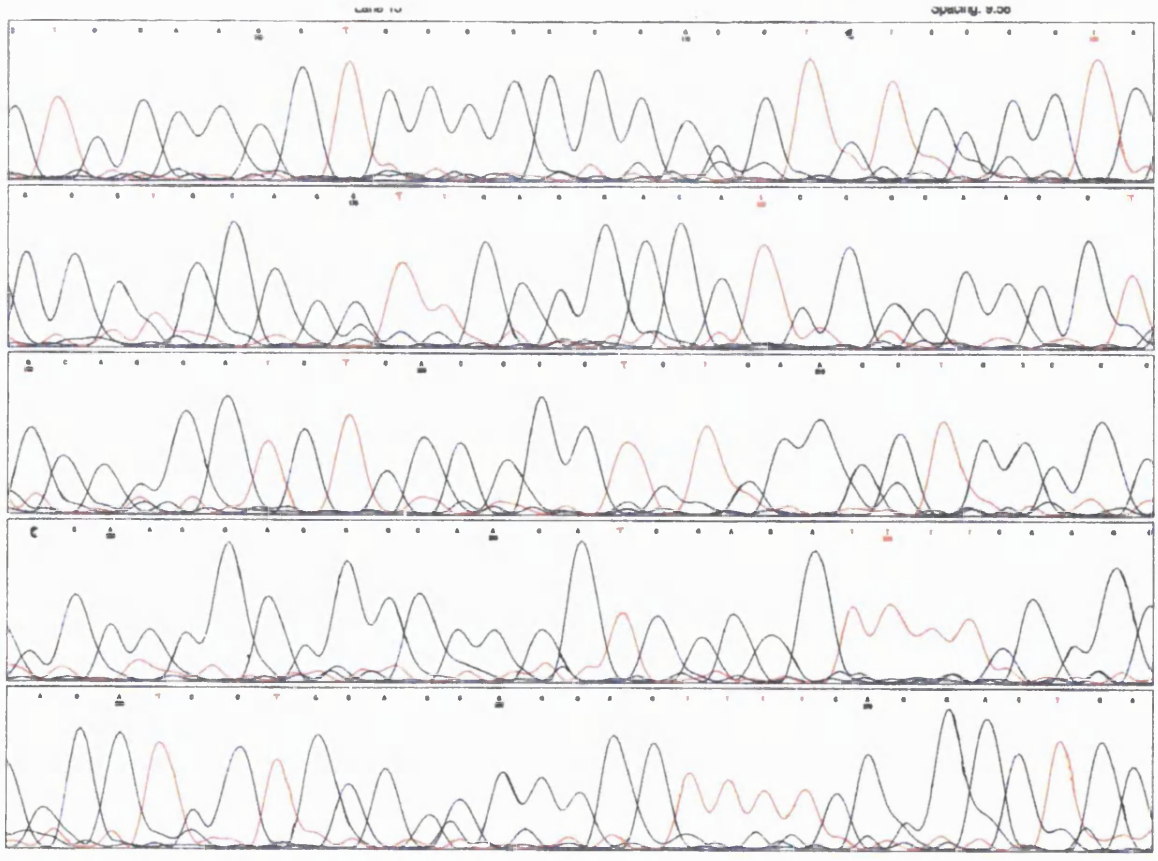

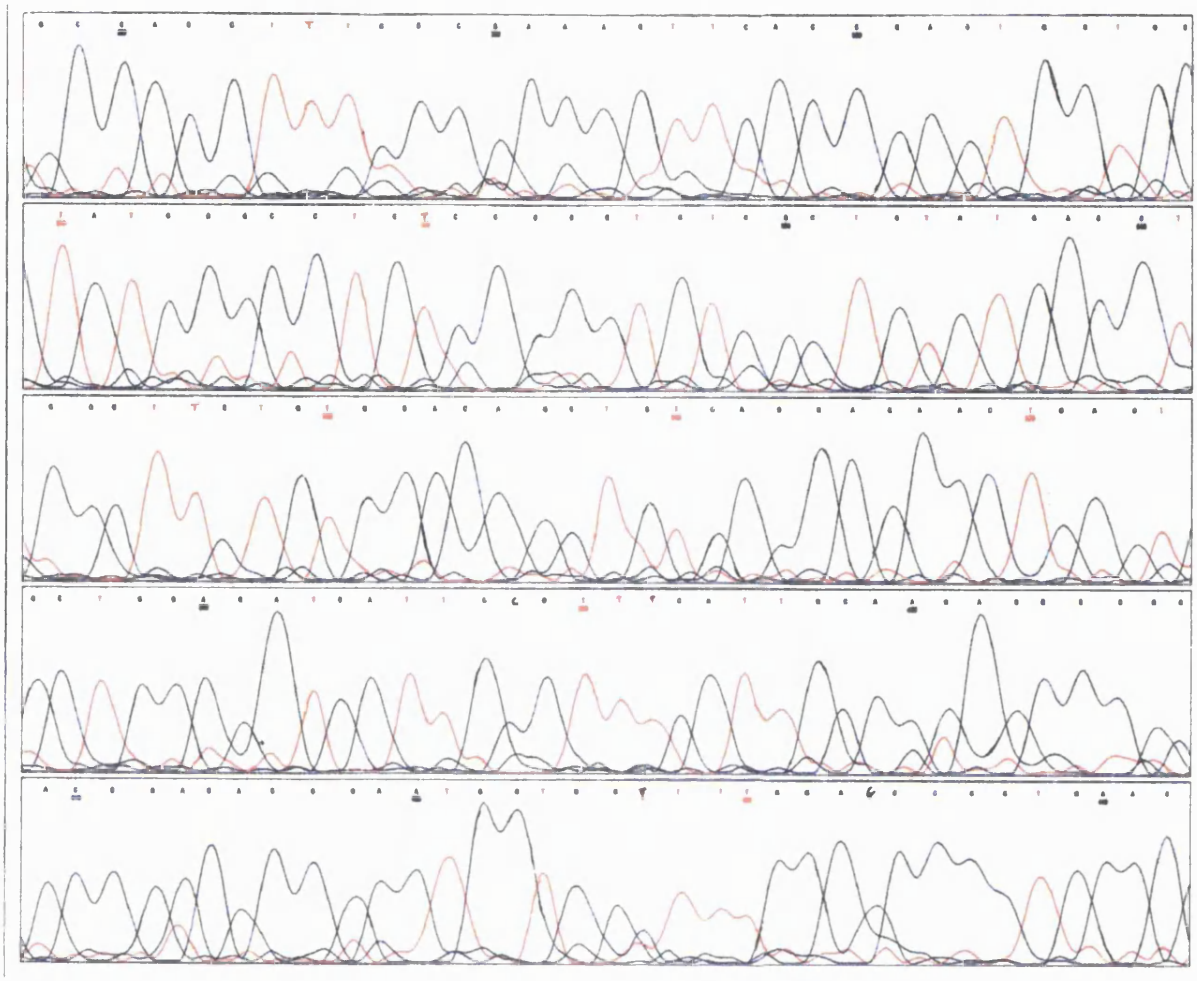

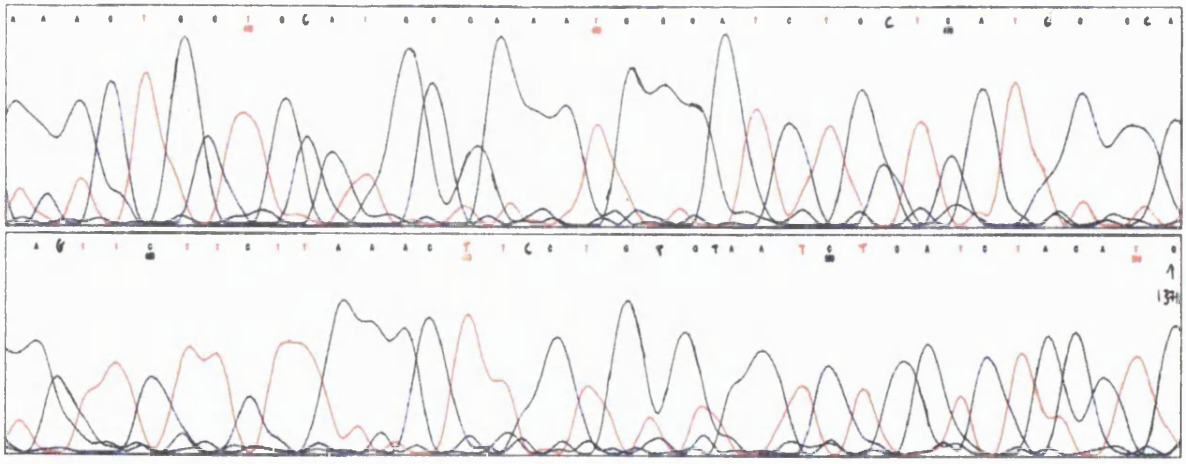

Appendix 1.3: 1372-1667bp of VR-L sequence. Primers used: J3,J4,J5

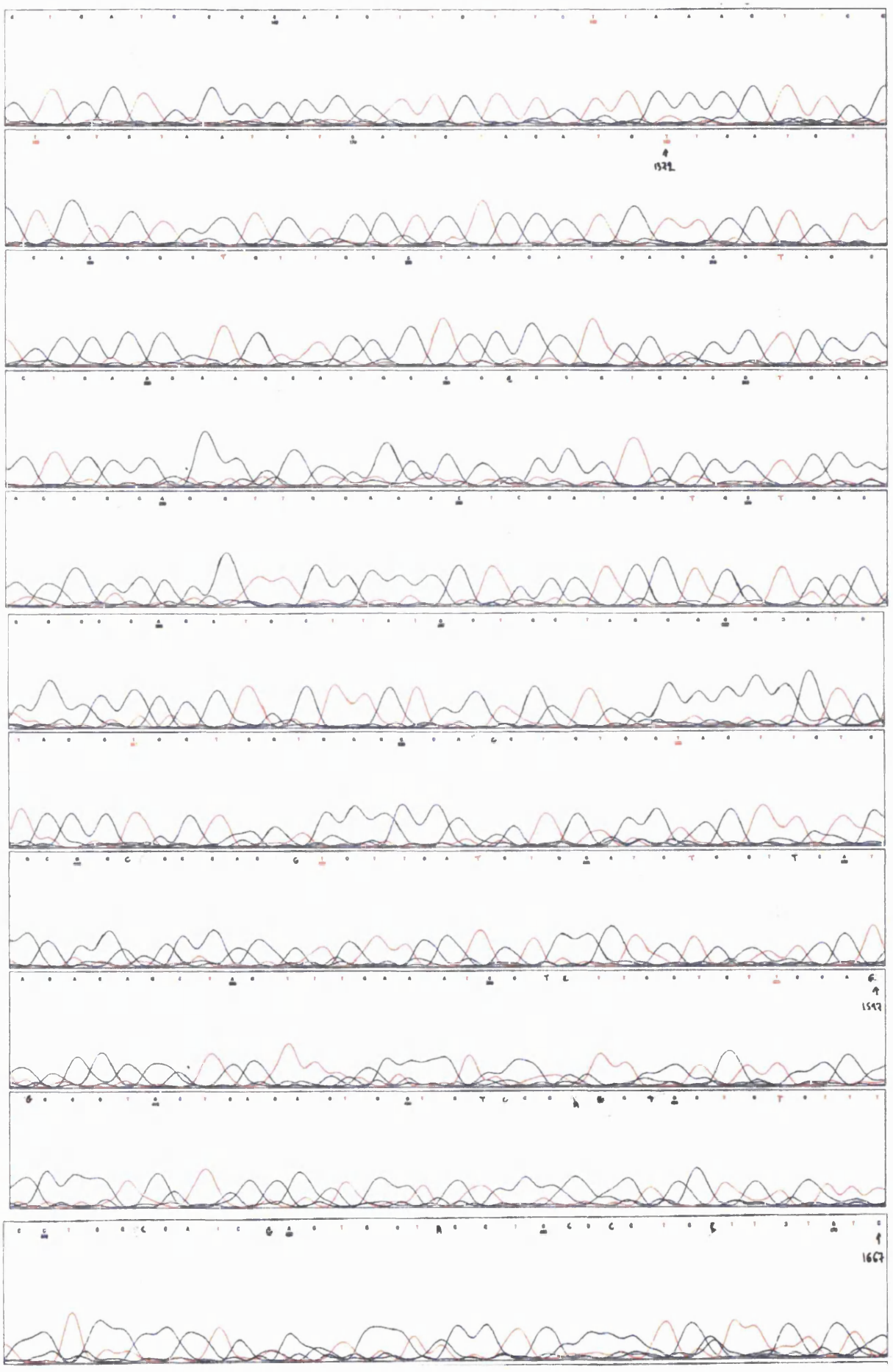

Appendix 1.3: sequences 1598-1988bp of human VR-L. Primers used: J6,J17

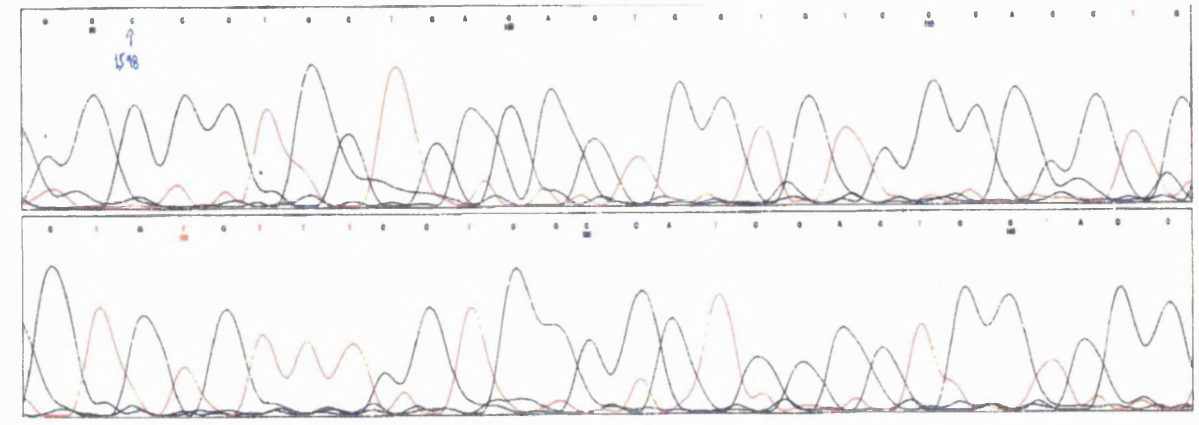

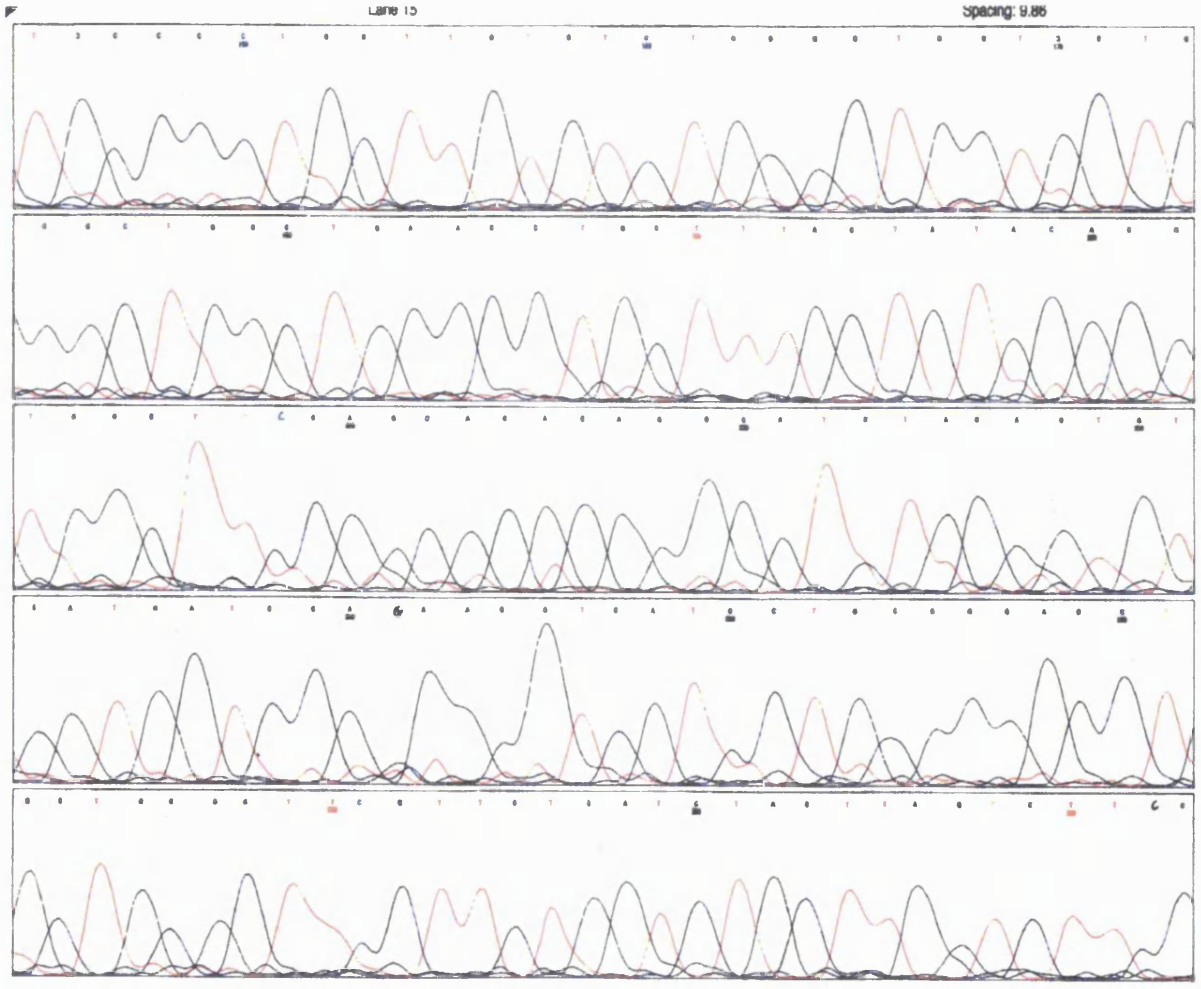

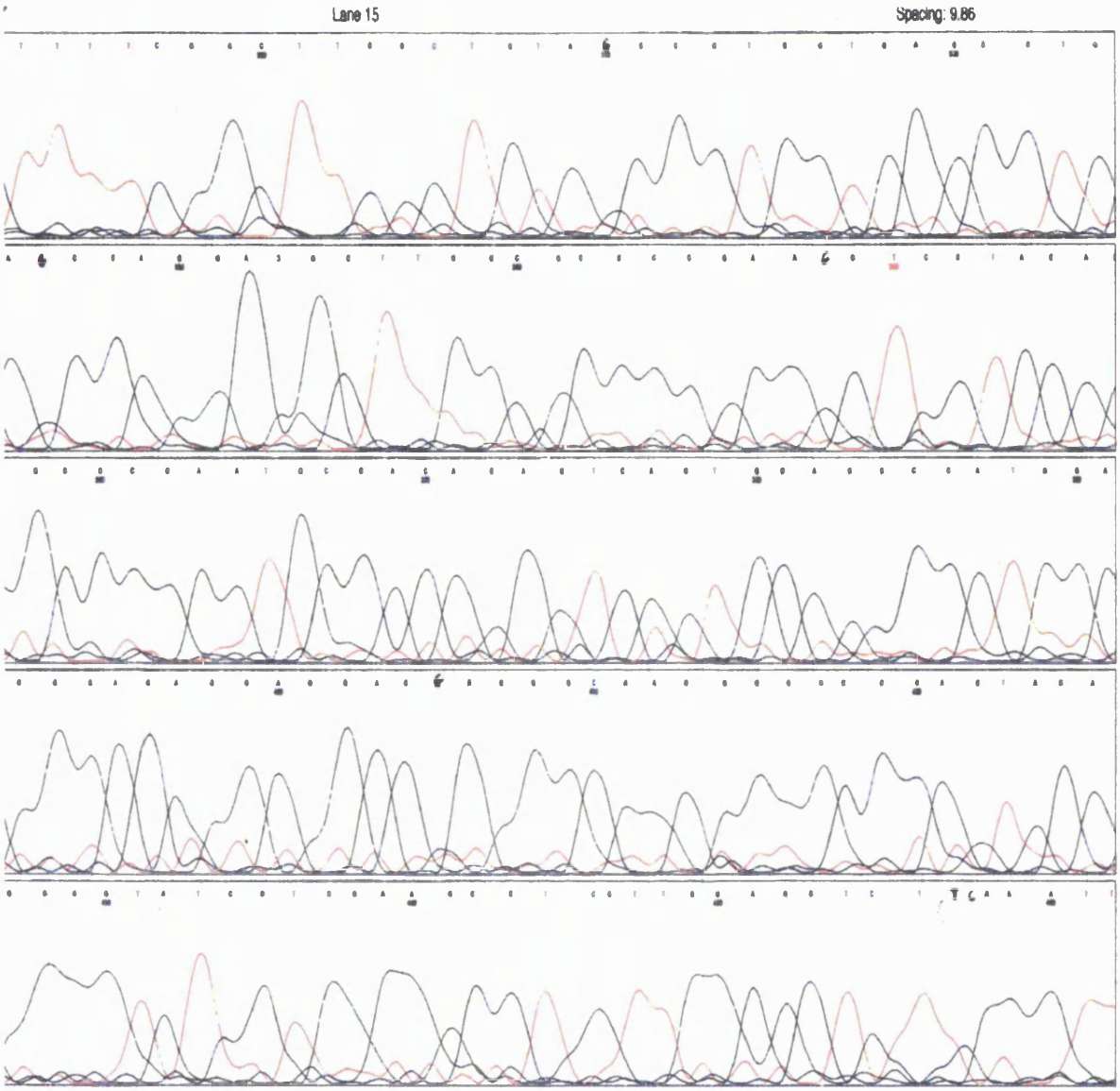
Lane 15
Spacing: 9.86

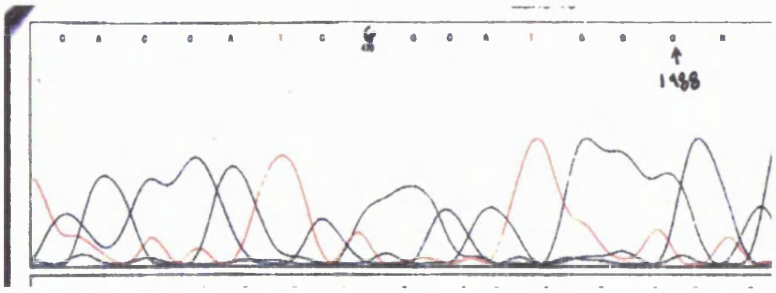

Appendix 1.3: 2255-1988 bp of VR-L sequence. Primers used: J8,J17

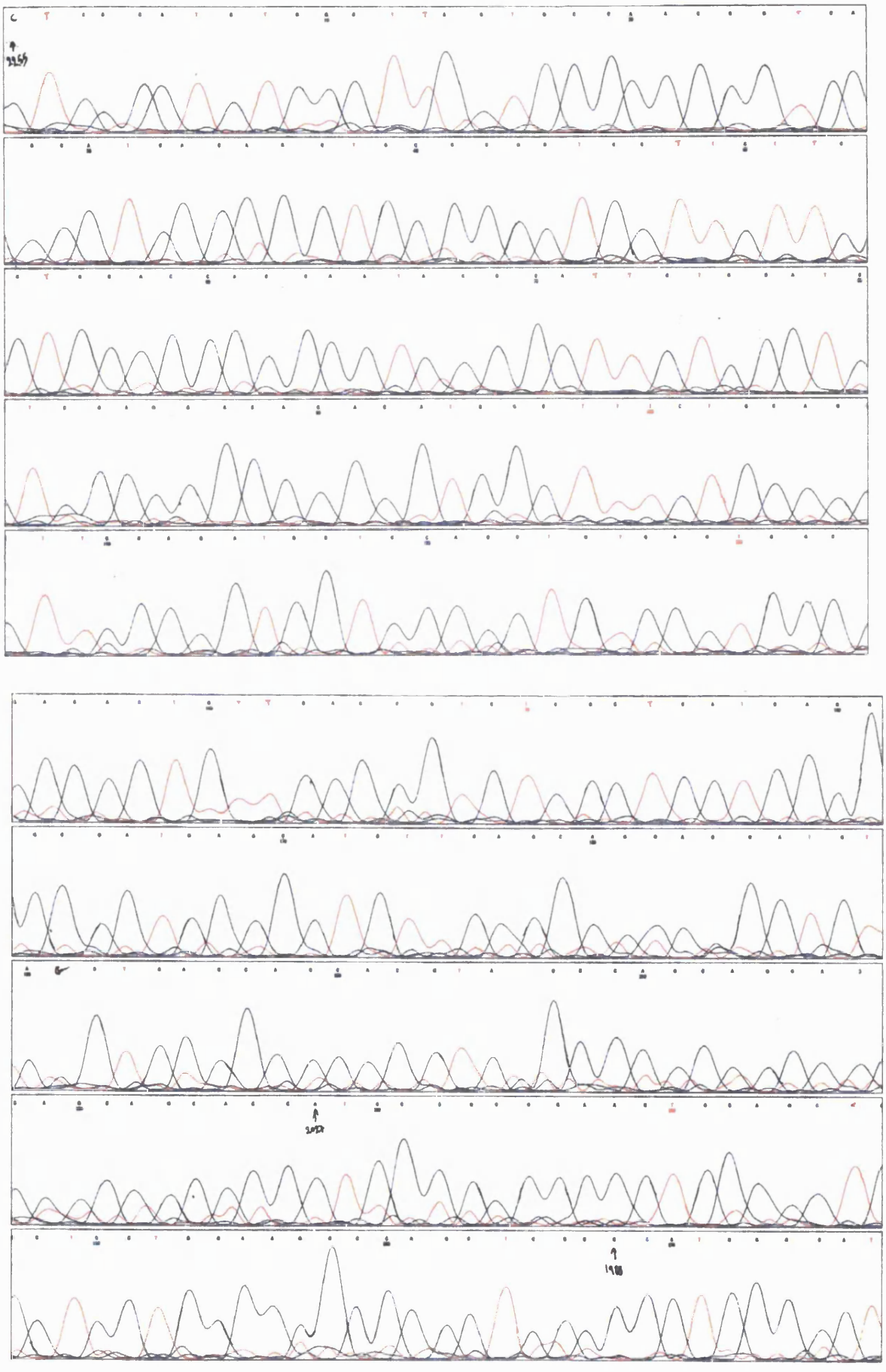

Appendix 1.3: 2507-2256. Primers used: J7,J14

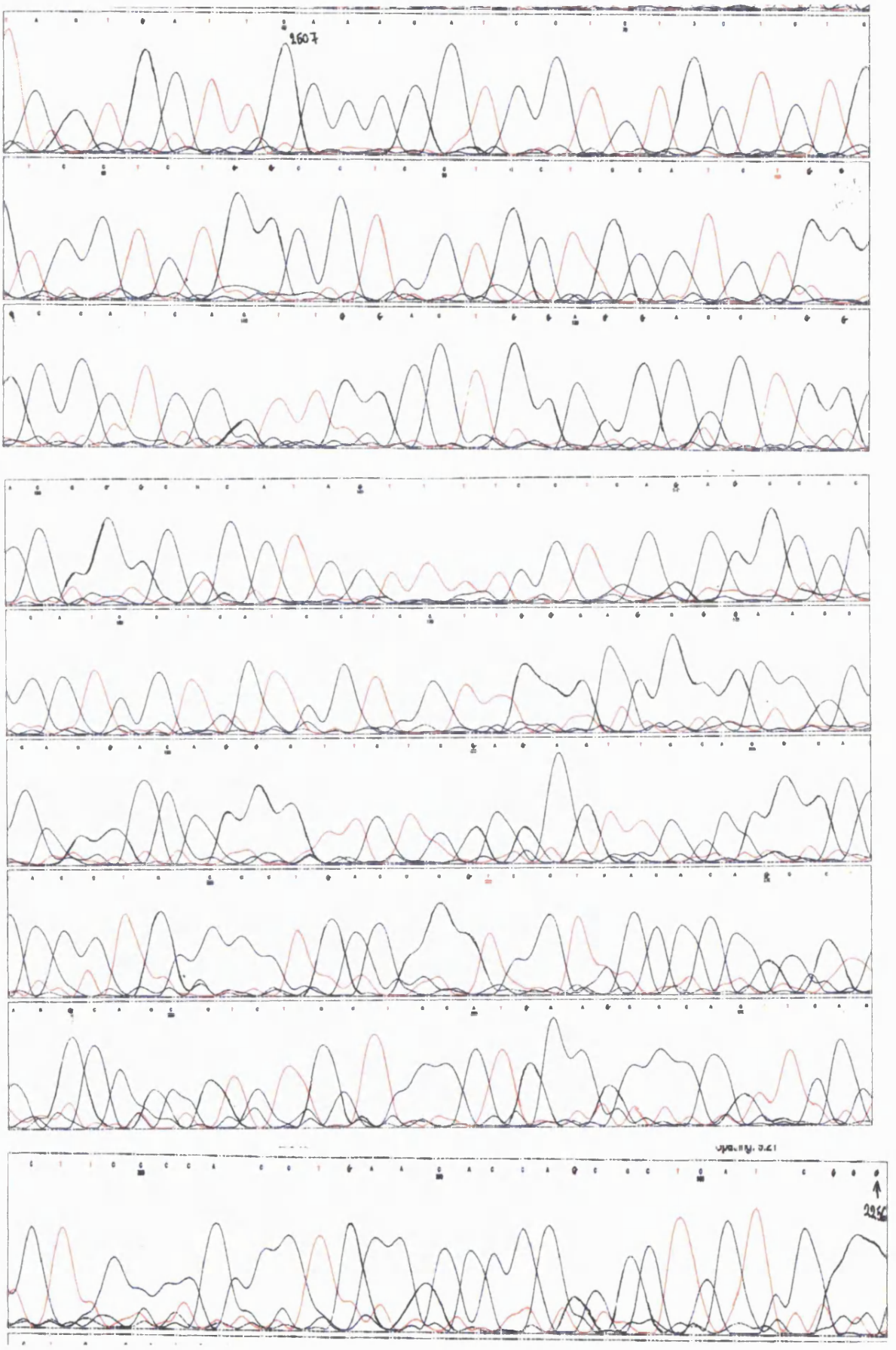

Appendix 1.4: Complete human VRL restriction map, showing the positions of the primers (underlined red regions) and the restriction sites used (highlighted gray regions). The start and stop codons are highlighted in yellow.

2766 base pairs

```
gctagcctgtcctgacaggggagagttaagctcccgttctccaccgtgccggctggcaggtgggctgagggtgac base pairs
cgatcggacaggactgtcccctctcaattcgagggcaagaggtggcacggccgaccgtccacccgactcccactg 1 to 75

cgagagaccagaacctgcttgctggagcttagtgctcagagctggggagggaggttccgccgctcctctgctgtc base pairs
gctctctggtcttggacgaacgacctcgaatcacgagtctcgacccctccctccaaggcggcgaggagacgacag 76 to 150
                                                  UTR
agcgccggcagcccctcccggcttcacttcctcccgcagcccctgctactgagaagctccgggatcccagcagcc base pairs
tcgcggccgtcggggagggccgaagtgaaggagggcgtcggggacgatgactcttcgaggccctagggtcgtcgg 151 to 225

gccacgccctggcctcagcctgcggggctccagtcaggccaacaccgacgcgcagctgggaggaagacaggaccc base pairs
cggtgcgggaccggagtcggacgccccgaggtcagtccggttgtggctgcgcgtcgaccctccttctgtcctggg 226 to 300
                                                  Met
ttgacatctccatctgcacagaggtcctggctggaccgagcagccccctcctcctaggatgacctcaccctccag base pairs
aactgtagaggtagacgtgtctccaggaccgacctggctcgtcgggggaggaggatcctactggagtgggaggtc 301 to 375


                                          BstXI
ctctccagttttcaggttggagacattagatggaggccaagaagatggctctgaggcggacagaggaaagctgga base pairs
gagaggtcaaaagtccaacctctgtaatctacctccggttcttctaccgagactccgcctgtctcctttcgacct 376 to 450


                     NcoI
ttttgggagcgggctgcctcccatggagtcacagttccagggcgaggaccggaaattcgcctctcagataagagt base pairs
aaaaccctcgcccgacggaggtacctcagtgtcaaggtcccgctcctggcctttaagcggagagtctattctca 451 to 525
                                                  J13
caacctcaactaccgaaagggaacaggtgccagtcagccggatccaaaccgatttgaccgagatcggctcttcaa base pairs
gttggagttgatggctttcccttgtccacggtcagtcggcctaggtttggctaaactggctctagccgagaagtt 526 to 600

tgcggtctcccggggtgtccccgaggatctggctggacttccagagtacctgagcaagaccagcaagtacctcac base pairs
acgccagagggccccacaggggctcctagaccgacctgaaggtctcatggactcgttctggtcgttcatggagtg 601 to 675
                                                  J12
cgactcggaatacacagagggctccacaggtaagacgtgcctgatgaaggctgtgctgaaccttaaggacggggt base pairs
gctgagccttatgtgtctcccgaggtgtccattctgcacggactacttccgacacgacttggaattcctgcccca 676 to 750

caatgcctgcattctgccactgctgcagatcgacagggactctggcaatcctcagcccctggtaaatgcccagtg base pairs
gttacggacgtaagacggtgacgacgtctagctgtccctgagaccgttaggagtcggggaccatttacgggtcac 751 to 825

cacagatgactattaccgaggccacagcgctctgcacatcgccattgagaagaggagtctgcagtgtgtgaagct base pairs
gtgtctactgataatggctccggtgtcgcgagacgtgtagcggtaactcttctcctcagacgtcacacacttcga 826 to 900


                                          NotI
cctggtggagaatggggccaatgtgcatgcccgggcctgcggccgcttcttccagaagggccaagggacttgctt base pairs
ggaccacctcttaccccggttacacgtacgggcccggacgccggcgaagaaggtcttcccggttccctgaacgaa 901 to 975
          J1
ttatttcggtgagctacccctctctttggccgcttgcaccaagcagtgggatgtggtaagctacctcctggagaa base pairs
aataaagccactcgatggggagagaaaccggcgaacgtggttcgtcaccctacaccattcgatggaggacctctt 976 to 1050
                                          J11
cccacaccagcccgccagcctgcaggccactgactcccagggcaacacagtcctgcatgccctagtgatgatctc base pairs
gggtgtggtcgggcggtcggacgtccggtgactgagggtcccgttgtgtcaggacgtacgggatcactactagag 1051 to 1125

ggacaactcagctgagaacattgcactggtgaccagcatgtatgatgggctcctccaagctggggcccgcctctg base pairs
cctgttgagtcgactcttgtaacgtgaccactggtcgtacatactacccgaggaggttcgaccccgggcggagac 1126 to 1200

ccctaccgtgcagcttgaggacatccgcaacctgcaggatctcacgcctctgaagctggccgccaaggagggcaa base pairs
gggatggcacgtcgaactcctgtaggcgttggacgtcctagagtgcggagacttcgaccggcggttcctcccgtt 1201 to 1275


                                                  DraIII
gatcgagattttcaggcacatcctgcagcgggagttttcaggactgagccacctttcccgaaagttcaccgagtg base pairs
ctagctctaaaagtccgtgtaggacgtcgccctcaaaagtcctgactcggtggaaagggctttcaagtggctcac 1276 to 1350

gtgctatgggcctgtccgggtgtcgctgtatgacctggcttctgtggacagctgtgaggagaactcagtgctgga base pairs
cacgatacccggacaggcccacagcgacatactggaccgaagacacctgtcgacactcctcttgagtcacgacct 1351 to 1425

gatcattgcctttcattgcaagagcccgcaccgacaccgaatggtcgttttggagcccctgaacaaactgctgca base pairs
ctagtaacggaaagtaacgttctcgggcgtggctgtggcttaccagcaaaacctcggggacttgtttgacgacgt 1426 to 1500

ggcgaaatgggatctgctcatccccaagttcttcttaaacttcctgtgtaatctgatctacatgttcatcttcac base pairs
ccgctttaccctagacgagtaggggttcaagaagaatttgaaggacacattagactagatgtacaagtagaagtg 1501 to 1575

cgctgttgcctaccatcagcctaccctgaagaagcaggccgcccctcacctgaaagcggaggttggaaactccat base pairs
gcgacaacggatggtagtcggatgggacttcttcgtccggcggggagtggactttcgcctccaacctttgaggta 1576 to 1650
```

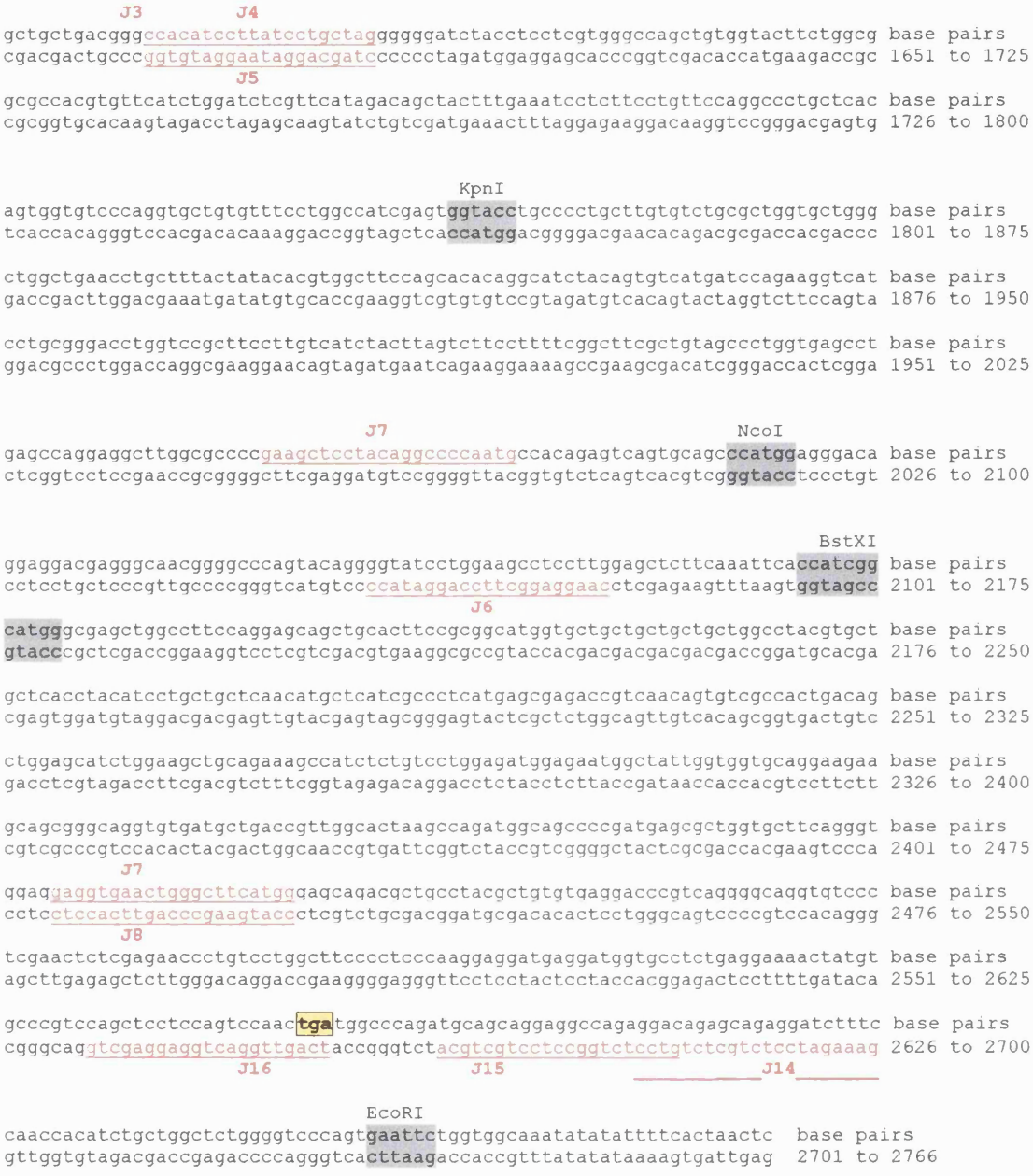
J3
J4
gctgctgacgggccacatccttatcctgctaggggggatctacctcctcgtgggccagctgtggtacttctggcg base pairs
cgacgactgcccggtgtaggaataggacgatccccccctagatggaggagcacccggtcgacaccatgaagaccgc 1651 to 1725
J5
gcgccacgtgttcatctggatctcgttcatagacagctactttgaaatcctcttcctgttccaggccctgctcac base pairs
cgcggtgcacaagtagacctagagcaagtatctgtcgatgaaactttaggagaaggacaaggtccgggacgagtg 1726 to 1800
KpnI
agtggtgtcccaggtgctgtgtttcctggccatcgagtggtacctgcccctgcttgtgtctgcgctggtgctggg base pairs
tcaccacagggtccacgacacaaaggaccggtagctcaccatggacggggacgaacacagacgcgaccacgaccc 1801 to 1875
ctggctgaacctgctttactatacacgtggcttccagcacacaggcatctacagtgtcatgatccagaaggtcat base pairs
gaccgacttggacgaaatgatatgtgcaccgaaggtcgtgtgtccgtagatgtcacagtactaggtcttccagta 1876 to 1950
cctgcgggacctggtccgcttccttgtcatctacttagtcttccttttcggcttcgctgtagccctggtgagcct base pairs
ggacgccctggaccaggcgaaggaacagtagatgaatcagaaggaaaagccgaagcgacatcgggaccactcgga 1951 to 2025
J7
NcoI
gagccaggaggcttggcgcccc gaagctcctacaggccccaatg ccacagagtcagtgcagccatggagggaca base pairs
ctcggtcctccgaaccgcggggcttcgaggatgtccggggttacggtgtctcagtcacgtcgggtacctccctgt 2026 to 2100
BstXI
ggaggacgagggcaacggggcccagtacaggggtatcctggaagcctccttggagctcttcaaattcaccatcgg base pairs
cctcctgctcccgttgccccgggtcatgtcccccataggaccttcggaggaacctcgagaagtttaagtggtagcc 2101 to 2175
J6
catgggcgagctggccttccaggagcagctgcacttccgcggcatggtgctgctgctgctggcctacgtgct base pairs
gtacccgctcgaccggaaggtcctcgtcgacgtgaaggcgccgtaccacgacgacgacgacgaccggatgcacga 2176 to 2250
gctcacctacatcctgctgctcaacatgctcatcgccctcatgagcgagaccgtcaacagtgtcgccactgacag base pairs
cgagtggatgtaggacgacgagttgtacgagtagcgggagtactcgctctggcagttgtcacagcggtgactgtc 2251 to 2325
ctggagcatctggaagctgcagaaagccatctctgtcctggagatggagaatggctattggtggtgcaggaagaa base pairs
gacctcgtagaccttcgacgtctttcggtagagacaggacctctacctcttaccgataaccaccacgtccttctt 2326 to 2400
gcagcgggcaggtgtgatgctgaccgttggcactaagccagatggcagccccgatgagcgctggtgcttcagggt base pairs
cgtcgcccgtccacactacgactggcaaccgtgattcggtctaccgtcggggctactcgcgaccacgaagtccca 2401 to 2475
J7
ggaggaggtgaactgggcttcatgg gagcagacgctgcctacgctgtgtgaggacccgtcaggggcaggtgtccc base pairs
cctcctccacttgacccgaagtacc ctcgtctgcgacggatgcgacacactcctgggcagtccccgtccacaggg 2476 to 2550
J8
tcgaactctcgagaaccctgtcctggcttcccctcccaaggaggatgaggatggtgcctctgaggaaaactatgt base pairs
agcttgagagctcttgggacaggaccgaaggggagggttcctcctactcctaccacggagactccttttgataca 2551 to 2625
gcccgtccagctcctccagtccaactgatggcccagatgcagcaggaggccagaggacagagcagaggatctttc base pairs
cgggcag gtcgaggaggtcaggttgact accgggtct acgtcgtcctccggtctcctgtctcgtctcctagaaag 2626 to 2700
J16
J15
J14
EcoRI
caaccacatctgctggctctggggtcccagtgaattctggtggcaaatatatattttcactaactc base pairs
gttggtgtagacgaccgagaccccagggtcacttaagaccaccgtttatatataaaagtgattgag 2701 to 2766

Appendix 1.5: alignment of VRs and TRP sequences. Identities are highlighted in red colour. Conservative substitutions are indicated with blue colour.

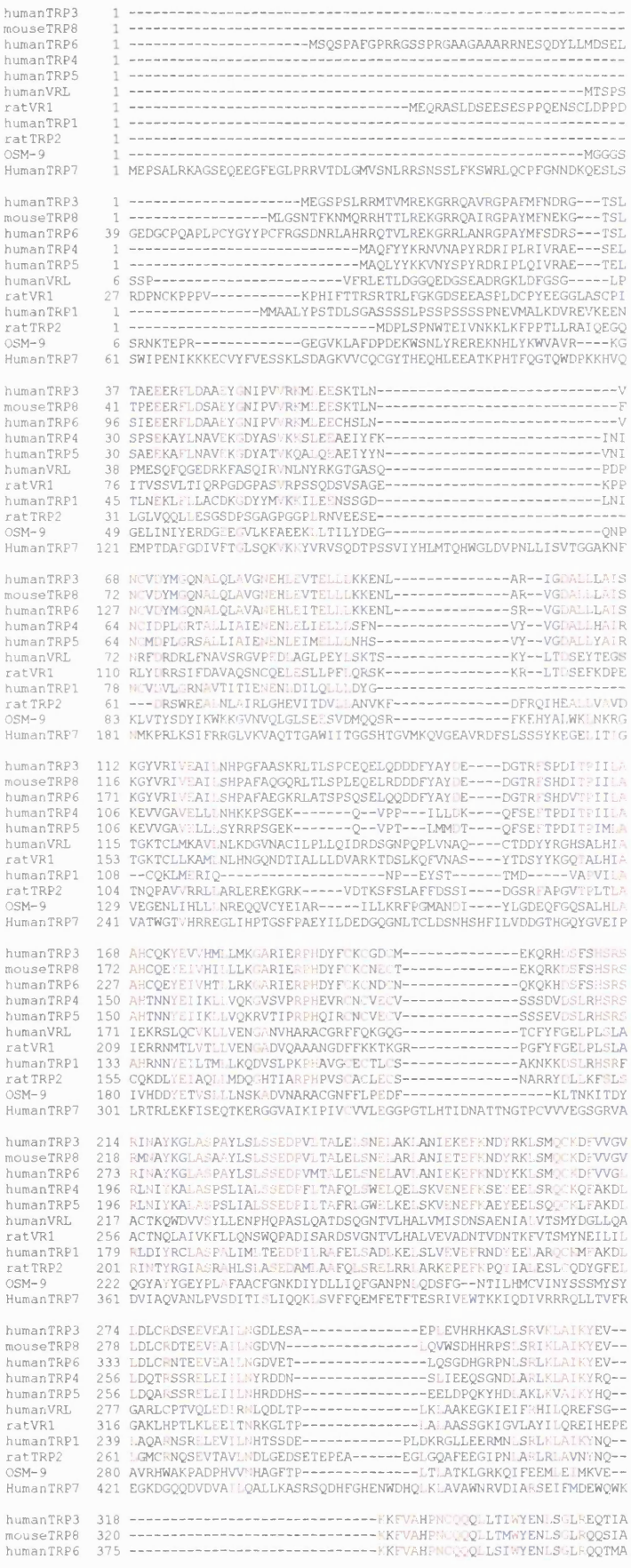

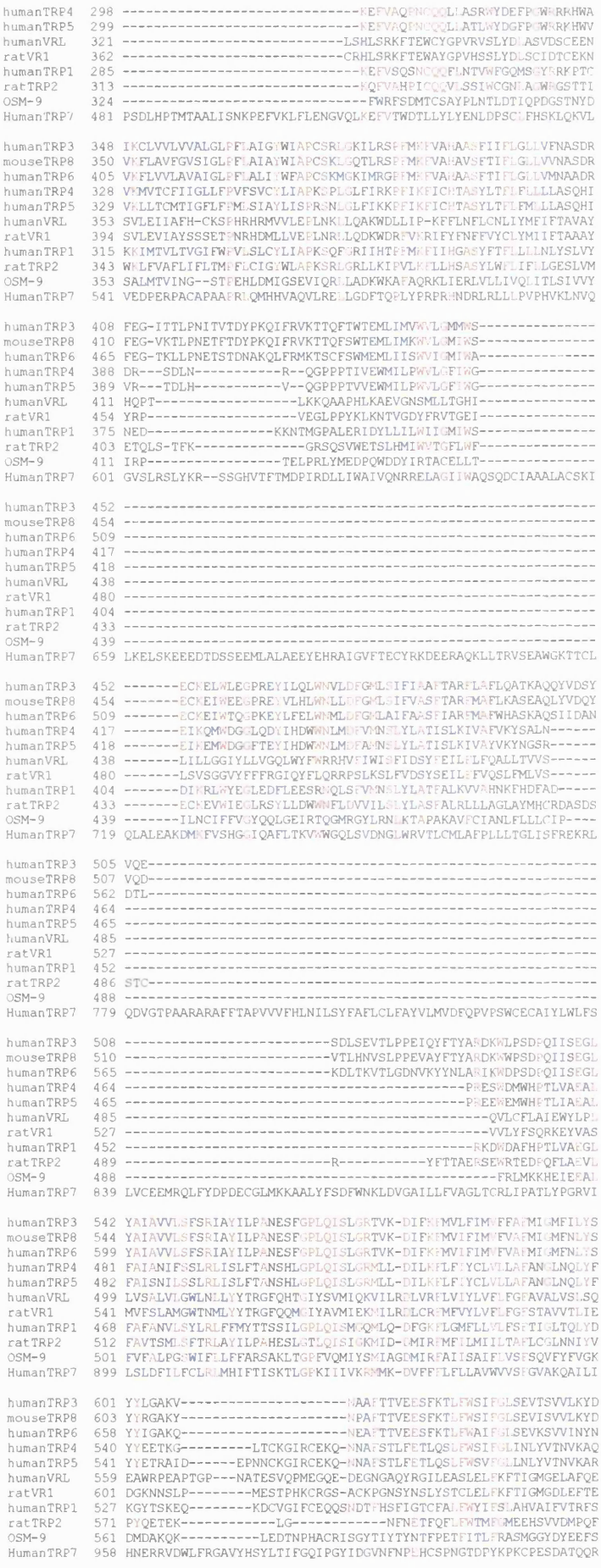

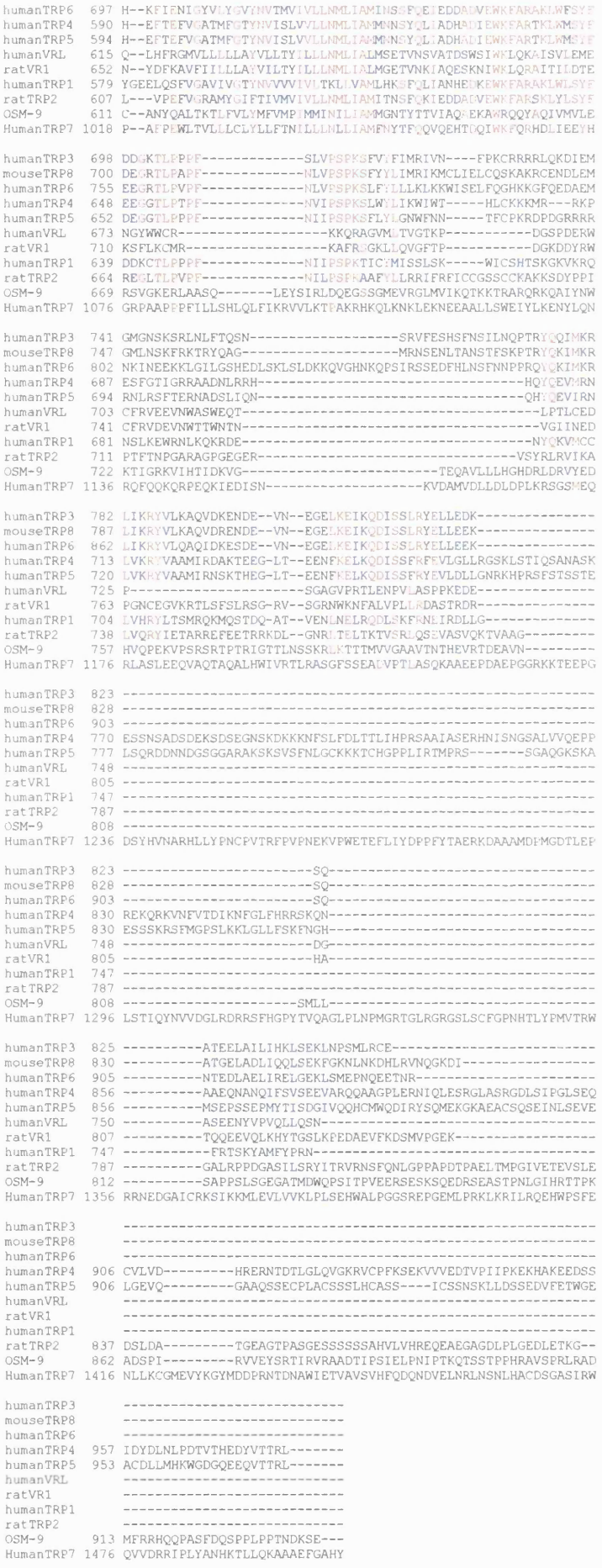

Appendix 1.6: the position of primers on the corresponding EST sequences

W44731

AA357145

N24224

W92895

AA281348

AA321554

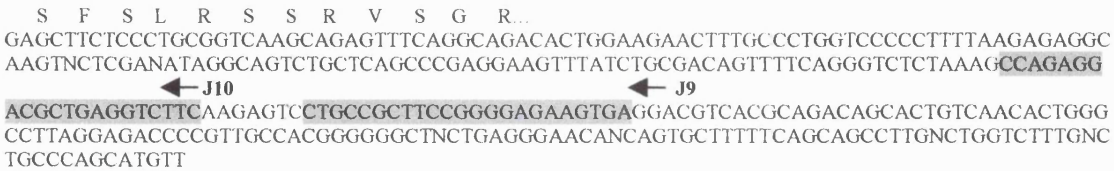

H21490

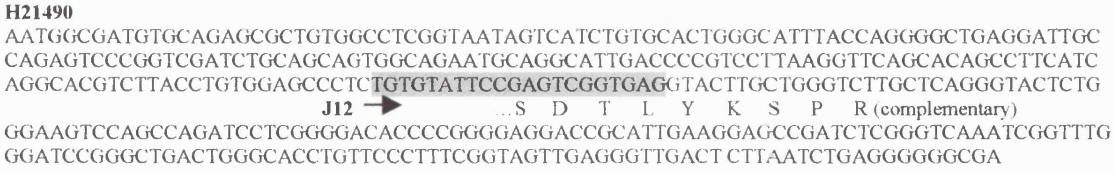

H20025

AATGGCGATGTGCAGAGCGCTGTGGCCTCGGTAATAGTCATCTGTGCACTGGGCATTTACCAGGGGCTGAGGATTGC
CAGAGTCCCGGTCGATCTGCAGCAGTGGCAGAATGCAGGCATTGACCCCGTCCTTAAGGTTCAGCACAGCCTTCATC
AGGCACGTCTTACCTGTGGAGCCCTCTGTGTATTCCGAGTCGGTGAGGTACTTGCTGGTCTTGCTCAGGTACTCTGGA
AGTCCAGC CAGATCCTCGGGGACACCCCGGGAGACCGCATTGAAGAGCCGATCTCGGTCAAATCGGTTTGGATCCG

J13 ...P D P
GCTGACTGGCACCTGTTCCCTTTCGGTAGTTGAGGTTGACTCTTATCTGAGG
Q S A (complementary)
GGCGAATTTCCGGTCCTCGCCCTGGGAACTGTGACTCCATGGGAGGCA

W92895

Y L P L L V S A L V L G...
TGTTTCCTGGCCATCGAGTGGTACCTGCCCCTGCTTGTGTCTGCGCTGGTGCTGGGCTGGCTGAACCTGCTTTACTATA
CACGTGGCTTCCAGCACACAGGCATCTACAGTGTCATGATCCAGAAGCCCTGGTGAGCCTGAGCCAGGANNTTGGCG
J17
CCCCGAAGCTCCTACAGGCCCCAATGCCACAGAGTCAGTGCAGCCCATGGAGGGACAGGAGGACGAGGGCAACGGG
GCCCAGTACAGGGGTATCCTGGAAGCCTCCTTGGAGCTCTTCAAATTCACCATCGGCATGGGCGAGCTGGCCTTCCAG
GAGCAGCTGCACTTCCGCGGCATGGGTGCTGCTGCTGCTNCTGGCCTACGTGCTGCTCACCTACATCCTGCTGCTCAA
CATGCTCATCGCCCTCATGGAGCGAGACCGTCAACAGGTNTCGC

THC176254

GCTAGCCTGTCCTGACAGGGgAGAGTTAAGCTCCCGtTCTCCACCGTGCCGGCTGgCAGGTGGGCTGAGGGTGACCGAGA
GACCAGAACCTGCTTGCTGGAGCTTAGTGCTCAGAGCTGGGGAGGGAGGTTCCGCCGCTCCTCTGCTGTCAGCGCCGGCA
GCCCCTCCCGGCTTCACTTCCTCCCGCAGCCCCTGCTACTGAGAAGCTCCGGGATCCCAGCAGCCGCCACGCCCTGGCCT
CAGCCTGCGGGGCTCCAGTCAGGCCAACACCGACCCGCAnTGGnGAGGAAGACAGGACCCTTGACATCTCCATCTGCACA
GAGGTCCTGGCTGGACgAGCAGCCTCCTCCTCCTAGGATGACCTCACCCTCCAGCTCTCCAGTTTTCAGGTTGGAGACAT
TAGATGGAGGCCAAGAAGATGGCTCTGAGGCGGACAGAGGAAAGCTGGATTTTGGGAGCGGGCTGCCTCCCATGGAGTCA
CAGTTCCAGGGCGAGGACCGGAAATTCGCCCCTCAGATAAGAGTCAACCTCAACTACCGAAAGGGAACAGGTGCCaGTCA
GCCGGATCCAAACCGATTTGACCgAGATCGGCTcTTCAATGCGGTCTCCCgGGGTGTCCCCGAGGATCTGGCTGGACTTC
CAGAGTACCTGAGCAAGACCAGCAAGTACCTCACCGACTCGGAATACACAGAGGGCTcCACAGGTAAGACGTGCCTGATG
AAGGCTGTGCTGAACCTTAAGGACGGGGTCAATGCCTGCATTCTGCCACTGCTGCAGATCGACCGGGACTCTGGCAATCC
TCAGCCCCTGGTAAATGCCCAGTGCACAGATGACTATTACCGAGGCCACAGCGCTCTGCACATCGCCATT

THC 161190 **J14**
TTAGTTAGTGAAAATATATATTTGCCACCAGAATTCACTGGGACCCCAGAGCCAGCAGATGTGGTTGGAAAGATCCT
J15 (complementary) ....Stop **J16**
CTGCTCTGTCCTCTGGCCTCCTGCTGCATCTGGGCCATCAGTTGGACTGGAGGAGCTGGACGGGCACATAGTTTTCCT
CAGAGGCACCATCCTCATCCTCCTTGGGAGGGGAAGCCAGGACAGGGTTCTCGAGAGTTCGAGGGACACCTGCCCCT
GACGGGTCCTCACACAGCGTAGGCAGCGTCTGCTCCCATGAAGCCCAGTTCACCTCCTCCACCCTGAAGCACCAGCG
CTCATCGGGGCTGCCATCTGGCTTAGTGCCAACGGTCAGCATCACACCTGCCCGCTGCTTCTTCCTGCACCACCAATA
GCCATTCTCCATCTCCAGGACAGAGATGGCTTTCTGCAGCTTCCAGATGCTCCAGCTGTCAGTGGCGACACTGTTGAC
GGTCTCGCTCATGAGGGCGATGAGCATGTTGAGCAGCAGGATGTAGGTGAGCAGCACGTAGGCCAGCAGCAGCAGC
AGCACCATGCCGCGGAAGTGCAGCTGCTCCTGGAAGGCCAGCTCGCCCATGCCGATGGTGAATTTGAAGAGCTCCAA
GGAGGCTTCCAGGATACCCCTGTACTGGGCCCCGTTGCCCTCGTCCTCCTGTCG

Appendix 1.7: DNA ladders used in experiments (information provided by GibcoBRL)

1 Kb DNA Ladder

1 Kb DNA Ladder is suitable for sizing linear double-stranded DNA fragments from 500 bp to 12 kb. Prepared from a plasmid containing repeats of a 1,018-bp DNA fragment (1), the ladder consists of 12 fragments ranging from 1,018 bp to 12,216 bp. In addition to these 12 bands, the ladder contains vector DNA fragments that range from 75 to 1,636 bp. The double-stranded ladder can be visualized on 0.5 to 1% agarose gels after ethidium bromide staining. This ladder may be radiolabeled using T4 polynucleotide kinase, T4 DNA polymerase, DNA polymerase I, or the large fragment of DNA polymerase I (Klenow fragment).

Concentration in storage buffer:

1 µg/µl in 10 mM Tris-HCl (pH 7.5), 50 mM NaCl, 0.1 mM EDTA.

100 bp DNA Ladder

100 bp DNA Ladder is suitable for sizing double-stranded DNA from 100 to 1,500 bp. Prepared from a plasmid containing repeats of a 100-bp DNA fragment, the ladder consists of 15 blunt-ended fragments ranging in length from 100 to 1,500 bp, at 100-bp increments, and an additional fragment at 2,072 bp. The double-stranded ladder can be visualized on 1% to 2% agarose gels after ethidium bromide staining. For easy reference on agarose gels, the 600-bp band is two- to three-times brighter than the other bands in the ladder. This ladder can be stained with ethidium bromide or radiolabeled using T4 polynucleotide kinase or T4 DNA polymerase.

Concentration in storage buffer:

1 µg/µl in 10 mM Tris-HCl (pH 7.5), 1 mM EDTA.

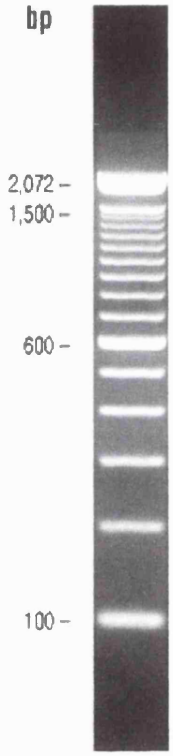

Appendix 1.8: restriction map of pcDNA3 (information provided by Invitrogen)

Comments for pcDNA3:
5446 nucleotides

CMV promoter: bases 209-863
T7 promoter: bases 864-882
Polylinker: bases 889-994
Sp6 promoter: bases 999-1016
BGH poly A: bases 1018-1249
SV40 promoter: bases 1790-2115
SV40 origin of replication: bases 1984-2069
Neomycin ORF: bases 2151-2945
SV40 poly A: bases 3000-3372
ColE1 origin: bases 3632-4305
Ampicillin ORF: bases 4450-5310

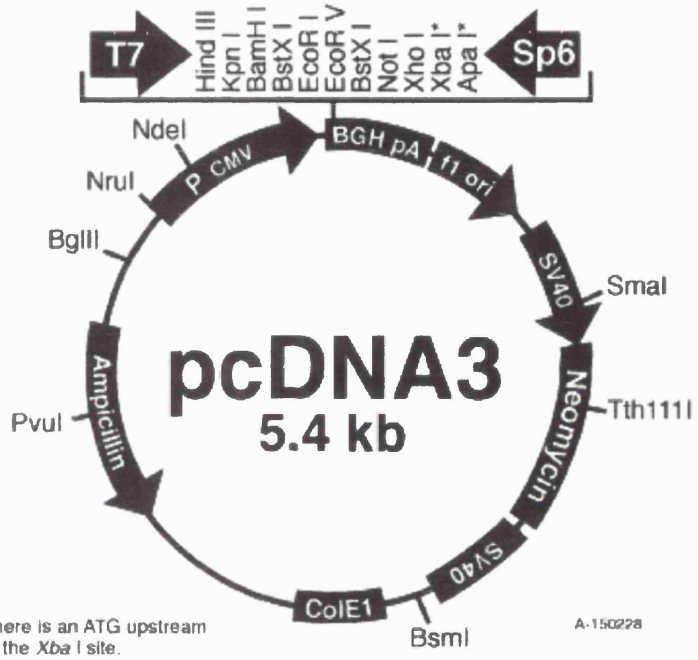

CHAPTER 2

Investigating the functional role of VR-L

APPENDIX

Appendix 2.1: prediction of transmembrane domains for rat VR-L

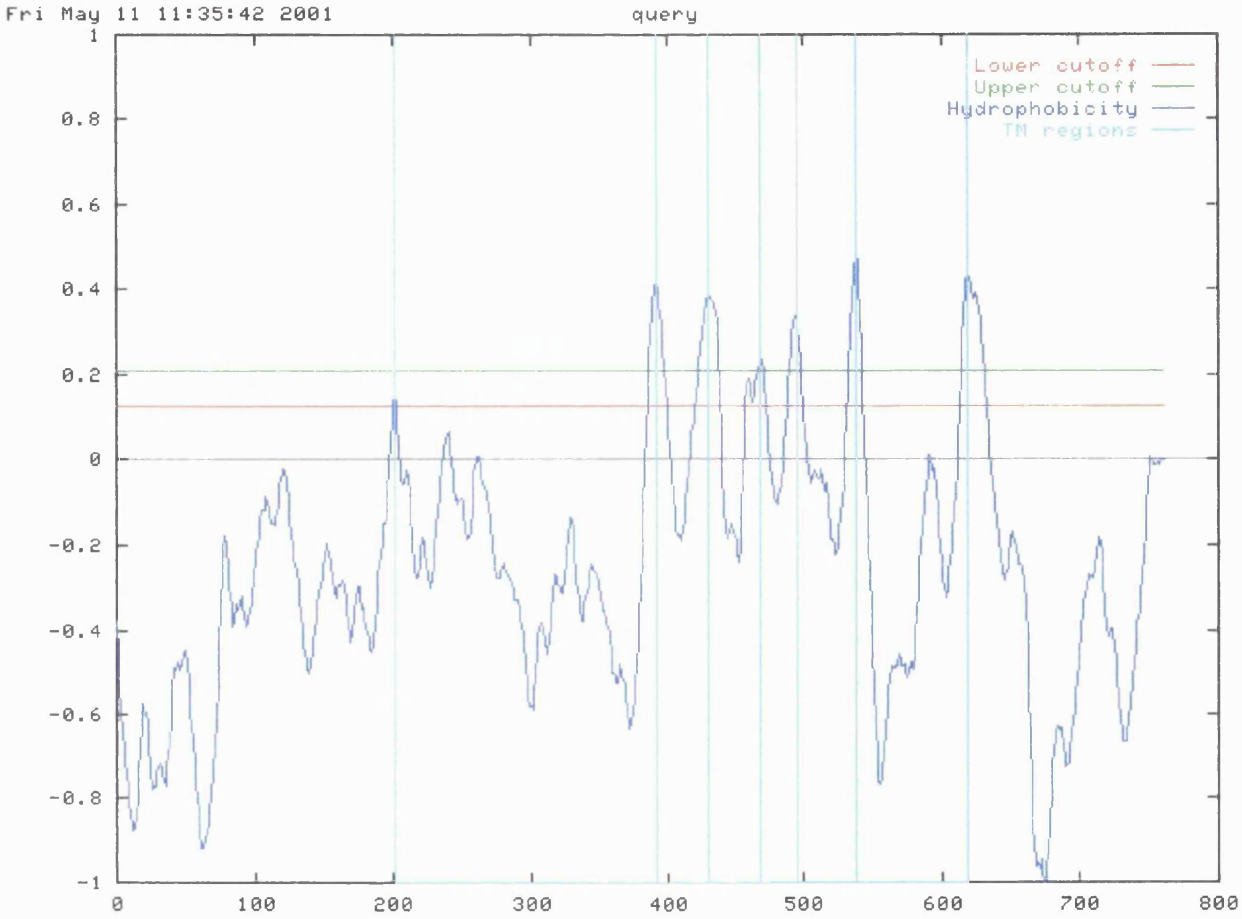

Number of helix	From amino acid No	To amino acid No	Length (a.a.)	orientation
1	393	412	20	Inside-outside
2	435	457	23	Outside-inside
3	471	489	19	Inside-outside
4	498	516	19	Outside-inside
5	540	556	17	Inside-outside
6	623	645	23	Outside-inside

Appendix 2.2: rat VR-L sequence cut with NarI and Eco47III. The position of the primers and enzyme restriction sites used for the insertion of the MYC epitope are shown.

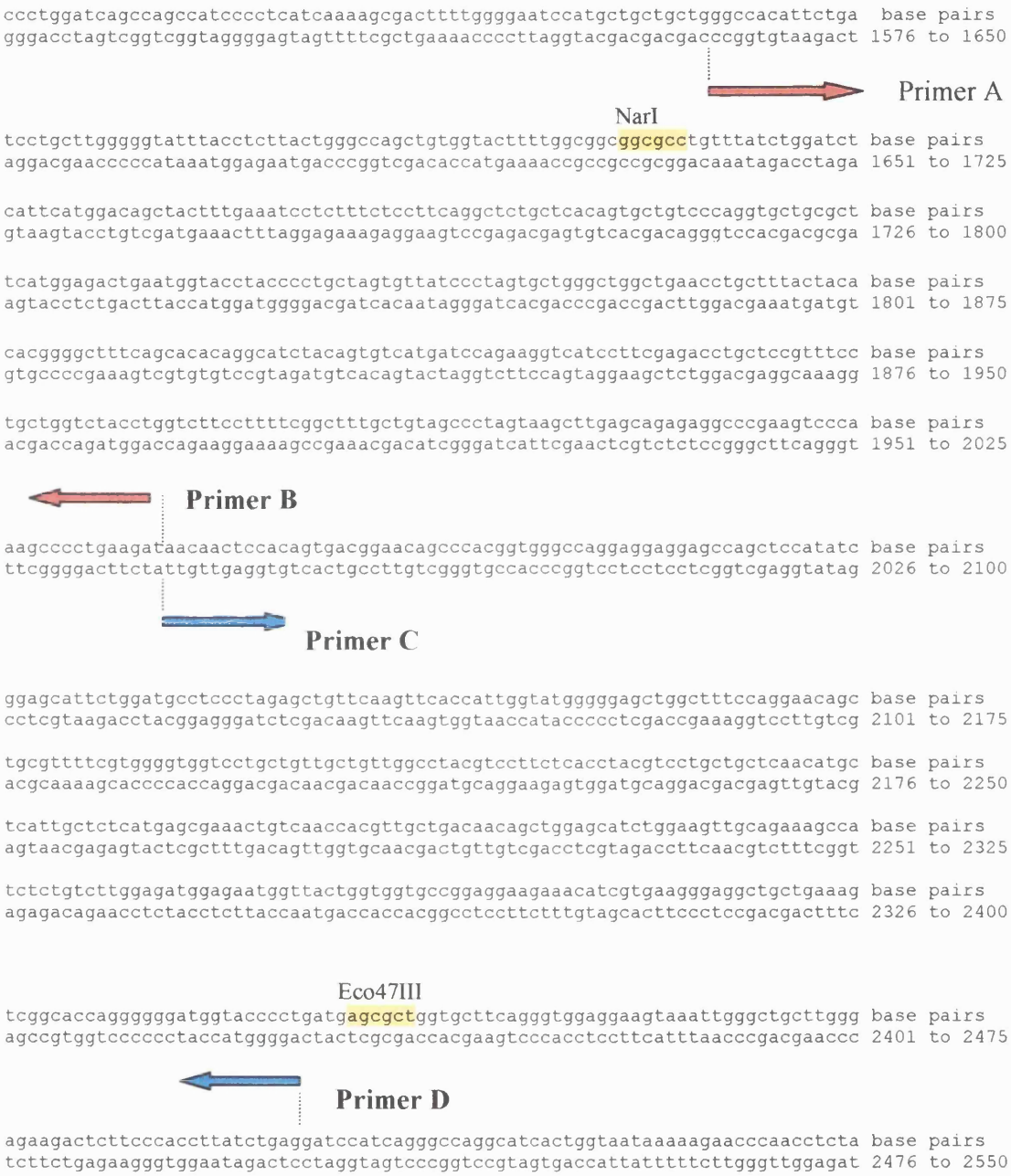

Appendix 2.3: rat VR-L cloned into pcDNAI. The positions of the primers and enzyme restriction sites used for the insertion of the MYC epitope are shown.

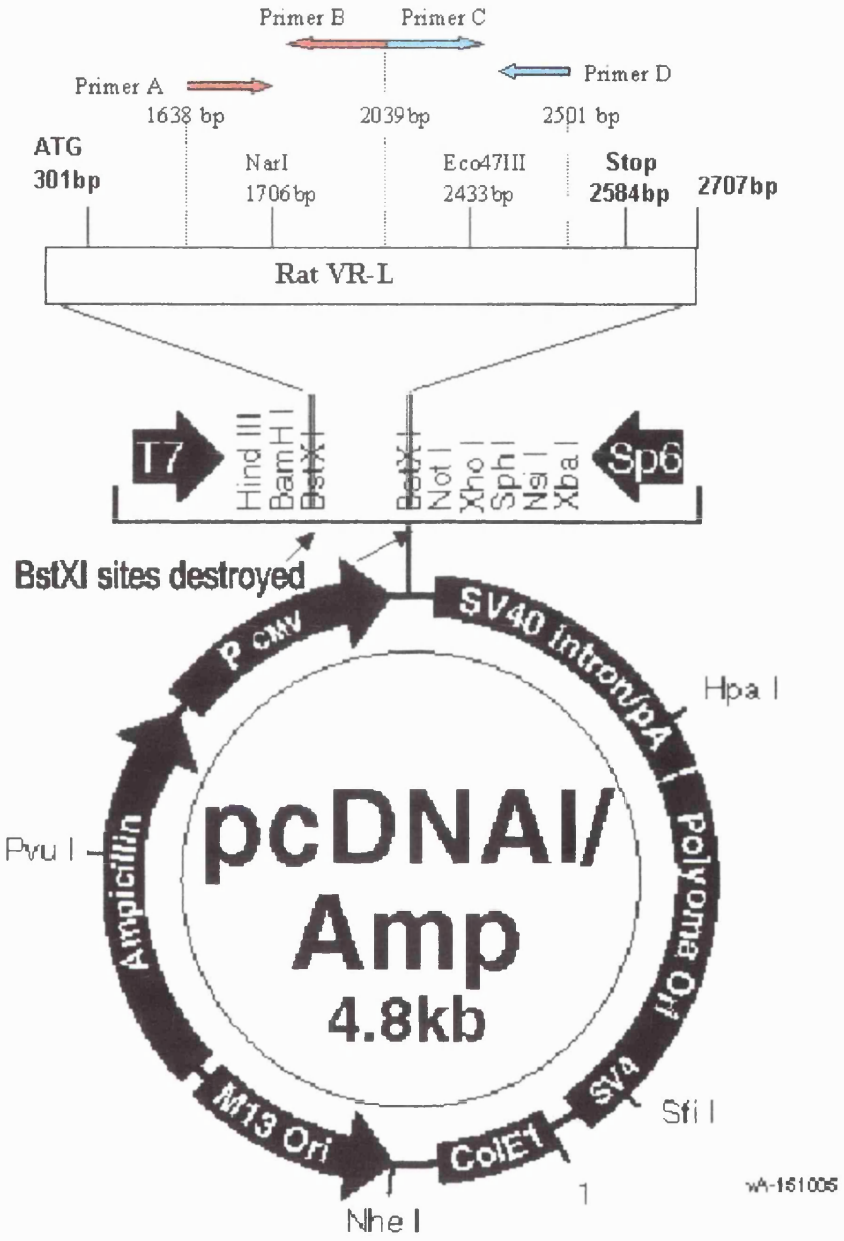

Appendix 2.4: DNA sequencing of the MYC epitope insertion between amino acids 561 and 562 of the rat VR-L sequence.

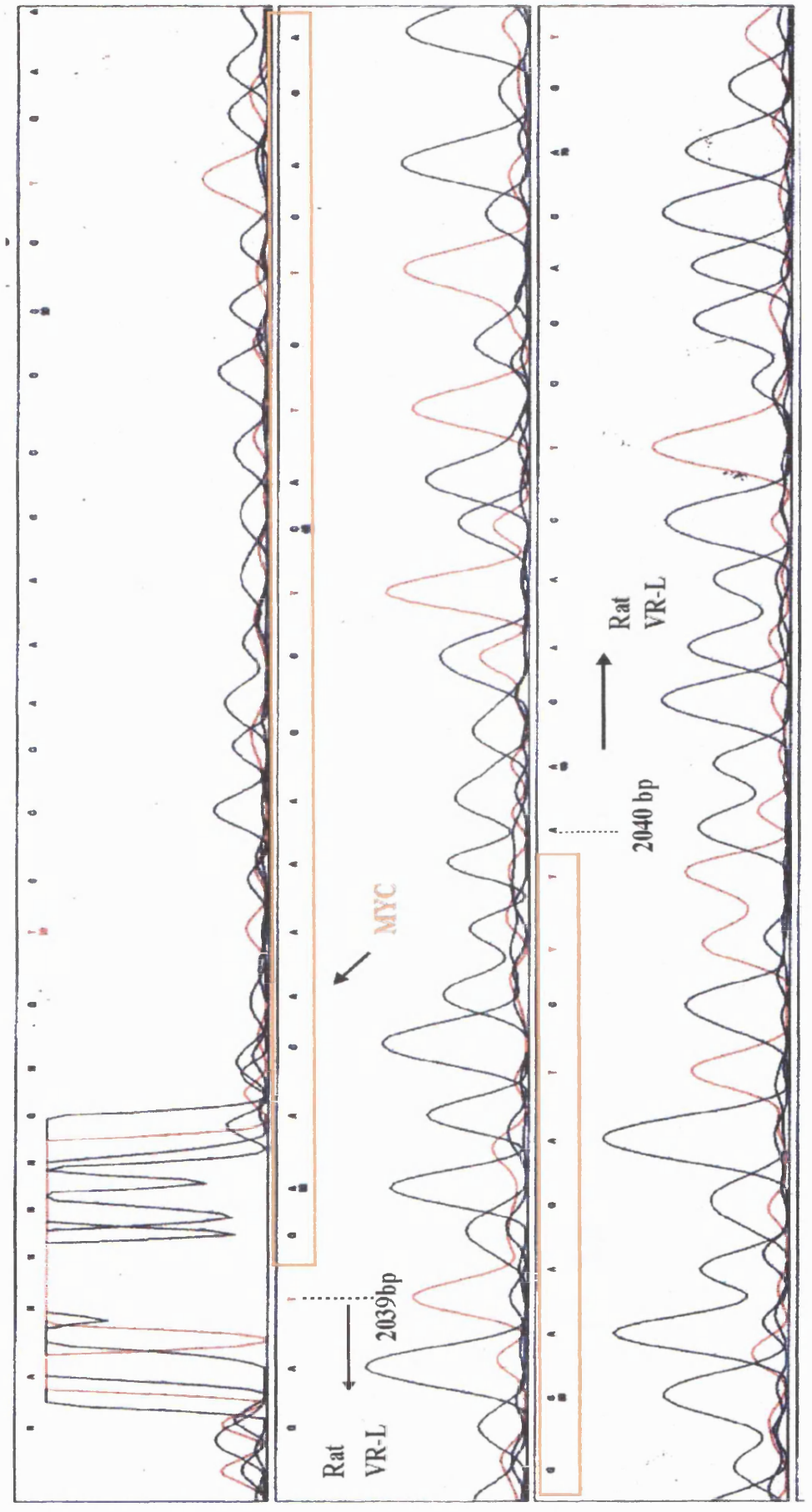

CHAPTER 3

Interactions between vanilloid receptors and members of the Transient Receptor Potential family of receptors

APPENDIX

Appendix 3.1: sequencing of constructs

Rat VR1/FLAG **Rat VR1/MYC**

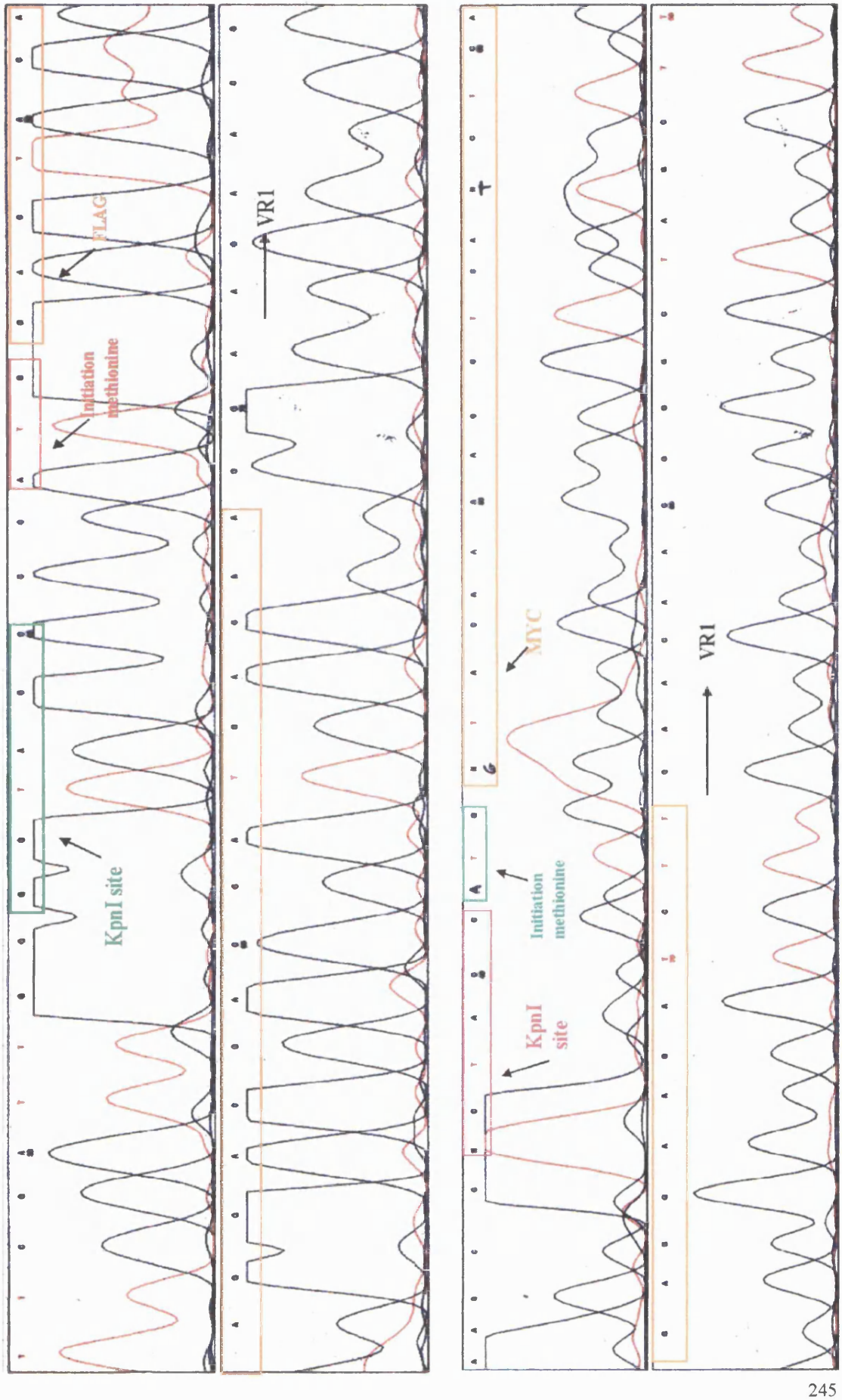

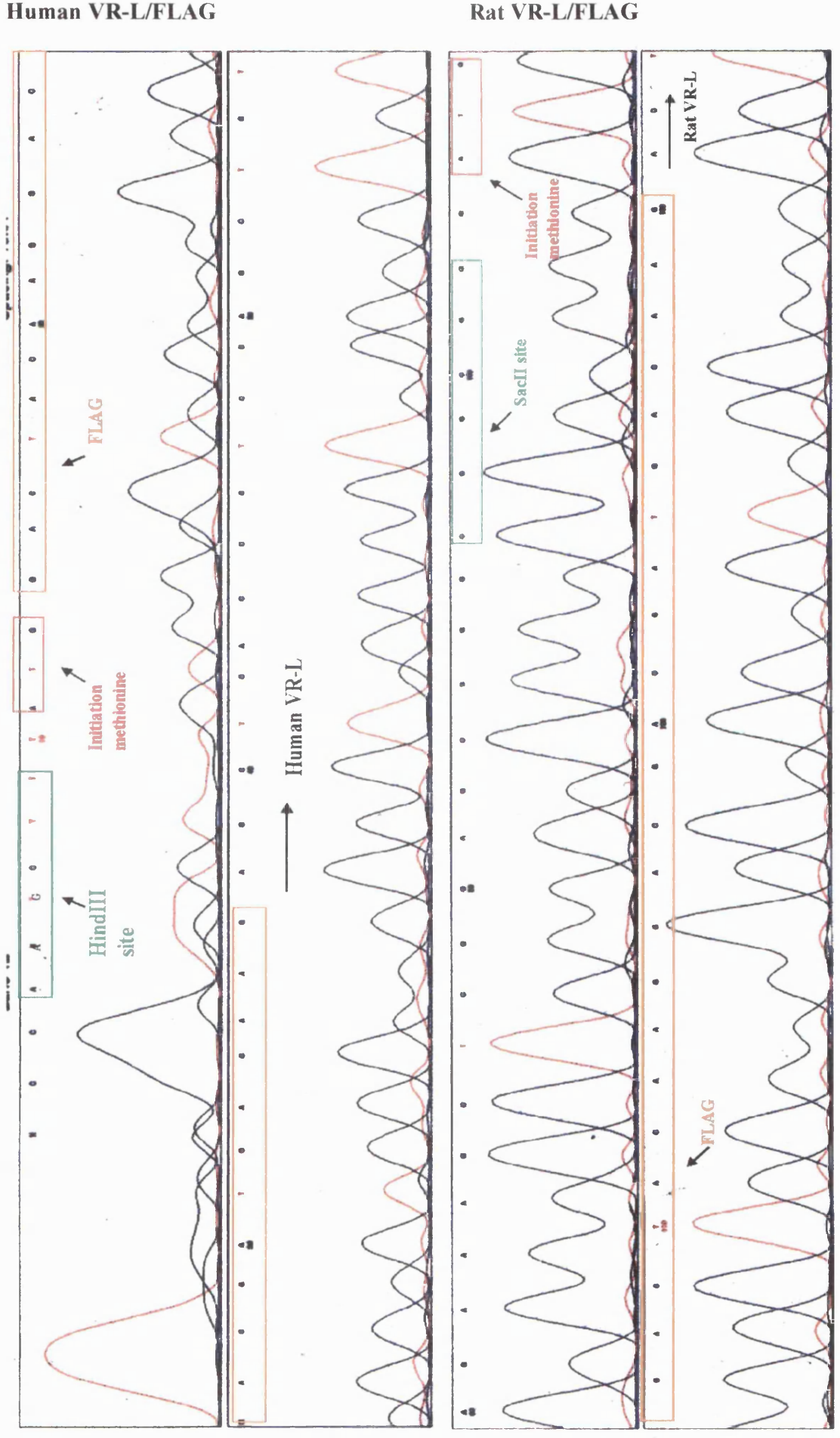
Human VR-L/FLAG
Rat VR-L/FLAG
HindIII site
Initiation methionine
FLAG
Human VR-L
SacII site
Initiation methionine
Rat VR-L
FLAG

Rat VR-L/MYC

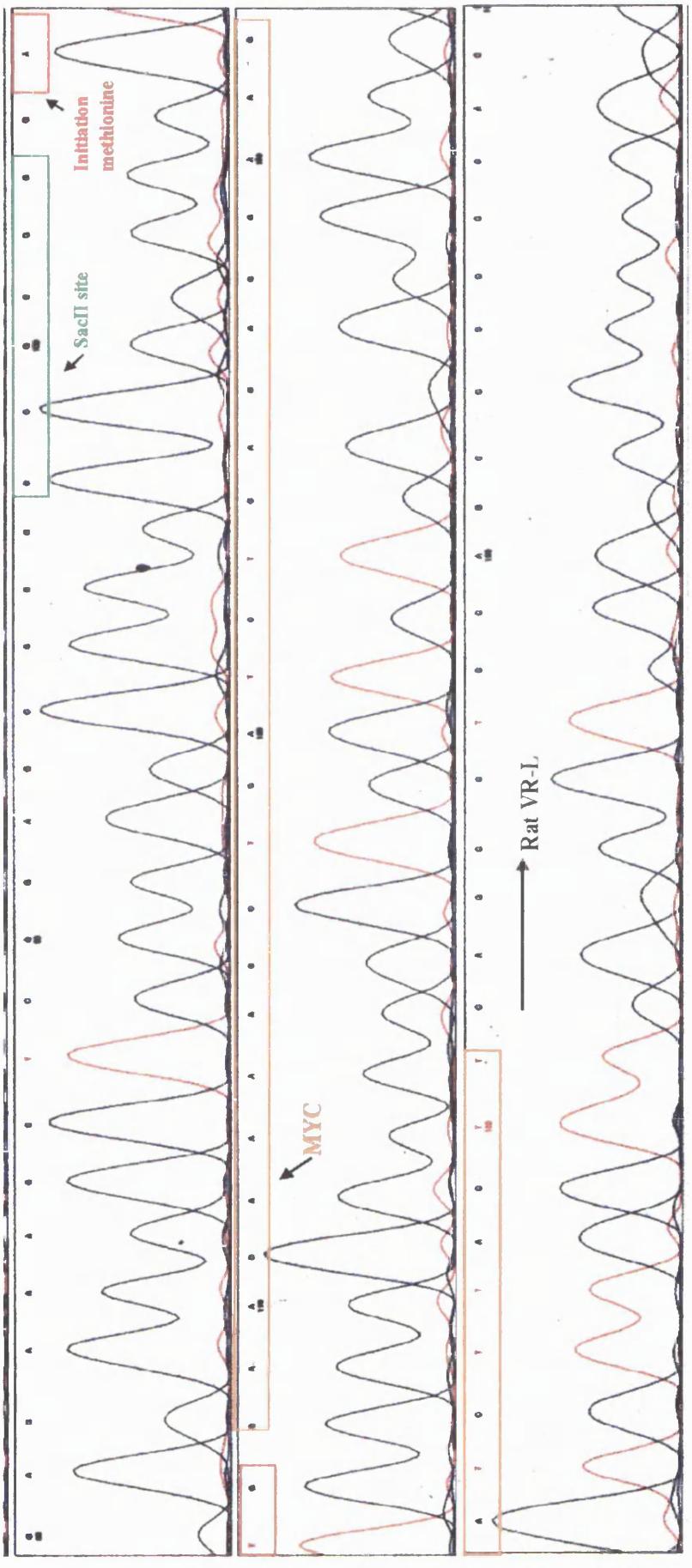

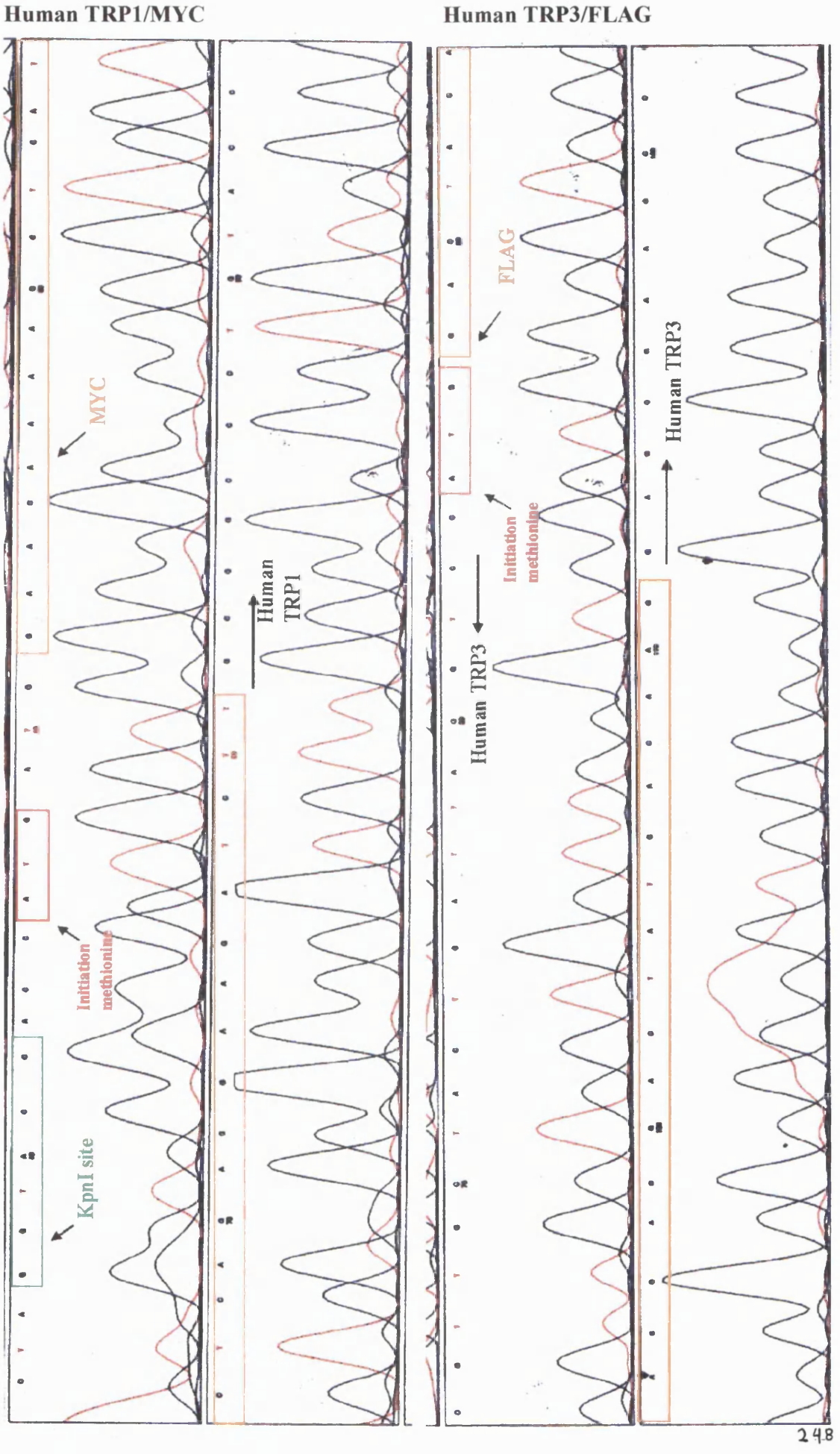
Human TRP1/MYC
Human TRP3/FLAG
MYC
Initiation methionine
KpnI site
Human TRP1
FLAG
Initiation methionine
Human TRP3
Human TRP3

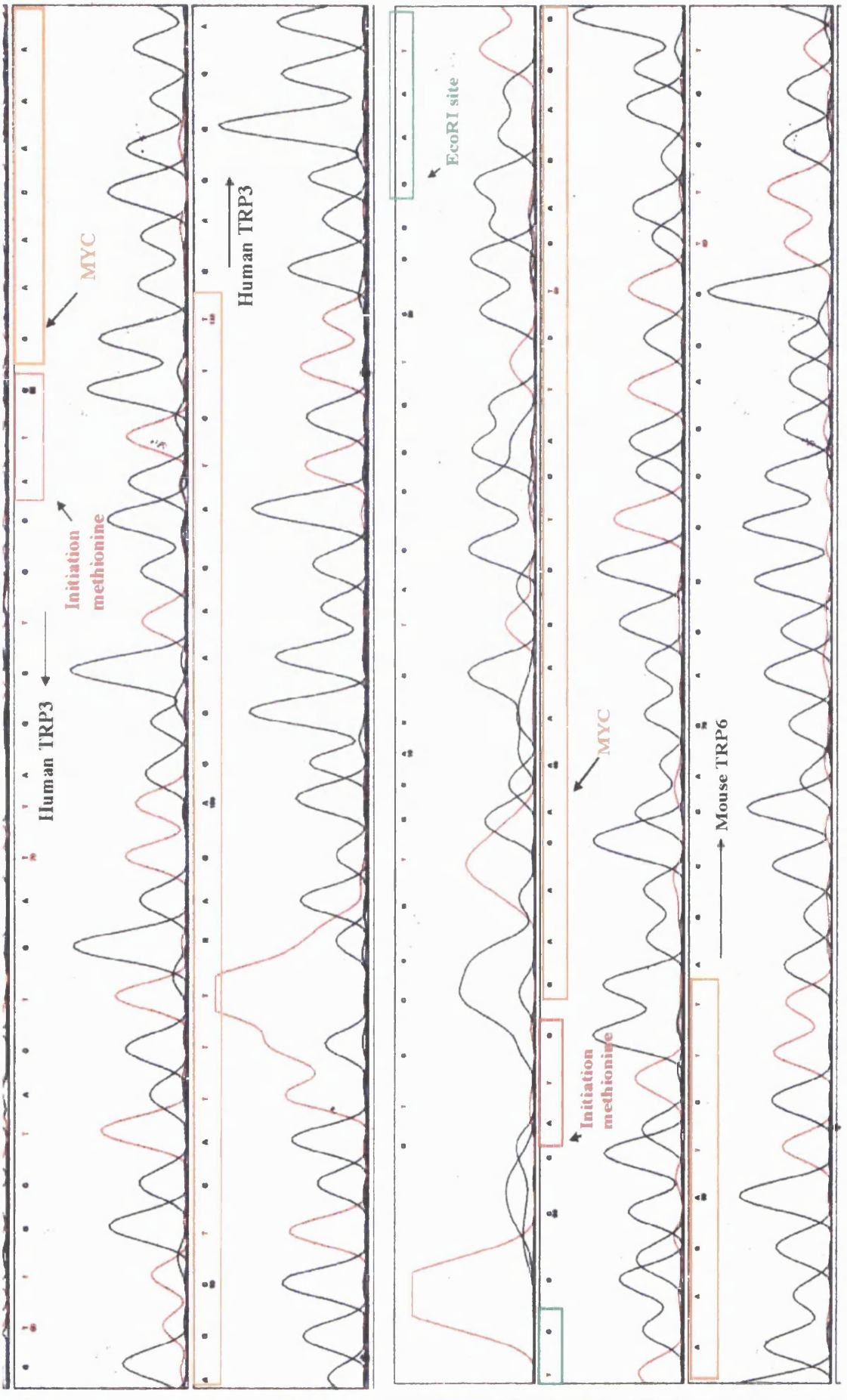
Human TRP3/MYC
Mouse TRP6/MYC
MYC
Initiation methionine
Human TRP3
Human TRP3
EcoRI site
MYC
Initiation methionine
Mouse TRP6

Appendix 3.2

3.2a: Rat VR1 cloned into pcDNA3. Caterina M. *et al.* Nature 389:816-824. Accession number: AAC53398

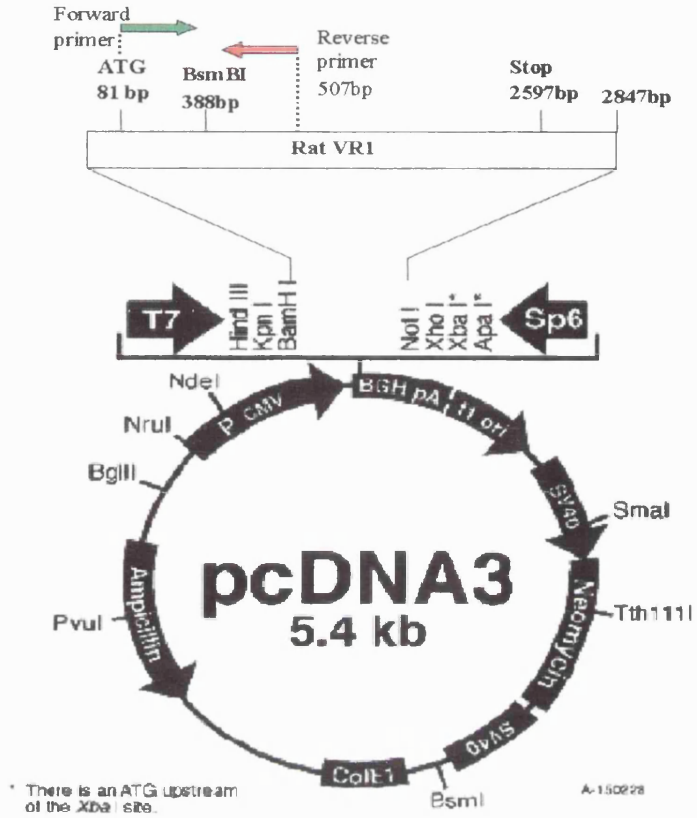

3.2b: Human VR-L cloned into pcDNA3. Caterina M. *et al.* Nature 398: 436-441. Accession number: AF129112 and AF103906

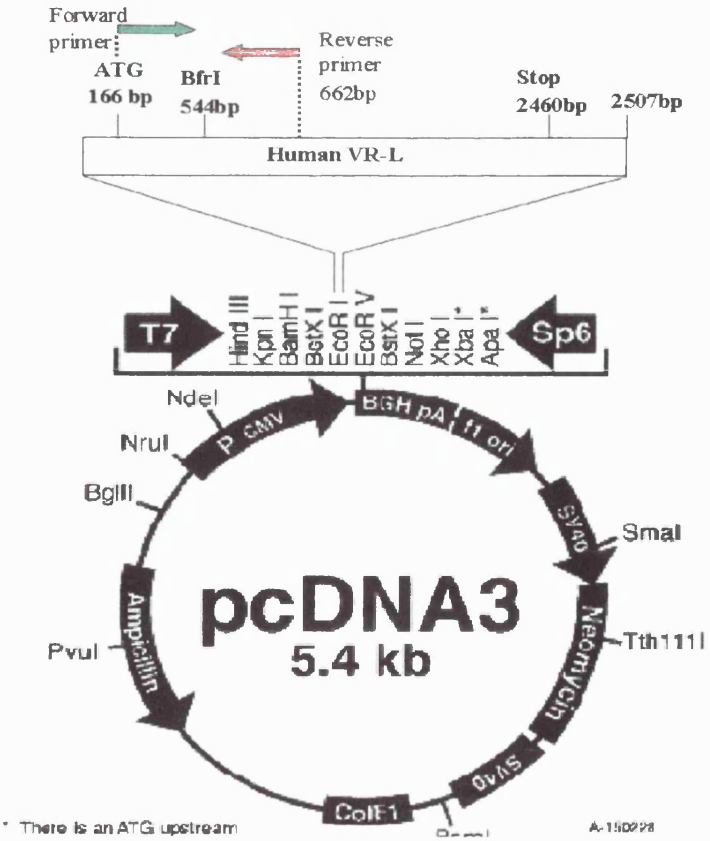

3.2c: Rat VR-L cloned into pcDNAI. Caterina M. *et al.* Nature 398: 436-441. Accession number :AF129113

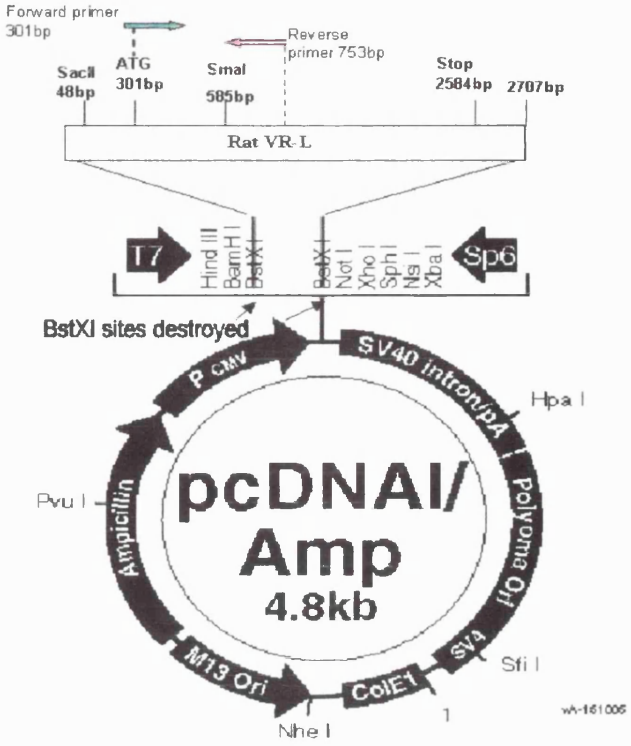

3.2d: Human TRP1 cloned into pcDNA3/Zeo. Zitt C. *et al.* Neuron 16: 1189-1196. Accession number: Z73903

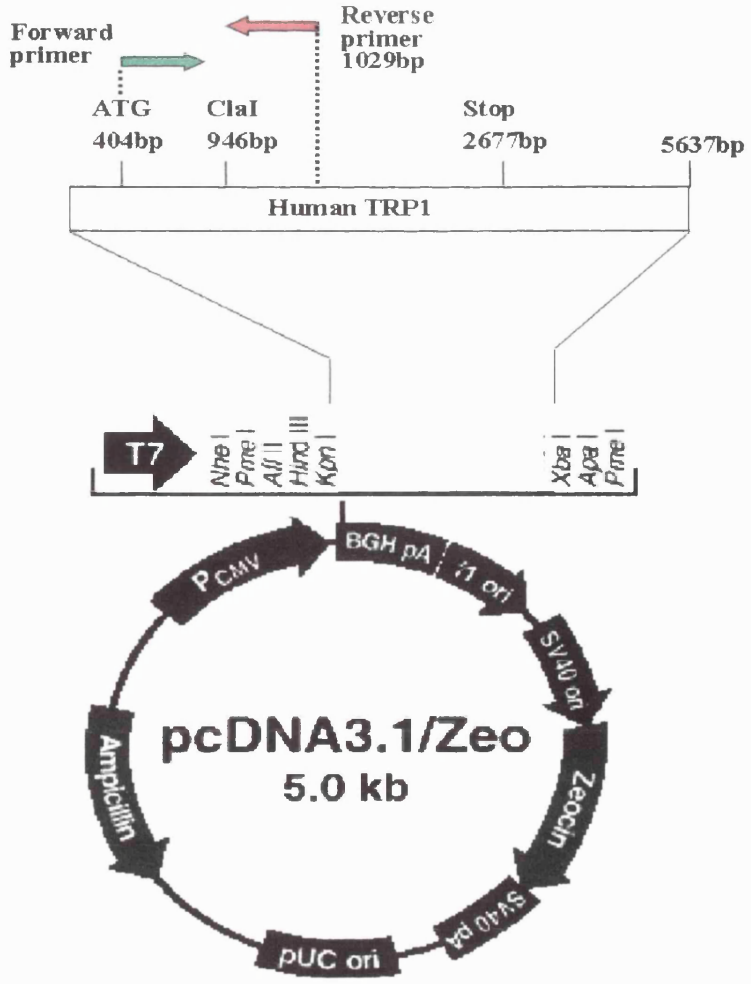

3.2e: Human TRP3 cloned into pcDNA3. Xu *et al.* Cell 89: 1155-1164. Accession number: NM_003305

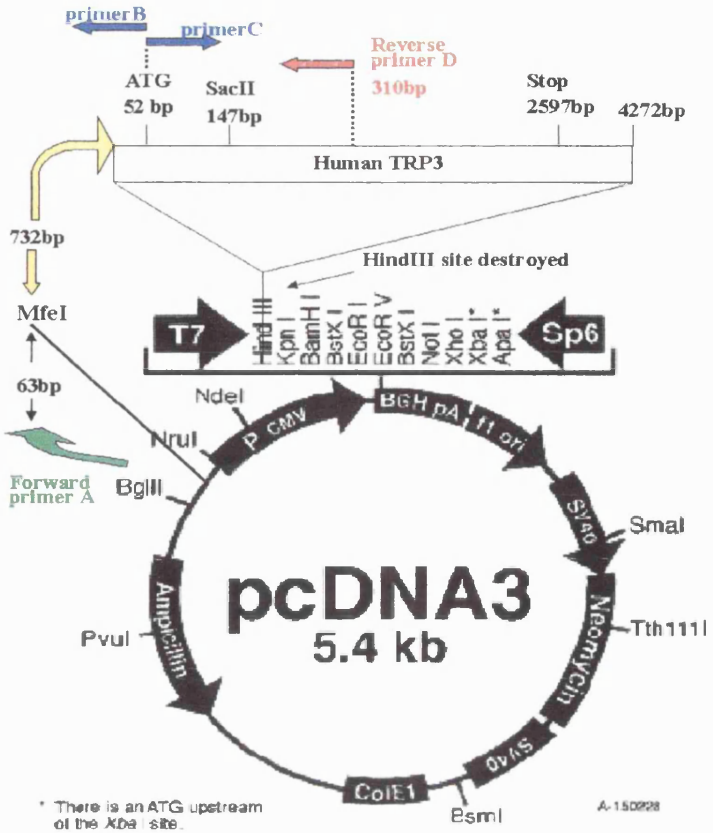

3.2f: Mouse TRP6 cloned into pSV.SPORT1. Zhu *et al.* Cell 85: 661-671. Accession number: MMU49069

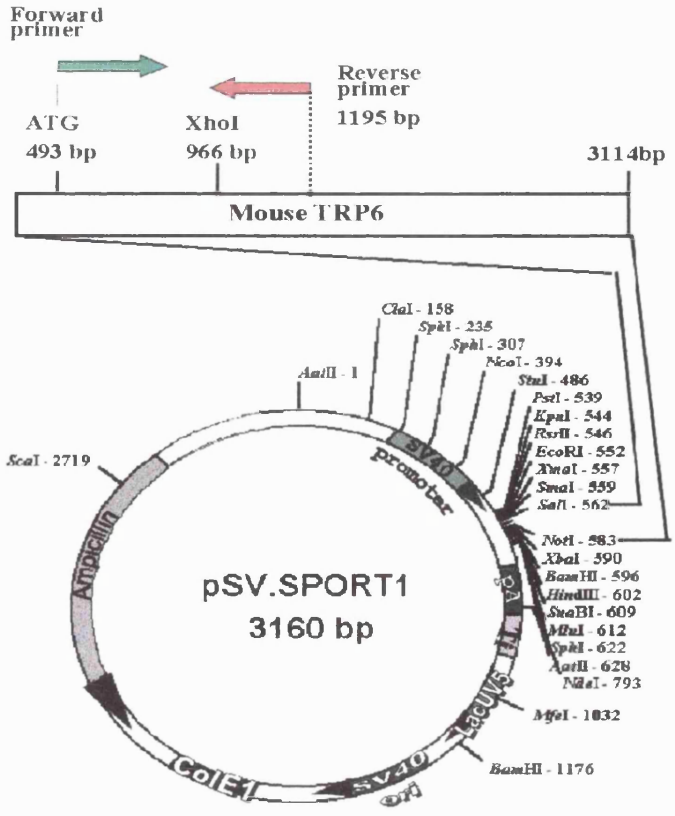

3.2g: rat VR-L subcloned into pcDNA3 via a SacII containing adaptor.

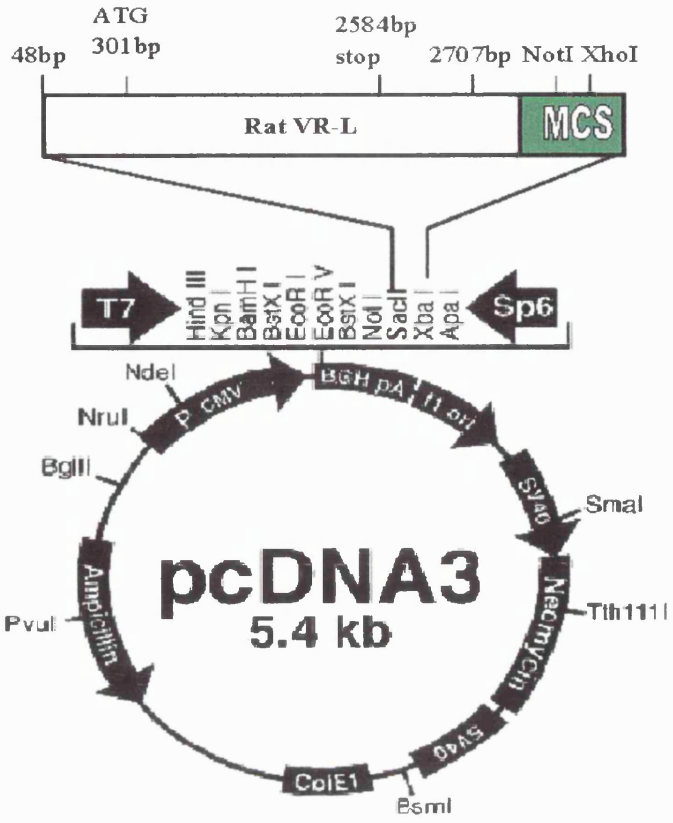

Appendix 3.4: Companies information

Alpha Diagnostics Intl.,Inc. 5415 Lost Lane , San Antonio, TX 78238 USA

Amersham Pharmacia Biotech UK Limited, Amersham Place, Little Chalfont, Buckinghamshire HP7 9NA, UK

BDH, VWR International Ltd – Poole, (UK Headquarters), Merck House, Poole, Dorset, BH15 1TD, UK

CALBIOCHEM-NOVABIOCHEM CORPORATION, 10394 Pacific Center Court, San Diego, California 92121 USA

CLONTECH Laboratories UK Ltd., Unit 2, Intec 2 Wade Road, Basingstoke, Hampshire RG24 8NE, UK

GibcoBRL, Invitrogen Ltd, 3 Fountain Drive, Inchinnan Business Park, Paisley PA4 9RF, UK

GlaxoSmithKline, Glaxo Wellcome UK Ltd., Stockley Park West, Uxbridge, Middlesex, UB11 1BT, UK

Jackson Immunoresearch Laboratories, Inc., 872 W. Baltimore Pike / P.O. Box 9 West Grove, PA 19390 USA

LabSales, Over Industrial Park, Norman Way, Over, Cambridgeshire CB4 5GR, UK

Merck, The Neuroscience Research Centre, Merck Sharp & Dohme Terlings Park Eastwick Road Harlow Essex CM20 2QR, UK

Metamorph Imaging system, Universal Imaging CorporationTM, 402 Boot Road, Downingtown PA 19335, UK

The Novartis Foundation, 41 Portland Place, London W1N 4BN, UK

Peptide Institute Inc., 4-1-2 INA, MINOH-SHI, OSAKA 562-8686, JAPAN

PerkinElmer Detection Systems, Unit 2 Astro House, Brants Bridge, Bracknell, Berkshire, RG129HW, UK

Promega UK, Delta House, Chilworth Research Centre, Southampton SO16 7NS, UK

Qiagen Ltd., Boundary Court, Gatwick Road, Crawley, West Sussex, RH10 9AX, UK

Roche Diagnostics Ltd., Bell Lane, Lewes East Sussex BN7 1LG, UK

Santa Cruz Biotechnology, Inc., 2161 Delaware Avenue, Santa Cruz, California 95060, USA

Sigma-Aldrich Company Ltd., Dorset, UK

Sigma-Genosys Ltd., London Road, Pampisford, Cambridge CB2 4EF, UK

Stratagene, 11011 North Torrey Pines Road, La Jolla, CA 92037 USA

REFERENCES

• Acs G., Lee J., Marquez V.E., Blumberg P.M. (1996) Distinct structure-activity relations for stimulation of 45Ca uptake and for high affinity binding in cultured rat dorsal root ganglion neurons and dorsal root ganglion membranes. Brain Res. Mol. Brain Res. 35(1-2):173-82

•Acs G., Biro T., Acs P., Modarres S., Blumberg P.M. (1997) Differential activation and desensitization of sensory neurons by resiniferatoxin. J. Neurosci. 17(14):5622-8

•Ahluwalia J., Urban L., Capogna M., Bevan S., Nagy I. (2000) Cannabinoid 1 receptors are expressed in nociceptive primary sensory neurons. Neuroscience 100(4): 685-688

• Albers K.M., Wright D.E., Davis B.M. (1994) Overexpression of nerve growth factor in epidermis of transgenic mice causes hypertrophy of the peripheral nervous system. J. Neurosci.14(3 Pt 2):1422-32

• Averbeck B., Izydorczyk I., Kress M. (2000) Inflammatory mediators release calcitonin gene-related peptide from dorsal root ganglion neurons of the rat. Neuroscience 98(1):135-40

• Basbaum A.I., Jessell T.M. (1991) The perception of pain Principles of neural science. Edited by Eric R. Kandel, James H. Schwartz, Thomas M. Jessell. New York, Elsevier p.p.473-489

• Basbaum A.I., Woolf C.J. (1999) Pain. Curr. Biol. 9(12): R429-431

• Bevan S., Forbes C.A. (1988) Membrane effects of capsaicin on dorsal root ganglion neurons in cell culture. J. Physiol. 398: 28P

• Bevan S., Szolcsanyi J. (1990) Sensory neuron-specific actions of capsaicin: mechanisms and applications. Trends Pharmacol. Sci. 11(8):330-3

•Bevan S., Yeats J. (1991) Protons activate a cation conductance in a sub-population of rat dorsal root ganglion neurones. J. Physiol. 433:145-61

• Bevan S., Hothi S., Hughes G., James I.F., Rang H.P., Shah K., Walpole C.S., Yeats J.C. (1992) Capsazepine: a competitive antagonist of the sensory neurone excitant capsaicin. Br. J. Pharmacol. 107(2):544-52

• Birder L.A., Kanai A.J., Kiss S., Burke N., Dineley K., Watkins S.C., Reynolds I.J., de Groat W.C., Caterina M.J. (2000) Evidence for functional VR1 receptors in bladder epithelial cells. Society for Neuroscience meeting, N.Orleans, abstract id: 6863

•Biro T., Maurer M., Modarres S., Lewin N.E., Brodie C., Acs G., Acs P., Paus R., Blumberg P.M. (1998a) Characterization of functional vanilloid receptors expressed by mast cells. Blood 91(4):1332-40

• Biro T., Brodie C., Modarres S., Lewin N.E., Acs P., Blumberg P.M. (1998b) Specific vanilloid responses in C6 rat glioma cells. Brain Res. Mol. Brain Res. 56(1-2):89-98

•Blumberg P.M., Szallasi A., Acs G. (1993) Resiniferatoxin-an ultrapotent capsaicin analogue. Capsaicin in the Study of Pain, New York: Academic, edited by J.N. Wood p.p. 45-62

• Boucher T.J., Okuse K., Bennett D.L., Munson J.B., Wood J.N., McMahon S.B. (2000a) Potent analgesic effects of GDNF in neuropathic pain states. Science 290(5489):124-7

•Boucher T.J., Kerr B.J., Ramer M.S., Thompson S.W.N., McMahon S.B. (2000b) Neurotrophic factor effects on pain-signaling systems. Proceedings of the 9th congress on pain. Progress in pain research and management.Vol 16, edited by Devor M., Rowbotham M.C. and Wiesenfeld-Hallin Z.IASP Press, Seattle, p.p.175-189

•Boulay G., Zhu X., Peyton M., Jiang M., Hurst R., Stefani E., Birnbaumer L. (1997) Cloning and expression of a novel mammalian homolog of Drosophila transient receptor potential (Trp) involved in calcium entry secondary to activation of receptors coupled by the Gq class of G protein. J. Biol. Chem. 272(47):29672-80

• Brand L., Berman E., Schwen R., Loomans M., Janusz J., Bohne R., Maddin C., Gardner J., Lahann T., Farmer R. *et al.* (1987) NE-19550: a novel, orally active anti-inflammatory analgesic. Drugs Exp. Clin. Res. 13(5): 259-265

•Caterina M.J. Schumacher M.A., Tominaga M., Rosen T.A., Levine J.D., Julius D. (1997) The capsaicin receptor: a heat-activated ion channel in the pain pathway. Nature 389(6653): 816-824

• Caterina MJ, Rosen TA, Tominaga M, Brake AJ, Julius D. (1999) A capsaicin-receptor homologue with a high threshold for noxious heat. Nature 398(6726):436-41

• Caterina M.J., Leffler A., Malmberg A.B., Martin W.J., Trafton J., Petersen-Zeitz K.R., Koltzenburg M., Basbaum A.I., Julius D. (2000) Impaired nociception and pain sensation in mice lacking the capsaicin receptor. Science 288(5464):306-13

•Cesare P., Dekker L.V., Sardini A., Parker P.J., McNaughton P.A. (1999a) Specific involvement of PKC-ε in sensitisation of the neuronal response to painful heat. Neuron 23: 617-624

•Cesare P., Young J., Wafford K., Clark S., England S., Delmas P., McNaughton P. Wood J.N. (1999b) Endogenous proton-gated cation channels in cell lines and *Xenopus* oocytes. J. Physiol. 518P p.p. 116P

• Chapman C.R., Stillman M. (1996) Chapter 7: Pathological pain. Pain and Touch. 2nd edition, edited by L.Kruger. London Academic Press, p.p. 315-341

•Chuang H.H., Prescott E.D., Kong H., Shields S., Jordt S.E., Basbaum A.I., Chao M.V, Julius D. (2001) Bradykinin and nerve growth factor release the capsaicin receptor from PtdIns(4,5)P2-mediated inhibition. Nature 411(6840):957-62

•Chyb S., Raghu P., Hardie R.C. (1999) Polyunsaturated fatty acids activate the Drosophila light-sensitive channels TRP and TRPL. Nature 397(6716):255-9

•Clapham D.E., Runnels L.W., Strubing C. (2001) The TRP ion channel family. Nat. Rev. Neurosci. 2(6):387-96

•Colbert H.A., Smith T.L., Bargmann C.I.(1997) OSM-9, a novel protein with structural similarity to channels, is required for olfaction, mechanosensation, and olfactory adaptation in Caenorhabditis elegans. J. Neurosci. 17(21):8259-69

•Colquhoun E.Q., Eldershaw T.P., Bennett K.L., Hall J.L., Dora K.A., Clark M.G. (1995) Functional and metabolic evidence for two different vanilloid (VN1 and VN2) receptors in perfused rat hindlimb. Life Sci. 57(2):91-102

•Davis J.B., Gray J., Gunthorpe M.J., Hatcher J.P., Davey P.T., Overend P., Harries M.H., Latcham J., Clapham C., Atkinson K., Hughes S.A., Rance K., Grau E., Harper A.J., Pugh P.L., Rogers D.C., Bingham S., Randall A., Sheardown S.A. (2000) Vanilloid receptor-1 is essential for inflammatory thermal hyperalgesia. Nature 405(6783):183-7

•De Petrocellis L., Bisogno T., Davis J.B., Pertwee R.G., Di Marzo V. (2000) Overlap between the ligand recognition properties of the anandamide transporter and the VR1 vanilloid receptor: inhibitors of anandamide uptake with negligible capsaicin-like activity. FEBS Lett. 483(1):52-6

• De Petrocellis L., Bisogno T., Maccarrone M., Davis J.B., Finazzi-Agro A., Di Marzo V. (2001) The activity of anandamide at vanilloid VR1 receptors requires facilitated transport across the cell membrane and is limited by intracellular metabolism. J. Biol. Chem. 276(16):12856-63

• Dedov V.N., Roufogalis B.D. (2000) Mitochondrial calcium accumulation following activation of vanilloid (VR1) receptors by capsaicin in dorsal root ganglion neurons. Neuroscience 95(1):183-8

•Delany N.S., Hurle M., Facer P., Alnadaf T., Plumpton C., Kinghorn I., See C.G., Costigan M., Anand P., Woolf C.J., Crowther D., Sanseau P., Tate S.N. (2001)

Identification and characterization of a novel human vanilloid receptor-like protein, VRL-2. Physiol. Genomics. 4(3):165-74

• Docherty R.J., Robertson B., Bevan S. (1991) Capsaicin causes prolonged inhibition of voltage-activated calcium currents in adult rat dorsal root ganglion neurons in culture. Neuroscience. 40(2):513-21

• Docherty R.J., Yeats J.C., Bevan S., Boddeke H.W. (1996) Inhibition of calcineurin inhibits the desensitization of capsaicin-evoked currents in cultured dorsal root ganglion neurones from adult rats. Pflugers Arch.431(6):828-37

• Doyle D.A., Morais Cabral J., Pfuetzner R.A., Kuo A., Gulbis J.M., Cohen S.L., Chait B.T., MacKinnon R. (1998) The structure of the potassium channel: molecular basis of K+ conduction and selectivity. Science 280(5360):69-77

• Dray A., Bettaney J., Forster P. (1990a) Actions of capsaicin on peripheral nociceptors of the neonatal rat spinal cord-tail in vitro: dependence of extracellular ions and independence of second messengers. Br. J. Pharmacol. 101(3):727-33

• Dray A., Forbes C.A., Burgess G.M. (1990b) Ruthenium red blocks the capsaicin-induced increase in intracellular calcium and activation of membrane currents in sensory neurones as well as the activation of peripheral nociceptors in vitro. Neurosci. Lett. 110(1-2):52-9

•Duncan L.M., Deeds J., Hunter J., Shao J., Holmgren L.M., Woolf E.A., Tepper R.I., Shyjan A.W. (1998) Down-regulation of the novel gene melastatin correlates with potential for melanoma metastasis. Cancer Res. 58(7): 1515-1520

•Fasolato C., Hoth M., Penner R. (1993) A GTP-dependent step in the activation mechanism of capacitative calcium influx. J. Biol. Chem. 268(28):20737-40

• Funayama M., Goto K., Kondo H. (1996) Cloning and expression localization of cDNA for rat homolog of TRP protein, a possible store-operated calcium (Ca2+) channel. Brain Res. Mol. Brain Res. 43(1-2):259-66

• Garcia R., Liapi A., Cesare P., Bonnert T., Wafford K., Clark S., Young J., Delmas P., Whiting P., McNaughton P. and Wood J.N. (1999) VR-L, a vanilloid receptor-like orphan receptor is expressed in T-cells and sensory neurons. Physiological Society meeting in University College London 518P: 126P

•Garcia-Martinez C., Morenilla-Palao C., Planells-Cases R., Merino J.M., Ferrer-Montiel A. (2000) Identification of an aspartic residue in the P-loop of the vanilloid receptor that modulates pore properties. J. Biol. Chem. 275(42):32552-8

•Grynkiewich G., Poenie M., Tsien R.Y. (1985) A new generation of Ca^{+2} indicators with greatly improved fluorescence properties. J. Biol. Chem. 260(6): 3440-3450

• Guo A., Vulchanova L., Wang J., Li X., Elde R. (1999) Immunocytochemical localization of the vanilloid receptor 1 (VR1): relationship to neuropeptides, the P2X3 purinoceptor and IB4 binding sites. Eur. J. Neurosci. 11(3):946-58

•Guo A., Olson T., Wang J., Elde R. (2000) A comparative study of thermal and pH sensitive transducers in sensory neurons of rats and mice. Society for Neuroscience meeting, N.Orleans, abstract id: 12998

• Habelt C., Kessler F., Distler C., Kress M., Reeh P.W. (2000) Interactions of inflammatory mediators and low pH not influenced by capsazepine in rat cutaneous nociceptors. Neuroreport 11(5):973-6

• Hawkins L.M., Chazot P.L., Stephenson F.A. (1999) Biochemical evidence for the co-association of three N-methyl-D-aspartate (NMDA) R2 subunits in recombinant NMDA receptors. J. Biol. Chem. 274(38):27211-8

• Hayes P., Meadows H.J., Gunthorpe M.J., Harries M.H., Duckworth D.M., Cairns W., Harrison D.C., Clarke C.E., Ellington K., Prinjha R.K., Barton A.J., Medhurst A.D., Smith G.D., Topp S., Murdock P., Sanger G.J., Terrett J., Jenkins O., Benham C.D., Randall A.D., Gloger I.S., Davis J.B. (2000) Cloning and functional expression of a human orthologue of rat vanilloid receptor-1. Pain 88(2):205-15

•Hoenderop J.G., van der Kemp A.W., Hartog A., van de Graaf S.F., van Os C.H., Willems P.H., Bindels R.J. (1999a) Molecular identification of the apical Ca2+ channel in 1, 25-dihydroxyvitamin D3-responsive epithelia. J. Biol. Chem. 274(13):8375-8

•Hoenderop J.G., van der Kemp A.W., Hartog A., van Os C.H., Willems P.H., Bindels R.J. (1999b) The epithelial calcium channel, ECaC, is activated by hyperpolarization and regulated by cytosolic calcium. Biochem. Biophys. Res. Commun.261(2):488-92

• Hofmann T., Obukhov A.G., Schaefer M., Harteneck C., Gudermann T., Schultz G. (1999) Direct activation of human TRPC6 and TRPC3 channels by diacylglycerol. Nature 397(6716):259-63

• Hu Y., Vaca L., Zhu X., Birnbaumer L., Kunze D.L., Schilling W.P. (1994) Appearance of a novel Ca2+ influx pathway in Sf9 insect cells following expression of the transient receptor potential-like (trpl) protein of Drosophila. Biochem. Biophys. Res. Commun. 201(2):1050-6

•Hudson L.J., Bevan S., Wotherspoon G., Gentry C., Fox A., Winter J. (2001) VR1 protein expression increases in undamaged DRG neurons after partial nerve injury. Eur. J. Neurosci. 13: 2105-2114

•Huminiecki L., Bicknell R. (2000) In silico cloning of novel endothelial-specific genes. Genome Res. 10(11):1796-806

• Hwang S.W., Cho H., Kwak J., Lee S.Y., Kang C.J., Jung J., Cho S., Min K.H., Suh Y.G., Kim D., Oh U. (2000) Direct activation of capsaicin receptors by products of lipoxygenases: endogenous capsaicin-like substances. Proc. Natl. Acad. Sci. U S A. 97(11):6155-60

•Inoue R., Okada T., Onoue H., Hara Y., Shimizu S., Naitoh S., Ito Y., Mori Y. (2001) The transient receptor potential protein homologue TRP6 is the essential component of vascular alpha(1)-adrenoceptor-activated Ca(2+)-permeable cation channel. Circ. Res. 88(3):325-32

• Jancso N., Jancso-Gabor A., Szolcsanyi J. (1967) Direct evidence for neurogenic inflammation and its prevention by denervation and by pretreatment with capsaicin. Br. J. Pharmacol. 31(1):138-51

• Jancso G., Wollemann M. (1977) The effect of capsaicin on the adenylate cyclase activity of rat brain. Brain Res. 123(2):323-9

•Jancso G., Kiraly E. (1981) Sensory neurotoxins: chemically induced selective destruction of primary sensory neurons. Brain Res. 210(1-2):83-9

•Jancso G., Kiraly E., Joo F., Such G., Nagy A. (1985) Selective degeneration by capsaicin of a subpopulation of primary sensory neurons in the adult rat. Neurosci. Lett. 59(2):209-14.

•Jordt S.E., Tominaga M., Julius D. (2000) Acid potentiation of the capsaicin receptor determined by a key extracellular site. Proc. Natl. Acad. Sci. U S A. 97(14): 8134-9

• Jung J., Hwang S.W., Kwak J., Lee S.Y., Kang C.J., Kim W.B., Kim D., Oh U. (1999) Capsaicin binds to the intracellular domain of the capsaicin-activated ion channel. J. Neurosci. 1999 Jan 15;19(2):529-38.

•Jungnickel M.K., Marrero H., Birnbaumer L., Lemos J.R., Florman H.M. (2001) Trp2 regulates entry of Ca2+ into mouse sperm triggered by egg ZP3. Nat. Cell Biol. 3(5):499-502

• Kanzaki M., Nie L., Shibata H., Kojima I. (1997) Activation of a calcium-permeable cation channel CD20 expressed in Balb/c 3T3 cells by insulin-like growth factor-I. J. Biol. Chem. 272(8):4964-9

•Kanzaki M., Zhang Y.Q., Mashima H., Li L., Shibata H., Kojima I. (1999) Translocation of a calcium-permeable cation channel induced by insulin-like growth factor-I. Nat. Cell Biol.1(3):165-70

•Kedei N., Szabo T., Lile J.D., Treanor J.J., Olah Z., Iadarola M.J., Blumberg P.M. (2001) Analysis of the native quaternary structure of vanilloid receptor 1. J. Biol. Chem. 276(30): 28613-28619

• Khasar S.G., Lin Y.H., Martin A., Dadgar J., McMahon T., Wang D., Hundle B., Aley K.O., Isenberg W., McCarter G., Green P.G., Hodge C.W., Levine J.D., Messing R.O. (1999) A novel nociceptor signaling pathway revealed in protein kinase C epsilon mutant mice. Neuron 24(1):253-60

•Kiselyov K., Muallem S. (1999) Fatty acids, diacylglycerol, Ins(1,4,5)P3 receptors and Ca2+ influx. Trends Neurosci. 22(8):334-7

•Kwak J., Wang M.H., Hwang S.W., Kim T.Y., Lee S.Y., Oh U. (2000) Intracellular ATP increases capsaicin-activated channel activity by interacting with nucleotide-binding domains. J. Neurosci. 20(22):8298-304

• Lawson S.N. (1996) Peptides and cutaneous polymodal nociceptor neurones. Prog. Brain Res. 113:369-85

•Lee Y.S., Lee J.A., Jung J., Oh U., Kaang B.K. (2000) The cAMP-dependent kinase pathway does not sensitize the cloned vanilloid receptor type 1 expressed in Xenopus oocytes or Aplysia neurons. Neurosci. Lett. 288(1):57-60

• Levine J.D., Lam D., Taiwo Y.O., Donatoni P., Goetzl E.J. (1986) Hyperalgesic properties of 15-lipoxygenase products of arachidonic acid. Proc. Natl. Acad. Sci. U S A. 83(14):5331-4

•Li H.S., Xu X.Z., Montell C. (1999) Activation of a TRPC3-dependent cation current through the neurotrophin BDNF. Neuron 24(1):261-73

•Liedtke W., Choe Y., Marti-Renom M.A., Bell A.M., Denis C.S., Sali A., Hudspeth A.J., Friedman J.M., Heller S. (2000) Vanilloid receptor-related osmotically activated channel (VR-OAC), a candidate vertebrate osmoreceptor. Cell 103(3):525-35

•Liman E.R., Corey D.P., Dulac C. (1999) TRP2: a candidate transduction channel for mammalian pheromone sensory signaling. Proc. Natl. Acad. Sci. U S A. 96(10):5791-6

•Lindsay R.M., Lockett C., Sternberg J., Winter J. (1989) Neuropeptide expression in cultures of adult sensory neurons: modulation of substance P and calcitonin gene-related peptide levels by nerve growth factor. Neuroscience 33(1):53-65

• Liu L., Simon S.A. (1996) Similarities and differences in the currents activated by capsaicin, piperine, and zingerone in rat trigeminal ganglion cells. J. Neurophysiol. 6(3):1858-69

• Liu L., Simon S.A. (2000) Capsaicin, acid and heat-evoked currents in rat trigeminal ganglion neurons: relationship to functional VR1 receptors. Physiol. Behav. 69(3):363-78

• Lopshire J.C., Nicol G.D. (1998) The cAMP transduction cascade mediates the prostaglandin E2 enhancement of the capsaicin-elicited current in rat sensory neurons: whole-cell and single-channel studies. J. Neurosci. 18(16):6081-92

• Mannion R.J., Costigan M., Decosterd I., Amaya F., Ma Q.P., Holstege J.C., Ji R.R., Acheson A., Lindsay R.M., Wilkinson G.A., Woolf C.J. (1999) Neurotrophins: peripherally and centrally acting modulators of tactile stimulus-induced inflammatory pain hypersensitivity. Proc. Natl. Acad. Sci. U S A. 96(16):9385-90

•Mantyh P.W., Allen C.J., Rogers S., DeMaster E., Ghilardi J.R., Mosconi T., Kruger L., Mannon P.J., Taylor I.L., Vigna S.R. (1994) Some sensory neurons express neuropeptide Y receptors: potential paracrine inhibition of primary afferent nociceptors following peripheral nerve injury. J. Neurosci. 14(6): 3958-3868

• McMahon S.B., Priestley J.V. (1995) Peripheral neuropathies and neurotrophic factors: animal models and clinical perspectives. Curr. Opin. Neurobiol. 5(5):616-24

• Melck D., Bisogno T., De Petrocellis L., Chuang H., Julius D., Bifulco M., Di Marzo V. (1999) Unsaturated long-chain N-acyl-vanillyl-amides (N-AVAMs): vanilloid receptor ligands that inhibit anandamide-facilitated transport and bind to CB1 cannabinoid receptors. Biochem. Biophys. Res. Commun. 262(1):275-84

• Mezey E., Toth Z.E., Cortright D.N., Arzubi M.K., Krause J.E., Elde R., Guo A., Blumberg P.M., Szallasi A. (2000) Distribution of mRNA for vanilloid receptor subtype 1 (VR1), and VR1-like immunoreactivity, in the central nervous system of the rat and human. Proc. Natl. Acad. Sci. U S A. 97(7):3655-60

• Michael G.J., Averill S., Nitkunan A., Rattray M., Bennett D.L., Yan Q., Priestley J.V. (1997) Nerve growth factor treatment increases brain-derived neurotrophic factor selectively in TrkA-expressing dorsal root ganglion cells and in their central terminations within the spinal cord. J. Neurosci. 17(21):8476-90

• Michael G.J., Priestley J.V. (1999) Differential expression of the mRNA for the vanilloid receptor subtype 1 in cells of the adult rat dorsal root and nodose ganglia and its downregulation by axotomy. J. Neurosci. 19(5): 1844-54

•Michael G.S., Averill S., Shortland P.J., Yan Q., Priestley J.V. (1999) Axotomy results in major changes in BDNF expression by dorsal root ganglion cells: BDNF expression in large trkB and trkC cells, in pericellular baskets and in projections to deep dorsal horn and dorsal column nuclei. Eur. J. Neurosci. 11: 3539-3551

• Millns P.J., Chapman V., Kendall D.A. (2001) Cannabinoid inhibition of the capsaicin-induced calcium response in rat dorsal root ganglion neurones. Br. J. Pharmacol. 132(5):969-71

• Montell C., Jones K., Hafen E., Rubin G. (1985) Rescue of the Drosophila phototransduction mutation trp by germline transformation. Science 230(4729):1040-3

•Munaron L., Pla A.F. (2000) Calcium infux induced by activation of tyrosine kinase receptors in cultured bovine aortic endothelial cells. J. Cell. Physiol. 185: 454-463

• Nagamine K., Kudoh J., Minoshima S., Kawasaki K., Asakawa S., Ito F., Shimizu N. (1998) Molecular cloning of a novel putative Ca2+ channel protein (TRPC7) highly expressed in brain. Genomics 54(1):124-31

• Nagy J.I., Vincent S.R., Staines W.A., Fibiger H.C., Reisine T.D., Yamamura H.I. (1980) Neurotoxic action of capsaicin on spinal substance P neurons. Brain Res. 186(2):435-44

• Nagy J.I., van der Kooy D. (1983) Effects of neonatal capsaicin treatment on nociceptive thresholds in the rat. J. Neurosci. 3(6):1145-50

• Nagy I., Rang H.P. (1999) Similarities and differences between the responses of rat sensory neurons to noxious heat and capsaicin. J. Neurosci.19(24):10647-55

• Nagy I., Rang H. (2000) Comparison of currents activated by noxious heat in rat and chicken primary sensory neurons. Regul Pept. 96(1-2):3-6

•Nakatsuka T. Gu J.G. (2000) ATP-sensitive and capsaicin-sensitive central synapses to lamina V and lamina II neurons in rat spinal cord. Society for Neuroscience meeting, N.Orleans, abstract id:431

• Nanki T., Hayashida K., El-Gabalawy H.S., Suson S., Shi K., Girschick H.J., Yavuz S., Lipsky P.E. (2000) Stromal cell-derived factor-1-CXC chemokine receptor 4 interactions play a central role in CD4+ T cell accumulation in rheumatoid arthritis synovium. J. Immunol. 165(11):6590-8

•Nicholas R.S., Winter J., Wren P., Bergman R., Woolf C.J. (1999) Peripheral inflammation increases the capsaicin sensitivity of dorsal root ganglion neurons in a nerve growth factor-dependent manner. Neuroscience 91(4): 1425-1433

•Niemeyer B.A., Bergs C., Wissenbach U., Flockerzi V., Trost C. (2001) Competitive regulation of CaT-like-mediated Ca^{+2} entry by protein kinase C and calmodulin. PNAS 98(6): 3600-3605

• Ninkina N.N., Willoughby J.J., Beech M.M., Coote P.R., Wood J.N. (1994) Molecular cloning of a resiniferatoxin-binding protein. Brain Res. Mol. Brain Res.22(1-4):39-48

•Ogun-Muyiwa P., Helliwell R., McIntyre P., Winter J. (1999) Glial cell line derived neurotrophic factor (GDNF) regulates VR1 and substance P in cultured sensory neurons. Neuroreport 10(10):2107-11

• Oh U., Hwang S.W., Kim D. (1996) Capsaicin activates a nonselective cation channel in cultured neonatal rat dorsal root ganglion neurons. J. Neurosci.16(5):1659-67

•Oh S.B., Tran P.B., Gillard S.E., Hurley R.W., Hammond D.L., Miller R.J. (2001) Chemokines and glycoprotein 120 produce pain hypersensitivity by directly exciting primary nociceptive neurons. J. Neurosci. 21(14): 5027-5035

•Okada T., Shimizu S., Wakamori M., Maeda A., Kurosaki T., Takada N., Imoto K., Mori Y. (1998) Molecular cloning and functional characterization of a novel receptor-activated TRP Ca2+ channel from mouse brain. J. Biol. Chem. 273(17):10279-87

•Okada T., Inoue R., Yamazaki K., Maeda A., Kurosaki T., Yamakuni T., Tanaka I., Shimizu S., Ikenaka K., Imoto K., Mori Y. (1999) Molecular and functional characterization of a novel mouse transient receptor potential protein homologue TRP7. Ca(2+)-permeable cation channel that is constitutively activated and enhanced by stimulation of G protein-coupled receptor. J. Biol. Chem. 274(39):27359-70

• Olah Z., Karai L., Iadarola M.J. (2001a) Anandamide Activates Vanilloid Receptor 1 (VR1) at Acidic pH in Dorsal Root Ganglia Neurons and Cells Ectopically Expressing VR1. J. Biol. Chem. 276(33):31163-70

• Olah Z., Szabo T., Karai L., Hough C., Fields R.D., Caudle R.M., Blumberg P.M., Iadarola M.J. (2001b) Ligand-induced dynamic membrane changes and cell deletion conferred by vanilloid receptor 1. J. Biol. Chem. 276(14):11021-30

• Oxford G.S., Kuzhikandathil E.V., Szabo T., Wang H., Blumberg P.M. (2000) Use of a dominant negative mutant of VR1 to explore capsaicin receptor stoichiometry. Society for Neuroscience meeting, N.Orleans, abstract id: 13707

•Pandey A., Lewitter F. (1999) Nucleotide sequence databases: a gold mine for biologists. Trends Biochem. Sci. 24(7):276-80

•Peng J.B., Chen X.Z., Berger U.V., Vassilev P.M., Tsukaguchi H., Brown E.M., Hediger M.A. (1999) Molecular cloning and characterization of a channel-like transporter mediating intestinal calcium absorption. J. Biol. Chem. 274(32):22739-46

• Perl E.R. (1996) Cutaneous polymodal receptors: characteristics and plasticity. Prog. Brain Res. 113:21-37

• Perl E.R., Kruger L. (1996) Chapter 4: Nociception and pain. Evolution of Concepts and Observations. Pain and Touch. 2nd edition, edited by L.Kruger. London Academic Press, p.p. 179-211

• Petersen M., LaMotte R.H. (1993) Effect of protons on the inward current evoked by capsaicin in isolated dorsal root ganglion cells. Pain 54(1):37-42

•Philipp S., Cavalie A., Freichel M., Wissenbach U., Zimmer S., Trost C., Marquart A., Murakami M., Flockerzi V. (1996) A mammalian capacitative calcium entry channel homologous to Drosophila TRP and TRPL. EMBO J. 15(22):6166-71

•Philipp S., Hambrecht J., Braslavski L., Schroth G., Freichel M., Murakami M., Cavalie A., Flockerzi V. (1998) A novel capacitative calcium entry channel expressed in excitable cells. EMBO J. 1998 17(15):4274-82.

• Phillips A.M., Bull A., Kelly L.E. (1992) Identification of a Drosophila gene encoding a calmodulin-binding protein with homology to the trp phototransduction gene. Neuron 8(4):631-42

•Planells-Cases R., Aracil A., Merino J.M., Gallar J., Perez-Paya E., Belmonte C., Gonzalez-Ros J.M., Ferrer-Montiel A.V. (2000) Arginine-rich peptides are blockers of VR1 channels with analgesic activity. FEBS Lett. 481: 131-136

• Porreca F., Lai J., Bian D., Wegert S., Ossipov M.H., Eglen R.M., Kassotakis L., Novakovic S., Rabert D.K., Sangameswaran L., Hunter J.C. (1999) A comparison of the potential role of the tetrodotoxin-insensitive sodium channels, PN3/SNS and NaN/SNS2, in rat models of chronic pain. Proc. Natl. Acad. Sci. U S A. 96(14):7640-4

• Prawitt D., Enklaar T., Klemm G., Gartner B., Spangenberg C., Winterpacht A., Higgins M., Pelletier J., Zabel B. (2000) Identification and characterization of MTR1, a novel gene with homology to melastatin (MLSN1) and the trp gene family located in the BWS-WT2 critical region on chromosome 11p15.5 and showing allele-specific expression. Hum. Mol. Genet. 9(2):203-16

• Premkumar L.S., Ahern G.P. (2000) Induction of vanilloid receptor channel activity by protein kinase C. Nature 408(6815):985-90

•Prigent C., Gill R., Trower M., Sanseau P. (1999) In silico cloning of a new protein kinase, Aik2, related to Drosophila Aurora using the new tool: EST Blast. In Silico Biol. 1(2):123-8

•Putney J.W. Jr. (1986) A model for receptor-regulated calcium entry. Cell Calcium 7(1):1-12

•Putney J.W. Jr, McKay R.R. (1999) Capacitative calcium entry channels. Bioessays 21(1):38-46

•Ringkamp M., Peng Y.B., Wu G., Hartke T.V., Campbell J.N., Meyer R.A. (2001) Capsaicin responses in heat-sensitive and heat-insensitive A-fiber nociceptors. J. Neurosci. 21(12):4460-8

•Runnels L.W., Yue L., Clapham D.E. (2001) TRP-PLIK, a bifunctional protein with kinase and ion channel activities. Science 291(5506):1043-7

•Russell J.W., Windebank A.J., Schenone A., Feldman E.L. (1998) Insulin-like growth factor-I prevents apoptosis in neurons after nerve growth factor withdrawal. J. Neurobiol. 36(4): 455-467

•Ryazanov A.G., Pavur K.S., Dorovkov M.V. (1999) Alpha-kinases: a new class of protein kinases with a novel catalytic domain. Curr. Biol. 9(2):R43-R45

• Sadeghi H.M., Innamorati G., Birnbaumer M. (1997) Maturation of receptor proteins in eukaryotic expression systems. J Recept. Signal Transduct. Res. 17(1-3):433-45

• Sasamura T., Sasaki M., Tohda C., Kuraishi Y. (1998) Existence of capsaicin-sensitive glutamatergic terminals in rat hypothalamus. Neuroreport 9(9):2045-8

• Schaefer M., Plant T.D., Obukhov A.G., Hofmann T., Gudermann T., Schultz G. (2000) Receptor-mediated regulation of the nonselective cation channels TRPC4 and TRPC5. J. Biol. Chem. 275(23): 17517-17526

•Schultz J., Doerks T., Ponting C.P., Copley R.R., Bork P. (2000) More than 1,000 putative new human signalling proteins revealed by EST data mining. Nat. Genet. 25(2):201-4

•Schumacher M.A., Moff I., Sudanagunta S.P., Levine J.D. (2000a) Molecular cloning of an N-terminal splice variant of the capsaicin receptor. Loss of N-terminal domain suggests functional divergence among capsaicin receptor subtypes. J. Biol. Chem. 275(4):2756-62

• Schumacher M.A., Jong B.E., Frey S.L., Sudanagunta S.P., Capra N.F. Levine J.D. (2000b) The stretch-inactivated channel, a vanilloid receptor variant, is expressed in small diameter sensory neurons in rat. Neurosci. Lett. 287: 215-218

• Shin J.S., Wang M.H., Hwang S.W., Cho H., Cho S.Y., Kwon M.J., Lee S.Y., Oh U. (2001) Differences in sensitivity of vanilloid receptor 1 transfected to human embryonic kidney cells and capsaicin-activated channels in cultured rat dorsal root ganglion neurons to capsaicin receptor agonists. Neurosci. Lett. 299(1-2):135-9

•Short protocols in molecular biology: a compendium of methods from Current protocols in molecular biology. Edited by F.M. Ausubel *et al.* 4th edition, N.York 1999, section 4.2.5

• Shu X., Mendell L.M. (1999) Nerve growth factor acutely sensitizes the response of adult rat sensory neurons to capsaicin. Neurosci. Lett. 274(3):159-62

•Sinkins W.G., Vaca L., Hu Y., Kunze D.L., Schilling W.P. (1996) The COOH-terminal domain of Drosophila TRP channels confers thapsigargin sensitivity. J. Biol. Chem. 271(6):2955-60

•Sinkins W.G., Estacion M., Schilling W.P.(1998) Functional expression of TrpC1: a human homologue of the Drosophila Trp channel. Biochem. J. 331 (Pt 1):331-9

• Smart D., Jerman J.C., Gunthorpe M.J., Brough S.J., Ranson J., Cairns W., Hayes P.D., Randall A.D., Davis J.B. (2001) Characterisation using FLIPR of human vanilloid VR1 receptor pharmacology. Eur J Pharmacol. 417(1-2):51-8

• Snider W.D., McMahon S.B. (1998) Tackling pain at the source: new ideas about nociceptors. Neuron 20(4):629-32

•Sossey-Alaoui K., Lyon J.A., Jones L., Abidi F.E., Hartung A.J., Hane B., Schwartz C.E., Stevenson R.E., Srivastava A.K. (1999) Molecular cloning and characterization of TRPC5 (HTRP5), the human homologue of a mouse brain receptor-activated capacitative Ca2+ entry channel. Genomics 60(3):330-40

•Strotmann R., Harteneck C., Nunnenmacher K., Schultz G., Plant T.D. (2000) OTRPC4, a nonselective cation channel that confers sensitivity to extracellular osmolarity. Nat. Cell Biol. 2(10):695-702

•Strubing C., Krapivinsky G., Krapivinsky L., Clapham D.E. (2001) TRPC1 and TRPC5 form a novel cation channel in mammalian brain. Neuron 29: 645-655

•Suzuki M., Sato J., Kutsuwada K., Ooki G., Imai M. (1999) Cloning of a stretch-inhibitable nonselective cation channel. J. Biol. Chem. 274(10):6330-5

• Szallasi A., Blumberg P.M. (1990) Specific binding of resiniferatoxin, an ultrapotent capsaicin analog, by dorsal root ganglion membranes. Brain Res. 524(1):106-11

• Szallasi A., Blumberg P.M. (1991) Molecular target size of the vanilloid (capsaicin) receptor in pig dorsal root ganglia. Life Sci.48(19):1863-9

• Szallasi A. (1994) The vanilloid (capsaicin) receptor: receptor types and species differences. Gen. Pharmac. 25(2): 223-243

•Szallasi A., Blumberg P.M., Lundberg J.M. (1995a) Proton inhibition of [3H]resiniferatoxin binding to vanilloid (capsaicin) receptors in rat spinal cord. Eur. J. Pharmacol. 289(2):181-7

•Szallasi A., Nilsson S., Farkas-Szallasi T., Blumberg P.M., Hokfelt T., Lundberg J.M. (1995b) Vanilloid (capsaicin) receptors in the rat: distribution in the brain, regional differences in the spinal cord, axonal transport to the periphery, and depletion by systemic vanilloid treatment. Brain Res. 703(1-2): 175-83

•Szallasi A., Blumberg P.M., Annicelli L.L., Krause J.E., Cortright D.N. (1999) The cloned rat vanilloid receptor VR1 mediates both R-type binding and C-type calcium response in dorsal root ganglion neurons. Mol. Pharmacol. 56(3):581-7

•Szolcsanyi J., Jancso-Gabor A. (1975) Sensory effects of capsaicin congeners I. Relationship between chemical structure and pain-producing potency of pungent agents. Arzneim.-Forsch. (Drug Res.) 25(12): 1877-1881

•Tang Y., Tang J., Chen Z., Trost C., Flockerzi V., Li M., Ramesh V., Zhu M.X. (2000) Association of mammalian trp4 and phospholipase C isozymes with a PDZ domain-containing protein, NHERF. J. Biol. Chem. 275(48):37559-64

•Tang J., Lin Y., Zhang Z., Tikunova S., Birnbaumer L., Zhu M.X. (2001) Identification of common binding sites for calmodulin and inositol 1,4,5-trisphosphate receptors on the carboxyl termini of trp channels. J. Biol. Chem. 276(24):21303-10

• Tham T.N., Lazarini F., Franceschini I.A., Lachapelle F., Amara A., Dubois-Dalcq M. (2001) Developmental pattern of expression of the alpha chemokine stromal cell-derived factor 1 in the rat central nervous system. Eur. J. Neurosci. 13(5):845-56

• Tominaga M., Caterina M.J., Malmberg A.B., Rosen T.A., Gilbert H., Skinner K., Raumann B.E., Basbaum A.I., Julius D. (1988) The cloned capsaicin receptor integrates multiple pain-producing stimuli. Neuron 21: 531-543

•Tominaga M., Wada M., Masu M. (2001) Potentiation of capsaicin receptor activity by metabotropic ATP receptors as a possible mechanism for ATP-evoked pain and hyperalgesia. Proc. Natl. Acad. Sci. U S A. 98(12):6951-6

•Tsavaler L., Shapero M.H., Morkowski S., Laus R. (2001) Trp-p8, a novel prostate-specific gene, is up-regulated in prostate cancer and other malignancies and shares high homology with transient receptor potential calcium channel proteins. Cancer Res. 61: 3760-3769

•Vaca L., Sinkins W.G., Hu Y., Kunze D.L., Schilling W.P. (1994) Activation of recombinant trp by thapsigargin in Sf9 insect cells. Am. J. Physiol. 267(5 Pt 1):C1501-C1505.

• Vannier B., Zhu X., Brown D., Birnbaumer L. (1998) The membrane topology of human transient receptor potential 3 as inferred from glycosylation-scanning mutagenesis and epitope immunocytochemistry. J. Biol. Chem. 273(15):8675-9

• Vannier B., Peyton M., Boulay G., Brown D., Qin N., Jiang M., Zhu X., Birnbaumer L. (1999) Mouse trp2, the homologue of the human trpc2 pseudogene, encodes mTrp2, a store depletion-activated capacitative Ca2+ entry channel. Proc. Natl. Acad. Sci. U S A. 96(5):2060-4

•Vasmatzis G., Essand M., Brinkmann U., Lee B., Pastan I. (1998) Discovery of three genes specifically expressed in human prostate by expressed sequence tag database analysis. Proc. Natl. Acad. Sci. U S A. 95(1):300-4

• Vlachova V., Vyklicky L. (1993) Capsaicin-induced membrane currents in cultured sensory neurons of the rat. Physiol. Res. 42(5):301-11

• Vyklicky L., Knotkova-Urbancova H., Vitaskova Z., Vlachova V., Kress M., Reeh P.W. (1998) Inflammatory mediators at acidic pH activate capsaicin receptors in cultured sensory neurons from newborn rats. J. Neurophysiol. 79(2):670-6

• Waldmann R., Lazdunski M. (1998) H(+)-gated cation channels: neuronal acid sensors in the NaC/DEG family of ion channels. Curr. Opin. Neurobiol. 8(3):418-24

• Wang W., O'Connell B., Dykeman R., Sakai T., Delporte C., Swaim W., Zhu X., Birnbaumer L., Ambudkar I.S. (1999) Cloning of Trp1beta isoform from rat brain: immunodetection and localization of the endogenous Trp1 protein. Am. J. Physiol. 276(4 Pt 1):C969-79

• Watson C.P., Evans R.J., Watt V.R. (1988) Post-herpetic neuralgia and topical capsaicin. Pain 33(3):333-40

• Wei M.H., Karavanova I., Ivanov S.V., Popescu N.C., Keck C.L., Pack S., Eisen J.A., Lerman M.I. (1998) In silico-initiated cloning and molecular characterization of a novel human member of the L1 gene family of neural cell adhesion molecules. Hum. Genet. 103(3):355-64

•Welch J.M., Simon S.A., Reinhart P.H. (2000) The activation mechanism of rat vanilloid receptor 1 by capsaicin involves the pore domain and differs from the activation by either acid or heat. Proc. Natl. Acad. Sci. U S A. 97(25):13889-94

•Wes P.D., Chevesich J., Jeromin A., Rosenberg C., Stetten G., Montell C. (1995) TRPC1, a human homolog of a Drosophila store-operated channel. Proc. Natl. Acad. Sci. U S A. 92(21):9652-6

•Wissenbach U., Bodding M., Freichel M., Flockerzi V. (2000) Trp12, a novel Trp related protein from kidney. FEBS Lett. 485(2-3):127-34

•Wissenbach U., Niemeyer B.A., Fixemer T., Schneidewind A., Trost C., Cavalie A., Reus K., Meese E., Bonkhoff H., Flockerzi V. (2001) Expression of CaT-like, a novel calcium-selective channel, correlates with the malignancy of prostate cancer. J. Biol. Chem. 276(22):19461-8

• Winston J., Toma H., Shenoy M., Pasricha P.J. (2001) Nerve growth factor regulates VR-1 mRNA levels in cultures of adult dorsal root ganglion neurons. Pain 89(2-3): 181-6

• Winter J. (1987) Characterization of capsaicin-sensitive neurones in adult rat dorsal root ganglion cultures. Neurosci. Lett. 80(2):134-40

• Winter J., Forbes C.A., Sternberg J., Lindsay R.M. (1988) Nerve growth factor (NGF) regulates adult rat cultured dorsal root ganglion neuron responses to the excitotoxin capsaicin. Neuron 1(10): 973-81

• Winter J., Dray A., Wood J.N., Yeats J.C., Bevan S. (1990) Cellular mechanism of action of resiniferatoxin: a potent sensory neuron excitotoxin. Brain Res. 520(1-2):131-40

•Winter J., Walpole C.S., Bevan S., James I.F. (1993) Characterization of resiniferatoxin binding sites on sensory neurons: co-regulation of resiniferatoxin binding and capsaicin sensitivity in adult rat dorsal root ganglia. Neuroscience 57(3):747-57

• Wood J.N., Winter J., James I.F., Rang H.P., Yeats J., Bevan S. (1988) Capsaicin-induced ion fluxes in dorsal root ganglion cells in culture. J. Neurosci. 8(9):3208-20

• Wood J.N., Coote P.R., Minhas A., Mullaney I., McNeill M., Burgess G.M. (1989) Capsaicin-induced ion fluxes increase cyclic GMP but not cyclic AMP levels in rat sensory neurones in culture. J. Neurochem. 53(4):1203-11

•Wood J.N., Walpole C., James I.F., Dray A., Coote P.R. (1990) Immunochemical detection of photoaffinity-labelled capsaicin-binding proteins from sensory neurons. FEBS Lett. 269(2):381-5

•Wood J.N., Docherty R. (1997) Chemical activators of sensory neurons. Annu. Rev. Physiol. 59: 457-482

•Wu X., Babnigg G., Villereal M.L. (2000) Functional significance of human trp1 and trp3 in store-operated Ca(2+) entry in HEK-293 cells. Am. J. Physiol. Cell Physiol. 278(3):C526-36

•Xu X.Z., Li H.S., Guggino W.B., Montell C. (1997) Coassembly of TRP and TRPL produces a distinct store-operated conductance. Cell 89(7):1155-64

• Xu X.Z., Chien F., Butler A., Salkoff L., Montell C. (2000) TRPgamma, a Drosophila TRP-related subunit, forms a regulated cation channel with TRPL. Neuron 26(3):647-57

•Yue L., Peng J.B., Hediger M.A., Clapham D.E. (2001) CaT1 manifests the pore properties of the calcium-release-activated calcium channel. Nature 410(6829):705-9

• Zhu X., Chu P.B., Peyton M., Birnbaumer L. (1995) Molecular cloning of a widely expressed human homologue for the Drosophila trp gene. FEBS Lett. 373(3):193-8

• Zhu X., Jiang M., Peyton M., Boulay G., Hurst R., Stefani E., Birnbaumer L. (1996) trp, a novel mammalian gene family essential for agonist-activated capacitative Ca2+ entry. Cell 85(5):661-71

• Zhu X., Jiang M., Birnbaumer L. (1998) Receptor-activated Ca2+ influx via human Trp3 stably expressed in human embryonic kidney (HEK)293 cells. Evidence for a non-capacitative Ca2+ entry. J. Biol. Chem. 273(1):133-42

•Zitt C., Zobel A., Obukhov A.G., Harteneck C., Kalkbrenner F., Luckhoff A., Schultz G. (1996) Cloning and functional expression of a human Ca2+-permeable cation channel activated by calcium store depletion. Neuron 16(6):1189-96

•Zitt C., Obukhov A.G., Strubing C., Zobel A., Kalkbrenner F., Luckhoff A., Schultz G. (1997) Expression of TRPC3 in Chinese hamster ovary cells results in calcium-activated cation currents not related to store depletion. J. Cell Biol. 138(6):1333-41

•Zou Y.R., Kottmann A.H., Kuroda M., Taniuchi I., Littman D.R. (1998) Function of the chemokine receptor CXCR4 in haemotopoiesis and cerebellar development. Nature 393(6685): 595-599

• Zygmunt P.M., Petersson J., Andersson D.A., Chuang H., Sorgard M., Di Marzo V., Julius D., Hogestatt E.D. (1999) Vanilloid receptors on sensory nerves mediate the vasodilator action of anandamide. Nature 400(6743):452-7

• Zygmunt P.M., Chuang H., Movahed P., Julius D., Hogestatt E.D. (2000) The anandamide transport inhibitor AM404 activates vanilloid receptors. Eur. J. Pharmacol. 396(1):39-42